

Context-Dependent Modulators of Cardiac Fibroblast Phenotype

A Thesis

Presented to

the faculty of the School of Engineering and Applied Science

University of Virginia

in partial fulfillment
of the requirements for the degree

Doctor of Philosophy

by

Angela Courtney Zeigler

August 2018

APPROVAL SHEET

This Thesis
is submitted in partial fulfillment of the requirements for the degree of
Doctor of Philosophy

Author Signature: _____

This Thesis has been read and approved by the examining committee:

Advisor: Jeffrey Saucerman

Committee Member: Jason Papin

Committee Member: Jeffrey Holmes

Committee Member: Thomas Barker

Committee Member: Coleen McNamara

Committee Member: Jennifer Munson

Accepted for the School of Engineering and Applied Science:



Craig H. Benson, School of Engineering and Applied Science

August 2018

Context-Dependent Modulators of Cardiac Fibroblast Phenotype

A DISSERTATION

Presented to the faculty of the School of Engineering and Applied Science,
University of Virginia,
in partial fulfillment of the requirements for the degree of

DOCTOR OF PHILOSOPHY

by ANGELA COURTNEY ZEIGLER

December 2017

This thesis is dedicated to the memory of
Frederick Christopher Gehlken
a man with a wonderful heart

“I am among those who think that science has great beauty”

-Marie Curie

“We are not afraid to follow truth wherever it may lead, nor to tolerate any error so long as
reason is left free to combat it.”

-Thomas Jefferson

Abstract

Fibrosis, the accumulation of excess extracellular matrix, is a characteristic of many pathologies. But it is currently poorly understood, partially because it was long thought to be simply a reaction to injury or a side effect of healing, rather than a treatable disease process. However, fibrosis is increasingly a focus of research as anti-fibrotic therapy has the potential to improve the prognosis for patients with fibrosis. In most organs fibrosis is associated with increased mortality because it disrupts normal organ function, and it can be progressive and permanent. In the heart, fibrosis is particularly devastating because increased extracellular matrix stiffens cardiac tissue and the mechanical properties of the heart are crucial to efficient pumping. Even post-myocardial infarction, when fibrosis is necessary to prevent rupture of the ventricular wall, the character and extent of matrix production is an important determinant of cardiac health. This is particularly true since cardiomyocytes do not repopulate the infarct scar, leaving the matrix and the fibroblasts who maintain it the important role of preserving pump function.

Another reason the mechanisms of fibrosis remain unknown is that it is a complex, heterogeneous response to a variety of injuries. In order for fibrosis to develop, a multitude of signals from the extracellular matrix, inflammatory cells, injured parenchymal cells, and endothelial cells drive matrix protein production or degradation. Often the relative amount of different matrix proteins, cell types, and chemical stimuli are specific to the organ and the initiating injury, meaning each fibrosis type is unique. Furthermore, fibroblasts, thought to be the main cell type involved in fibrosis development, are highly plastic. That is, they are capable of adopting a variety of phenotypes in response to different signaling contexts, and that results in a

variety of effects on the extracellular matrix. Fully investigating the complex signaling milieu and consequent cell decision-making is a difficult, almost intractable, experimental challenge. What drives fibrosis is exactly the sort of question that is suited to a systems biology approach. With computational modeling it is easier to interrogate fibrosis as a system to determine which cell type, which signaling pathway, or which protein is the major modulator of fibrosis development in a given setting. Ultimately, a systems biology investigation of fibrosis could identify potential therapeutic approaches for prevention or reversal of fibrosis through targeting fibroblast signaling.

This study represents a first step in that direction by focusing on cardiac fibroblast signaling and decision-making. We used the literature on cardiac fibroblast and general fibroblast signaling interactions to compile a manually curated network of fibroblast signaling pathways. This network is effectively a review of the current understanding of fibroblast signaling. This network was used in a logic-based ODE model that can predict changes in relative activity of network members given an extracellular signaling context (both mechanical and chemical).

We applied this model to the question: how does signaling context determine which node or pathway can modulate collagen expression? We first investigated how pathways are organized into modules and how these modules are affected by which stimulus is applied to the model. This led us to the prediction that mechanical signaling depends on the TGF β pathway to induce α SMA production, and this was validated in rat cardiac fibroblasts. The model was also used to predict how dynamic signaling in the post-MI setting affects collagen I expression in fibroblasts. We predicted that IL1 signaling is the dominant pathway determining fibroblast phenotype in the early (0.5 day) post-MI signaling context, and that TGF β is the dominant pathway at the 7 day

time-point. We found that ROS is a context-dependent regulator of collagen I mRNA expression in both dynamic and steady-state simulations. We also hypothesize, based on model predictions, that nodes such as PKC or IL1RI are pro-fibrotic modulators of fibroblast signaling in the post-MI dynamic signaling context. This use of a model to investigate wound healing process is an important advance, as the dynamics of acute wound healing are difficult to study. Ultimately, the model predicted that up-regulation of a node is more likely to be pro-fibrotic than anti-fibrotic. This leads to the general hypothesis that cardiac fibroblasts are primed to increase collagen production in response to a variety of stimuli.

As drug discovery is an important use of computational modeling, we developed a pipeline for *in silico* drug screening using the fibroblast signaling model. With this pipeline we were able to predict drugs that can improve (triflusal) or worsen (arsenic trioxide or anti-thymocyte globulin) cardiac remodeling post-MI through regulation of collagen I expression by fibroblasts.

In this study we developed a signaling network and computational model that together provide a framework for understanding how fibroblasts decide to adopt a certain phenotype. I outline in this dissertation a few important applications for this model: linking topological structure to function, screening for potential pro- or anti- fibrotic activity of drugs, and determining the context-dependence of collagen modulators. But this network and model are flexible enough to be applied to other questions. Gene expression data could be used to inform model parameters and make predictions about how organ-specific or patient-specific fibroblasts respond to different signaling contexts. This model could be incorporated into a multi-scale model of tissue-level fibrosis, or stochastic variation could be added to the model to predict how populations of fibroblasts lead to changes in matrix composition. Finally, pathways could be

added onto this network either through further manual curation or through network expansion using inference techniques and high-throughput expression or proteomics data. The capabilities of this model highlight how it can be useful in organizing current knowledge to make hypotheses about fibroblast behavior.

Acknowledgements

All scientific advancement is dependent on the support of family, friends and advisors. I have so many people to thank for helping this thesis become reality.

I first need to thank my PhD advisor. Jeff, your mentorship has been instrumental to my success. I am grateful to you for letting me join your lab even though I had zero computational or engineering experience. Your patient teaching has turned me from a student who was dependent on an undergrad to help write new code to a student who can teach her undergrad how to write cleaner, more efficient code. As difficult as the years of frustrating experimental failures have been for me, I appreciate you trying to keep me cheerful and motivated.

I have been lucky enough to have an amazing PhD committee. First, Jeff Holmes, I am thankful to you for always challenging me to improve myself - whether that's in my communication or in my experimental design. I have no doubt I hold myself to a higher standard of excellence because of you. Jason, it's important for scientists to have some level of optimism to keep going in the face of frustration, so thank you for teaching me to always look for the positive lessons from failure. Jenny, I am forever grateful to you for letting me work closely with you in your lab. Your advice goes through my head every time I design a new experiment. Your encouragement boosted my excitement for science, and seeing some my own characteristics in

you made me think for the first time that I could be a successful PI. Borna, I am thankful you pushed me to think deeply about every statement I make. Tom, I learned so much about fibroblasts from our conversations, and I appreciate you validating my experience that these cells are difficult to study. Coleen, you have been inspiring to me since you spoke to the MSTP ladies over coffee, and I am grateful you joined my committee so that I can hear your practical advice for my future career.

I have had other mentors who have contributed to my scientific development. Sandy and John Wheeler, you are the main reason I love research. You saw a budding physician scientist where I didn't, and I'm glad I have finally realized this career path was the right choice. To my other Furman professors, Brian Goess and Karen Buchmueller, your continued advice over the years I've been in graduate school has given me a helpful dose of perspective on this brief phase of my career. Mark Mendelsohn, my preceptor in medical school, you encouraged me to pursue my interest in science, and are the original reason I joined the MD, PhD program. You are the most amazing clinician I have ever met, and if I am anywhere near as calm and thoughtful as you are with both patients and students, I will consider myself a huge success.

The MSTP has been hugely supportive of me. Dori Williams and Gary Owens were kind enough to consider my application to the program when I was a medical student. Dean Kedes, you always have an open ear for a struggling MSTP student, and I am encouraged to know you believe in my ability to become a good scientist. The other students of the MSTP, especially Annie Carlton, Ricky Bayliss, Bert Cortina, Jeff Xing, Ali Kahn, Sam Adamson, Sowmya Narayanan, Kristen Penberthy, and Joe Walpole, have provided so much inspiration and commiseration. I couldn't have done it without you.

There have been many students throughout the BME department who have shared ideas and support throughout the years: Millie Shah, Liz Periera, Laura Dunphy, Anna Blazier, Laura Caggiano, Matt Biggs, Phil Yen, Kelly Virgilio, Kellen Chen, and the entire Munson lab, Matt Perez, Jess Yuan, Katherine Kingsmore, Chase Cornelison, and Ali Harris.

Nicole, Courtney, and Veronica, throughout grad school you have let me visit you and listened to me and given me advice and cheered me on. No matter how far away you live, your friendship is valuable to me.

To the rest of the Saucerman lab, it was “awesomesauce” working with you! Karen Ryall and Eric Greenwald, thank you for letting me pester you with questions both before and after you graduated. Laura Woo, thank you for always seeing the logical side of every scenario and listening to be talk for hours about how I feel. I wouldn’t have made it without all the Costco, Starbucks, and bubble tea trips. Philip Tan and Bryan Chun, thank you for pushing me to consider the details of all of my projects. Will Richardson, I am so lucky I somehow got the chance to work with you. You have, in so many ways, shaped my scientific thinking, and I’m grateful you’ve let me continue going to you for advice. Matthew Sutcliffe, you were the best desk-mate I could have asked for - always ready to share puppy pictures or take trips to Insomnia Cookies or critique my coding. Your friendship has made me a more thoughtful and better person. Debbie Frank, I look up to you so much, and it has been amazing visiting you in the PICU and chatting with you in lab. And thank you to the other lab members who have helped shaped my work: Alex Paap, Jingyuan Zhang, Astor Liu, Matthew Van de Graaf (for “who’s to say”), and Darius Hossainian. I especially want to thank Ani Chandrabatla. I am so proud of the scientist that you have become, and thank you for being patient with me while I learn how to be a better mentor.

Finally, I need to thank my family - the original supporters of my young scientific career. My grandparents, who have come through plenty of hardships unphazed, have inspired me to think of any obstacle as trivial. Melinda and Kahli have always been cheerfully supportive. My “little” brother, Chris, is always ready to provide perspective on how normal non-grad students think. Even though he doesn’t share my love of academia, his support of my career choice means more than anyone’s. My mom has provided endless support from listening to me cry over failed experiments to making me a month’s worth of food right before my thesis was due. She always challenges me to look beyond just scientific success and to have empathy for those around me. Because of this, I am a better student, teacher, and scientist. My dad is the person who initially sparked my interest in science. He got me a telescope for my birthday one year and enlisted my help in electrically wiring our new house. He got me a typing game and pushed me to learn to type quickly. My dad believes I can do anything, and because of him, I sometimes believe that too. Thank you to my entire family for encouraging me to be my nerdy self.

Angela C. Zeigler

December 2017

Contents

[Abstract](#)

[Acknowledgements](#)

[Contents](#)

[List of Figures](#)

[List of Tables](#)

[Abbreviations](#)

1. [Background and Significance](#)
 - 1.1 [Foreword](#)
 - 1.2 [Introduction](#)
 - 1.3 [Electrophysiological Modeling](#)
 - 1.4 [Fibroblasts and Tissue Remodeling](#)
 - 1.5 [Signaling Networks and Fibroblast Phenotype](#)
 - 1.6 [Future Directions](#)
 - 1.7 [Conclusions](#)
2. [A computational model of cardiac fibroblast signaling predicts context-dependent drivers of myofibroblast differentiation.](#)
 - 2.1 [Foreword](#)
 - 2.2 [Introduction](#)

-
- 2.3 [Methods](#)
 - 2.4 [Results](#)
 - 2.4.1 [A predictive computational model of cardiac fibroblast signaling](#)
 - 2.4.2 [Context-Dependent Roles of Cardiac Fibroblast Signaling Driver](#)
 - 2.4.3 [Relationship Between Network Structure and Function](#)
 - 2.4.4 [Cross-Talk Between Mechanical and TGF \$\beta\$ Pathways](#)
 - 2.5 [Discussion](#)
 - 2.6 [Conclusions](#)
 - 3. [Identifying Potential Modulators of Adverse Remodeling Post-Myocardial Infarction](#)
 - 3.1 [Foreword](#)
 - 3.2 [Introduction](#)
 - 3.3 [Methods](#)
 - 3.4 [Results](#)
 - 3.4.1 [Adapting the computational model to predict post-MI phenotype](#)
 - 3.4.2 [Predicting the role of exo. signaling in collagen dynamics during wound healing](#)
 - 3.4.3 [Predicting endogenous modulators of fibroblast phenotype during infarct healing](#)
 - 3.4.4 [IL1 and TGF \$\beta\$ cross talk](#)
 - 3.5 [Discussion](#)
 - 3.6 [Conclusion](#)
 - 4. [In silico screening for potential modulators of adverse remodeling post-myocardial infarction](#)
 - 4.1 [Foreword](#)
 - 4.2 [Introduction](#)
 - 4.3 [Methods](#)

-
- 4.4 [Results](#)
 - 4.4.1 [Simulation of competitive and non-competitive drugs in logic-based ODE model](#)
 - 4.4.2 [Identifying drugs with targets in the fibroblast network](#)
 - 4.4.3 [Predicting the effect of drug simulation on drug target](#)
 - 4.4.4 [Context-Dependent drug simulations](#)
 - 4.5 [Discussion](#)
 - 4.6 [Conclusion](#)
 - 5. [Comparisons between cultured primary fibroblasts](#)
 - 5.1 [Foreword](#)
 - 5.2 [Introduction](#)
 - 5.3 [Methods](#)
 - 5.4 [Results](#)
 - 5.4.1 [\$\alpha\$ SMA levels in different cell culture conditions and fibroblast types](#)
 - 5.4.2 [Contractile properties of different fibroblast types](#)
 - 5.4.3 [Collagen production from different fibroblast types](#)
 - 5.5 [Discussion](#)
 - 5.6 [Conclusion](#)
 - 6. [Dissertation discussion](#)
 - 6.1 [Aims](#)
 - 6.1.1 [Relationship between network topology and function](#)
 - 6.1.2 [Post-MI wound healing](#)
 - 6.1.3 [Pipeline for *in silico* drug screening](#)
 - 6.1.4 [Context-dependent signaling and cell decision-making](#)

6.2 [Future](#)

6.3 [Conclusion](#)

[Appendix A: Large-scale fibroblast signaling model description](#)

[Appendix B: Modeling the dynamic post-MI environment](#)

[Appendix C: Drug-target pairs](#)

[Bibliography](#)

List of Figures

- 1.1 [Electrical behavior of fibroblasts](#)
- 1.2 [Agent-based modeling of infarct wound healing](#)
- 1.3 [Fibroblast signaling network](#)
- 1.4 [Summary of future directions](#)
- 2.1 [Reconstruction of the cardiac fibroblast signaling network](#)
- 2.2. [Example of model validation with combined stimuli](#)
- 2.3 [Validation of network input-output relationships predicted by the model](#)
- 2.4 [Sensitivity analysis reveals context-dependent functional roles for regulators of cardiac fibroblast signaling](#)
- 2.5 [Relationships between functional modules are context-dependent](#)
- 2.6 [Metrics of network topology are insufficient to predict network function](#)
- 2.7 [Exp. validation of predicted role for TGF \$\beta\$ in mechanical-induced expression of \$\alpha\$ SMA.](#)
- 3.1 [Generation and validation of a dynamic post-MI model of cardiac fibroblast](#)
- 3.2 [Model prediction of the result of random expression](#)
- 3.3 [Effect of altered input profiles](#)
- 3.4 [Relationship b/w sustained, simplified inputs and select time points of the dyn. prediction](#)
- 3.5 [Predicted fibroblast phenotype in the dynamic and steady state simulations](#)
- 3.6 [Screen for modulators of post-MI collagen](#)
- 3.7 [Screen for collagen modulators in representative steady state simulations](#)
- 3.8 [Effect of specific modulators of collagen output](#)
- 3.9 [Validation of interaction between IL1 and TGF \$\beta\$.](#)

-
- 4.1 [Drug screen pipeline schematic](#)
 - 4.2 [Effect of competitive or non-competitive inhibitors on interactions of different topologies](#)
 - 4.3 [Effect of increasing drug strength on activity of drug target](#)
 - 4.4 [Effect of competitive vs. non-competitive modeling of increasing drug strength](#)
 - 4.5 [Drug effect in different contexts](#)
 - 4.6 [Post-MI dynamic drug simulations](#)
 - 4.7 [Effect of specific drugs on post-MI phenotype](#)
 - 5.1 [\$\alpha\$ SMA expression in adult rat cardiac fibroblasts in 2D and 3D culture.](#)
 - 5.2 [\$\alpha\$ SMA expression in human dermal and human ventricular fibroblasts](#)
 - 5.3 [Contraction of human primary fibroblasts](#)
 - 5.4 [Collagen production by primary human fibroblasts](#)
 - A.1 [Full simulation of TGF- \$\beta\$ versus forskolin treatment](#)
 - A.2: [Other validated relationships](#)
 - A.3: [Robustness of validation accuracy to changes in baseline input levels](#)
 - A.4: [Full sensitivity analysis.](#)
 - A.5: [Clustering analysis](#)
 - A.6: [Full comparison of topological features versus influence](#)
 - B.1: [Network modifications](#)
 - B.2: [Training mechanical input levels to validation data](#)
 - B.3: [Inputs to dynamic post-MI simulations](#)
 - B.4: [Inputs to tissue-level model for control \(pre-infarct\) simulations.](#)

List of Tables

- 1.1 [Summary of approaches used to model fibroblasts and fibrosis](#)
- 2.1 [Model-predicted functional modules](#)
- 3.1 [Input alterations](#)
- 4.1 [Unique drug-target pairs](#)
- A.1 [Network description](#)
- A.2 [References for validation of the large-scale fibroblast signaling model](#)
- A.3 [Definitions of network topology metrics](#)
- B.1 [Post-Infarct Measurements of Model Inputs](#)
- C.1 [All drug-target pairs](#)

Abbreviations

Abbreviation	Description
AngII	angiotensin II
inputAngII	Input angiotensin II
AngIImRNA	Angiotensin II mRNA
AT1R	angiotensin II receptor type 1
AGT	angiotensinogen
ACE	angiotensin converting enzyme
NOX	NAD(P)H oxidase
ROS	reactive oxygen species
ET1	endothelin I
inputET1	Input endothelin I
ET1mRNA	Endothelin I mRNA
ETAR	endothelin 1 receptor A
DAG	diacyl-glycerol
PKC	protein kinase C
TRPC	transient receptor potential canonical
NE	norepinephrine
inputNE	Input norepinephrine
BAR	beta adrenergic receptor 1 or 2
Forskolin	Forskolin
inputForskolin	Input forskolin
AC	adenylate cyclase
cAMP	cyclic adenosine monophosphate
PKA	protein kinase A
CREB	cAMP response-element binding protein

CBP	CREB - binding protein
TGFB or TGF β	transforming growth factor beta 1
inputTGFB	Input transforming growth factor beta I
TGFB1R	TGFB receptor
smad3	small mothers against decapentaplegic 2 and 3
smad7	Small mothers against decapentaplegic 7
TGFBmRNA	TGFB1 with latent protein complex
BAMBI	BMP and activin bound inhibitor
PDGF	platelet derived growth factor
inputPDGF	Input platelet derived growth factor
PDGFR	platelet derived growth factor receptor
NP	natriuretic peptide
inputNP	Input natriuretic peptide
NPRA	natriuretic peptide receptor
cGMP	cyclic guanosine monophosphate
PKG	protein kinase G
mechanical	stretch
inputMechanical	Input mechanical
B1int	beta 1 integrin
Rho	a Rho-dependent GTPase
ROCK	rho associated protein kinase
Ca	calcium
calcineurin	calcineurin
NFAT	nuclear factor of activated T-cells
IL6	interleukin-6
inputIL6	Input interleukin-6
IL6mRNA	Interleukin-6 mRNA
gp130	IL-6 receptor complexed to gp130 for signal transduction

STAT	signal transducers and activators of transcription 1 and 3
IL1	interleukin-1 alpha and beta
inputIL1	Input interleukin 1
IL1RI	Interleukin 1 receptor type I
TNF α or TNF α	tissue necrosis factor alpha
inputTNF α	Input tissue necrosis factor alpha
TNF α R	Tissue necrosis factor alpha receptor
NFKB	nuclear factor kappa-light-chain-enhancer of activated B cells
PI3K	phosphoinositide 3-kinase
Akt	protein kinase B
p38	Mitogen activated protein kinase 11, mitogen activated protein kinase 12, mitogen activated protein kinase 13, mitogen activated protein kinase 14
TRAF	tnf receptor associated factor either 2/6
ASK1	apoptosis signal related kinase 1
MKK3	mitogen activated protein kinase kinase
PP1	protein phosphatase 1
JNK	c-Jun N-terminal kinases
abl	abl tyrosine kinase
Rac1	a Rho-dependent GTPase
MEKK1	Mitogen activated protein kinase kinase kinase 1
MKK4	Mitogen activated protein kinase kinase 4
ERK	Extracellular-signal related kinases
Ras	representing the family of GTPases
Raf	family of raf protein serine/threonine kinases
MEK1	a MAP2K mainly specific to ERK
FAK	focal adhesion kinase
epac	exchange protein activated by cAMP 1

Factin	polymerized actin
FA	formation of focal adhesions
migration	mobility
cmyc	avian myelocytomatosis viral oncogene homolog
CTGF	connective tissue growth factor
proliferation	proliferation
SRF	serum response factor
EDAFN	extra domain A of fibronectin
α SMA or α SMA	alpha-smooth muscle actin
AP1	activator protein 1
TIMP1	tissue inhibitor of metalloproteinase 1
TIMP2	tissue inhibitor of metalloproteinase 2
PAI1	plasminogen activator inhibitor 1
proMMP14	Matrix metalloproteinase 14 mRNA
proMMP1	Matrix metalloproteinase 1 mRNA
proMMP2	Matrix metalloproteinase 2 mRNA
proMMP9	Matrix metalloproteinase 9 mRNA
MMP1	Matrix metalloproteinase-1
MMP2	Matrix metalloproteinase-2
MMP9	Matrix metalloproteinase-9
MMP14	Matrix metalloproteinase-14
CImRNA	Collagen I mRNA
CIII mRNA	Collagen III mRNA
CI	collagen I
CIII	collagen III
LOX	lysyl oxidase
xlinkFibers	crosslinked collagen fibers
HDF	Human dermal fibroblast
HVF	Human ventricular fibroblast

MI	Myocardial infarction
ODE	Ordinary differential equation
ECM	extracellular matrix

Chapter 1

Background and Significance

Reprinted from: AC Zeigler, WJ Richardson, JW Holmes, JJ Saucerman, “Computational Modeling of Cardiac Fibroblasts and Fibrosis.” *Journal of Molecular and Cellular Cardiology* Vol. 93 pp 73-83 (2016), with permission from Elsevier

1.1 Foreword

In order to properly introduce this thesis, it's important to explain why I initially wanted to pursue this project. I joined the Saucerman lab because I find the heart fascinating, and I felt it would be beneficial to gain skills in systems biology, as this is rapidly becoming an essential tool for solving problems of complex diseases. This dissertation underscores my deep interest in cardiac and systems level research. However, this project is first and foremost about a wonderfully plastic and multi-tasking cell - the fibroblast. When given the choice of projects to work on, I chose to work on fibrosis because I was taught in medical school how intractable a problem it was. In almost every system we studied, fibrosis emerged as the end-point to many pathologies. Despite years of futile research, there is no cure for fibrosis, which means it is often presented as a boring clinical problem, a basic sign that the body is injured rather than a disease state to be treated. Although in some organs treatment of the underlying cause can reverse fibrosis, in many organs, fibrosis is a death knell. I specifically remember meeting a patient with idiopathic pulmonary fibrosis just after learning this diagnosis had a median survival rate of two years. It was hard to listen to him speaking because all I could think about was how soon he was going to die. This is the kind of problem that attracted me, and many others, to a career as a physician scientist. There are patients for whom there is little hope, and we seek to provide some sliver of additional opportunity for them through research.

Since I began working on this dissertation, I have learned that fibrosis is a complex and terrifying process - often utilizing aggressive feed-forward signaling to perpetuate further matrix production. This is, I think, the type of problem most suited to a systems biology approach. There is no one single cell type, one single stimulus, or one single matrix protein that makes fibrosis. Instead it is a complex interplay between many signals and many cells, which can easily

tip matrix production from helpful to harmful. The matrix itself is a complex meshwork whose composition and arrangement can determine everything from a single cell's phenotype to an organ's mechanical properties. Even the most well designed *in vivo* experimental study cannot fully investigate all the temporal, cell-specific, and organ-specific drivers of fibrosis. The question of what drives fibrosis is one that can benefit from the power of computational experimentation where variation in all of these factors can be investigated quickly and cheaply. This thesis uses computational modeling to understand how fibroblasts, the cell type central to fibrosis, integrate complex stimuli and respond to the benefit or harm of the heart. In this chapter, I review what had been accomplished in the area of computational modeling of fibroblasts in the heart.

1.2 Introduction

Altered fibroblast behavior can lead to pathologic changes in the heart such as arrhythmia, diastolic dysfunction, and systolic dysfunction. Computational models are increasingly used as a tool to identify potential mechanisms driving a phenotype or potential therapeutic targets against an unwanted phenotype. In this chapter, we review how computational models incorporating cardiac fibroblasts have clarified the role for these cells in electrical conduction and tissue remodeling in the heart. Models of fibroblast signaling networks have primarily focused on fibroblast cell lines or fibroblasts from other tissues rather than cardiac fibroblasts, specifically, but they are useful for understanding how fundamental signaling pathways control fibroblast phenotype. In the future, modeling cardiac fibroblast signaling, incorporating -omics and drug-interaction data into signaling network models, and utilizing multi-scale models will improve the

ability of in silico studies to predict potential therapeutic targets against adverse cardiac fibroblast activity.

Fibroblasts are integral to the normal structure and function of the heart. During development, fibroblasts deposit extracellular matrix (ECM) to provide structural integrity of the myocardium (K T Weber 1989; Souders, Bowers, and Baudino 2009). Throughout life, fibroblasts maintain and remodel the ECM in response to the environment and act as sentinel cells, integrating the tissue's response to various mechanical, chemical, and electrical cues (Miragoli, Gaudesius, and Rohr 2006; Souders, Bowers, and Baudino 2009). For example, fibroblasts play a role in initiating and resolving the inflammatory response following myocardial injury such as infarction (Díaz-Araya et al. 2015). Finally, it is increasingly clear that fibroblasts are electrically coupled to myocytes and contribute to the electrical properties of the myocardium (Shibukawa et al. 2005; Souders, Bowers, and Baudino 2009; Miragoli, Gaudesius, and Rohr 2006).

Cardiac injury, such as an infarct, prompts changes in fibroblast activity that can be helpful or pathologic. Following an infarct, inflammatory cytokines induce migration of fibroblasts into the tissue that are, at later stages of healing, induced to deposit collagen and differentiate into pro-fibrotic myofibroblasts. A balance of ECM production and degradation is necessary to prevent excessive loss of matrix proteins which can increase risk of wall rupture and infarct expansion (Ma et al. 2013), or excessive matrix production which can lead to increased interstitial fibrosis even in areas distant from the infarct (Sun and Weber 2000). Activated myofibroblasts have been observed in human cardiac tissue many years after an infarct, indicating the potential for long-term tissue remodeling by fibroblasts (Willems et al. 1994). Fibroblast activation can be triggered by many other forms of cardiac injury including pressure

overload (K T Weber 1989), diabetes (Asbun and Villarreal 2006), and infectious diseases such as Chagas disease (Galvão and Miranda 2010) or Coxsackie B3 infection (Nishtala et al. 2011).

Not only does fibroblast activity change in response to injury and disease, but altered fibroblast matrix production can also provoke disease. For example, myxomatous valve disorders are associated with an increase in matrix metalloproteinase (MMP) production by myofibroblasts without an increase in collagen expression leading to a loss of structural integrity in the valve (Rabkin et al. 2001). Increased ventricular fibrosis is associated with a worse prognosis and worsened diastolic dysfunction (Wong et al. 2012; Moreo et al. 2009). Fibrosis is also implicated in conduction abnormalities that increase risk for arrhythmia (Krul et al. 2015; Miragoli, Gaudesius, and Rohr 2006). Restoring the balance of fibroblast activity could be a valuable therapeutic approach, which would rely on a more complete understanding of fibroblast regulation and function.

Yet the complexity of cardiac fibroblasts and fibrotic tissue hinders such an understanding. Teasing apart the competing roles of fibroblasts in response to mechanical, chemical, and electrical cues is difficult to do experimentally. When closely integrated with experimental studies, computational models can provide a powerful framework for developing a quantitative understanding of complex biological systems. Indeed, computational models of cardiomyocytes have long been employed to make substantial insights into cardiac electrophysiology, mechanics, and signaling networks, as recently reviewed elsewhere (Trayanova and Boyle 2014; J. H. Yang and Saucerman 2011). Increasingly, computational models have also begun to provide important insights into cardiac fibroblasts and cardiac fibrosis. Here, we review the contributions of computational modeling to the field's understanding of how fibroblasts modulate electrical conduction, coordinate tissue remodeling,

and integrate signals. We then outline future directions for improving modeling of cardiac fibroblasts toward a better understanding of the role of fibroblasts in heart disease and targeted design of therapeutic strategies.

1.3 Electrophysiological Modeling

Fibroblasts play a role in electrical conduction through the heart both indirectly through regulation of extracellular matrix proteins and directly by connecting to cardiac myocytes (Rohr 2009; Spach and Boineau 1997). Fibroblasts have been shown to conduct electrical activity through direct connection to myocytes via gap junctions composed of Cx43 and Cx45 (Gaudesius et al. 2003; Miragoli, Gaudesius, and Rohr 2006). Their resting membrane potential *in vitro* is primarily determined by K⁺ currents and was measured around at -60mV (Shibukawa et al. 2005). Fibroblasts alter myocyte electrical behavior *in vitro* by raising their resting membrane potential and by slowing conduction velocity (Chilton et al. 2005). Here we review how computational modeling has been used to better understand how electrical coupling to fibroblasts modulates both cardiac myocyte and tissue electrophysiology.

Linking Fibroblasts to Cardiac Myocytes

Kohl et al. developed the first computational model linking fibroblasts and cardiac myocytes, applying it to test the hypothesis that mechanosensitive fibroblasts modulate the spontaneous firing rate of the sinoatrial node (SAN) (P Kohl et al. 1994). They modeled fibroblasts as electrically passive (lacking voltage-dependent ion currents) but responsive to mechanical

stretch. When coupled to a single myocyte, this model predicted that fibroblasts increased the rate of SAN firing in response to stretch, consistent with previous studies. Further, the model was able to predict how variations in the coupling between fibroblasts and myocytes would affect these responses (P Kohl et al. 1994). The Oxsoft model was later expanded by linking it with the Kurata rabbit SAN model and was used to examine how fibroblasts affect SA node activity (Oren and Clancy 2010). The model predicted that fibroblasts act as electrical sinks and slow conduction from SAN to atrium. This could provide a mechanistic link between age-associated increases atrial conduction times and atrial fibroblast numbers.

While early models represented fibroblasts as electrically passive, the MacCannell model was the first to incorporate active, voltage-dependent ion currents based on patch clamp measurements from isolated cardiac fibroblasts (MacCannell et al. 2007). This electrically active fibroblast model was coupled to the ten Tusscher model of cardiac myocyte electrophysiology, which has experimentally-based parameters for ion current densities and gating kinetics from human ventricular myocytes and *in vivo* data (ten Tusscher et al. 2004). The MacCannell model described the fibroblast's electrical activity based on four currents: a delayed-rectifier K⁺ current, an inward-rectifying K⁺ current, a Na⁺-K⁺ pump, and a "leak" Na⁺ current. The parameters for the delayed-rectifier K⁺ current were derived experimentally, while the parameters for the inward-rectifying K⁺ current were estimated from the ten Tusscher model. This "active" model was more accurate than a comparable "passive" model of fibroblast activity, which lacked voltage-dependent ion currents. This model predicted that fibroblasts would partially depolarize the resting membrane potential for myocytes and shorten the action potential duration (Fig. 1.1A), which agrees with experimental studies (Miragoli, Gaudesius, and Rohr

2006). This model was subsequently adapted for use in several models of tissue-level conduction as described below.

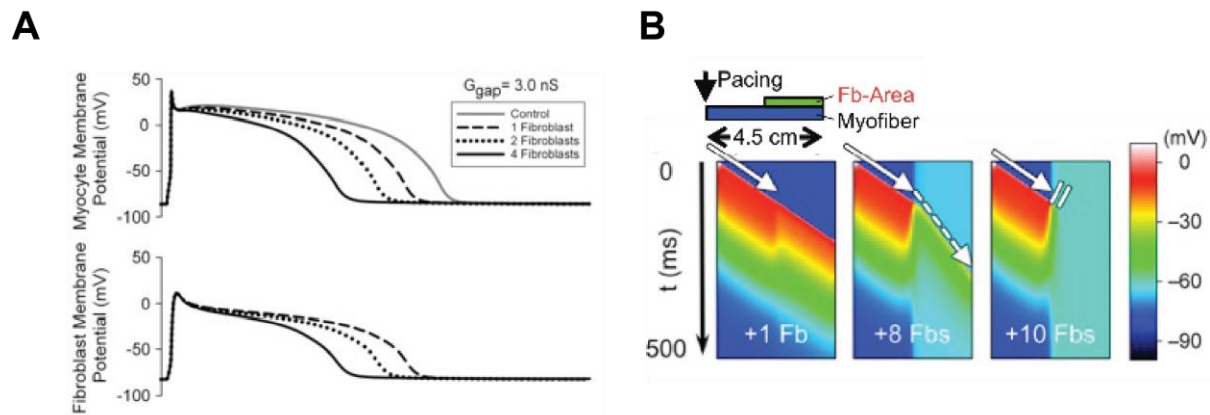


Figure 1.1: Electrical behavior of fibroblasts. (A) The MacCannell model predicts myocyte action potential duration and fibroblast potential elevation are shortened as the number of fibroblasts connected to myocytes is increased. Figure adapted with the permission by Biophysical Journal from MacCannell et al 2007. (B) Predictions from the Ashihara model show that increased numbers of fibroblasts connected to a myocyte can slow conduction (dashed arrow) or even cause conduction block (double lines). Figure adapted with permission by Circulation Research from Ashihara et al 2012.

Around the same time, Jacquemet et al. published a more phenomenological model that described the voltage-dependence of fibroblast ion currents as a polynomial fit to *in vitro* data (Jacquemet and Henriquez 2007). They coupled the fibroblast to a model of a mouse myocyte (Bondarenko et al. 2004) as a single fibroblast-myocyte pair or a strand of myocytes covered with a layer of fibroblasts. Increasing myocyte-fibroblast coupling and increasing fibroblast activity decreased the conduction velocity and prolonged action potential duration. Importantly, they predicted that the fibroblast's resting membrane potential was an important determinant of the effect on the myocyte. When the myocyte membrane potential was more negative than the fibroblast, the fibroblast acted as a source of current, but the fibroblast acted as

current sink when the myocyte potential was less negative. A later modification of this model retained the same fibroblast-myocyte organization but used a model of a canine atrial myocyte (Ramirez, Nattel, and Courtemanche 2000) coupled to the MacCannell model (Jacquemet and Henriquez 2008). This model predicted the myocyte resting membrane potential would be higher with increased fibroblast-myocyte coupling, in agreement with the MacCannell model. They determined that a lower fibroblast resting membrane potential shortens the action potential duration (APD), while a higher resting membrane potential prolongs the APD. This reconciles the apparent contradiction between the findings in their previous study and those in the MacCannell study using the same conclusion that the relative difference between the myocyte and fibroblast membrane potentials determines the effect on electrical conduction.

Others have used a more detailed Markov model of the fibroblast time- and voltage-dependent outward K^+ current and reached the same conclusion that the relative membrane potentials of the two cells is important for determining the effect of fibroblasts on electrical activity (Sachse, Moreno, and Abildskov 2008). Additionally, the model predicted that increased heterocellular coupling (through decreased myocyte-fibroblast resistance) intensified the effect of fibroblasts on electrical activity. Overall, these studies and others (Xie, Garfinkel, Weiss, et al. 2009; Xie, Garfinkel, Camelliti, et al. 2009; Sachse et al. 2009), provide quantitative support for hypothesis that fibroblasts affect the electrical activity of cardiomyocytes by acting as a current source or sink depending on the context. The Sachse model used four arrangements of myocytes and fibroblasts that are simplifications of organizations that could be observed *in vivo*. For example, fibroblasts forming a bridge between chains of myocytes, as would be found in focal fibrosis, were predicted to lead to conduction block, which was consistent with *in vitro* studies (Gaudesius et al. 2003). Together these studies provide a basis for understanding how

coupling to a fibroblast affects myocyte resting potential and action potential, and applying these simplified models to more complex heterocellular arrangements allows for an increased understanding of tissue-level electrical conduction and arrhythmia.

Modeling Fibroblast Contribution to Ventricular Arrhythmia

A number of studies have built upon these models of conduction velocity to examine the impact of fibroblasts on ventricular arrhythmia. In a highly influential study, Zlochiver et al. combined experimental and computational approaches to examine the role of myofibroblast-myocyte coupling on reentrant arrhythmias (Zlochiver et al. 2008). Their model coupled an active myofibroblast model to the Viswanathan model of a ventricular myocyte (Viswanathan, Shaw, and Rudy 1999; Zlochiver et al. 2008) to simulate electrical propagation in a co-culture of myofibroblasts and myocytes. The arrangement of the cells was designed to match the experimental arrangements measured *in vitro*. Their model predicted that increased myofibroblasts would decrease reentry of a spiral wave but would increase the complexity of the electrical propagation (increased phase singularities). Further, an increase in myofibroblast-myocyte and myofibroblast-myofibroblast coupling decreased phase singularities but had a biphasic relationship with conduction velocity, with the lowest conduction velocity occurring at intermediate myofibroblast density. These findings were remarkably consistent with data from their co-culture experiments (Zlochiver et al. 2008). The biphasic relationship between conduction velocity and myofibroblast coupling highlights the potential for fibroblasts either to contribute to or protect against conduction abnormalities.

Other models have expanded on the detailed MacCannell fibroblast model to explore how fibroblasts contribute to arrhythmia development. The Zlochiver group later developed a model based on the MacCannell model linked to the ten Tusscher model with fibroblasts arranged as a layer on top of a sheet of myocytes (bilayer model) or interspersed between the myocytes as a monolayer (Greisas and Zlochiver 2012). This model predicted a biphasic relationship between spontaneous depolarization frequency that peaks at intermediate fibroblast/myocyte ratios. However, they found that stability of the reentrant wave decreases with increased fibroblast density and increased fibroblast-myocyte coupling, which is in contrast to the Zlochiver model. The most likely reason they cited for the discrepancy was that the previous model assumed that fibroblasts and myocytes were the same size. While this assumption may be appropriate *in vitro*, this newer model represented the *in vivo* case where fibroblasts are much smaller than myocytes.

There are also other factors regarding fibroblasts and extracellular matrix that differ between *in vitro* and *in vivo* experiments. Ashihara et al. adapted the MacCannell model to model fibroblasts or myofibroblasts and coupled it to the Courmanche human atrial model (Ashihara et al. 2012). Myofibroblasts were represented as fibroblasts with increased capacitance. They found that both fibroblasts and myofibroblasts shortened action potential duration and that areas of high fibroblast or myofibroblast density slow conduction (Fig. 1.1B) and are arrhythmogenic, but that fewer myofibroblasts than fibroblasts are sufficient to induce conduction block. Simulation of ablation in those areas prevented reentry, providing a rationale for the treatment of arrhythmia with ablation.

Myocardial infarction is a risk factor for the development of arrhythmia. McDowell et al. integrated the MacCannell model into a finite element model (FEM) based on an MRI of a rabbit heart to investigate how fibroblasts in the infarct zone and peri-infarct zone affect electrical

conduction throughout the heart (McDowell et al. 2011). As predicted by the Jacquemet model (Jacquemet and Henriquez 2008), this model predicted that the fibroblasts act as a current sink during the action potential to shorten APD, but during rest the fibroblasts act as a current source and raise the resting membrane potential. Furthermore, the resting membrane potential was higher with increased myofibroblast-myofibroblast coupling within the scar and was further increased with a higher density of myofibroblasts in the infarct zone. Their model also predicted that intermediate levels of myofibroblasts in the peri-infarct zone are arrhythmogenic because there is a dispersal of the APD, but at higher densities the myofibroblasts act as a current sink to limit reentry. Together these studies indicate that fibroblasts can support arrhythmia by increasing the heterogeneity of electrical conduction, but they can limit arrhythmia by slowing conduction or facilitating conduction depending on the strength of fibroblast-myocyte or fibroblast-fibroblast connection. As the electrical properties of fibroblasts *in vivo* are clarified (recently reviewed by Kohl et al. (Peter Kohl and Gourdie 2014)), updates on these models can incorporate more accurate parameters and improve our understanding of the role of fibroblasts in modulating electrical activity in the heart.

1.4 Fibroblasts and Tissue Remodeling

The extracellular matrix is a critical determinant of cardiac mechanics, and abnormal quantity or organization of matrix can lead to both systolic and diastolic dysfunction. Many past studies have used computational modeling to demonstrate the acute mechanical effects of cardiac matrix structure and organization (Bogen et al. 1980; Fomovsky et al. 2011; Moyer et al. 2015; Wall et al. 2006; Wenk et al. 2011). Herein, we focus our review on models that predict fibroblast-

mediated, long-term changes in scar structure, i.e. growth and remodeling during wound healing and/or fibrosis. Cardiac fibroblasts drive matrix turnover through an orchestrated balance of matrix protein secretion and processing (e.g., collagen I, collagen III, fibronectin, elastin, etc.), proteinase secretion and activation (e.g., MMP 1, 2, 3, 7, 8, 9, 12, 13, 14, etc.), and proteinase inhibitor secretion and activation (e.g., tissue inhibitor of metalloproteinases (TIMP) 1, 2, 3, 4) (see reviews by Creemers (Creemers et al. 2001), Lindsey (Lindsey and Zamilpa 2012), and Vanhoutte (Vanhoutte et al. 2006)). Fibroblasts can also organize matrix structure by exerting acto-myosin generated contractile forces on matrix fibers via focal adhesions (Hailong Wang et al. 2014; Harris, Stopak, and Wild 1981), and by directing the deposition of matrix fibers with preferred orientations parallel to the cells' own orientations (Birk and Trelstad 1986; Trelstad and Hayashi 1979; Canty et al. 2004). Fibroblast-mediated turnover and fibroblast-mediated remodeling are both sensitive to chemical and mechanical environmental cues that can dramatically change during disease conditions (Nahrendorf M, Sam F 2016; Richardson WJ, Clarke SA 2016). The relationships between local signals and long-term matrix remodeling have therefore been the focus of a number of computational studies, which have varied in modeling framework and biological complexity. Here we divide the studies by the biological components explicitly included in their simulations: matrix only, matrix plus fibroblasts, or matrix plus multiple cell types.

Matrix-Only Models

Extracellular matrix growth and remodeling across diverse tissues has been predicted using a variety of computational frameworks including simple ODE (ordinary differential equation) models, FEMs, constrained mixture models, agent-based models, and others. To our knowledge,

the first simulations focusing specifically on cardiac matrix remodeling were performed by Driessen and colleagues to test the effects of mechanical loading on collagen fiber orientations in the aortic valve. In a series of studies (N. J. Driessen et al. 2003; N. J. B. Driessen, Bouten, and Baaijens 2005; N. J. B. Driessen et al. 2008), they used an FEM of the aortic valve geometry and loading to calculate strain and stress distributions throughout the valve. Assuming that steady-state fiber content increases linearly with stretch² and that fibers tend to align according to positive principal strain directions, matrix remodeling simulations were conducted stepwise with new matrix structure (and corresponding new material parameters) calculated in remodeling steps, then new tissue strains calculated in FEM steps. Over time, these straight-forward assumptions proved to be sufficient to successfully generate the distinctive, fiber architecture experimentally observed in mature valves with fibers running from commissure to commissure.

Matrix & Fibroblast Models

Some of the earliest models explicitly combining fibroblasts with matrix remodeling were formulated by Dallon and colleagues, who simulated fibroblast-mediated dermal wound healing by simulating matrix properties as a continuous 2D-vector field and fibroblasts as discrete elements migrating in that field (J. C. Dallon, Sherratt, and Maini 1999; J. Dallon et al. 2000). In these simulations, fibroblasts oriented themselves by averaging their previous orientation direction with the local collagen fiber direction, then migrated, reoriented existing collagen, and laid down new collagen according to prescribed rate parameters. Not surprisingly, the long-term matrix alignment and content was highly dependent on a variety of parameters including initial cell positions, cell speed, cell persistence, fiber reorientation rate, initial fiber alignment, fiber production rate and others. In two later studies, Dallon et al. (J. C. Dallon, Sherratt, and Maini)

and McDougall et al. (McDougall et al. 2006) improved upon their basic model to include the effects of chemical signals in the wound territory. Specifically, the concentrations of tissue growth factor beta (TGF β) and a generic chemoattractant were included in the simulations as functions of position and time in order to modulate a variety of rate parameters according to experimental observations (e.g., TGF β increases collagen deposition, and chemotactic gradients enhance wound infiltration rates). These important model additions improved the match between model and experimental data, and also enabled more explicit testing of specific therapeutic interventions.

In the first model of cardiac infarct wound healing, Rouillard and Holmes adapted Dallon and McDougall's agent-based model (ABM) to simulate cardiac fibroblast infiltration and collagen remodeling in infarct tissue (Fig. 1.2) (Rouillard and Holmes 2012). A critical extension of Rouillard was the addition of a mechanical cue to combine with local chemical and structural cues to guide fibroblast proliferation, orientation, migration, apoptosis, collagen production, collagen degradation, and collagen reorientation. An additional advance was that nearly every parameter value was determined directly from independent experimental data in the literature. With this framework, Rouillard found that a uniaxial strain environment lead to an anisotropic collagen matrix with both cells and fibers aligned in parallel to the strain direction, while a biaxial strain environment lead to an isotropic collagen matrix with cells and fibers more randomly oriented. Importantly, both these predictions matched experimental data from rat infarcts subjected to either uniaxial or biaxial loading environments for 3 weeks (Fomovsky, Rouillard, and Holmes 2012; Fomovsky and Holmes 2010). Moreover, the model also correctly recapitulated a transmural variation in infarct collagen alignment experimentally observed in pig infarcts (Holmes, Nuñez, and Covell 1997): collagen alignment is highest at the midwall where

the mechanical cue and pre-existing fiber cue are parallel, and alignment is lowest at the endocardial and epicardial surfaces where mechanical cue and pre-existing fiber cue are competing. These findings demonstrate the ability of these types of models to integrate information about multiple different mechanisms of matrix remodeling to predict their combined effects *in vivo*, which is vital to the ability to develop effective therapeutic interventions to control matrix structure and thereby improve cardiac function in disease conditions.

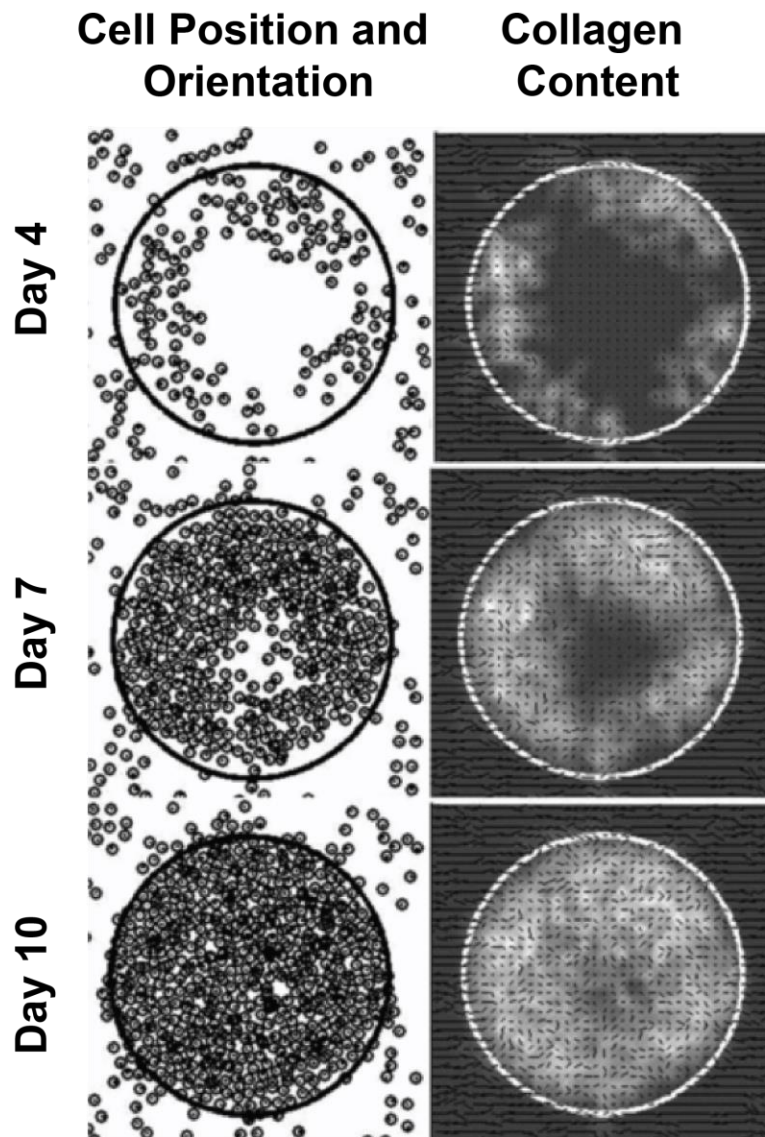


Figure 1.2: Agent-based modeling of infarct wound healing. Rouillard and Holmes used an agent-based framework to capture fibroblast proliferation, orientation, migration, and collagen remodeling in response to mechanical, chemical, and structural cues. During the healing time course, high chemokine levels in the wound lead to fibroblast infiltration and collagen accumulation, and the strain pattern (biaxial vs. uniaxial) determine fibroblast and collagen orientations (random vs. aligned, respectively). Figure is adapted with permission by the Journal of Physiology from Rouillard and Holmes 2012.

Rouillard and Holmes have recently updated their original framework by coupling ABM predictions to an FEM of infarct mechanics (Rouillard and Holmes 2014). Those simulations used the previously developed ABM to predict changes in scar structure, which is passed as fiber-based constitutive material properties to an FEM of a 2D infarct section. New strains are then calculated by the FEM and passed back to ABM to provide updated mechanical cues for the next remodeling time step, and so forth. This coupled ABM-FEM allowed Rouillard to correctly predict not only scar fiber structure but also regional deformations seen following coronary ligation in rats (Fomovsky and Holmes 2010). It also suggested that fibroblast alignment parallel to a strain cue actually provides negative feedback to drastic changes in local fiber orientations: as fiber orientation deviates from an aligned direction, the tissue becomes stiffer parallel to the new orientation and strain becomes greater perpendicular to the new orientation, driving fibroblasts and subsequent fiber orientations away from the deviation direction and back toward the original alignment direction. We should note one limitation to their approach is that fibroblast-mediated reorientation of collagen was represented by phenomenologically modifying local fiber orientation distributions. As an alternative, several groups have simulated cell compaction of collagen gels by explicitly calculating the mechanical equilibrium between each cell's contractile forces and nearby collagen fibers' mechanical properties (Reinhardt and Gooch 2014; Checa et al. 2014).

Multiple Cell Type Models

While the addition of fibroblasts to matrix remodeling simulations offers many benefits, fibroblasts are of course not the only cell type contributing to changes in cardiac matrix structure, and several groups have included a variety of other cells in efforts to more faithfully capture

important cell-cell interactions. For example, Neagu and colleagues developed a lattice-based ABM of endothelial-mesenchymal transformation (EMT) during cardiac morphogenesis based on the interactions of endothelial cells, mesenchymal cells, and local matrix (Neagu et al. 2010). Each component interacts with neighboring components by cohesion and adhesion, and migration. Proliferation, or EMT occur according to a decision-tree of component interactions and remodeling probabilities. With the assumed behavior rules and cohesion/adhesion interaction parameters, simulations predicted not just the occurrence of EMT but also the morphological formation of cushion tissue. Additionally, simulations predicted that cell-matrix adhesion is more critical than cell-cell adhesion for promoting EMT – a finding with potential therapeutic implications.

Jin and colleagues also investigated the role of interacting cell types as well as fibrosis-related cytokines by developing an ODE model of fibroblast, macrophage, collagen, TGF β , and MMP9 mass action kinetics in post-infarction myocardium (Jin et al. 2011). The basic interactions included the following: macrophages secrete TGF β and MMP9, TGF β stimulates fibroblasts to secrete collagen, TGF β stimulates macrophage infiltration, TGF β inhibits MMP9, and MMP9 degrades collagen. Interaction parameters were set to experimentally-estimated values, and myocardial remodeling was simulated for 30 days, which correctly predicted biphasic macrophage, TGF β , and MMP levels, and monotonically increasing fibroblast and collagen levels. Perhaps surprisingly, simulating reduced TGF β actually raised collagen levels while elevated TGF β reduced collagen levels. This finding was due to TGF β -induced macrophage infiltration leading to 1) high MMP9 levels and collagen degradation, and 2) lower early fibroblast levels because of macrophage crowding. Experimentally, there is in fact evidence that elevating TGF β delays wound healing after cardiac injury (Nakajima 2000).

Galvao and colleagues have developed 2D and 3D ABMs of Chaga's cardiomyopathy by including not just fibroblasts and fibrosis but also the *Trypanosoma cruzi* parasites, inflammatory cells, cardiomyocytes, bone marrow stem cells (BMSC), and tumor necrosis factor- α (Galvão, Miranda, and Ribeiro-dos-Santos 2008; Galvão and Miranda 2010). In their lattice-based simulations, each grid location is designated as one of these component types or left empty, and successive time steps updates each location designation according to simple, experimentally-motivated rules based on which component types are nearby. For example, a cardiomyocyte location near a fibroblast will transition to a fibrotic location to simulate fibroblast deposition of matrix, or an empty location near a parasite will transition to a parasite to simulate *T. cruzi* replication. Using just a handful of these transition rules was sufficient for the model to reproduce experimentally-observed, biphasic temporal dynamics of fibrotic area, inflammatory cell fraction, and parasite nest numbers over 7 months of disease progression in infected mice, and subsequent 6 months of BMSC injection therapy (M. B. Soares et al. 2001; M. B. P. Soares et al. 2004). The simulations also found that the spatial pattern of fibrosis was the most critical determinant of the kinetics of BMSC-induced regeneration in the Chagastic heart and should therefore be an important therapeutic consideration.

The above studies highlight the utility of computational approaches to investigate cardiac fibroblast behavior and matrix remodeling in a variety conditions, and it is clear that modeling approaches can range in system complexity by including not just matrix but also fibroblasts, not just fibroblasts but also other cell types, and not just cell types but also specific signaling molecules. Additional levels of complexity, while requiring more experimental data for model generation and validation, offer new layers of therapeutic relevance by enabling simulations to both elucidate mechanisms and screen novel treatment approaches. Not surprisingly, similar

modeling frameworks have been applied to fibroblasts and fibrosis in non-cardiac tissues as well including pulmonary fibrosis (Brown et al. 2011), cystic fibrosis (Voit 2014), liver fibrosis (Dutta-Moscato et al. 2014), and kidney fibrosis (Hao, Rovin, and Friedman 2014).

1.5 Signaling Networks and Fibroblast Phenotype

Fibroblasts are a plastic cell type – able to respond to chemical, mechanical, and electrical cues with large alterations in cell behavior. For example, fibroblasts break down the extracellular matrix by producing MMPs in response to inflammatory cytokines. However, growth factors prompt fibroblasts to increase their expression of collagens and fibronectin, leading to tissue-level fibrosis. Fibroblasts migrate in response to inflammatory cues in order to infiltrate an infarct. Phenotypic alterations also occur such as endothelial to mesenchymal transitions, which increase the number of fibroblasts or differentiation into the contractile, pro-fibrotic myofibroblast phenotype. Ultimately, these changes lead to tissue-level remodeling and altered electrical conduction as described above. To our knowledge, there are no published models of cardiac fibroblast-specific signaling. However, such models are useful for investigating how external cues are translated into changes in cell behavior and for predicting which signaling players are necessary for a specific cellular response. Here we review models of fundamental signaling pathways, migration, and phenotype switching in non-cardiac fibroblasts as they are likely useful for understanding cardiac fibroblast physiology.

Several kinetic models based on data in other cell types have been built of signaling pathways that are relevant to fibroblast physiology. For example, a large-scale model of epidermal growth factor (EGF) signaling with 94 different signaling isoforms was used to

examine how EGF receptor dynamics affect MAPK activation in HeLa cells. This model predicted that increasing the concentration of EGF or the EGF receptor was translated in the signaling network as an increase in the rate or duration of ERK activation rather than an increase in peak ERK activation (Schoeberl et al. 2002). Extracellular signaling models have also been developed such as Vempati et al.'s model of a network of 17 MMPs and TIMPs that predicted active MMP9 can deactivate other active MMP9 molecules (Vempati, Karagiannis, and Popel 2007). Previously it had been assumed that only TIMPs deactivated MMP9, but that mechanism was insufficient to quantitatively explain the experimental dynamics of MMP9 activity. Both of these studies point to the benefit of large-scale models of signaling networks as a method for hypothesizing key determinants of phenotypes.

Models of Signaling Networks Regulating Migration

Migration is important for recruitment of fibroblasts into the cardiac tissue. Importantly, inhibiting migration of fibroblasts affects wound healing after an infarct (Shinde and Frangogiannis 2014). The Lauffenberger group used decision-tree modeling to investigate how EGF and fibronectin signaling integrate to affect cell migration speed. This data-driven modeling approach was based on a 3T3 lineage cell line expressing human EGF-receptor. The initial model was based on one time point and found that ERK phosphorylation level was sufficient to predict whether a fibroblast was moving slowly or not, but determining whether migration was at medium or high speed required information on MLC (myosin light chains), PKC (protein kinase C), and PLC (phospholipase C) phosphorylation levels (Hautaniemi et al. 2005). A later model from this group incorporated data from two time points. This model predicted a biphasic relationship between migration speed and MLC levels, so that at low levels of MLC, migration

speed is paradoxically increased. This new model also predicted ERK was necessary for medium or high-speed migration (Kharait et al. 2007).

Rangamani et al. built a stochastic cell-spreading model regulated by a curated kinetic model of integrin signaling based on data from MEFs (mouse embryonic fibroblasts) (Rangamani et al. 2011). This model was used to make predictions about mechanical determinants of migration kinetics. In this study, they concluded that initiation of migration depends on the signaling environment, but, once triggered, migration depends on membrane mechanics and is robust to changes in integrin-mediated signaling. These models demonstrate how *in silico* studies of signaling can provide potential mechanisms for how dynamic signals are translated into cell behavior.

Models of Signaling Networks Regulating Phenotype Switching

Cardiac injury triggers EMT and differentiation of fibroblasts into myofibroblasts to increase the number and activity of fibroblasts. Myofibroblasts express high levels of collagen and fibronectin as well as contractile proteins such as α SMA (alpha smooth muscle actin). Schroer et al. used a kinetic model based on experimental data from wild type and FAK^{-/-} (focal adhesion kinase knock out) MEFs to explore how TGF β , FGF(fibroblast growth factor), and integrin signaling pathways combine to influence expression of alpha smooth muscle actin. In this study they compared different mechanistic models and found that including a time-dependent negative regulation of ERK in the model was important for explaining the adaptive kinetics observed experimentally (Fig. 1.3). The model also predicted that FAK KO increases the sensitivity of α SMA to substrate stiffness (Schroer, Ryzhova, and Merryman 2014). This study highlights how

signaling network models can be used to test potential signaling interactions and identify likely mechanisms that can be validated experimentally.

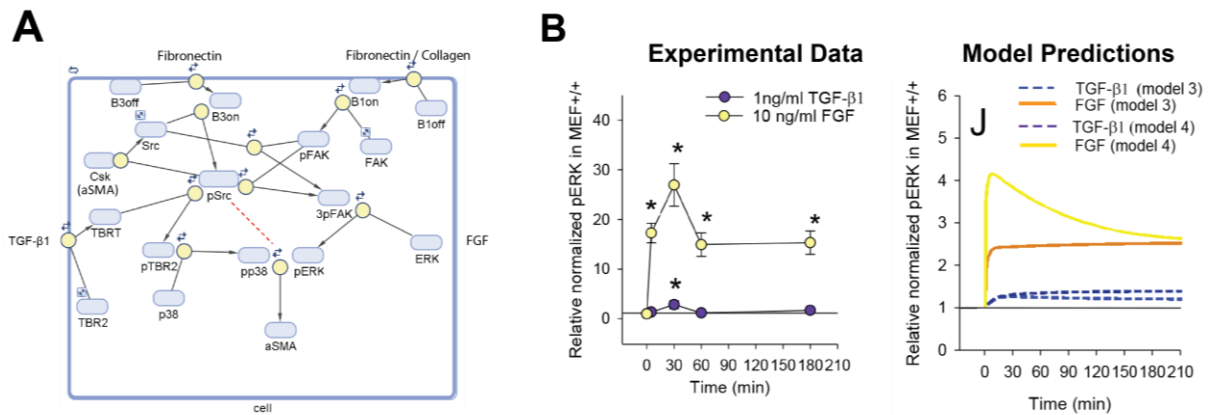


Figure 1.3: Fibroblast signaling network. (A) Schematic of signaling network incorporating integrin, TGF β , and FGF pathways. The red line indicates the time-dependent ERK regulation included in model 4. (B) Comparison of the experimental levels of ERK phosphorylation with TGF β or FGF treatment with the model prediction that demonstrates that including ERK regulation improved the model prediction. Figures adapted with permission by Cellular and Molecular Bioengineering from Schroer et al 2014.

Similarly, data-driven models can be used to hypothesize how signaling is changing in different phenotypic contexts. Desai et al. used phosphorylation data from an airway epithelial cell line to build a mixed-effects model to study the signaling differences after epithelial-mesenchymal transition (EpMT) when the cells have become fibroblast-like. Epithelial-mesenchymal transition is analogous to the endothelial-mesenchymal transition that occurs in the heart during development or cardiac injury to increase the density of fibroblasts in the tissue (Zeisberg et al. 2007). Interestingly, they found that following EpMT there is a rewiring of the phosphorylation network (Desai et al. 2015). For example, they identified a novel loss of connection between IL6 and pSTAT3 and an increased correlation between pSMAD2 and

GSK3 α in cells that had undergone EpMT, which could be the basis for differential signaling in this phenotype.

Together these models indicate that context-specific signaling is important in determining phenotype. The role of the fibroblast in integrating mechanical, chemical, and electrical cues makes understanding context-dependent signaling important for identifying useful therapeutic targets against fibrosis. As there are significant differences between cardiac fibroblasts and other fibroblasts (Furtado et al. 2014) it would be important to apply a computational modeling approach to cardiac fibroblasts, specifically, to identify which key signaling components determine fibroblast behavior in the heart.

1.6 Future Directions

In this chapter, we have reviewed a wide variety of modeling approaches applied to exploring different aspects of cardiac fibroblast physiology. Different types of modeling are appropriate for answering different biological questions (see Table 1). While there are pros and cons to individual modeling approaches, in general models can be improved by incorporating more biological detail to increase relevance or by simplifying the model to improve computational efficiency and biological interpretation. Incorporating new data into computational models increases their predictive capability so that model interpretation can generate more plausible hypotheses. One way to incorporate data in an unbiased way is by developing models using high-throughput datasets as described in the next section. Additionally, model reduction approaches as described by Holland et al. can simplify highly detailed models without sacrificing predictive power, which can simplify interpretation of model predictions (Holland, Krainak, and Saucerman

2011). Here, we identify three major areas of significant potential for future computational models of cardiac fibroblasts: incorporation of high-throughput data, multi-scale modeling of tissue physiology, and a focus on using models to identify potential therapeutic targets.

Table 1.1: Summary of approaches used to model fibroblasts and fibrosis

Physiology	Model Type	Description	Model Size	Spatial Scale	Time Scale	References
Electrical	Ordinary Differential Equations (ODEs)	Based on conservation of charge and ion channel biophysics	~10-100 parameters; 2-10 ODEs	10 μm –1 cm	msec - minutes	[22–24,30,34,36,37]
	Finite Element Method (FEM)	Tissue modeled as continuum of elements, constrained by conservation of mass and charge.	~10 ⁶ elements	10 cm	msec - minutes	[38]
Remodeling	FEM	Tissue modeled as continuum of elements, constrained by conservation of mass and momentum	100-500 elements	10 μm –1 cm	hours - weeks	[55–57,88]
	Agent Based Model (ABM)	Treats cells as agents responding to a set of rules.	1-5 agents, 10-50 parameters	10 μm – 1 cm	hours -weeks	[10,58–62,69,71]
	ODEs	Predicts changes in cells and proteins over time.	15 parameters; 4 ODEs	1 cm	weeks	[70]
Signaling	ODEs	Predicts changes in proteins, constrained by mass-action kinetics	10-200 parameters; 4-100 ODEs	10 μm	seconds - hours	[78,79,83,84]
	Decision tree model	Predicts outcome based on a sequence of branching decisions	5 nodes	10 μm	NA	[81,82]
	Mixed-effects model	Statistical model calibrated to experimental data	13 parameters; one equation	10 μm	minutes	[86]

Inference from High-Throughput Data Sets

As high-throughput sequencing and proteomic methods become more common, integrating these datasets into computational models will be an important tool for understanding the functional consequences of the many simultaneous changes revealed by these data. There are available datasets of gene expression in cardiac fibroblasts and myofibroblasts [42,43], and there are algorithms for combining high-throughput datasets with some manual curation to increase biological relevance of the predicted hits [44,45]. Using gene expression data to generate predictive models allows an unbiased method for determining context-dependent effects on phenotype.

Proteomics datasets can also be used to infer networks, which can be adapted into predictive computational models. For example, statistical modeling has been applied to a proteomics dataset to generate hypotheses about crosstalk in coxsackievirus B3 infection in cardiomyocytes (Jensen et al. 2013). Kupfer et al. used the NetGenerator algorithm to infer an ODE signaling model of gene expression from synovial fibroblasts from rheumatoid arthritis patients^[47,48]. These types of approaches could be applied to cardiac fibroblasts in order to generate testable hypotheses linking gene expression to phenotype. Ultimately, this could lead to an understanding of the genetic predisposition for cardiac fibrosis and heart failure.

Multi-Scale Modeling

This review highlights the breadth of cardiac fibroblast-related computational studies extending across length scales from subcellular signaling, to local cell-cell and cell-matrix interactions, to tissue remodeling, and to organ level conduction properties. Of course, processes across these scales do not occur in isolation but operate as an interconnected system with every level passing

information to other levels. In fact, many phenomena emerge specifically out of these multi-scale interactions. For a more complete understanding of fibroblast functions within such a system, researchers are now developing multi-scale modeling frameworks. Such approaches have shown benefit in many contexts including morphogenesis, wound healing, blood flow, arterial growth and remodeling, bone mechanics, cardiac mechanics, and many others (Walpole, Papin, and Peirce 2013; Bajikar and Janes 2012; Fedosov, Noguchi, and Gompper 2014; Vermolen and Gefen 2013; Hayenga et al. 2013; Weinberg, Shahmirzadi, and Mofrad 2010; Hunter et al. 2006; Campbell and McCulloch 2011), but multi-scale models involving cardiac fibroblasts and fibrosis are still rare.

As described above, Rouillard and Holmes extended their multi-cell ABM of myocardial infarct growth and remodeling by coupling it with an FEM of infarct mechanics to iteratively update both local scar structures and tissue-level deformations (Rouillard and Holmes 2014). It is easy to imagine how to extend such a model to an even larger scale by replacing the prescribed tissue loading with a whole-ventricle FEM for computing new boundary loads. Additionally, the ABM framework is well-suited for extending to a smaller scale as well by replacing prescribed turnover rate constants with an intracellular signaling model to calculate collagen and MMP synthesis rates based on each cell's local chemical and/or mechanical signals. Such an approach could be useful for modeling other tissue-level behaviors as well. For example, a multi-scale model linking intracellular signaling to a tissue-level ABM could be useful for modeling fibroblast reprogramming to myocytes and the effect on tissue function (see review on reprogramming in this issue by Czubryt et al. (Czubryt MP, Safi HA 2016)). While multi-scale modeling brings computational challenges, it offers enormous potential for integrating biological processes within the context of a broader system to determine functional responses to diseases

and therapies.

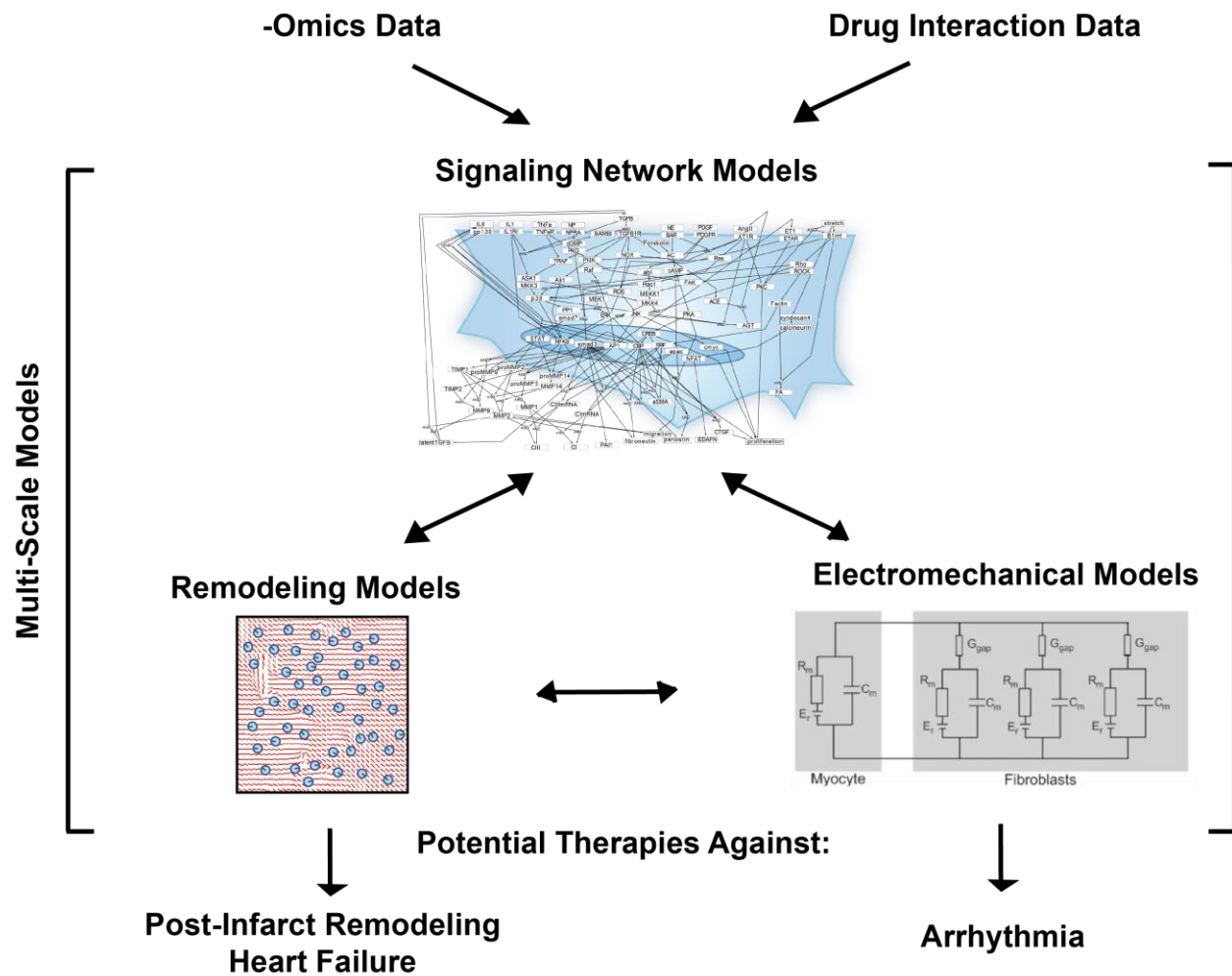


Figure 1.4: Summary of future directions. Currently used models of electrical conduction, cardiac tissue remodeling, and signaling networks could be integrated with –omics data and drug interaction data and combined into multi-scale models to identify potential therapeutics against heart disease.

Prioritizing Therapeutic Targets Against Fibrosis

Current heart failure therapies such as ACE inhibitors and aldosterone antagonists can affect cardiac fibrosis, and promising drugs such as nintedanib and pirfenidone have been approved to reverse lung fibrosis. However, it's unclear how these drugs limit fibrosis. Computational

models can help identify the mechanisms by which these drugs suppress fibrosis and can identify therapeutic strategies that could be more targeted and efficacious against cardiac fibrosis.

Computational models of cardiomyocyte signaling have successfully been used to predict which signaling nodes are most important for cardiomyocyte hypertrophy *in vitro* (Ryall et al. 2012, 2014) or how phenomena such as compartmentalization affect hypertrophy (J. H. Yang et al. 2014; Greenwald et al. 2014). Markov models are also useful for determining the effect of ion channel mutations on electrical conduction (Clancy and Rudy 2002). Integrating molecular level models into tissue level models can help clarify how mutations develop into tissue-level phenotype changes (Fig. 1.4). A well-designed model can save money by testing all potential therapeutic targets *in silico* and identifying the most likely hits. Pharmaceutical companies are already using modeling to direct research focus in an effort to increase the likelihood of success and lower costs (Visser et al. 2014). It is likely this approach will benefit academic research in the same manner.

1.7 Conclusions

This chapter reviews how computational models have been useful for clarifying the role of cardiac fibroblasts in electrical conduction and tissue remodeling in the heart. Although cardiac-specific models of fibroblast signaling had not yet been developed prior to this thesis, models of general fibroblast signaling have generated hypotheses about how fibroblasts integrate signaling cues. Future work will benefit from incorporating large -omics datasets into computational models. Multi-scale models allow researchers to explore how molecular- and cellular-level

changes affect tissue function. This can be useful for identifying potential therapeutic targets against cardiac fibrosis.

Chapter 2:

A computational model of cardiac fibroblast signaling predicts context-dependent drivers of myofibroblast differentiation.

Adapted from AC Zeigler, WJ Richardson, JW Holmes, JJ Saucerman “A computational model of cardiac fibroblast signaling predicts Context-Dependent Drivers of Myofibroblast Differentiation” *Journal of Molecular and Cellular Biology* Vol 94 pp 72-81 (2016), with permission from Elsevier

Author Contribution: A.C. Zeigler - developed computational model, performed all computational analysis, wrote paper, W.J. Richardson - performed experiments, assisted in writing the paper, J.W. Holmes - assisted in designing the model and experiments and in writing the paper, J.J. Saucerman - assisted in designing the model and experiments and in writing the paper.

2.1 Foreword

In chapter 1, I highlighted the previous efforts to develop computational models of cardiac fibroblasts. Importantly, prior to this study, there were no large-scale models of fibroblast signaling. Previous models focused on a single pathway or were not cell-type specific. In this chapter, I describe the development of a manually-curated fibroblast signaling network and its application in a logic-based ODE model. The model serves as a systems framework for predicting modulators of fibroblast phenotype in different signaling contexts (as we demonstrate in chapter 3 and 4).

2.2 Introduction

Cardiac fibroblasts play an important role in cardiac physiology by maintaining the extracellular matrix (ECM), linking with myocytes to participate in electrical propagation, and by actin as a sentinel cell mediating response to cardiac injury (Souders, Bowers, and Baudino 2009). These cells are critical to the heart's ability to adapt to mechanical, chemical, and electrical changes, and dysregulation of fibroblast activity leads to cardiac pathology. Increased fibrosis in the heart is associated with tissue dysfunction such as arrhythmias, diastolic failure, and systolic failure (Moreo et al. 2009; Wong et al. 2012). Moreover, increased ECM is an independent risk factor for the development of heart failure and is associated with a worse prognosis (Maschi et al. 2014). In a failing heart, a major source of ECM is the population of myofibroblasts – differentiated fibroblasts characterized by increased contractility (α SMA) and increased expression of collagens, fibronectin, and tissue inhibitors of matrix metalloproteinases

(TIMPs), which increase the stiffness of the extracellular matrix. Identifying key drivers of this fibrotic phenotype could be the key to understanding the pathogenesis of heart failure.

Cardiac fibroblasts experience competing cues from growth factors, inflammatory cytokines and mechanical signals, among others, and integrate these diverse signals to produce increases or decreases in matrix turnover. Therefore, appropriate therapeutic strategies to modulate cardiac fibrosis must function within the rich milieu of diverse signaling cues present in the diseased heart, and designing such therapies relies on understanding how cells integrate these signals (Angela C Zeigler et al. 2015). Large-scale computational models have been used to describe hypertrophic signaling in cardiac myocytes and have successfully identified signaling mechanisms and key regulatory hubs for cardiac hypertrophy (Ryall et al. 2012, 2014; J. H. Yang and Saucerman 2011).

In this study we developed a large-scale computational model of the cardiac fibroblast signaling network in order to identify context-dependent drivers of myofibroblast differentiation and extracellular matrix remodeling. The model integrates multiple signaling pathways in order to predict changes in gene expression and protein activity across different signaling contexts. The model identifies a context-dependent functional role for transforming growth factor β receptor (TGF β -R) and reactive oxygen species (ROS). Additionally, TGF β -R was found to be important for up-regulation of alpha smooth muscle actin (α SMA) under many signaling contexts. The model predicted that regulation of α SMA by TGF β -R is dependent on the level of mechanical stimulation, and this novel cross-talk mechanism was experimentally validated in rat cardiac fibroblasts.

2.3 Materials and Methods

Model Development

A cardiac fibroblast consensus signaling network was manually reconstructed from previous experimental studies from the literature. This network integrates 10 pathways with 11 mechanical or biochemical stimuli that are altered during cardiac injury or heart failure including: IL1 (interleukin 1), IL6 (interleukin 6), TNF α (tissue necrosis factor α), NE (norepinephrine), NP (natriuretic peptide), β -integrins, TGF β (tissue growth factor β), angiotensin II, PDGF (platelet derived growth factor), ET1 (endothelin 1), mechanical stimulation, and forskolin.

A review of the literature on cardiac fibroblast signaling was conducted, with a focus on the pathways described above. During literature review, studies were separated for use in validation (see Model Validation section below) if the cell type used was human or rat cardiac fibroblasts and the study investigated input (biochemical or mechanical stimulus) to pathway output (e.g. collagens, α SMA, cell migration, proliferation, and other ECM proteins) responses.

Alternatively, studies that focused on direct signaling mechanisms were used to identify interactions to define the structure of the signaling network. Initially, interactions were added based on direct experimental evidence in mammalian cardiac fibroblasts (112 reactions). Then, we performed gap filling of each pathway with intermediate reactions (20 reactions) between those that had support in cardiac fibroblasts if they were well-characterized in other cell types and there was evidence for the interaction in a fibroblast-related cell type. Each reaction in the network is supported by two independent studies, at least one of which was performed in

fibroblasts, with a majority of the reactions supported by data in cardiac fibroblasts. Extracellular interactions were included from cell-free measurements. The network includes 91 nodes (mRNA, proteins, and cell processes) connected by 142 reactions. Full documentation of the experimental evidence supporting each reaction is provided in Database S1.

The network reconstruction was converted into a predictive computational model using a previously described logic-based ordinary differential equation modeling approach used previously described (Ryall et al. 2012). Briefly, the activity of each node is modeled using a normalized Hill ODE with default parameters and logic gating. Default reaction parameters include weight (1), Hill coefficient (1.4), and EC50 (0.6), and species parameters include y_{init} (0), y_{max} (1), and τ . The τ parameter (time constant) was scaled according to the type of reaction: 6 minutes for signaling reactions, 1 hour for transcription reactions, and 10 hours for translation reactions. The system of ODEs was auto-generated from Database S1 using the Netflux software available at: <https://github.com/saucermanlab/Netflux> and implemented in MATLAB.

Model Validation

Literature for validating network input-output relationships (see Table S2) were identified by searching for each network input and output together with the phrase “cardiac fibroblast” in the Pubmed database. Other validation literature was identified while reviewing literature for the development of the network (see above). As a quality and reproducibility control, model validation used only studies that use rat or human cardiac fibroblasts and have at least two agreeing data points for that response (e.g., two methods of measurement, two dosages, two time points, or two independent studies). All supporting studies used in validation were independent

of those used to develop the model network. Validation was performed by comparing the qualitative increase, decrease, or no change in output activity of the model simulation to the experimental results. Changes of less than 0.1% were categorized as “no change”.

Sensitivity Analysis

A systematic functional analysis was performed by simulating full knockdown of each node and predicting the change in activity of every node in the network. First the steady-state activity of all nodes was computed under baseline conditions, serving as a control. Then, we knocked down the activity of each node one at a time and subtracted the basal activity levels from the activity in the knocked down case to calculate “ Δ Activity”. Influence is measured as the number of nodes with 25% change or greater in activity following knock out of the perturbed node, sensitivity is the number of nodes that will affect the target by a 25% change or greater when knocked out. The collagen sensitivity and α SMA sensitivity are defined as either the change in collagen I activity + change in collagen III activity or the change in α SMA activity respectively when the target node is knocked out. The topology of the fibroblast signaling network was analyzed using the NetworkAnalyzer plugin in Cytoscape (Shannon et al. 2003; Assenov et al. 2008). AND relationships were collapsed into their target node using MetaNodes plugin (developed by John Morris, University of California, San Francisco) and network analysis was performed on that topology. The correlation coefficient for matching topological to functional metrics was computed using the `fitlm` function in MATLAB.

Functional modules were identified using k-means clustering of the sensitivity analysis in the high TGF β context. Nodes were clustered based on both influence and sensitivity by

concatenating the sensitivity matrix with its transpose. Clustering was performed using MATLAB's kmeans function using the "correlation" distance measure. The clustering was performed 20 times with different initial centroid positions and nodes were grouped into the module that most frequently appeared. The number of clusters was set at 10 because that gave the highest inter-cluster vs intra-cluster distance without having clusters of single nodes.

Functional relationships between modules were derived from the high TGF β or high mechanical stimulus sensitivity analysis (described above) by summing the influence of all nodes in one module over all nodes in the second module. The line weights indicate the sum of influence of one module over another, with the shape of the target arrow indicating whether the overall relationship is positive or negative.

Cardiac Fibroblast Isolation

Adult rat cardiac fibroblasts were isolated and cultured as previously published (Thomopoulos, Fomovsky, and Holmes 2005). Briefly, Sprague-Dawley rats (6 weeks old, ~ 200g) were sacrificed and the ventricles removed, minced into ~1 mm pieces, and digested using Liberase Blendzyme 3 (Roche, Indianapolis, IN). Successive digestions were centrifuged for 10 min at 400x g and cells were resuspended into culture medium containing Dulbecco's modified Eagle medium (Sigma-Aldrich, St. Louis, MO) with 10% fetal bovine serum (FBS, Atlanta Biologicals, Flowery Branch, GA), 100 U/mL penicillin, 100 g/mL streptomycin, and 2 ng/mL amphotericin B (all Sigma-Aldrich). After incubating in culture flasks for 4 hrs at 37 C and 5% CO₂, flasks were rinsed with phosphate-buffered saline (PBS, Sigma-Aldrich) to remove nonadherent cells, and resupplied with culture medium.

After 7 d of culture, fibroblasts were removed from flasks with 0.25% Trypsin-EDTA (Sigma-Aldrich), and seeded into 3D collagen gels as previously published (Thomopoulos, Fomovsky, and Holmes 2005). Briefly, 0.2 M HEPES (Sigma-Aldrich), 10X MEM (Sigma-Aldrich), 3 mg/mL type I bovine collagen (PureCol, Advanced Biomatrix, San Diego, CA) and cells resuspended in low-serum culture medium (1% FBS) at respective ratios of 1:1:8:2 to yield a final collagen concentration of 2 mg/mL and final cell concentrations of 200k cells/mL (for restrained gel conditions) or 133k cells/mL (for floating gel conditions). The cell+collagen gel mixtures were rotated in an incubator for 5 min, then pipetted into 24-well plates (1mL in each well).

In order to apply a high mechanical stimulus cells were seeded into a collagen gel restrained at the boundary, and compared to a free-floating gel (low mechanical stimulus). Restrained gels were poured into non-treated wells and remained adhered to the well bottom and sides; floating gels were poured into wells pre-coated with bovine serum albumin (BSA, Sigma-Aldrich) by incubation in 2% BSA for 1 hr. After 4 hrs of incubation, the floating gels were released from the bottom of the wells with the addition of low-serum culture medium (1% FBS). All gels were then incubated for 2 d in low-serum medium. After 2 d, gels were cultured for an additional 2 d in one of three chemical conditions: low-serum culture medium control, TGF β -inhibitor treatment (30nM of SD208, Sigma-Aldrich), or TGF β treatment (100 ng/mL of human TGF β 1, Cell Signaling Technology, Danvers, MA).

Gel Compaction Measurements

Starting immediately after floating the gels, pictures of the floating gels were taken every 24 hrs with a handheld digital camera. Gel outlines were manually traced using ImageJ (Schneider, Rasband, and Eliceiri 2012), and relative gel compaction was assessed as the ratio of the area of each gel at a given time point to the initial area of that gel.

Microscopy and Image Analysis

After a total of 4 days of culture, gels were fixed overnight in 4% paraformaldehyde (Sigma-Aldrich), and washed 3x with PBS; cells were then permeabilized in 0.05% TritonX (Sigma-Aldrich) in 1% BSA overnight, stained with monoclonal anti- α smooth muscle actin (Sigma-Aldrich) overnight, washed 3x with PBS, stained with 4',6-diamidino-2-phenylindole, dihydrochloride (DAPI, Life Technologies, Carlsbad, CA), and washed again 3x with PBS. PBS was removed and gels were imaged on an Olympus IX81 inverted microscope with a 10x UPlanSApo 0.40 NA objective (Olympus, Center Valley, PA) and a C9300 cooled CCD digital camera (Hamamatsu, Bridgewater, NJ). An 800 μm x 600 μm area in the central region of every gel was scanned, capturing at least 100 cells per gel.

To quantify α SMA expression, an automated image analysis pipeline was employed in CellProfiler (Broad Institute) (Carpenter et al. 2006; Kametsky et al. 2011). Fibroblast nuclei were identified by DAPI signal, and fibroblast boundaries corresponding to each nuclei were segmented based on the α SMA signal using the “propagate” algorithm. α SMA signal was integrated within each cell's boundary, and then averaged across all cells in a given gel as a measure of average α SMA expression per cell for that particular gel condition.

Statistics

Fibroblasts were isolated from 7 different rats, each isolation was divided into 18-24 gels, and gels were divided into six experimental groups for a total of 3-4 gels per group per rat (150 gels total, 25 gels per experimental group). α SMA was averaged across the gels within each group and rat, yielding N=7 replicates (one for each rat isolation) across the six experimental conditions. We performed a two-way ANOVA on floating-baseline, floating-SD208, restrained-baseline, and restrained-SD208 groups with post-hoc Bonferroni tests comparing floating-baseline to restrained-baseline, and comparing restrained-baseline to restrained-SD. For the gel compaction assay, we performed a Student's t-test between floating-control vs. floating-SD208 and between floating-control vs. floating-TGF β groups with Bonferroni adjustments. Statistical significance was set at $p < 0.05$.

2.4 Results

2.4.1 A predictive computational model of cardiac fibroblast signaling

A cardiac fibroblast consensus signaling network was manually reconstructed from previous experimental studies from the literature. Literature papers on cardiac fibroblast signaling were placed into distinct “model development” and “model validation” groups, depending on whether that paper described direct molecular interactions (e.g. smad3 binds to the collagen I promoter) or network input-output relationships (e.g. TGF β induces collagen I protein expression in cardiac fibroblasts), respectively. The 177 papers in the “model development” literature group were used to define the structure of the cardiac fibroblast signaling network (Table A.1), while the 41

papers in the “model validation” literature group were used to validate model predictions of network function (Table A.2). The detailed procedure for literature review and network reconstruction is provided in Methods.

This cardiac fibroblast signaling network (Fig 1) integrates ten signaling pathways previously shown to regulate cardiac fibroblast phenotypes and are up- or down-regulated during cardiac injury or heart failure. The network includes 91 nodes (mRNA, proteins, and cell processes) connected by 142 reactions. Full documentation of the experimental evidence supporting each reaction is provided in Database S1.

The network reconstruction was then converted into a predictive computational model using a logic-based ordinary differential equation (ODE) approach that we described previously (Kraeutler, Soltis, and Saucerman 2010; Ryall et al. 2012). Briefly, the normalized activity of each node is modeled using ordinary differential equations, with reactions modeled using saturating Hill functions and continuous OR/AND logic gates. As in previous network models (Kraeutler, Soltis, and Saucerman 2010; Ryall et al. 2012), uniform default parameters were used, except that time constants (τ) were scaled to an order of magnitude appropriate for the type of molecule (mRNA, protein, process; see Methods). The baseline condition was defined as 25% signaling activity for all inputs, which represents fibroblasts cultured on a stiff substrate with ligands at basal constitutive levels. Given any combination of the 11 signaling inputs, the model can simulate the dynamic changes in activity for every node in the network.

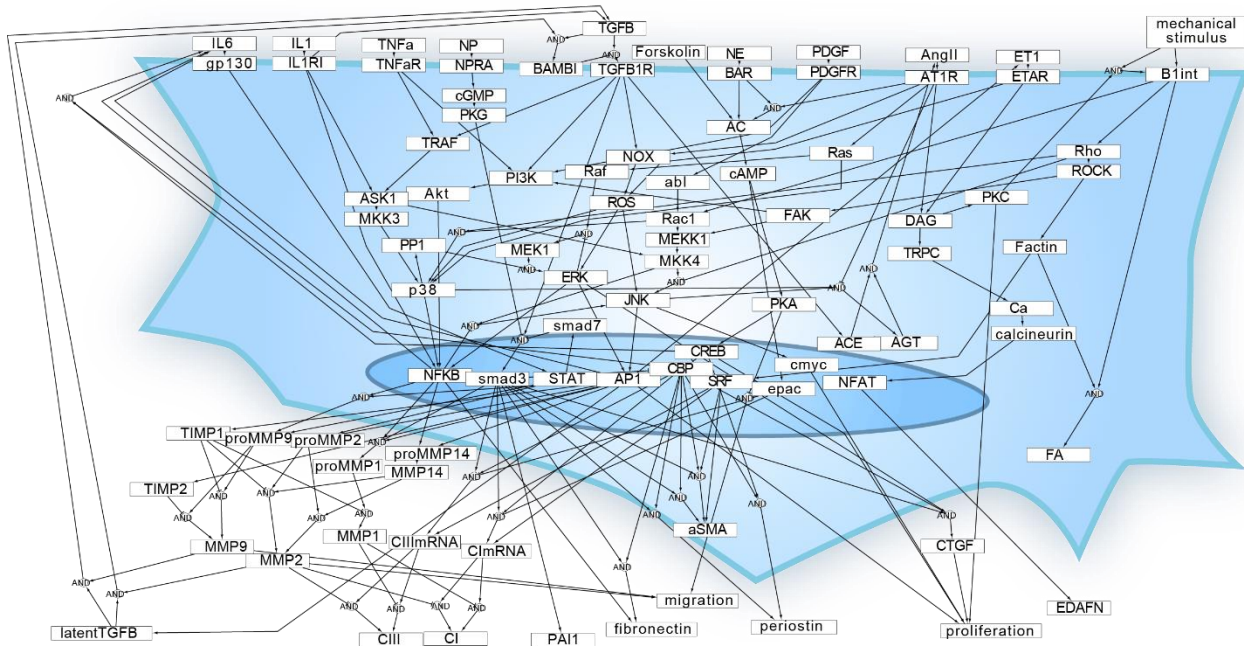


Fig. 2.1: Reconstruction of the cardiac fibroblast signaling network.

Each of the 91 nodes represents a gene product, modification of a gene product, or cell process in the model. Each arrow indicates a reaction based on experimental data of activation or inhibition from cardiac fibroblasts or a fibroblast-related cell line (142 reactions from 177 papers). Where shown, some reactions combine the influence of multiple reactants via AND gate logic. Multiple reactions affecting the same product are combined using OR gate logic.

Next, we predicted responses of the fibroblast signaling network to specific stimuli. These predictions were validated against experimental studies performed in rat or human cardiac fibroblasts that were independent from those studies used to reconstruct the signaling network. For example, the effect of a 4-day TGF β stimulus followed by a 2-day TGF β + forskolin stimulus was simulated and compared to experimental data from Lu et al (Lu et al. 2013) (Fig. 2.2A, with full simulation in Fig. A.1). The model predicted that the addition of TGF β initially increases collagen I mRNA, but forskolin treatment during the last two days partially reverses this increase. This prediction is qualitatively consistent with published data from rat cardiac fibroblasts showing that forskolin attenuates TGF β -dependent expression of collagen I (Lu et al. 2013) (Fig. 2.2B).

Overall, the model was validated against 82 input-output relationships from 34 papers (see Methods) and accurately predicts 66 of those 82 (80%). Fig. 2.3 summarizes the predicted relationship of each individual input stimulus to the outputs collagen I, collagen III, α SMA, and the MMPs (matrix metalloproteinases) and the agreement between model predictions and experimental data where available (40 relationships). Validations for the other 42 input-output relationships are shown in Fig. A.2, with complete annotation in Database S2. The validation accuracy was robust to a $\pm 50\%$ change in the baseline input levels as shown in Fig. A.3.

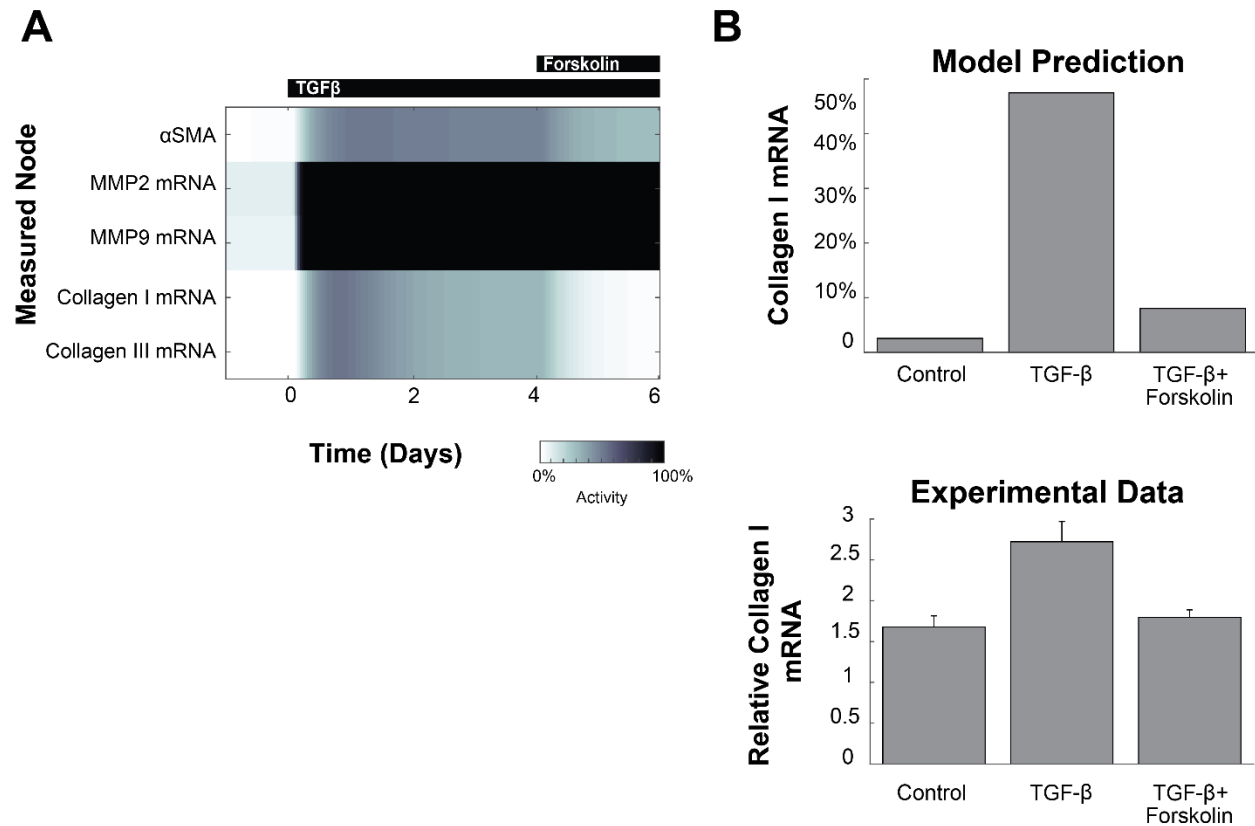


Fig. 2.2: Example of model validation with combined stimuli.

(A) Predicted dynamics of selected outputs in response to TGF β , followed by a combined TGF β + forskolin stimulus. Full dynamic prediction shown in Fig. S1 (B) The model prediction is compared to independent experimental data from Lu et al 2013 (Lu et al. 2013), showing the attenuation of collagen I mRNA by forskolin treatment. The model prediction is expressed as percent of maximal mRNA level. Experimental collagen mRNA is relative to the initial measurement at day 0.

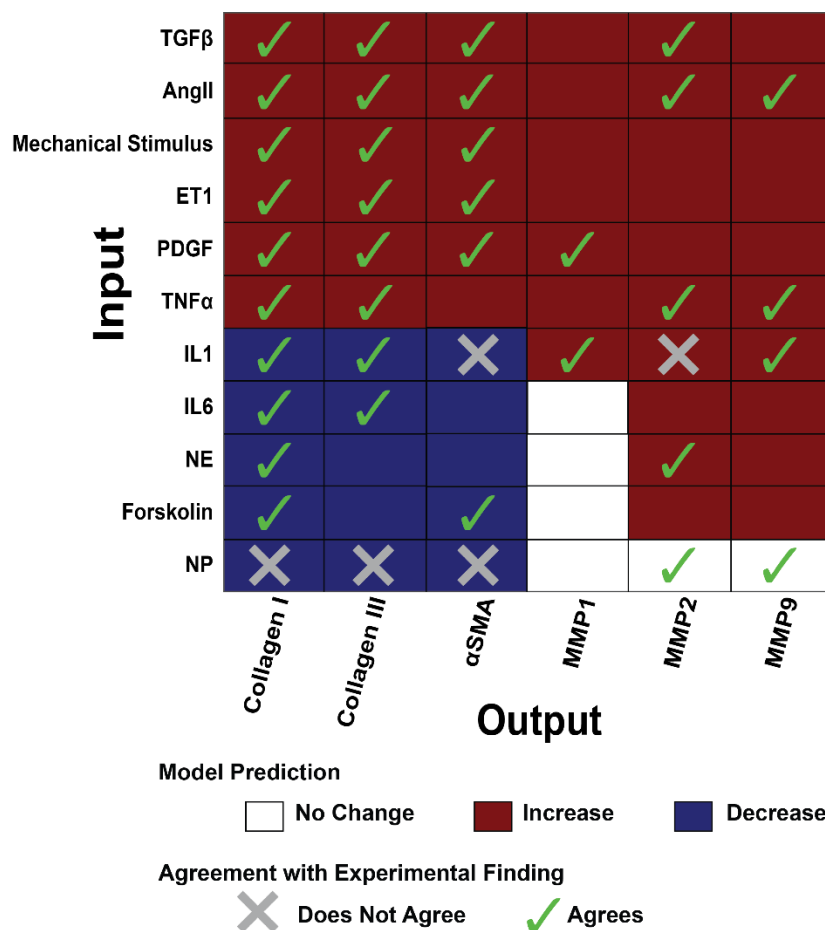


Fig. 2.3: Validation of network input-output relationships predicted by the model.

The qualitative response of selected fibrosis-related outputs is shown in response to each of 11 input stimuli. Agreement or disagreement with independent experimental data when available from the literature is indicated as a check or an X, respectively. *The model validates 35 of the 40 (88%) predictions shown in this Figure that have experimental data. Overall, the model validates 66 of 82 comparisons (80%), as shown in Figure S2 and Database S2.*

2.4.2 Context-Dependent Roles of Cardiac Fibroblast Signaling Drivers

Sensitivity analysis is one way to systematically characterize the functional roles of nodes in a signaling network. We first performed sensitivity analysis under baseline conditions (all inputs at 25%) by simulating complete knockdown of each node in the fibroblast network and quantifying the change in activity of all network nodes in response to each knockdown (Fig. S4). From this analysis, we identified the most influential nodes as those whose knockdown produced the greatest summed magnitude of change in the phenotypic outputs of the network. Fig 4A shows how knockdown of these 10 most influential nodes affected the outputs under baseline conditions. For example, knockdown of interleukin 6 (IL6) was predicted to strongly suppress expression of pro-MMP14 and pro-MMP2, consistent with Dawn et al and Luckett et al (Dawn et al. 2004; Luckett and Gallucci 2007).

As TGF β is a well-studied growth factor that is elevated following myocardial infarction (Swaney et al. 2005; Lu et al. 2013), we repeated the sensitivity analysis in a high TGF β context (TGF β input weight set to 90%, all other inputs at 25%) (Fig. A.4b). The role of influential nodes on phenotypic outputs differed substantially between the baseline and high TGF β contexts (Fig. 2.4a and b). For example, in the baseline condition proMMP2 and proMMP9 are sensitive to knockdown of IL6 pathway members. However in the high TGF β context, IL6 pathway members were predicted to regulate proMMP1 but proMMP2 or proMMP9. We also identified key regulators of the overall network. While knockdown of TGF β receptor (TGF β R) and ROS had broad network effects in both baseline and high TGF β conditions (Fig. S4), their influence on specific network nodes was highly context-dependent (Fig. 4C). For example, ROS knockdown decreased MMP9 expression under baseline conditions but increased MMP9 activity in the high TGF β context.

To more fully profile the context-dependent influence of the TGF β receptor and identify cross-talks between pathways, TGF β R knockdown was simulated in all 12 possible single-stimulus signaling contexts (90% activity of each stimulus, 25% activity of all other inputs). The network response to TGF β R knockdown varied considerably across the 12 signaling contexts (Fig. 2.4D). In particular, knockdown of TGF β R decreased expression of collagen I, collagen III, and α SMA in all single-stimulus contexts, but to different magnitudes in each context. TGF β R knockdown caused increases in periostin expression in the high NE or high forskolin signaling contexts but decreased expression in the 10 other contexts. Together, these analyses highlight the ability of the model to make predictions about how the influence of regulatory nodes in a signaling network vary as a function of the cell's environment.

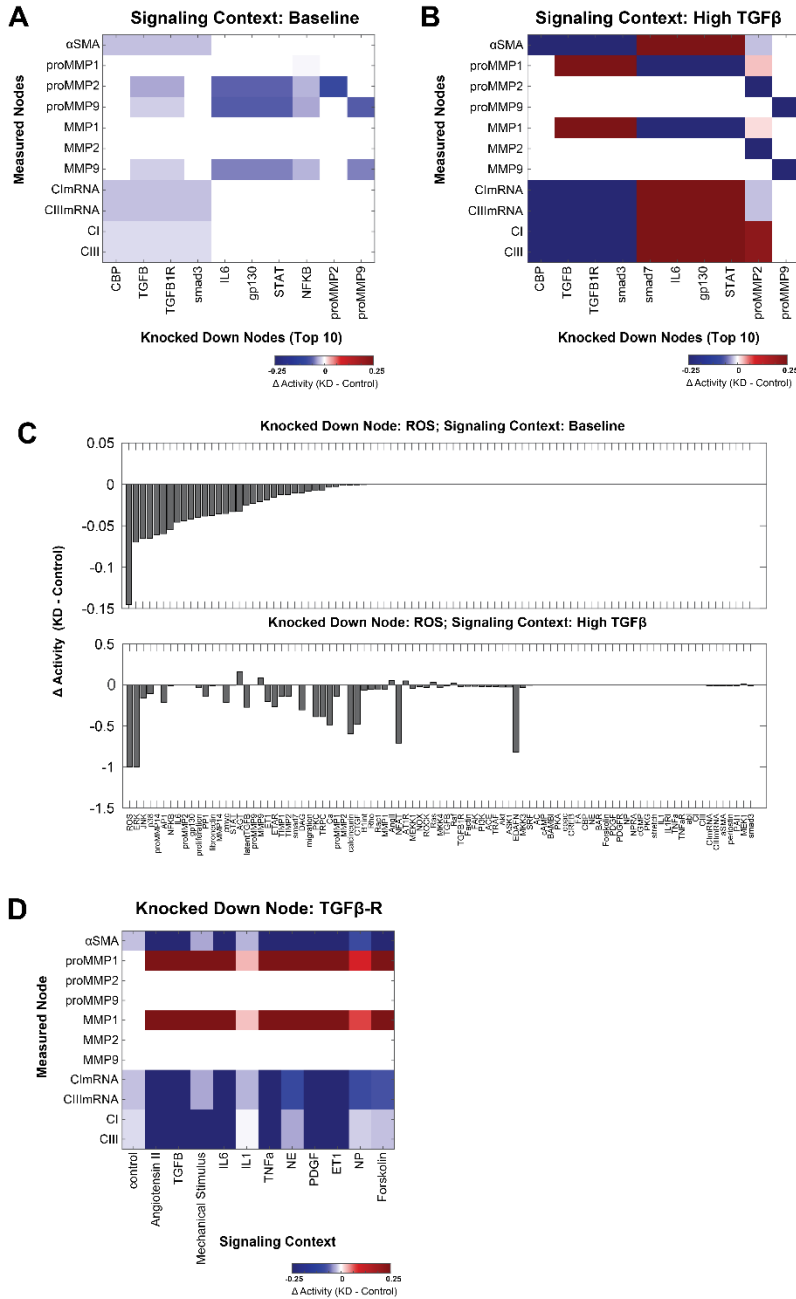


Fig. 2.4: Sensitivity analysis reveals context-dependent functional roles for regulators of cardiac fibroblast signaling.

Systematic knockdown (KD) simulations (see Fig. A.2) revealed that the top 10 most influential differed considerably between (A) baseline and (B) high TGFβ signaling contexts. At baseline all inputs are set to 25%, while for high TGFβ that input is further increased to 90% (see Methods).

(C) The response of network nodes to ROS knockdown differs substantially between baseline and high TGF β contexts. Nodes are rank-ordered by change in activity in the baseline context (note the difference in y-axis scales in upper and lower panels). (D) The effect of TGF β -R KD on fibrosis-related model outputs varies across baseline and all 11 single-input contexts.

Signaling nodes that have similar function within a network are often thought to form modules which maintain biological robustness and allow for signaling flexibility (Hartwell et al. 1999). Identification of network modules would allow for development of a hierarchical understanding of network function. To predict functional modules in the cardiac fibroblast network, we initially clustered network nodes based on both influence and sensitivity in the baseline signaling context (from Fig. A.4a) using k-means clustering. However, we found that clustering using sensitivity analysis from baseline conditions was highly variable due to many signaling nodes having relatively low influence or sensitivity. Therefore, we clustered nodes into functional modules based on both influence and sensitivity in the high TGF β context (Table 2.1 and Fig. A.5) and computed the strength of functional relationships between modules by summing the influence all nodes in one module had over another, as shown in Fig. 2.5a.

Because relationships between modules can vary depending on the signaling context (Hartwell et al. 1999), we also computed the relationships between functional modules in a high mechanical stimulus context that mimics the mechanical environment during myocardial infarction or volume overload. Fig. 2.5 compares the relationships between functional modules in the high TGF β and high mechanical stimulus contexts. This analysis indicated that in conditions of high TGF β , the TGF β module promotes and the cytokine module strongly inhibits activation of the fibrosis module, which contains network outputs such as expression of collagen

I, collagen III, and α SMA. Intriguingly, the autocrine module became more influential in the high mechanical stimulus context, predicting an important role for autocrine signals that amplify the fibrotic response to integrin stimulation.

Module	Members
PDGF	PDGF, PDGFR, TNF α , TNF α R, p38, PP1, JNK, abl, cmyc
Autocrine	ROS, ET1, ETAR, DAG, TRPC, latentTGF β , Ca, calcineurin, NFAT, ERK, EDAFN, AP1, TIMP1, TIMP2
Migration	Migration, proMMP14, proMMP2, MMP2, MMP14
Natriuretic	NP, NPRA, cGMP, PKG, proliferation
Cytokine	smad7, BAMBI, IL6, gp130, STAT, IL1, IL1RI, NF κ B, proMMP1, MMP1, fibronectin
Mechanical	PKC, mechanical stimulus, β 1int, Rho, ROCK, Rac1, MEKK1, FAK, Factin, FA, SRF
TGF β	ACE, NOX, TGF β , TGF β -R, PI3K, Akt, TRAF, ASK1, MKK3, MKK4
Angiotensin	AngII, AT1R, AGT, Ras, Raf, MEK1, proMMP9, MMP9
Beta Adrenergic	NE, BAR, forskolin, AC, cAMP, PKA, CREB, epac
Fibrosis	CBP, smad3, CTGF, α SMA, PAI1, periostin, CImRNA, CIII mRNA, CI, CIII

Table 2.1: Model-predicted functional modules

The members of each functional module identified using k-means clustering of the high TGF β sensitivity analysis.

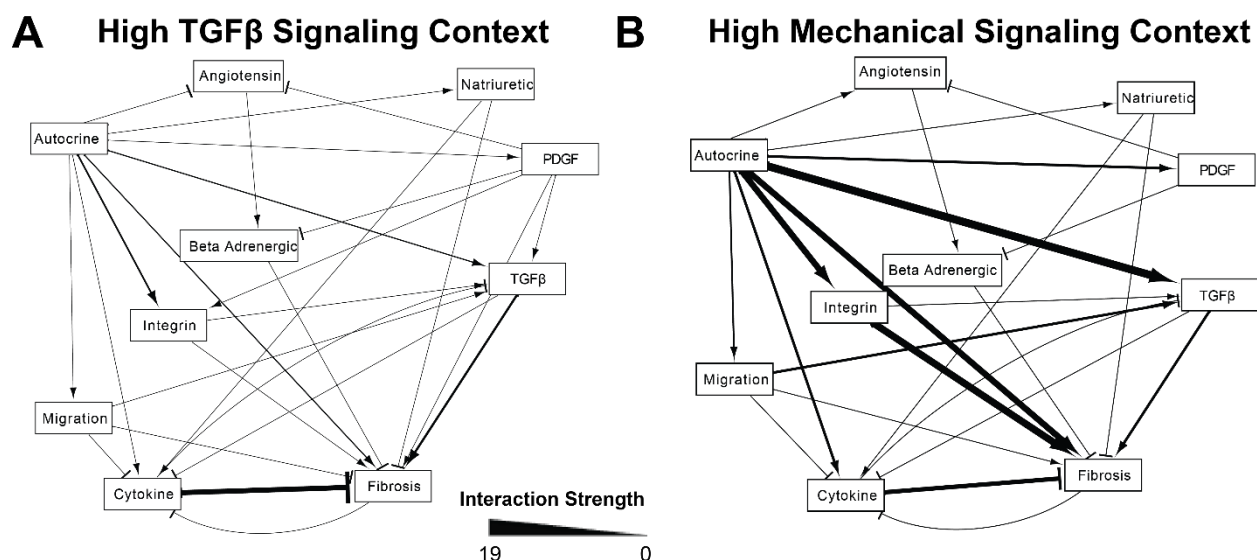


Fig. 2.5: Relationships between functional modules are context-dependent.

Relationships between functional modules (from Table 2) were quantified by the sum of influence of the members of one module over another in the specified signaling context. A) In the high TGF β context, the fibrosis module was positively regulated by the TGF β module and negatively regulated by the cytokine module. B) In the high mechanical signaling context, the autocrine module became a prominent regulator of the mechanical and fibrosis modules.

2.4.3 Relationship Between Network Structure and Function

While the above analyses used model simulations to predict function of nodes in the fibroblast signaling network, an alternative approach is to estimate function based on metrics of network topology (Albert 2007). Highly connected nodes, as determined by the topology metrics defined in Table 2, are generally expected to be more influential in a network (Albert 2005; Yu et

al. 2007). For example the fibroblast network contains 5 network hubs, defined as nodes with 8+ edges: AP1, smad3, NFκB, CBP, and p38. Topological analysis has been most often applied to large-scale biological networks where a predictive computational model is not available (Pržulj 2011; Albert 2005). However, the availability of this large-scale predictive signaling model provides a unique opportunity to examine the relationships between signaling network structure and function.

Accordingly, we examined the relationship between metrics of network structure and function as predicted by sensitivity analysis of the model under baseline conditions (from Fig. A.2). These functional metrics were: 1) influence, the number of nodes with an activity change of greater than 25% with knockdown of node n ; 2) sensitivity, the number of nodes that change the activity of node n by more than 25% when knocked down; 3) collagen sensitivity, the sum of the absolute value of the change in collagen I and collagen III with knockdown of node n ; and 4) α SMA sensitivity, the absolute value of the change in α SMA with knockdown of node n .

Betweenness centrality, defined as the number of shortest paths from all nodes to all other nodes that pass through node n , is one topological measure of connectivity. As shown in the comparison of betweenness centrality with influence (see Fig. 2.6a), a few nodes such as the TGFβR had both high topological and functional scores. Yet betweenness centrality was a poor predictor of influence for other nodes such as angiotensin II (underestimating influence) and smad3 (overestimating influence), with only moderate correlation overall ($r = 0.64$). A similar analysis was performed for all 10 topological metrics compared to influence (Fig. A.6), sensitivity, collagen sensitivity, and α SMA sensitivity (Fig. 2.6b). Overall, functional features were not strongly correlated with topological features, indicating the additional need for predictive signaling models as developed here. Betweenness centrality was the most useful

topological metric for predicting overall network influence, while measures of degree (in-degree, out-degree, and edge count, see Table A.1) were the most useful for predicting influence over the phenotypic outputs collagen and α SMA.

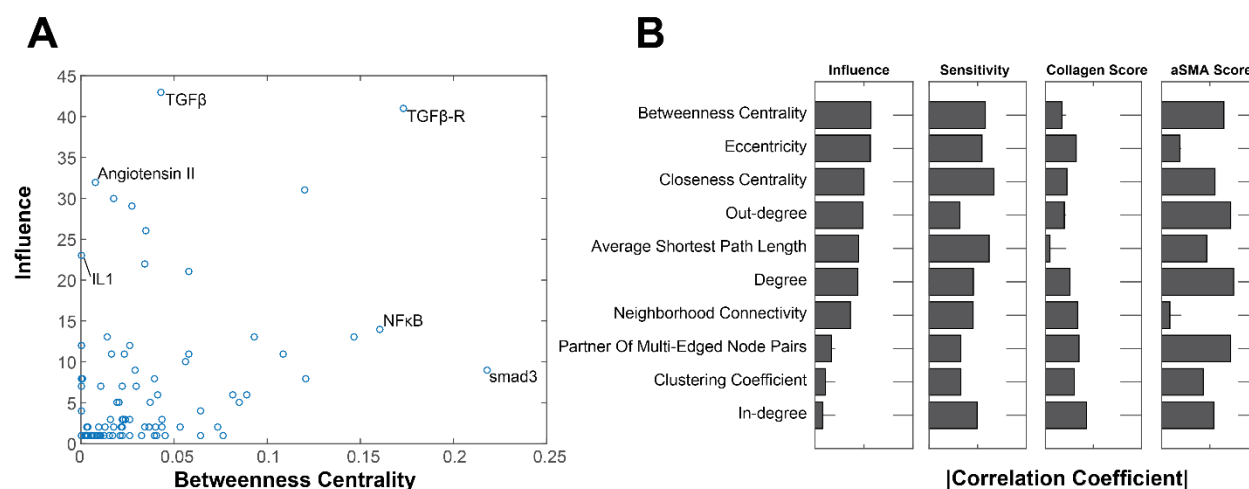


Fig. 2.6: Metrics of network topology are insufficient to predict network functions.

(A) Scatter plot showing the relationship of betweenness centrality (a metric of network topology) vs influence (predicted by the model). Influence is calculated by summing the absolute value of the changes in activity with knockdown of the target node. Several nodes of interest have been labeled. (B) The correlation coefficient for each topological feature vs 4 functional features. Sensitivity is the absolute value of the change in activity of the target node for all possible knockdowns. Collagen sensitivity and α SMA sensitivity are the change in collagen or α SMA respectively with knockdown of the target node.

2.4.4 Cross-Talk Between Mechanical and TGF β Pathways

The sensitivity and clustering analyses described above suggested substantial crosstalk between the mechanical stimulus pathway and the TGF β pathway. Simulated knockdown of the TGF β receptor lowered expression of α SMA, collagen I, and collagen III in conditions of high mechanical stimulus (Fig. 2.4d). Furthermore, at a more course-grained level, the TGF β module was an important regulator of the fibrosis module (which contains important output genes such as collagen I, collagen III, and α SMA) in conditions of both high TGF β and mechanical stimulus (Fig. 2.5). This led us to further investigate the potential role for TGF β in integrin-mediated differentiation of fibroblasts to myofibroblasts. The model predicted that inhibition of the TGF β receptor would have little effect on α SMA expression in baseline conditions but would attenuate mechanical-induced α SMA expression (Fig. 2.7a). To experimentally validate this prediction, we cultured rat cardiac fibroblasts in floating and mechanically restrained collagen gels, with and without a TGF β receptor inhibitor, SD-208 (see Methods). The restraint boundary condition provides mechanical resistance to intrinsic cell contractile forces, enabling cells to produce higher contractile tension and higher corresponding reaction tension in the gel(John et al. 2010). This restraint has been shown to activate integrin pathways(Rosenfeldt 2000). TGF β was used as a positive control. As shown in Fig. 2.7b-c, fibroblasts in the restrained gels had significantly increased α SMA expression, but SD-208 significantly attenuated the expression of α SMA in the restrained gels. Inhibition of the TGF β receptor in the floating gels did not significantly reduce α SMA expression. Further, the expression of α SMA in floating gels strongly correlated with the degree of gel compaction, a functional measure of cardiac fibroblast contraction (Fig. 2.7d-e).

Together, these experiments semi-quantitatively validate the model prediction that the TGF β receptor is an important regulator of mechanical-mediated myofibroblast differentiation.

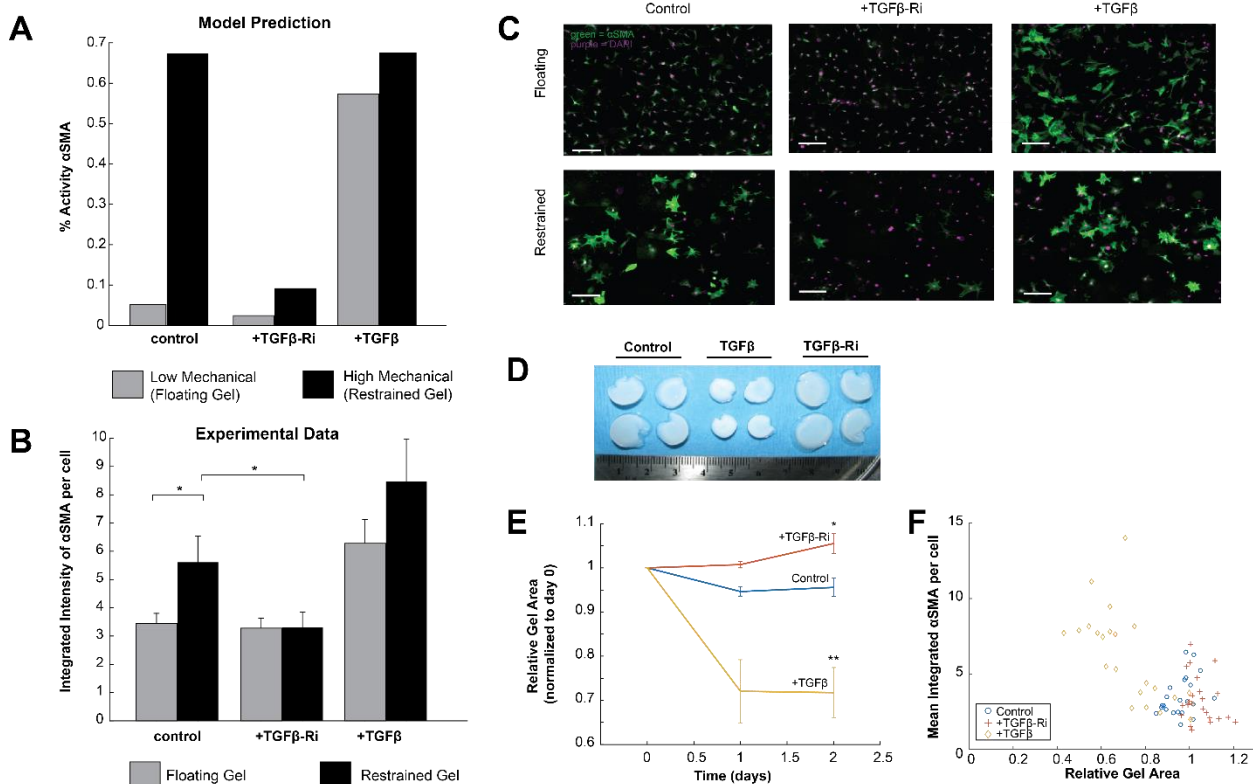


Fig. 2.7: Experimental validation of predicted role for TGF β in mechanical-induced expression of α SMA.

(A) The model predicted that high mechanical input would increase α SMA expression, but that this effect would be mitigated by a TGF β -R inhibitor. TGF β increased α SMA at both low and high mechanical input. (B) Experimental measurements of α SMA expression as measured by immunofluorescence in adult rat cardiac fibroblasts cultured in floating or restrained gels, in which fibroblasts experienced increased mechanical stimulation. As predicted by the model, restrained gels exhibited increased α SMA expression, which was mitigated by the TGF β -R inhibitor (TGF β -Ri) SD208. (C) Example images of cardiac fibroblasts cultured in restrained and floating gels, stained for α SMA (green) and DAPI (purple). Scale bar = 100 μ m. (D) Increased

compaction of floating gels treated with TGF β but not with TGF β -Ri. (E) Floating gels compact over time with TGF β and become more relaxed over time after treatment with TGF β -Ri. (F) The final size of floating gels was inversely correlated with α SMA expression. * indicates $p < 0.05$, and ** indicates $p < 0.01$. All error bars indicate standard error of the mean.

2.5 Discussion

Here we manually reconstructed a literature-based network of cardiac fibroblast signaling. This network was used to develop a logic-based predictive model of fibroblast signaling, which validated at a rate of 80% in comparison to independent, published studies in cardiac fibroblasts. A comprehensive sensitivity analysis revealed the context-dependent functional roles of nodes in the network, such as ROS and the TGF β receptor. Betweenness centrality was the topological metric that was most predictive of functional influence, but overall there was a low correlation between topological and functional characteristics. The model predicted substantial crosstalk between TGF β - and mechanical-induced myofibroblast differentiation, and this prediction was experimentally validated in rat cardiac fibroblasts.

Model validation

While the model validates 80% of input-output relationships for which there is independent data, 16 input-output relationships were incorrectly predicted by the model. Most incorrect predictions were in response to 3 inputs: NP (6), NE (4), and IL1 (4). For example, the model predicted some responses to NP and IL1 where no change was reported experimentally. As NP

counteracts fibrotic stimuli, those pathways may have a lower baseline activation than modeled currently. For IL1, validation data exhibited changes mRNA that were either not statistically significant (N. a Turner et al. 2010) or did not propagate to protein expression as predicted by the model (van Nieuwenhoven et al.). NE and forskolin both stimulate cAMP but have distinct effects(Lai, Sanderson, and Yu 2009; Swaney et al. 2005), indicating cAMP-independent roles of NE. However these are not yet sufficiently characterized for inclusion in the model. Together, these incorrect predictions highlight areas for future model revision and experiments.

Structure-Function Relationships in a Large Signaling Network

There are several approaches for using biological network reconstructions to identify key regulators of cell signaling. One way to predict the influence of a given node is through network topology analysis. Generally, well-connected nodes (those with high degree or betweenness centrality) are more likely to be essential nodes in the network(Albert 2005; Yu et al. 2007). We found that, although betweenness centrality was most strongly correlated with influence, topological features were not strongly predictive of functional influence as determined by sensitivity analysis of the logic-based model. This finding is in agreement with other studies which found degree was not able to fully predict essentiality in signaling and metabolic networks(Li, Assmann, and Albert 2006; Mahadevan and Palsson 2005). Topological metrics are simplified measures of connectivity, whereas the model utilizes the entire network structure to make functional predictions. This finding argues for the need for large-scale predictive network models as in this study rather than relying on simplified measures of connectivity of individual nodes to identify potential signaling drivers and therapeutic targets.

Context-Dependent Roles of Signaling Molecules

Cardiac fibroblasts play diverse functional roles in sensing and contributing to inflammation, remodeling extracellular matrix, and mediating wound healing. As a result their cellular signaling is highly context-dependent, which has implications for the effect of targeted therapy against fibrosis under these different signaling contexts. The large-scale model provides a unique opportunity to investigate context-dependent signaling roles in the cardiac fibroblast signaling network. TGF β is known to be up-regulated following cardiac injury and in heart failure, and in vitro it has been established as a strongly pro-fibrotic stimulus on cardiac fibroblasts (Bujak and Frangogiannis 2007; Swaney et al. 2005; Lu et al. 2013). Anti-oxidants that suppress ROS have been shown to decrease fibrosis following myocardial infarction and prevent cardiac dilation (S. Zhou et al. 2009; Kinugawa et al. 2000). In conditions of high TGF β , the model predicted that suppressing ROS would produce a larger decrease in the TGF β and ET1 autocrine feedback loops than in the baseline signaling context. Additionally, simulations of ROS suppression predicted decreases in collagen and α SMA activity in the high TGF β context, consistent with previous studies (Cucoranu et al. 2005). Interestingly, ROS suppression in the baseline signaling context decreased MMP-9 activity whereas it increased MMP-9 activity in the high TGF β context. This is likely due to the effect of ROS knock down on TIMP activity as MMP-9 mRNA levels were predicted to increase with ROS knock down regardless of the signaling context. This has implications for the treatment of heart failure-associated fibrosis with antioxidants as the model predicts antioxidants will be more effective in treating fibrosis under a high TGF β

signaling context (e.g. near a myocardial infarct) than in a baseline context (e.g. in the remote zone).

Additionally, the TGF β receptor, which is directly linked to only the TGF β pathway, was shown to be highly influential in both the baseline context and the high TGF β context. For this reason, we investigated the role of the TGF β receptor and, by extension, the involvement of the TGF β pathway, under the baseline context and all 11 single-input contexts. We found that the TGF β -R functions to increase collagen I, collagen III, and α SMA under all single-stimulus contexts, but the magnitude of the increase depends on the context. In contrast, the TGF β -R was predicted to up- or down-regulate periostin in a context-dependent manner. Blocking the TGF β -R was predicted to decrease periostin under 10 of 12 signaling contexts, but TGF β -R knockdown was predicted to increase periostin expression in contexts of high β -adrenergic or high forskolin signaling. Together these data demonstrate how a large-scale model that incorporates multiple pathways can be useful for interrogating how fibroblasts respond to different signaling contexts. These results also have implications for how cells in different signaling environments might respond differently to antioxidants (above) or to TGF β receptor inhibitors. Future studies can use this model to better understand how fibroblasts respond to more complex signaling contexts such as combinatorial- or dynamic-stimulus contexts and varied doses of inputs.

Cross-Talk and the Effect on Phenotype

Hypertension is a risk factor for the development of cardiac fibrosis, and understanding how cross-talk between mechanical and chemical stimuli affects the development of a pro-fibrotic phenotype could reveal possible mechanisms of pathogenesis. The model predicted a role for the TGF β -R in up-regulating collagen and α SMA under a high mechanical stimulus. Therefore we

tested this prediction using mechanically restrained or floating gels in order to activate the integrin pathway downstream of mechanical stimulus in the model (Rosenfeldt 2000).

Experimentally, we found that the TGF β -R inhibition abrogates mechanical-induced α SMA up-regulation, validating the model's prediction. To our knowledge this relationship has not been shown previously, reinforcing the value of large-scale modeling to elucidate novel signaling mechanisms via signal cross-talk. The precise mechanism by which the TGF β pathway amplifies myofibroblast differentiation in response to integrin stimulation requires further investigation. The model predicts that an autocrine loop involving an increase in TGF β expression is responsible for sensitizing the fibroblast to differentiation from multiple stimuli including mechanics, angiotensin II and ET1 (data not shown). However, stretch of extracellular matrix has also been shown to increase activation of extracellular stores of latent TGF β (Klingberg et al. 2014). For example, Sarrazy et al. demonstrated that integrins activate latent TGF β (Sarrazy et al. 2014). Both of these are testable potential mechanisms underlying this cross-talk.

Limitations

As with all modeling approaches, our logic-based ODE approach has inherent limitations. While this model uses default parameters, we have previously shown that this approach still exhibits strong predictive accuracy in comparison to a fully parametrized biochemical model (Kraeutler, Soltis, and Saucerman 2010). Further, the model's validation and predictions are robust to parameter variation (Fig. S3). Availability of more quantitative proteomic data could increase the quantitative and dynamic predictive power of the model. The model structure is not fully comprehensive, focusing instead on the consensus cardiac fibroblast signaling network that

meets specified inclusion criteria. However, this provides a framework for future expansion based on new experimental data.

2.6 Conclusions

We developed a predictive model of cardiac fibroblast signaling through manual curation of a signaling network, combining 10 pathways that are altered during cardiac injury or heart failure. Sensitivity analysis identified key signaling drivers of fibroblast function, and showed that these drivers vary across diverse signaling contexts. Specifically, TGF β and ROS were key drivers of fibrosis signaling under both the baseline and high TGF β context, but their relative effect on different nodes in the network was context-specific. The model also predicted a role for TGF β in amplifying myofibroblast differentiation and expression of extracellular matrix proteins in response to other signals such as mechanical stimulation. The role for the TGF β -R in mechanical stimulation-induced α SMA expression was validated experimentally. More generally, we found that functional influence and topological features are not well correlated, revealing the limited ability of topological analysis to predict functionality within a signaling network. The large-scale network modeling approach utilized here enables the prediction of global features of signaling networks that are often non-intuitive from local topological connections alone. In the following chapters we will expand on this study to investigate how dynamic inputs or pharmacologic treatments alter fibroblast phenotype.

Chapter 3

Identifying Potential Modulators of Adverse Remodeling Post-Myocardial Infarction

Contributors: Angela Zeigler (developed model, designed all analysis, performed all analysis, wrote paper), Philip Tan (editing text), Jeffrey Holmes (assisted in post-MI model design, developed tissue-level ODE), Jeffrey Saucerman (designed study, assisted in writing).

3.1 Forward

Wound healing is a complex process that involves a dynamic interplay between inflammatory and proliferative signaling. Therefore, wound healing is particularly suited to a systems biology approach. Although the healing process follows the same general trajectory throughout the body, it is slightly different in end result in each organ. In the heart, injury, such as myocardial infarction, is particularly problematic since cardiomyocytes do not proliferate and re-populate the infarct area. I described the development of a cardiac fibroblast-specific computational model in the previous chapter. In this chapter, I outline how this model can be used to investigate modulators of infarct healing.

3.2 Introduction

Patients who have a myocardial infarction are at high risk for developing heart failure (Gottdiener et al. 2000; J. He et al. 2001) — usually due to adverse remodeling associated with infarct wound healing (Beltrami et al. 1994). Myocardial infarcts follow the same healing course that occurs in other organs (Fishbein, Maclean, and Maroko 1978; Palatinus, Rhett, and Gourdie 2010). There is first an inflammatory phase characterized by extracellular matrix (ECM) breakdown and myocyte necrosis which lasts around 2 days in rats and 5 days in larger mammals (Virag and Murry 2003). Then, the proliferative phase lasts around 2-5 days in rats (2 weeks in large mammals), during which fibroblasts proliferate, migrate into the wound, differentiate into myofibroblasts, and generate large amounts of collagen I and III and other ECM proteins (Virag and Murry 2003; Chistiakov, Orekhov, and Bobryshev 2016). Ultimately, the wound matures into a stable scar with balanced ECM production and degradation. The heart is unique in that

cardiomyocytes do not proliferate and re-populate the wound, so the ultimate fate of cardiac tissue depends on the behavior of cardiac fibroblasts. Excessive degradation can lead to ventricular dilation and wall rupture due to the loss of structural integrity in the heart wall (Hwang et al. 2001). Conversely, excessive ECM deposition, particularly in healthy myocardium remote from the infarct, can lead to diastolic dysfunction (Volders PG1, Willems IE, Cleutjens JP, Arends JW, Havenith MG 1993; Litwin et al. 1991). Many patients with adverse remodeling post-MI have both dilation and fibrosis (Beltrami et al. 1994).

A beneficial infarct healing process involves a transient burst of high collagen deposition that replaces lost cardiomyocytes with strong ECM without a sustained increase in ECM that leads to adverse remodeling (N. A. Turner and Porter 2013). This “transient fibrosis” is likely facilitated by many different factors including inflammatory cell phenotype and number, the pre-infarct signaling state, the size of the infarct, and the health of the remaining cardiac vessels (Pfeffer and Braunwald 1990; Sun and Weber 2000). However, fibroblasts play a prominent role throughout the entire wound healing process, and therefore present a good system for studying how cells respond to the dynamic signaling environment of wound healing. Additionally, understanding how fibroblasts respond during the different phases of wound healing could identify mechanisms by which adverse healing processes develop in all organs.

This study leverages a large-scale model of cardiac fibroblast signaling (A. C. Zeigler et al. 2016) to identify the key exogenous and endogenous drivers of fibroblast phenotype during myocardial infarct wound healing. We found that using data-derived idealized input curves to the model accurately predicts the dynamics of collagen expression and development of increased collagen area fraction in the heart. The model predicts that the timing and intensity of inflammatory or TGF β signaling affects the process of wound healing. Additionally, the model

predicts a role for IL1 in improving ECM remodeling by increasing collagen expression early without inducing a prolonged increase in collagen long-term.

3.3 Methods

Model Modifications

For this study we adapted the large-scale fibroblast model of fibroblast signaling from chapter 2 to be more relevant for subsequent experimental study of fibroblast phenotype. The interactions and nodes added are shown in Fig. B.1. Specifically, the input nodes were separated from their associated ligands to facilitate the drug study in Chapter 4, and outputs associated with collagen maturation (e.g. LOX) and myofibroblast differentiation (e.g. contraction) were added.

In addition to updating the model network, the input levels of the model that are used for control simulations were trained to validation data used in Chapter 2. Specifically, we trained for a baseline level of inputMechanical activity such that when inputTGF β or inputIL1 activity were increased the predicted fold change in collagen I/III mRNA (TGF β) or MMP9 (IL1) would be quantitatively as close as possible to the experimentally determined values. To identify this level of mechanical input, we used brute force optimization to minimize the sum of squared error between the model prediction and experimental data (Fig. B.2). We found that a level of 0.725 for the inputMechanical node was the optimum control stimulus.

Modeling the Dynamics of Post-MI Signaling

To simulate a post-MI setting, we developed idealized input curves for all inputs except mechanical, which has been shown to remain a constant stimulation throughout the infarct healing time course (Fomovsky, Rouillard, and Holmes 2012). Initially data from both rat and mouse infarcts were combined, but the data were so inconsistent from mouse to rat, that it was difficult to identify a consensus to validate against. There was no published post-MI rat study where NE, ET1, or NP were measured at different time points, so human data was used for those inputs. We used post-MI data (summarized in Table B.1) to identify when each input peaked and to what extent. If a stimulus experimentally peaked to greater than 3 times the pre-infarct levels, that was defined as a “high” peak and set to a normalized input value of 0.5. If the experimental peak was less than 3 times pre-infarct levels, this was defined as a “low” peak and the input was set to a normalized value of 0.25. Production and degradation curves were defined for each input to peak at approximately the correct time and to the approximate height as was shown experimentally. The production rate is modeled as being faster than the degradation rate for all curves because that is most consistent with the data outlined in Table B.1. The idealized input curves for each output is plotted against the dynamics of expression or protein content post-MI in Figure B.3.

Tissue-Level Model

In addition to the previously described logic-based ODE signaling model (Chapter 2), we coupled an adapted model of tissue-level collagen accumulation dynamics to the signaling model to predict how single-cell changes in collagen expression lead to changes in percent collagen area fraction in the infarct scar (Richardson WJ, Clarke SA 2016). This model incorporates an approximation of the MMP dynamics and fibroblast number as well as the collagen I and III

mRNA levels predicted by the signaling model (Figure C.4). The changes in collagen area fraction were defined by equation 1.

Equation 1

$$\frac{dAreaFraction}{dt} = k_g * c_n * n_f - k_d * m * AreaFraction$$

Where k_g is the collagen degradation rate (1.8 unit/day), c_n is the collagen I mRNA levels predicted by the network model, n_f is the number of fibroblasts (as shown in SF 4), k_d is the degradation rate (0.03 unit/day), and m is the level of MMP activity (as shown in Fig. B.4).

Validation of Post-MI Dynamics

We validated model predictions of post-MI collagen dynamics against data collected in rat infarcts (A Deten et al. 2001; Zimmerman et al. 2001). Only rat infarct data was used to validate output levels, since the model and input levels were primarily based on rat data. Experimental expression data (Figure 3.1b) were normalized to the max value (such that the max value = 1) because the experimentally determined highest expression value was very different between the two data sources (partially because expression was measured different in the two studies). However, this normalization facilitates comparison of the dynamics, as time to peak height and time to return to baseline are the main outcomes being validated. The predictions from the tissue-level model were validated against percent collagen area fraction measured in rat infarcts (Fomovsky and Holmes 2010).

Randomized Simulation

In order to simulate a population of fibroblasts with random variation in expression, we randomly sampled y_{\max} values (default = 1) from a normal distribution. First, we simulated 100 randomized models where all y_{\max} values were randomly sampled from a normal distribution with increasing standard deviation (data not shown). Figure 3.2a shows the comparison of sampling from a normal distribution with a standard deviation of 0.025 to the dynamics of collagen expression in rat infarcts. The variance of the randomized model predictions is smaller than the standard deviation of the experimental data, which justifies our use of this range for post-MI simulations.

Correlation to Single Input

Steady state predictions from the logic-based ODE model were compared to predictions at specific time points in the dynamic simulation that correspond to different phases of infarct healing. Specifically, a constant stimulus of each single inputs or the pairs of inputs that define the inflammatory or proliferative state was simulated. The predicted values of all outputs (MAP kinases, transcription factors, and phenotypic outputs) was correlated to the predicted values of all outputs at 0 day, 1 day, 7 day, or 42 days in the dynamic simulation.

Screen for Modulators of Collagen

To screen for modulators of collagen I mRNA using the model, each node was up-regulated, and the simulation with up-regulation was compared to the control simulation with no up-regulation. In the steady state screen, the comparison was made by predicting the fold change of collagen I mRNA (altered simulation / control). Up-regulation was simulated by setting the $dy/dt[\text{upregulated node}] = 0$ and setting $y_0 = 0.6$. This y_0 value was chosen because it was higher than the high peak height in the dynamic idealized input curves, and therefore should be higher than the value of most nodes. Notably, this doesn't apply to members of the mechanical pathway since the value of the mechanical input is 0.725. Therefore these screens show that setting mechanical signaling to 0.6 lowers collagen output in all contexts, and this should not be interpreted as a prediction mechanical stimulus down-regulating collagen mRNA.

In vitro collagen production

Human ventricular fibroblasts were purchased from PromoCell and grown on culture flasks in Fibroblast Growth Medium 3 (PromoCell) containing 10% fetal calf serum (except when indicated as serum free), 1ng/mL recombinant human basic fibroblast growth factor and 5ug/mL recombinant human insulin (all components from PromoCell). Cells were used within passages 4–8.

In order to measure collagen production, we adapted a tissue picrosirius protocol to a 2D in vitro setting (Kliment et al. 2011). In these experiments cells were plated on a 24 well plate and treated in media with 200uM ascorbic acid (3T3) or 250uM ascorbic acid and 100U/mL penicillin/streptomycin (human primary fibroblasts) for 72 hours. Collagen standards were made by plating 1, 5, 10, 20, or 50µg rat tail collagen on 96 well assay plate in triplicate and allowed to

dry in cell culture hood or oven. Then, cells were fixed and the cell plates and standards were stained with picosirius red for 1 hour. Stained plates were washed 4 times with 5% acetic acid and 1 time with DIH₂O, then the plates were de-stained with 200uL 0.1M NaOH for 30 minutes.

3.4 Results

3.4.1 Adapting the computational model to predict post-MI phenotype

The previously published large-scale model of cardiac fibroblast signaling (A. C. Zeigler et al. 2016) was adapted for use in predicting fibroblast phenotype during infarct healing (see Fig. B.1). This model is useful for such an application because it is capable of predicting semi-quantitative dynamic behavior and it incorporates many of the pathways involved in infarct healing (IL1, IL6, TGF β being the most prominent). First, control levels of mechanical signaling were trained to *in vitro* data due to a lack of such fibroblast-specific data *in vivo* (Fig. B.2, Table B.1).

Post-infarct levels of the model inputs (exogenous chemical cues) were derived from data collected from rat and human infarcts (Table B.1). There was no consistent measuring technique from the infarct vs remote zone vs whole heart. Therefore, these input curves are meant to convey signaling dynamics in the infarct although some values were measured outside the infarct. Notably, mechanical signaling remains constant throughout the healing process as was shown in Fomovsky et al. Fig. 3.1a shows the data-derived generated curves used to define the post-infarct inputs to the model. The signaling model alone predicts collagen mRNA expression dynamics that are comparable to rat infarct dynamics (Fig. 3.1b). Additionally, the model-predicted collagen I and III mRNA levels were used as inputs to a tissue-level model of collagen

deposition, and this model predicted changes in collagen area fraction consistent with those in a rat infarct (Fig. 3.1c).

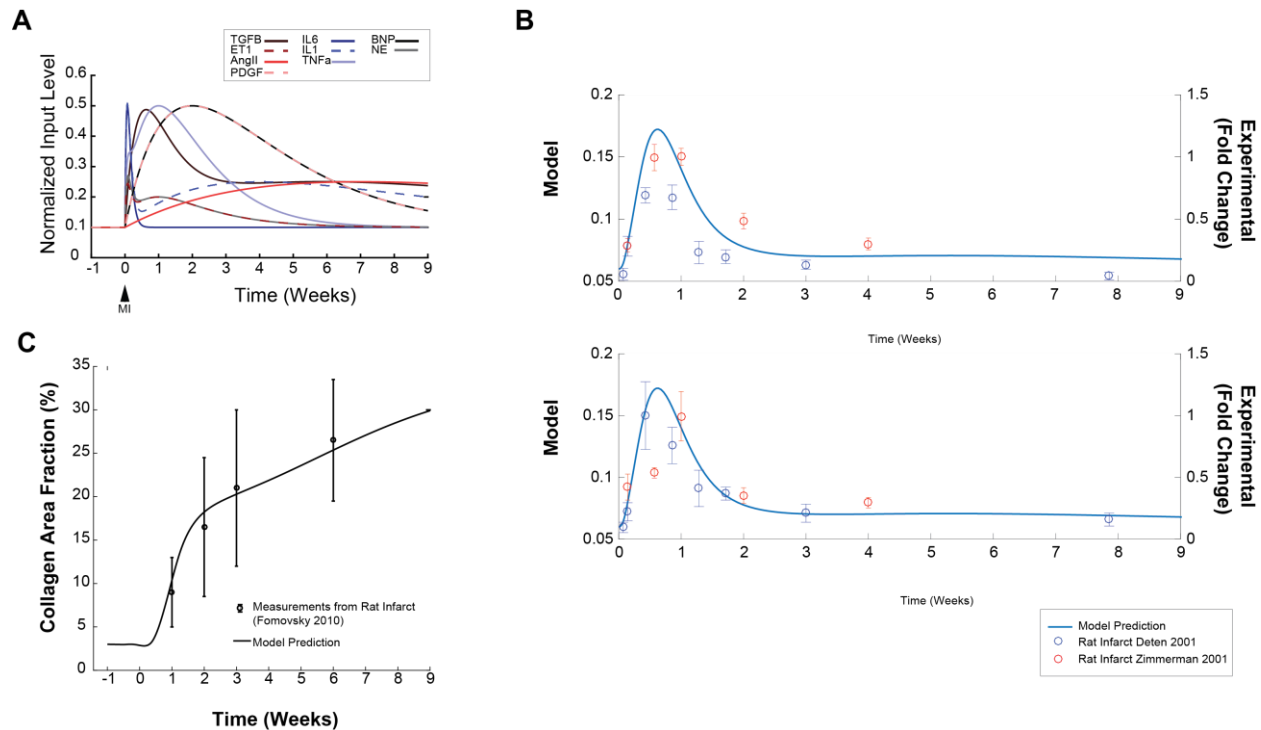
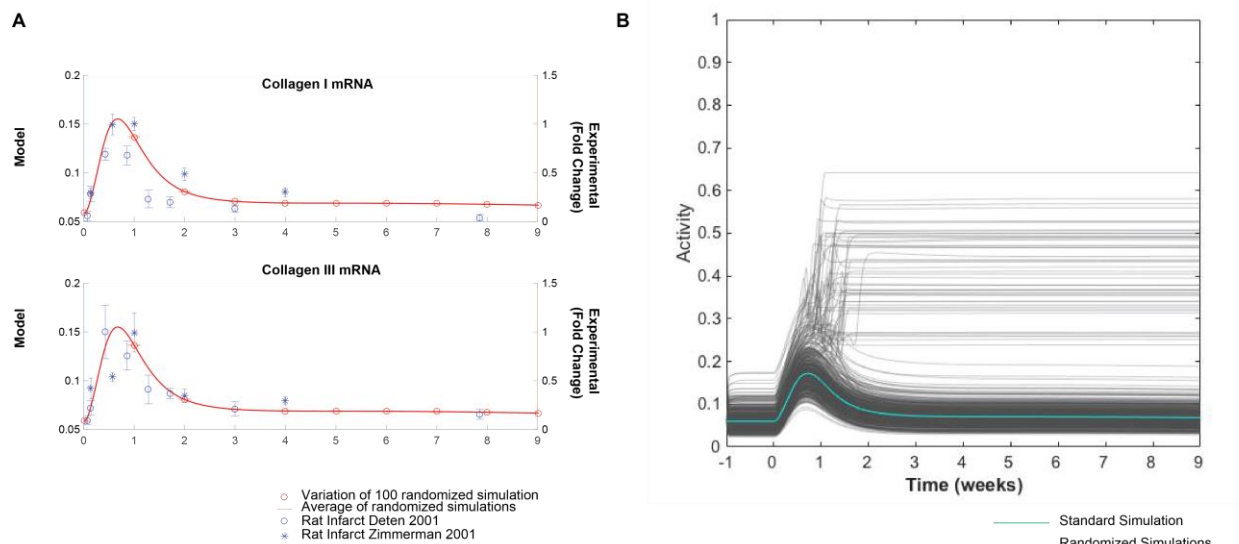


Figure 3.1: Generation and validation of a dynamic post-MI model of cardiac fibroblast signaling. A: Idealized input curves for each input (excluding mechanical) based on post-MI levels. B: validation of the predicted timing of collagen expression post MI against data from rat infarcts. C: validation of the collagen area fraction predicted from the tissue level ODE.

The sensitivity of the model prediction to random variation in y_{max} values (which can be interpreted as random variation in expression) was assessed. Fig. 3.2a shows the comparison of 500 stochastic simulations to the training data shown in Fig. B.2. In Figure 3.2b, the predicted collagen I mRNA activity from 100 dynamic post-MI simulations of fibroblasts with randomized y_{max} values is shown in comparison with the deterministic model prediction. This predicts that small, random variation in expression levels can lead to sustained collagen activation. This is consistent with the fact that some percentage of the fibroblast population becomes permanently



differentiated into myofibroblasts and persists in remodeling the infarct long-term (Cleutjens et al. 1995; Willems et al. 1994; Palatinus, Rhett, and Gourdie 2010).

3.4.2 Predicting the impact of variation in extracellular signaling dynamics post-MI.

The use of idealized generated input curves allows for the model to predict how variation in signaling dynamics alter the collagen dynamics. TGF β has been implicated as a driver of fibrosis in many signaling environments. To better clarify the role of TGF β signaling dynamics post-MI, we modeled a delay in TGF β peak signaling and an increase in the amplitude of TGF β signaling. Specific TGF β alterations are outlined in Table 3.1. As shown in Fig 3.3, the model predicts that delaying TGF β signaling leads to more of an increase in collagen area fraction than increasing

Figure 3.2: Model prediction of the result of random expression. A: the comparison of the variation of model predictions using a standard deviation of 0.025 to determine the normal distribution from which y_{max} values are sampled. B: Model prediction of 100 different simulations with randomized y_{max} values sampled from a normal distribution with a standard deviation of 0.025.

TGF β signaling (Fig. 3.3b).

Table 3.1: Input Alterations

Alteration Name	Inputs Altered	Peak Height Alteration	Timing Alteration
High TGFβ	TGF β	High peak height = 0.6	No change
Late TGFβ	TGF β	no change	High peak at 14 days

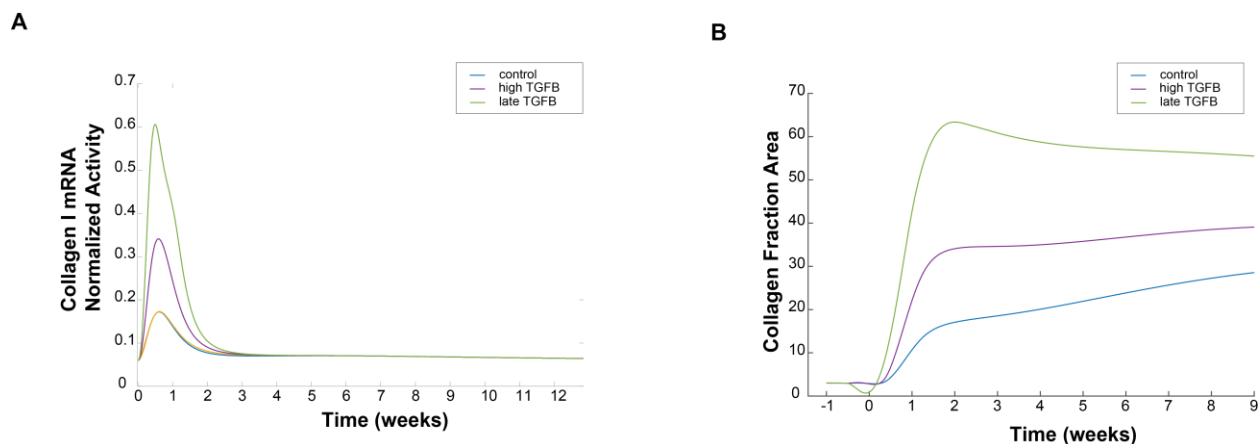


Figure 3.3: Effect of altered input profiles. Shown are the effect of altered input profiles outlined in Table 3.1 on collagen I expression (A) and collagen area fraction (B) predicted by the model.

Because cell signaling is more straightforward to study *in vitro*, we used the model to predict how a single sustained stimulus, analogous to an *in vitro* application, related to different stages of dynamic input. The model-predicted phenotypic profile at different stages of post-MI healing was compared to the predicted phenotypic profile of a fibroblast stimulated with a constant

single input as would occur in an *in vitro* setting. The control (unstimulated) condition had the highest correlation with pre-infarct, IL1 had the highest correlation with inflammatory (1 day) time, and TGF β had the highest correlation with the proliferative (7 day) time point (Fig. 3.4). The late (42 day) time point was well-correlated with several single stimuli and the control stimulus. Previous studies have shown that mouse fibroblasts at intermediate stages of MI healing are most similar to fibroblasts stimulated by TGF β (Squires et al. 2005). As shown in Fig. 3.5, the representative single stimulus is capable of reproducing most of the qualitative phenotype predicted by the dynamic stimulus.

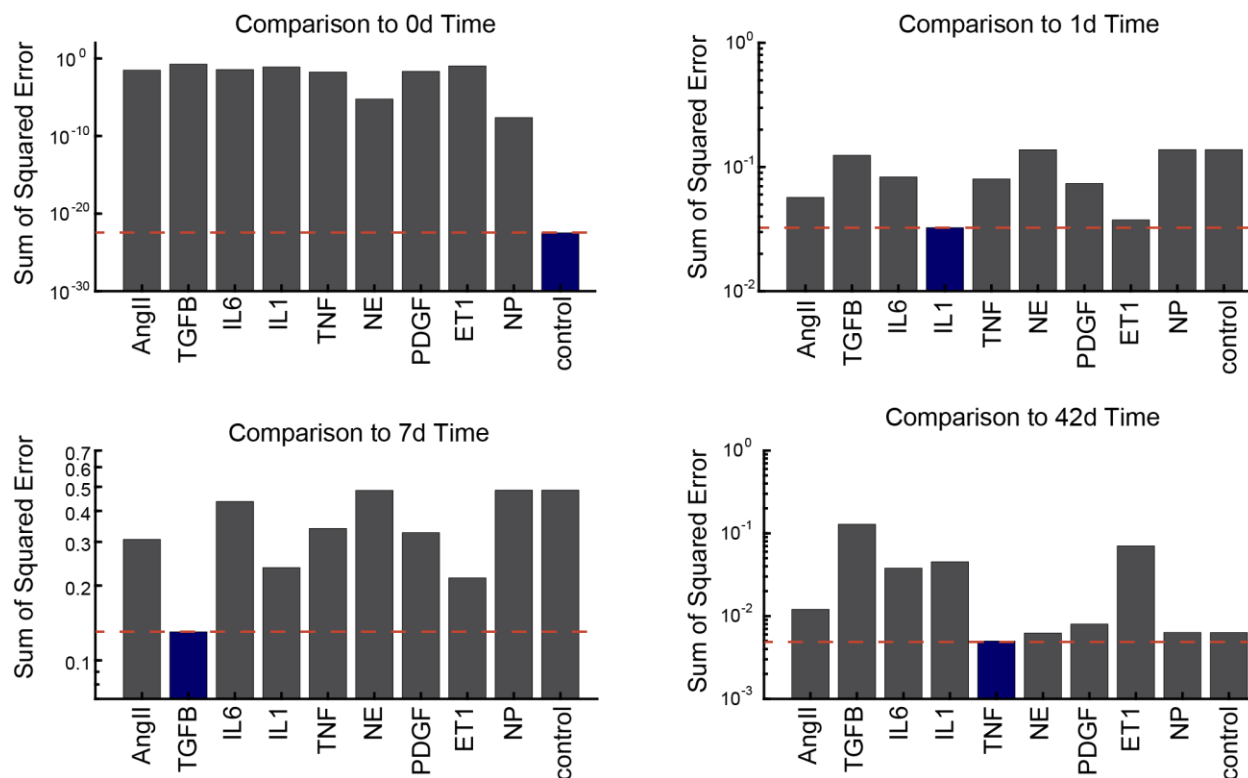


Figure 3.4: Relationship between sustained, simplified inputs and select time points of the dynamic prediction. Shown is the sum of squared error between the predicted output levels at steady state with sustained stimulation of the indicated inputs and the predicted output levels at the indicated time point in the dynamic simulation. Blue highlights most correlated single inputs.

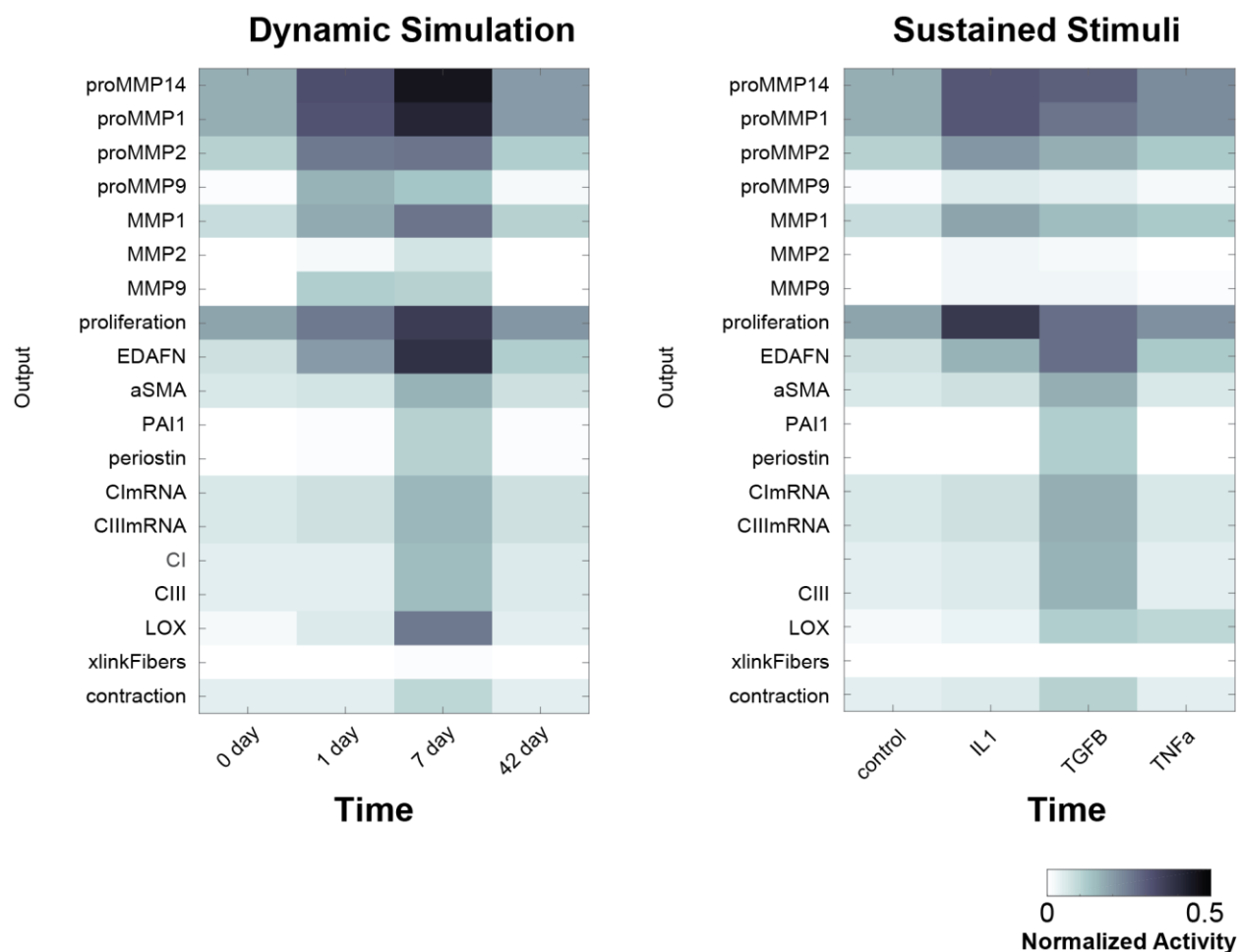


Figure 3.5: Predicted fibroblast phenotype in the dynamic and steady state simulations. Predicted output levels at pre (0 day), early (1 day), middle (7day), and late (42 day) time points in the dynamic stimulus is compared to the predicted output levels with sustained stimulus of representative inputs. Sustained stimuli are ordered by the time point with which they are most closely correlated.

3.4.3 Predicting endogenous modulators of fibroblast phenotype during infarct healing.

It is possible to interpret from the above analysis that IL1-pathway members will modulate fibroblast activity during early time points and TGF β -pathway members will modulate fibroblast activity during late time points. However, there are many intracellular signaling proteins that participate in multiple pathways that might play a more central role in affecting fibroblast

decision-making in signaling contexts with dynamic or competing cues. In order to identify putative context-dependent modulators, an *in silico* screen was performed using the dynamic inputs (Fig. 3.6). For each simulation, the generated input curves were applied to the model with no alteration (control) or with the indicated node up-regulated to 0.6 activity. The mechanical pathway is normally activated at 0.725 so this screen indicates that reducing mechanical signaling will inhibit collagen production during infarct healing. The qualitative effect of up-regulation of all other nodes is indicated by the colored bar in Figure 3.6.

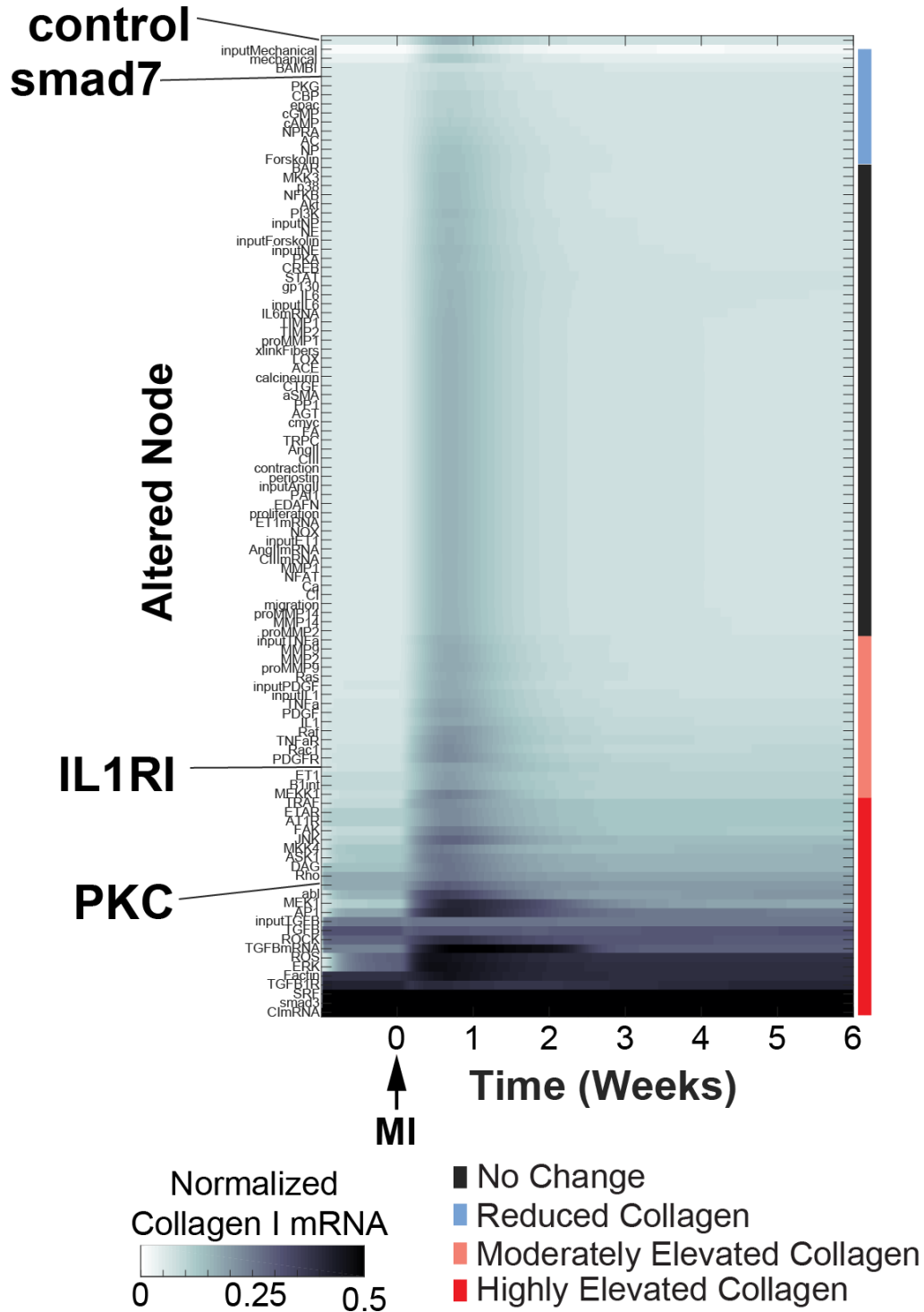


Figure 3.6: Screen for modulators of post-MI collagen. Simulations of the dynamic MI setting where each node (y-axis) is up-regulated to 0.6. Simulations were sorted by hierarchical clustering. The colored bar indicates the qualitative change in collagen predicted by the model. Control, smad7, PKC, and IL1RI simulations are highlighted.

The same screen (up-regulation to 0.6) was performed in representative single-input, steady state simulations with the inputs representative of inflammatory (IL1), proliferative (TGF β), or mature post-infarct healing as defined above (Figure 3.7). The predicted effect of up-regulation of many nodes is consistent between the two screens. Three of these inputs are highlighted: smad7, PKC, and IL1RI.

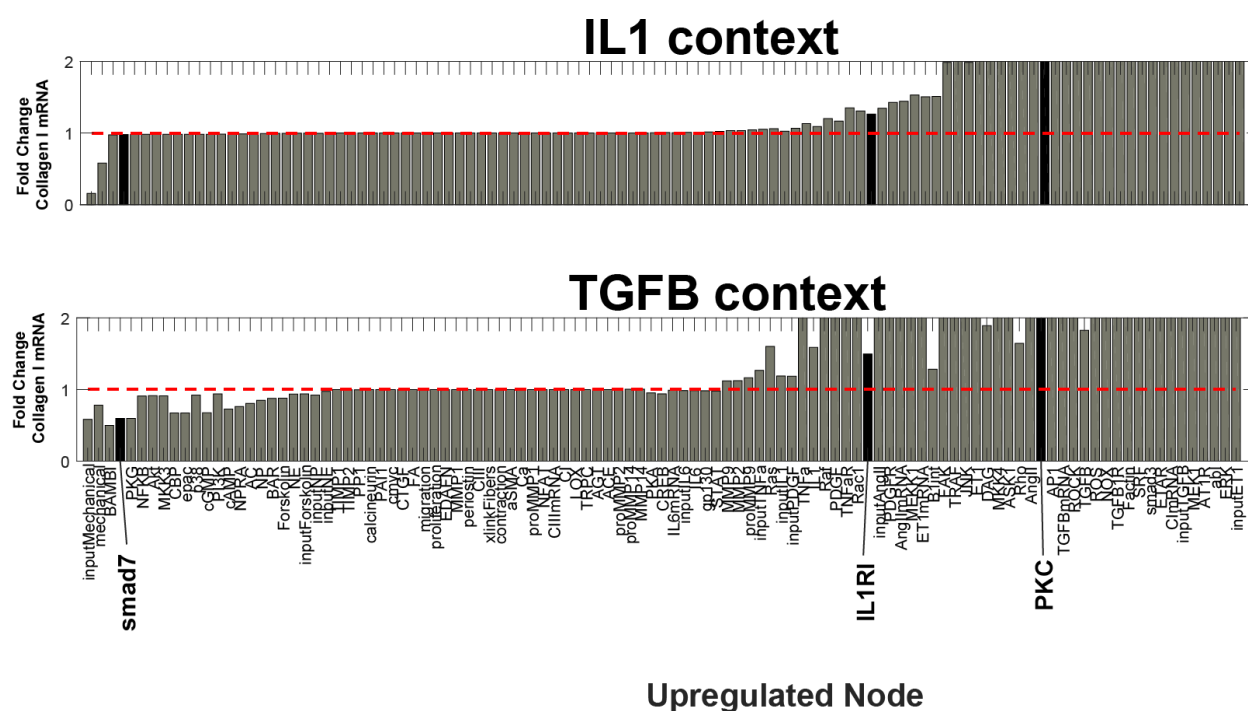


Figure 3.7: Screen for collagen modulators in representative steady-state simulations.

Shown is the predicted fold change in collagen I mRNA above the control simulations following a steady state stimulation with the indicated input to 0.5 activity. Predictions are rank-ordered by their effect in the control stimulus (data not shown). Specific predictions of smad7, PKC, and IL1RI are highlighted for comparison to figure 6.

The model predicted that increasing smad7 activity decreases collagen expression (Fig 3.7a), which is consistent with post-infarct studies showing reduced TGF β signaling impairs wound

healing (Ikeuchi et al. 2004). The model predicted a strong increase collagen expression and area fraction with increased PKC activity (Fig 3.7b). Increasing IL1 is predicted to improve collagen dynamics at moderate doses, but at high doses increases the risk for fibrosis (Fig.3.7c).

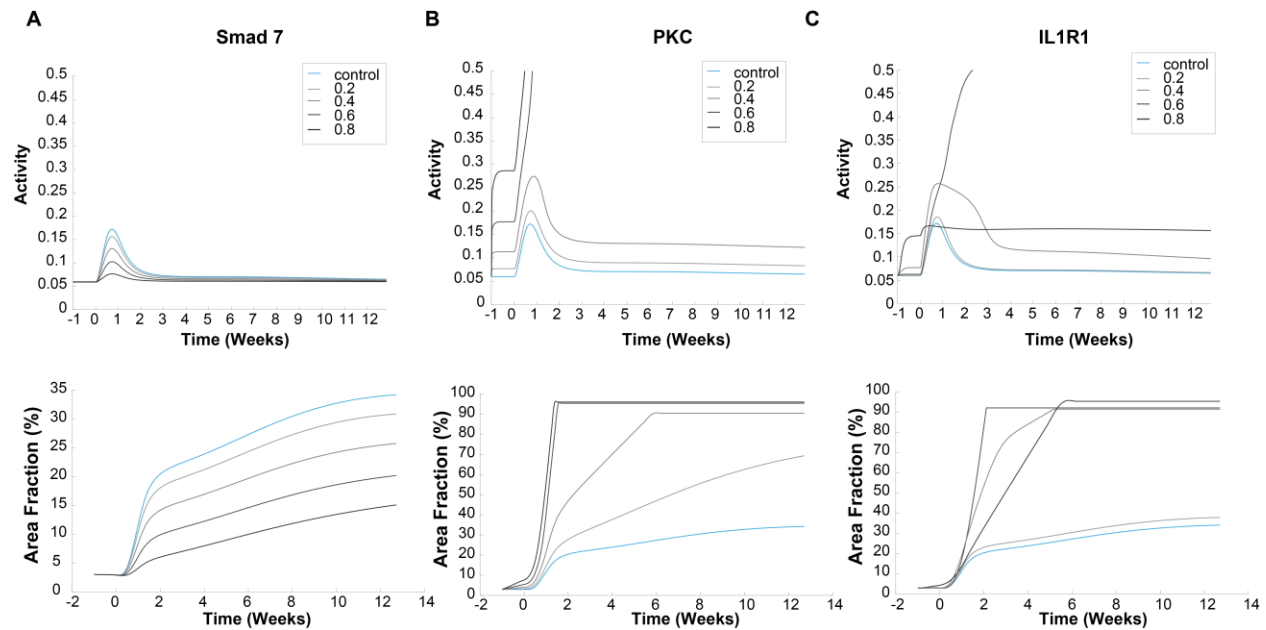


Figure 3.8: Effect of specific modulators of collagen output. The predicted effect of increasing doses of smad7 (A), PKC (B), and IL1R1 (C) on predicted collagen I mRNA and collagen area fraction. Control simulations are highlighted in blue.

3.4.4 IL1 and TGF β cross talk

Since it was shown that IL1 and TGF β are the major input pathways for inflammatory and proliferative phase signaling respectively, we investigated the relationship between these two signaling pathways. In Figure 3.9 we show that IL1 is predicted to increase collagen expression in control (0.1) or low (0.4) levels of TGF β , but that at high (0.55, higher than high peak post-MI) levels of TGF β , IL1 is predicted to slightly decrease collagen. We preliminarily validated

these predictions by measuring collagen production in 2D culture of human ventricular fibroblasts.

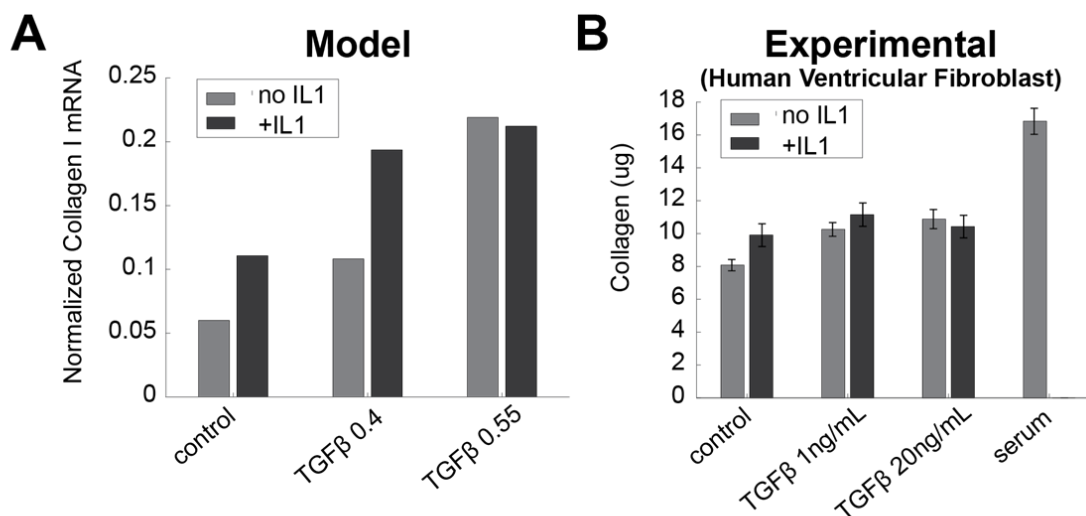


Figure 3.9: Validation of interaction between IL1 and TGFβ. The model predicts that when TGFβ levels are below peak height (as shown in Figure 1), IL1 increases collagen. However, for high levels of TGFβ there is no further increase in collagen expression. Experimental validation performed in human ventricular fibroblasts is shown where collagen was measured using picrosirius assay. n=1 experiment with 3 wells, error bars show standard deviation

3.5 Discussion

Not all myocardial infarctions are the same. It is difficult to predict which patients will have long-term remodeling which leads to heart failure and which patients will heal with no loss of cardiac function. Infarct size and wall stress can determine the health of the heart post-infarct healing (Pfeffer and Braunwald 1990). However, collagen expression dynamics can affect cardiac health post-MI (Dobaczewski et al. 2010; Frantz et al. 2008; Hwang et al. 2001). Excessive production can lead to fibrosis, which contributes to diastolic dysfunction (Volders

PG1, Willems IE, Cleutjens JP, Arends JW, Havenith MG 1993; Litwin et al. 1991), and excessive degradation immediately post-MI can contribute to dilation and wall rupture (Hwang et al. 2001; Frantz et al. 2008).

This study aims to predict some of the signaling characteristics both external and internal to cardiac fibroblasts that can affect collagen production post-MI. We predict that inflammatory signaling actually serves to increase collagen output in early post-MI healing and that late TGF β is more pro-fibrotic than increased TGF β signaling. Additionally, we predicted that smad7 is anti-fibrotic, IL1 is mildly pro-fibrotic, and PKC is strongly pro-fibrotic. Finally, the relationship between inflammatory (IL1) and proliferative (TGF β) signaling was predicted by the model and validated *in vitro* using human ventricular fibroblasts.

Exogenous regulators of post-MI collagen production

It would be important to find extracellular modulators of fibroblast activity to improve post-MI wound healing, but also to understand how fibroblasts participate in wound healing in any organ. The wound healing process is stereotyped, following the same inflammatory to proliferative to maturation phase progression and entailing the same involvement by fibroblasts (Palatinus, Rhett, and Gourdie 2010). Therefore, understanding how fibroblasts respond to these dynamic and complex stimuli could have clues for how fibrosis and progressive remodeling develop. This study predicts that the intensity of inflammatory signaling and the timing of TGF β signaling have implications for the dynamics of collagen production. It has been shown that reducing IL1 or IL6 signaling post-MI can worsen healing and increase risk for dilation, possibly through a reduction in collagen expression (Hwang et al. 2001).

Endogenous modulators of post-MI collagen production

It is also helpful to identify the key intracellular modulators of fibroblast phenotype during wound healing, as these could be considered therapeutic targets against fibrosis or adverse remodeling. (Chapter 4 utilizes this modeling approach to predict how FDA-approved drugs might affect fibroblast phenotype post-MI.) This study indicates that there are several nodes and pathways that up-regulate collagen activity (eg: PKC, Rho, and the PDGF pathway), but that there are not as many nodes that down-regulate collagen (Fig. 3.6 and 3.7). Additionally, we predicted that even small variation in expression values can lead to sustained collagen production post-MI, which could be a result of randomly increased signaling in more than one pathway at one time. This result could be explained by the fact that the manually curated network is biased toward well-studied pathways (see chapter 2). Perhaps, well-studied pathways happen to be primarily pro-fibrotic. However, it is also possible that fibroblasts are primed to increase collagen production in response to stimuli. This hypothesis is supported by the fact that fibroblasts tend to differentiate into pro-fibrotic myofibroblasts in response to a variety of stressors including pro-inflammatory ones (N. A. Turner and Porter 2013; Palatinus, Rhett, and Gourdie 2010). In chapter 5, we showed that human primary fibroblasts do not decrease their collagen production in response to any of the inflammatory stimuli (IL6, IL1, or TNF α). In fact, IL1 increased collagen production in ventricular fibroblasts, as is predicted by the model in this chapter (Fig. 3.9) and has been shown in murine infarcts (Hwang et al. 2001). That there is an abundance of pathways that up-regulate collagen expression has implications for potential therapeutics. It is possible that inhibiting multiple pro-fibrotic therapies with combined anti-fibrotic therapies might be more successful in treating fibrosis.

However, this trend toward pro-fibrosis might be organ specific. This model has only been validated against cardiac fibroblast data, but organ-specific regulation or expression might drive changes in wound healing. Myofibroblasts are present in both the infarct and remote regions of the heart long after infarct healing (Willems et al. 1994), but this is not true in dermal wound healing where the fibroblasts all apoptose following the maturation phase (Palatinus, Rhett, and Gourdie 2010). As shown in chapter 5, collagen production and baseline contractile properties are higher in human ventricular versus human dermal fibroblasts. Therefore, it is possible cardiac fibroblasts, specifically, are primed to be more pro-fibrotic.

Limitations and future directions

The main limitation of this study is that the model only predicts fibroblast responses to MI. Other cell types such as macrophage and cardiomyocytes do participate in signaling that can alter the remodeling process. Furthermore, events such as re-vascularization (which can improve infarct healing) or further cardiomyocyte injury (which can re-start or prolong wound healing and induce pathologic remodeling) are not captured by this model. However, this provides a first step toward a better understanding of both wound healing and cardiac remodeling. Further studies could incorporate this model into a multi-scale model that can predict the effect of cell-cell interactions between macrophage and cardiomyocytes. Additionally, the hypotheses generated by this study, including the role of delayed TGF β signaling or increased IL1 signaling in infarct healing will need to be validated *in vivo*.

3.6 Conclusion

In this chapter we demonstrated the application of a logic-based ODE model to investigate phenotypic modulators during a dynamic signaling process. We predicted that moderate IL1 stimulation has a beneficial effect on post-MI wound healing by increasing collagen expression early post-infarct without increasing expression levels in the mature infarct.

Chapter 4

Developing a Pipeline for *In Silico* Drug

Screening

Contributing Authors: Angela Zeigler (assisted in designing pipeline and writing code, ran all simulations, wrote chapter), Anirudha Chandrabatla (assisted in designing pipeline and writing code), Matthew Sutcliffe (paper editing), Jeffrey Saucerman (designed experiments).

4.1 Foreword

A better understanding of fibroblast signaling can help identify what predisposes a fibroblast toward a pro-fibrotic phenotype post MI (as outlined in chapter 3), but the ultimate goal is to identify potential therapeutics that can reduce the risk for cardiac fibrosis. In this chapter, I outline a novel pipeline for virtual drug screening using the fibroblast signaling model described in chapter 3. This method is unique among virtual drug screens in that it can predict a drug's effect in different contexts such as different expression levels and signaling contexts. This approach can also predict how drug dose and method of action affect the outcome. The potential flexibility outlined in this chapter makes this method attractive as a generalizable approach for drug screening.

4.2 Introduction

The process for bringing a drug to FDA approval is long and expensive, often taking 8-12 years to have (by a conservative estimate) a success rate of one in 5000 (Lipsky and Sharp 2001). One study found that, even after approval, approximately 30% of new approvals are subject to a postmarket safety event (withdrawal, black box warning, or safety communication), and the median time for these events to occur is 4.2 years after approval (Downing et al. 2017). Therefore, there is a need for a way to quickly identify useful therapeutics early in the discovery process without compromising safety.

The FDA has recently developed a method for using a computational model of cardiomyocyte electrical activity to screen for drugs that induce fatal arrhythmias (Colatsky et al. 2016). In

general, a growth in computational modeling and machine learning has facilitated large-scale *in silico* drug screening. If a target is known, biophysical methods like structural matching, chemical docking (Sohraby et al. 2017; Lavecchia and Cerchia 2016; March-Vila et al. 2017), and molecular networking (Quinn et al. 2017) can identify novel chemicals or off-target effects. Metabolic modeling can facilitate antibiotic and cancer drug discovery (Blais et al. 2017; Folger et al. 2011). High-throughput gene expression and proteomics datasets have allowed for comprehensive and unbiased target identification and adverse effect prediction (Hu and Agarwal 2009; Guney et al. 2016; Vanhaelen et al. 2017).

While these approaches have many benefits, with the exception of metabolic modeling, they cannot predict context-dependent drug action. To translate the benefits of metabolic modeling to other signaling pathways, it's necessary to use a large-scale signaling model to predict how a drug affects the outcome of interest in the context of different stimuli.

In this study we developed an *in silico* pipeline that utilizes DrugBank, a repository of drug target and use information, and a model of fibroblast signaling to predict how 114 drugs with targets in the fibroblast network affect cardiac fibroblast phenotype in a variety of disease contexts. Targeting fibroblast signaling is an ideal application for *in silico* drug screening as there are no current therapies specifically meant to reverse fibrosis. The development of fibrosis is due to the interplay between inflammatory and growth factor signaling (Wynn 2008; Murtha et al. 2017), so the use of a large-scale model of fibroblast signaling (A. C. Zeigler et al. 2016) allows for the investigation of drug action in complex signaling contexts. Therefore, we applied this pipeline to predict which drugs might limit or increase fibrosis development in different signaling contexts.

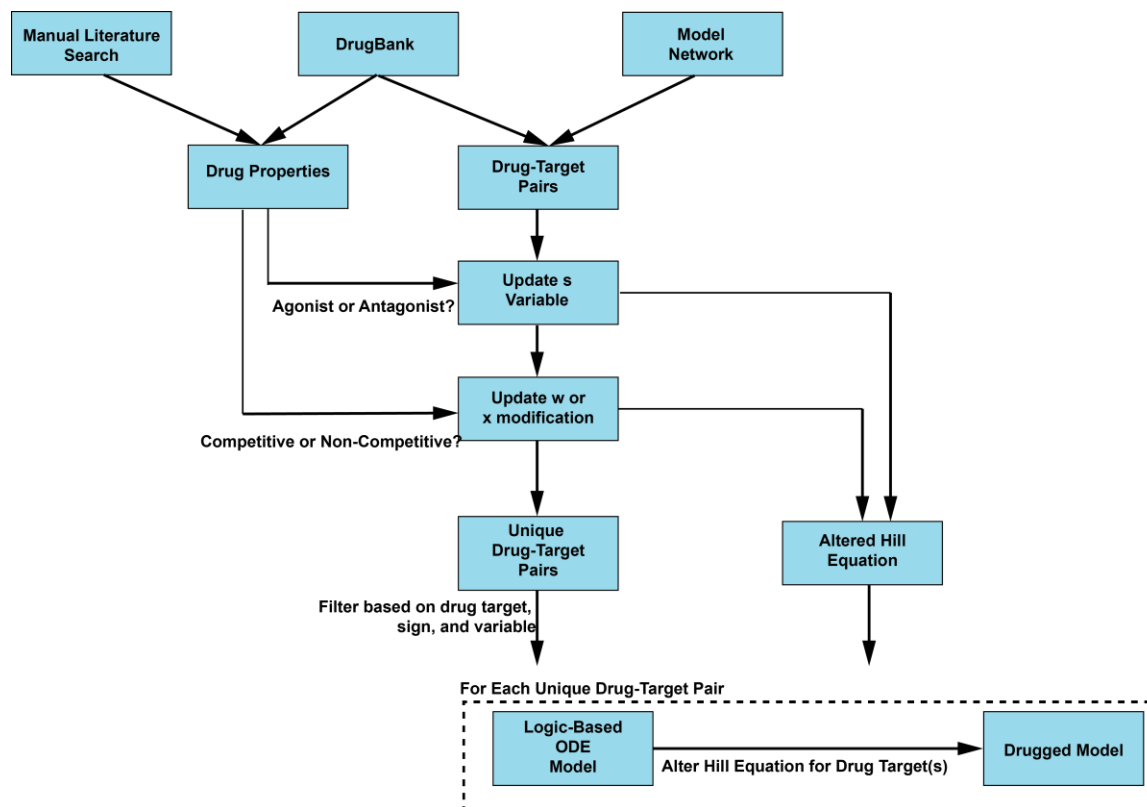


Figure 4.1: Drug screen pipeline schematic

4.3 Methods

Automation of pipeline

Figure 4.1 outlines the steps in the pipeline. First, the DrugBank database of FDA-approved drugs was downloaded (D. S. Wishart 2006; David S. Wishart et al. 2017). Then, the targets within the network were identified by matching the gene name of network members to the gene names of drug targets from DrugBank. Where a network node was associated with multiple genes, the drug was modeled as targeting the same node. The drug information for all drugs with a target within the network was compiled for use in generating parameters.

Modeling of specific drug properties

Whether the drug is an antagonist or agonist is pulled from the DrugBank database. A drug is labeled as competitive or non-competitive based on manual literature search. Biologically, drugs affect interactions downstream of the drug target. However, for drug simulations, the incoming interactions to the drug target node are modified to allow for predictions of drug target activity that is not muddled by cross talk that might affect nodes downstream of the target.

The signaling model utilizes a logic-based ODE approach (Kraeutler, Soltis, and Saucerman 2010), where each network interaction is modeled using a normalized Hill equation. An example of a simple activation interaction (associated with node C in the toy model) is shown in equation 4.1.

Equation 4.1:

$$\frac{dC}{dt} = \frac{1}{\tau_D} (w_{AC} * f_{act}(A) * C_{max} - C)$$

$$f_{act}(A) = \frac{BA^n}{K^n + A^n} \quad B = \frac{EC_{50}^n - 1}{2 * EC_{50}^n - 1}$$

Drugs are simulated through modifications of the normalized hill equation as shown in equation 4.2 (competitive) and equation 4.3 (non-competitive) for modification of the A->C interaction in the toy model (see Fig. 4.1).

Equation 4.2:

$$A_{drug} = A + s * d$$

Equation 4.3:

$$w_{drug} = w * (1 - s * d)$$

Where $s = +1$ for antagonists and $s = -1$ for agonists. The d variable indicates the dose of the drug, which must be between 0 and 0.6 for the normalized Hill equation. Unless otherwise indicated, the drug is classified as competitive or non-competitive based on literature curation.

Modeling drug application in simple contexts

To provide an example application of the drug simulation pipeline the fibroblast signaling model was used to predict candidate drug effects on fibroblast phenotype in signaling contexts characteristic of different cardiac stressors (MI, renal failure, heart failure). As outlined in chapter 3, the control input stimulation to the fibroblast model is 0.1 for all inputs except mechanical stimulation, which is set to 0.725. To simulate constant application of a new

stimulus, stimulus-associated inputs were set to 0.5. Then, each drug was simulated individually, with the simulation run out to steady state ($t = 500$ hours).

Modeling drug application in dynamic wound healing

To model how drugs would affect a dynamic wound-healing process, the same idealized input curves developed in chapter 3 were used.

4.4 Results

4.4.1 Simulation of competitive and non-competitive drugs in logic-based ODE model

We simulated application of competitive or non-competitive drugs to different interactions in a toy model (Fig. 4.2) in order to demonstrate how drugs with different action can be modeled. In each simulation we modeled stimulation with increasing doses of activator (either A or B) for 100 hours out to steady state. Modification of interactions with different logic is predicted to affect the target differently. For example, drugging a node that is part of a feed-forward (D) is less effective than drugging a node with a single activator (C).

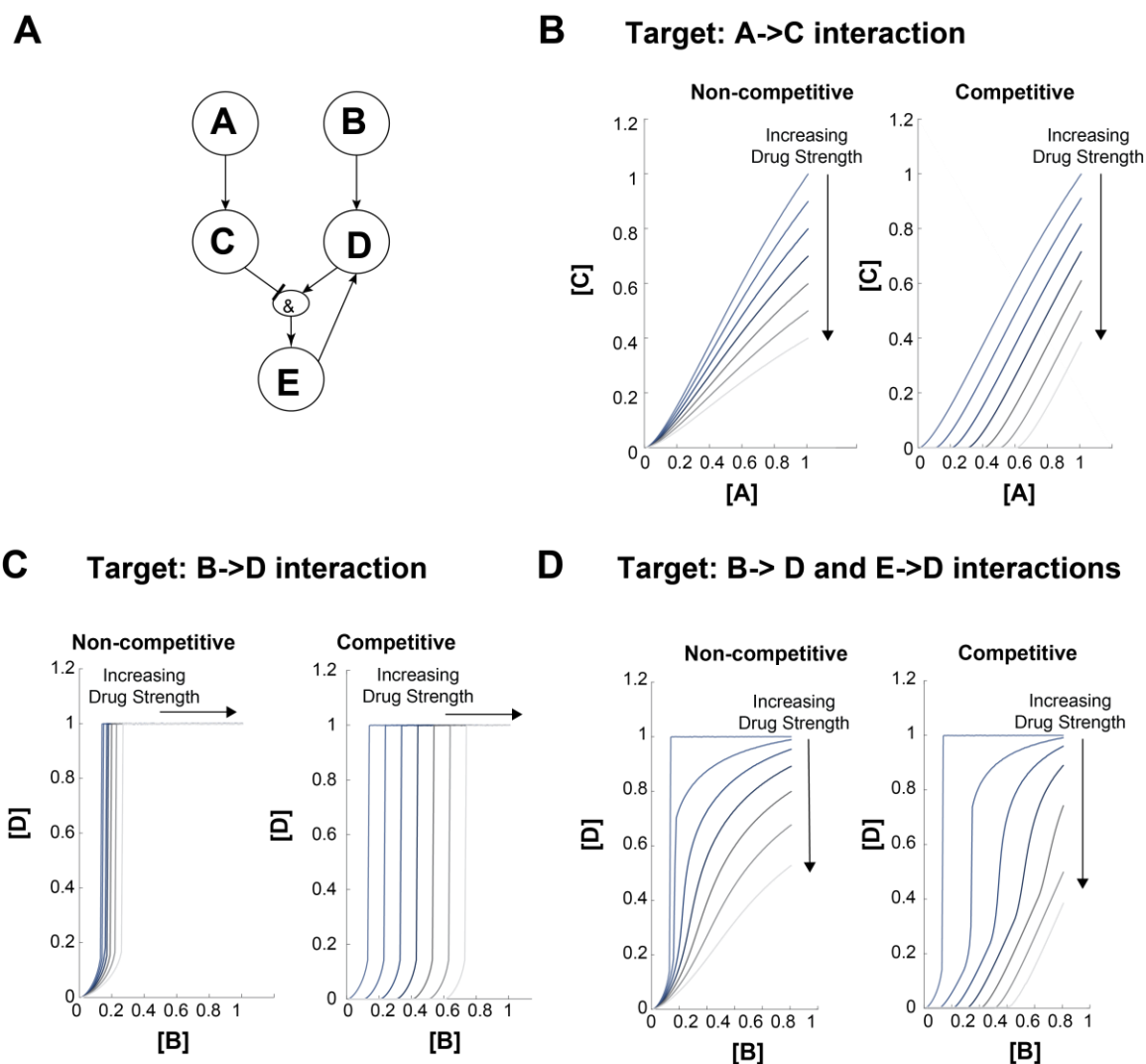


Figure 4.2: Effect of competitive or non-competitive inhibitors on interactions of different topologies. The toy model (A) was used to determine the effect of the competitive and non-competitive modeling approach on interactions with different logic. The effect of inhibiting the only activator of a node (B), one of two activators of a node (C) or all activators of a node (D). Strength of the drug simulated increases as the color goes from blue to light gray.

4.4.2 Identifying drugs with targets in the fibroblast network

The FDA-approved drug database and the drug naming database were downloaded from

DrugBank(D. S. Wishart 2006; David S. Wishart et al. 2017). The gene names associated with

each node in fibroblast signaling network (A. C. Zeigler et al. 2016) (see Appendix A) were used to search for all FDA-approved drugs with targets among the network members. After these drugs were identified, they were classified as an agonist or antagonist using the DrugBank database. If this information was not available, the drug was classified as an antagonist by default due to the fact that a majority of drugs in the database are antagonists. Each drug was then classified as a “non-competitive” or “competitive” drug through manual curation. The unique drug-target combinations are summarized in Table 4.1. The full list of drugs with a network target is shown in Table C.1.

Table 4.1: Unique drug-target pairs. Example drug shown is the first drug in an alphabetic list of all drugs with the same target, sign and action.

Node Name	Gene Name	Example Drug	Drug Sign	Drug Action
AT1R	ACTR1	Azilsartan medoxomil'	'antagonist'	'Competitive'
ACE	ACE	Benazepril'	'antagonist'	'Competitive'
ET1	'EDNRA'	'Ambrisentan'	'antagonist'	'Competitive'
BAR	ADRB1	'Acebutolol'	'agonist'	'Competitive'
BAR	ADRB1	'Alprenolol'	'antagonist'	'Competitive'
PDGFR	'PDGFRA'	'Becaplemin'	'None'	'Non-Competitive'
PDGFR	'PDGFRA'	'Pazopanib'	'antagonist'	'Non-Competitive'
NPRA	NPR1	'Amyl Nitrite'	'agonist'	'Competitive'
B1int	ITGB1	'Anti-thymocyte Globulin (Rabbit)'	'None'	'Non-Competitive'
IL6	IL6	'Siltuximab'	'antagonist'	'Non-Competitive'
IL1	IL1B	'Canakinumab'	'antagonist'	'Non-Competitive'
IL1RI	IL1R1	'Anakinra'	'antagonist'	'Competitive'
TNFa	TNF	'Adalimumab'	'antagonist'	'Non-Competitive'
NFKB	NFKB1	'Triflusal'	'antagonist'	'Non-Competitive'
abl	ABL1	'Bosutinib'	'antagonist'	'Non-Competitive'
abl	ABL1	'Dasatinib'	'None'	'Non-Competitive'
Raf	RAF1	'Dabrafenib'	'antagonist'	'Non-Competitive'
MEK1	MAP2K1	'Cobimetinib'	'antagonist'	'Competitive'
EDAFN, FN	FN1	'Ocriplasmin'	'antagonist'	'Non-Competitive'
PAI1	'SERPINE1'	'Urokinase'	'None'	'Non-Competitive'
MMP9	MMP9	'Glucosamine'	'antagonist'	'Non-Competitive'
ERK, AP1	'MAPK1; MAPK3; FOS; JUN; '	'Arsenic trioxide'	'agonist'	'Non-Competitive'
MMP1; MMP2; MMP9; MMP14;'	MMP1; MMP2; MMP9; MMP14;'	'Marimastat'	'antagonist'	'Non-Competitive'
PDGFR, abl, Raf	'PDGFRA; PDGFRB; ABL1; ABL2; RAF1; '	'Regorafenib'	'antagonist'	'Non-competitive'
PDGFR, Raf	'PDGFRA; PDGFRB; RAF1; '	'Sorafenib'	'antagonist'	'Non-competitive'
TNFa, NFKB	TNF; NFKB1;'	'Thalidomide'	'antagonist'	'Non-Competitive'

4.4.3 Predicting the effect of drug simulation on drug target

Each of the drugs in Table 4.1 was simulated using the fibroblast model where all inputs were set to 0.5. This equal stimulation of all pathways to 50% allows for the differentiation between agonists and antagonists. The drugs were modeled as competitive or non-competitive according to Table 4.1. The activity of the drug target was predicted at steady state (Fig. 4.3). Because it was demonstrated in Fig 4.2 that competitive and non-competitive drugs are predicted to have a different effect on target activity, we show in Fig 4.4 that this is true in the context of a larger network.

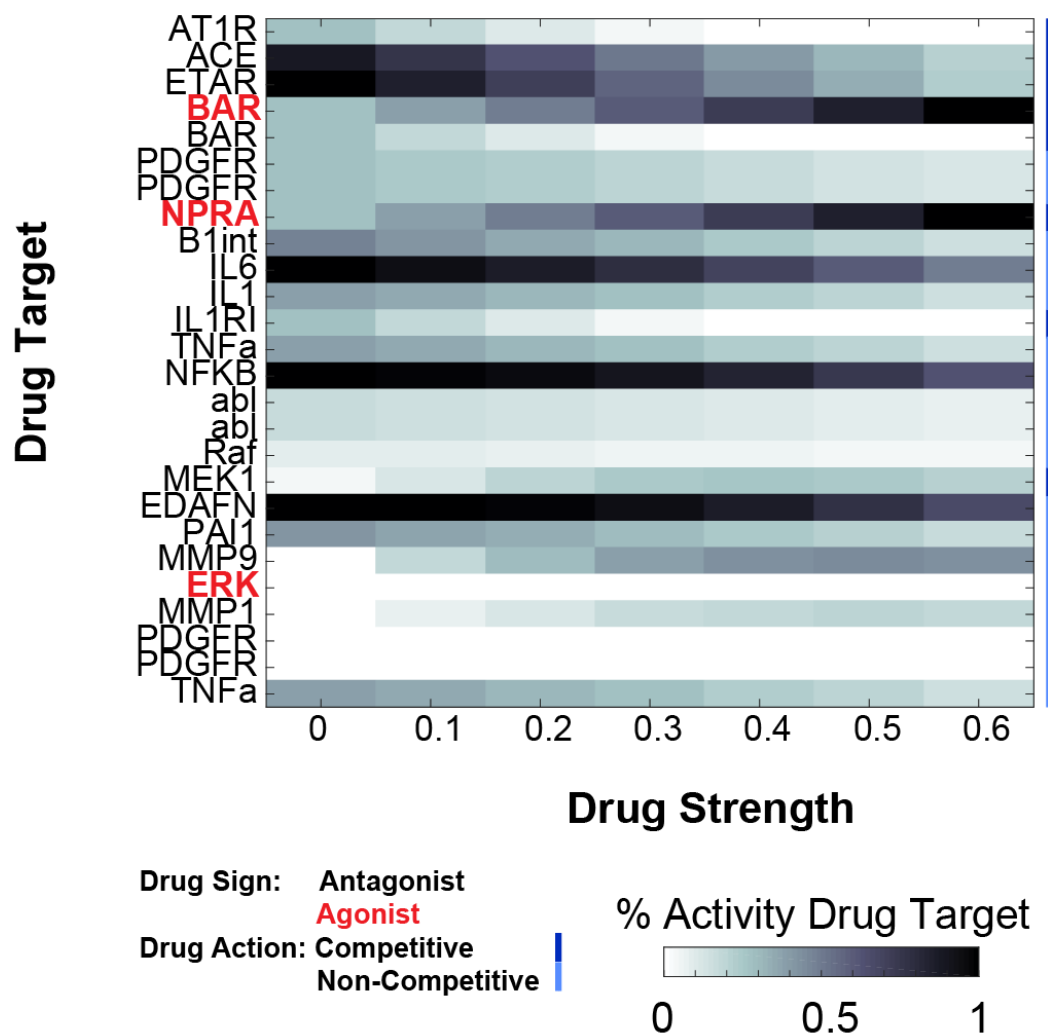


Figure 4.3: Effect of increasing drug strength on activity of drug target. Shown is the effect of each drug in Table 1 on the fibroblast network when all inputs are set to 0.5. For increasing drug dose, there is an increased effect on the drug target. In the case of multiple targets, one example target from each drug-target pair is shown.

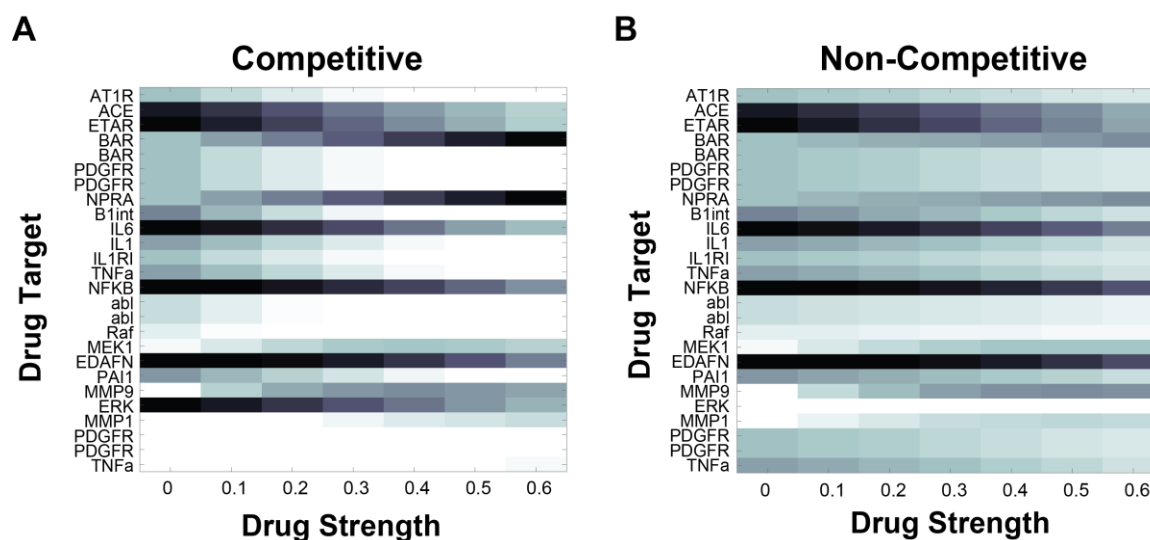


Figure 4.4: Effect of competitive vs. non-competitive modeling of increasing drug strength on drug target. Simulations were performed as in Figure 3 with all drugs simulated as either competitive (A) or non-competitive (B).

4.4.4 Context-Dependent drug simulations

As mentioned above, the benefit of using an *in silico* model for drug screening is the ability to quickly screen for drug efficacy in a variety of contexts. In order to investigate the context-dependent role for the drugs in Table 4.1, we performed the drug screen in simulations with each single input raised to 0.5 and in simulations where inputs representative of the inflammatory phase post-MI (IL1+IL6) the proliferative phase post-MI (TGF β +NP), renal failure (AngII+NP) and heart failure (AngII+NE) were raised to 0.5 (Herskowitz et al. 1995; A Deten et al. 2001; Alexander Deten et al. 2002; White et al. 2001; Haug et al. 1994; L. Zhou and Liu 2016; Matsubara 1998; Wei et al. 2016). The results of these simulations are shown in Figure 4.5. Both the drug target and collagen I mRNA have a context-dependent response to drug application. For example, many drugs are predicted to have the same effect on Collagen I mRNA in the

context of either TGF β or ET1 stimulation. One notable exception to this is Situximab which is predicted to decrease Collagen I mRNA with TGF β stimulus and increase it with ET1 stimulus.

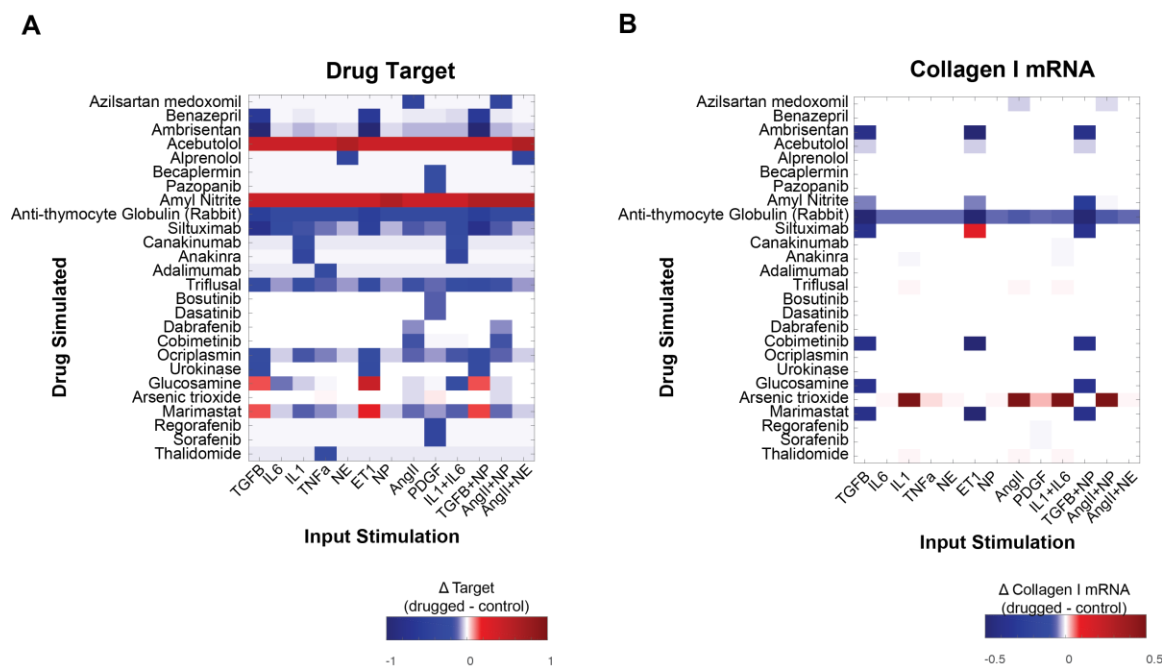


Figure 4.5: Drug effect in different contexts. Shown are the effects of simulating the drugs from Table 1 in the model stimulated with single or paired inputs. All drugs are modeled as competitive or non-competitive based on their true action.

These drugs were then applied to a dynamic post-MI simulation as defined in chapter 3. The effect of each drug on collagen I mRNA and proliferation was predicted at times representative of pre-infarct (0 day), inflammatory (1 day), proliferation (7 day) and mature (42 day) time points post-MI (Figure 4.6). Notably, some drugs have context-dependent activity such as canakinumab which is predicted to decrease collagen I mRNA and fibroblast proliferation only during early (day 1) healing. Specific drugs were predicted to increase collagen (arsenic trioxide), decrease collagen (anti-thymocyte globulin), and increase collagen only in the early phases of healing (triflusal). These drugs were then simulated in more detail. Alterations in full

collagen I mRNA dynamics in response to these drugs are shown in Figure 4.7. Then, the tissue level model (as described in chapter 3) was used to predict collagen area fraction. As shown in Figure 4.7. Arsenic trioxide is predicted to increase fibrosis, anti-thymocyte globulin is predicted to decrease collagen below control, and triflusal is predicted to raise collagen I area fraction without raising it above the range of experimental values.

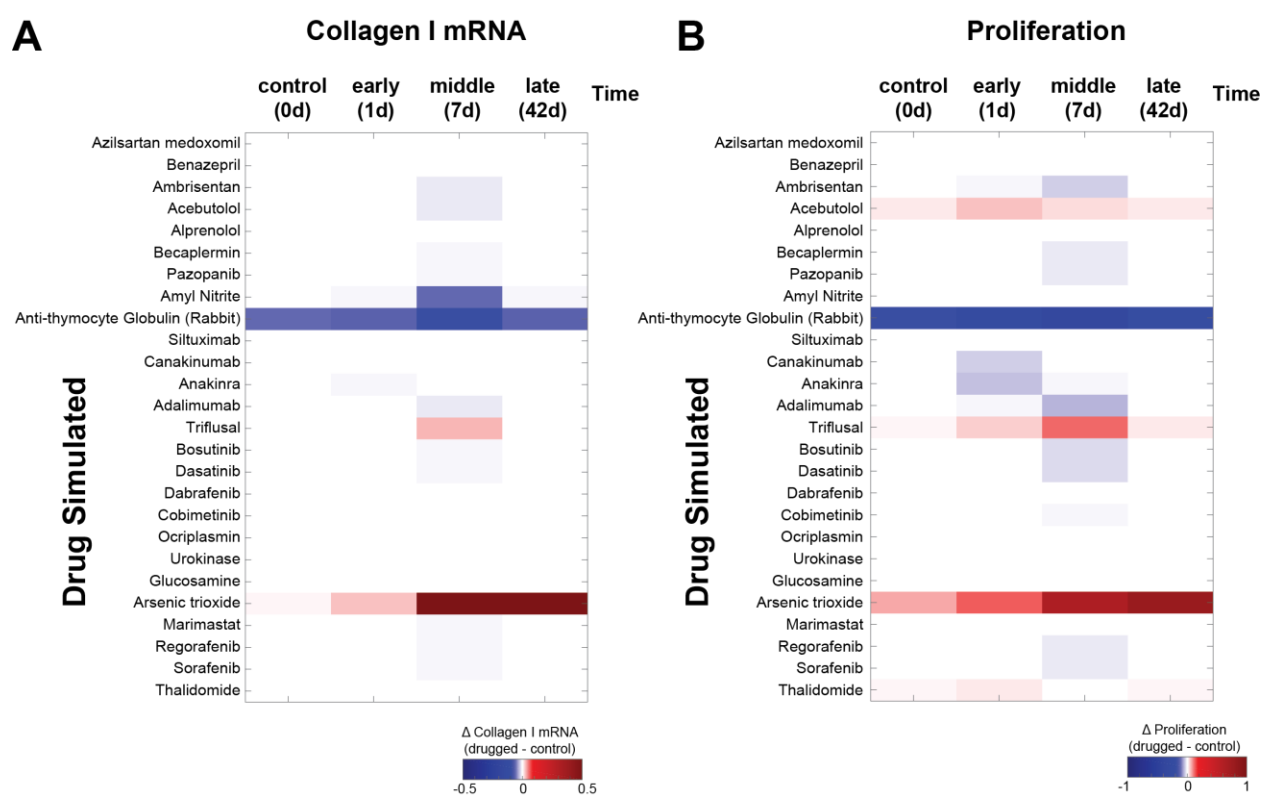


Figure 4.6: Post-MI dynamic drug simulations. Drug application was simulated with a dynamic input profile representative of post-MI wound healing. Drug effect on collagen and proliferation is shown at specific time points of interest.

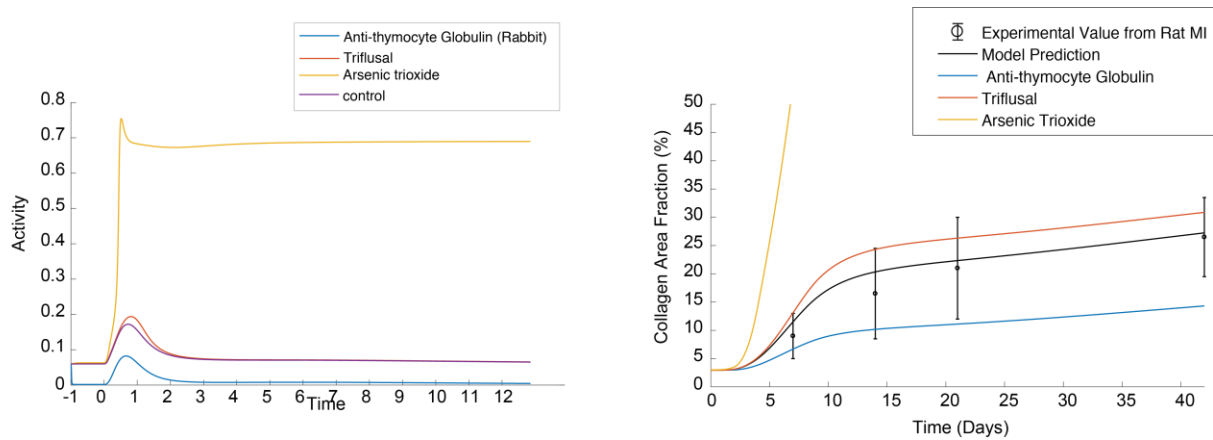


Figure 4.7: Effect of specific drugs on post-MI phenotype. The predicted dynamics of collagen I mRNA (A) and collagen area fraction (B) with no drug (control) or with representative drugs with post-MI inputs.

4.5 Discussion

In this study we developed a pipeline for high-throughput *in silico* drug screening and applied it to identify potentially anti- or pro-fibrotic drugs. Specifically, we predicted the role of certain drugs in affecting fibroblast phenotype in different contexts including dynamic wound healing post-MI. We predicted two drugs would have a detrimental effect on MI wound healing (arsenic trioxide and antithymocyte globulin) and one drug that might improve healing (triflusal).

Putative effect of drugs on cardiac fibroblast biology

Arsenic trioxide was predicted to increase risk of fibrosis by stimulating sustained collagen I mRNA expression in the post-MI context. It was also predicted to be pro-fibrotic in a variety of sustained single-input conditions. Although arsenic trioxide was shown to have a TGF β -blocking and anti-fibrotic effect *in vitro* in human pulmonary fibroblasts (Luo et al. 2014), this

drug was shown to be pro-fibrotic in guinea pig hearts(Chu et al. 2012) and to cause QT prolongation (a marker of cardiac fibrosis) in cancer patients (Soignet et al. 2001; Yeh and Bickford 2009). This could be a prediction that is specific to cardiac fibroblasts - again highlighting the benefit of using a manually curated model specific to the biologic question.

In contrast, anti-thymocyte globulin was predicted to decrease collagen I mRNA even pre-infarct. Therefore, the model predicts this drug will decrease collagen area fraction in response to post-MI signaling, and this indicates an increased risk for dilation and wall rupture(Frantz et al. 2008). Anti-thymocyte globulin has successfully reduced dermal fibrosis in patients with systemic sclerosis(Nash et al. 2007). Future studies will be needed to determine whether this applies to cardiac fibroblasts as well.

Finally, triflusal is predicted to increase the height of the transient collagen I expression in post-MI healing while only slightly increasing collagen area fraction. This could be an ideal drug for increasing the patency of a scar during healing without increasing the risk for fibrosis. Triflusal has been used as an anti-coagulant post-MI to prevent secondary vascular events, and has been shown to decrease mortality rates in that setting (Bover et al. 2009; Cruz-Fernández et al. 2000; J. Costa et al. 2006). Triflusal also has been shown to inhibit pressure-induced cardiac hypertrophy by blocking NFκB signaling in cardiomyocytes (Planavila et al. 2006). Further studies will be needed to determine the effect of triflusal in cardiac fibroblasts, but the data is promising in that this drug could improve post-MI healing and reduce the risk of pathologic cardiac remodeling.

Generalizable drug screening method

This study presents a method for high-throughput *in silico* drug screening with a manually curated signaling model. This method could be applied to any Hill ODE-based signaling model to determine the effect of any drug in the DrugBank database on any signaling model. Therefore, this method could be generalized to determine a drug's effect on multiple organs.

4.6 Conclusion

In this chapter, I outlined a novel pipeline for incorporating drug information from DrugBank into a large-scale computational model of fibroblast signaling to perform an *in silico* screen for drugs that affect cardiac fibroblast phenotype. The context-dependent action of drugs was predicted for both drug targets and the major outcome of interest, collagen I mRNA. We identified two drugs that are likely to increase the risk of pathological post-MI healing (arsenic trioxide and anti-thymocyte globulin), and we predicted that triflusal could improve post-MI healing and limit the risk of both wall rupture and fibrosis. Future studies can experimentally validate these predictions and use this approach to predict how network topology, drug action, and drug dose affect drug efficacy.

Chapter 5

Comparisons between cultured primary fibroblasts

Author Contribution: Angela Zeigler, Kellen Chen (isolated adult cardiac fibroblasts), Laura Woo (editing text), Jeffrey Holmes (experimental design), Jennifer Munson (experimental design), Jeffrey Saucerman (experimental design).

5.1 Foreword

In chapters 2, 3, and 4 we used a computational model of fibroblast signaling to generate testable hypotheses regarding the context-dependent regulation of cardiac fibroblast phenotype. We predicted in chapter 4 that triflusal might increase collagen I mRNA expression in IL1- or TGF β -treated fibroblasts but not in untreated fibroblasts. We also predicted that IL1, like mechanical signaling in chapter 2, activates the TGF β pathway and thereby induces a pro-fibrotic phenotype. It was my goal to validate both of these predictions using cultured rat cardiac fibroblasts or human cardiac fibroblasts. This project, however, faced many obstacles, as fibroblast phenotype is highly variable and experiment-to-experiment variability as well as challenges related to measuring collagen in 3D hydrogels led to many unsuccessful experiments. However, there is always something to be learned from experimental investigation. Therefore, in this chapter, I outline a few of the observations made during these preliminary experiments. To my knowledge, there is no previously published head-to-head comparison of cultured human dermal and human ventricular fibroblasts, so this study provides some unique characterization of these cells.

5.2 Introduction

Studying what modulates fibroblast phenotype is important because fibroblasts (or a fibroblast-like cell type) are present in all organs, and these cells preserve the normal function of a tissue by facilitating stress sensing and response, wound healing, development, and maintenance of the extracellular matrix (ECM) (Squires et al. 2005; Palatinus, Rhett, and Gourdie 2010; Murtha et al. 2017; Rinn et al. 2006). Fibroblasts can participate in so many functions because they are a

highly plastic cell type, capable of adopting very different phenotypes depending on the signaling environment (Rinn et al. 2006). Therefore, it can be difficult to identify which pathways are dysregulated when fibroblasts adopt a pathological phenotype that leads to fibrosis. This thesis has developed a computational model of cardiac fibroblast signaling for studying fibroblast-specific responses to complex signaling environments with the goal of understanding which pathways or signaling nodes are driving fibroblast phenotype. As shown in chapters 1-4, this computational studies are useful for generating hypotheses that can ultimately be tested experimentally in cardiac fibroblasts.

In vitro experimentation is ideal for studying cell-specific responses, as you can isolate a cell of interest from other cell types or environmental effects such as genetic differences or variance in microbiota. However, fibroblasts are notoriously difficult to study *in vitro* due to their sensitivity to mechanical stiffness, which is supra-physiological (~10,000x tissue stiffness) on 2D tissue culture plates (Sadeghi et al. 2017; Huan Wang et al. 2012; Benton, Fairbanks, and Anseth 2009; Huang et al. 2012). This study outlines some organ-specific fibroblast characteristics that were identified in preliminary validation studies. Specifically, we show that α SMA expression is more dependent on cell type and stiffness of culture substrate than on chemical stimuli. However, we show that other aspects of myofibroblast phenotype such as increased collagen production and contraction of fibroblasts are not always directly related to α SMA expression. Increased collagen expression and contraction are hallmarks of myofibroblasts *in vivo* (Van Den Borne et al. 2010; N. A. Turner and Porter 2013; Grinnell 1994), and therefore should potentially be used as more reliable indicators of functional myofibroblast differentiation. Furthermore, we show that TGF β -dependent increases in collagen production can be observed using picrosirius staining in 2D culture conditions, despite the fact

that the fibroblasts are likely differentiated at baseline in this condition and already producing high levels of collagen. Finally, we show that fibroblasts from different organs respond differently to the same stimuli, which is not fully captured by computational model predictions (chapters 2 and 3). These observations indicate further study is needed to fully understand the mechanism by which dermal and ventricular fibroblasts respond differently to IL1 and mechanical stimuli.

5.3 Methods

Adult rat cardiac fibroblasts

Adult rat cardiac fibroblasts were isolated and cultured as previously published (Thomopoulos, Fomovsky, and Holmes 2005). Briefly, Sprague-Dawley rats (6 weeks old, ~ 200g) were sacrificed and the ventricles removed, minced into ~1 mm pieces, and digested using Liberase Blendzyme 3 (Roche, Indianapolis, IN). Successive digestions were centrifuged for 10 min at 400x g and cells were resuspended into culture medium containing Dulbecco's modified Eagle medium (Sigma-Aldrich, St. Louis, MO) with 10% fetal bovine serum (FBS, Atlanta Biologicals, Flowery Branch, GA), 100 U/mL penicillin, 100 g/mL streptomycin, and 2 ng/mL amphotericin B (all Sigma-Aldrich). After incubating in culture flasks for 4 hrs at 37° C and 5% CO₂, flasks were rinsed with phosphate-buffered saline (PBS, Sigma-Aldrich) to remove nonadherent cells, and resupplied with culture medium.

Human dermal fibroblasts

Human foreskin fibroblasts were purchased from ATCC and grown on culture flasks in dermal media containing Dulbecco's modified Eagle medium (Sigma-Aldrich, St. Louis, MO) with 10% fetal bovine serum (FBS, Atlanta Biologicals, Flowery Branch, GA) except when indicated as serum free. These cells were used from passages 4-7.

Human cardiac fibroblasts

Human ventricular fibroblasts were purchased from PromoCell and grown on culture flasks in Fibroblast Growth Medium 3 (PromoCell) containing 10% fetal calf serum (except when indicated as serum free), 1ng/mL recombinant human basic fibroblast growth factor and 5ug/mL recombinant human insulin (all components from PromoCell). Cells were used within passages 4-8.

Treatments

Cells are treated with 1-50ng/mL transforming growth factor beta (TGF β , Cell Signaling Technology), 1-50ng/mL interleukin 1 (IL1, Cell Signaling), 1-50ng/mL interleukin 6 (IL6, Cell Signaling), 1-50ng/mL tumor necrosis factor alpha (TNF α , Cell Signaling).

2D imaging of alpha smooth muscle actin

In order to determine the extent of myofibroblast differentiation, alpha smooth muscle actin (aSMA) was measured using immunofluorescence. Cells were cultured for 2 days on

CellBIND® 96 well plates (Corning). Cells were fixed for 15 minutes in 4% paraformaldehyde (Sigma-Aldrich), and washed 3x with PBS; cells were then permeabilized in 0.05% TritonX (Sigma-Aldrich) in 1% BSA for 30 minutes. Then, samples were stained with monoclonal anti-alpha smooth muscle actin (Sigma-Aldrich) overnight at 4 degrees Celsius, washed 3x with PBS, stained with 4',6-diamidino-2-phenylindole, dihydrochloride (DAPI, Life Technologies, Carlsbad, CA) for 10 minutes, and washed again 3x with PBS. PBS was removed and gels were imaged on an Olympus IX81 inverted microscope with a 10x UPlanSApo 0.40 NA objective (Olympus, Center Valley, PA) and a C9300 cooled CCD digital camera (Hamamatsu, Bridgewater, NJ). An 800 µm x 600 µm area in the central region of every gel was scanned.

3D imaging of alpha smooth muscle actin in adult rat cardiac fibroblasts

Similarly, the differentiation state of fibroblasts in 3D gels was determined by measuring αSMA amount using immunofluorescence (IF). After 7 days of culture following the isolation, fibroblasts were removed from flasks with 0.25% Trypsin-EDTA (Sigma-Aldrich), and seeded into 3D collagen gels as previously published (Thomopoulos, Fomovsky, and Holmes 2005). Briefly, 0.2 M HEPES (Sigma-Aldrich), 10X MEM (Sigma-Aldrich), 3 mg/mL type I bovine collagen (PureCol, Advanced Biomatrix, San Diego, CA) and cells were resuspended in low-serum culture medium (1% FBS) at respective ratios of 1:1:8:2 to yield a final collagen concentration of 2 mg/mL and final cell concentrations of 200k cells/mL. Gels were plated at 500µL of gel per well in 48 well plate.

Gels were fixed overnight in 4% paraformaldehyde (Sigma-Aldrich), and washed 3x with PBS; cells were then permeabilized overnight, stained with monoclonal anti- alpha smooth

muscle actin overnight, washed 3x with PBS, stained with DAPI for 20 minutes and washed again 3x with PBS. Then gels were imaged as described for 2D imaging.

3D imaging of alpha smooth muscle actin in human primary fibroblasts

Primary fibroblasts at passage 5-8 were trypsinized and seeded into 3D collagen gels with a final collagen concentration of 1.8 mg/mL and a final cell concentration of ~75,000 cells/well for human dermal and ~50,000 cells/well for human ventricular. Gels were made using 10x PBS, deionized sterile water, 1N NaOH, rat tail collagen I (Corning), serum free media, matrigel at 0.5mg/mL, and ~50k cells per gel. Gels were plated at 500uL of gel per well in 48-well tissue culture treated plate (Olympus Plastics) and treated for 24 hours. Gels were fixed and stained as described above for 3D gels. Gels were imaged on an EVOS XL cell imaging system (ThermoFisher).

3D contraction of hydrogels

Another metric for determining fibroblast differentiation is to measure the contractile capability of a fibroblast. For these experiments primary fibroblasts were seeded into a collagen hydrogel as described above. The gels were treated for 24 hours in serum free media and then were transferred to a new 48 well plate in 10% serum media and allowed to contract for 6 hours. Images were taken from a set height using a ring stand. Contraction was measured in FIJI (Schindelin nature methods 2012) by freeform tracing the base of the well and the rim of the gel

in order to remove artifact from slight differences in the camera angle, and contraction was calculated by taking the area of the gel / area of the well.

2D picrosirius assay

In order to measure collagen production, we adapted a tissue picrosirius staining protocol to a 2D *in vitro* setting. In these experiments primary human fibroblasts are plated on a 24 well plate and treated in media with 250uM ascorbic acid and 100U/mL penicillin/streptomycin for 72 hours. All treatment media was serum free except for serum treatment which was 10% serum. Collagen standards were made by plating 1, 5, 10, 20, or 50ug rat tail collagen on 96 well assay plate in triplicate and allowed to dry in a cell culture hood or oven. Then, cells were fixed and the cell plate and standard were stained with picrosirius red for 1 hour. Stained plates were washed 4x with 5% acetic acid and 1x with de-ionized water to dilute any residual acid, then the plates were de-stained with 200uL 0.1M NaOH for 30 minutes until all stain was dissolved. De-stained base wash was transferred to a fresh assay plate and read using a plate reader at 550nm. All collagen measurements are shown as fold change from control.

Statistics

All primary human fibroblasts were used from the same lot of human dermal or human ventricular cells, but for each measurement at least one experiment was performed with cells thawed from a different vial. For each experiment, the cells were divided into three gels per

condition, and the experiments were independently performed a total of 4 times for an N = 4 replicates across all experimental conditions. We performed a two-tailed students t-test to compare each condition to the untreated control. Statistical significance was set at $p < 0.05$.

5.4 Results

5.4.1 Alpha smooth muscle actin levels in different cell culture conditions and fibroblast types

We aimed to use α SMA levels in rat and human fibroblasts as a measure of myofibroblast differentiation (Willems et al. 1994; Squires et al. 2005; Huan Wang et al. 2012) in order to experimentally validate model predictions. As has been previously shown (Sadeghi et al. 2017; Huan Wang et al. 2012), culturing fibroblasts on a stiff 2D surface induces spontaneous differentiation (Fig. 5.1). However, when cultured in a 3D collagen hydrogel, we observed that rat cardiac fibroblasts, human dermal fibroblasts, and human ventricular fibroblasts do not exhibit spontaneous α SMA expression, which is consistent with previous findings (Huan Wang et al. 2012; Benton, Fairbanks, and Anseth 2009; Huang et al. 2012). Rat cardiac and human dermal fibroblasts have very low α SMA expression levels in untreated 3D control conditions (Fig. 5.1 and 5.2). Human ventricular fibroblasts have more baseline expression of α SMA (as shown in the untreated control in Fig. 5.2), but these levels are still lower than observed in rat cardiac fibroblasts in 2D culture (control condition, Fig. 5.1). Furthermore, primary fibroblasts cultured in 3D demonstrate no increase in α SMA expression with TGF β or serum (positive control) treatment (Fig. 5.1 and 5.2).

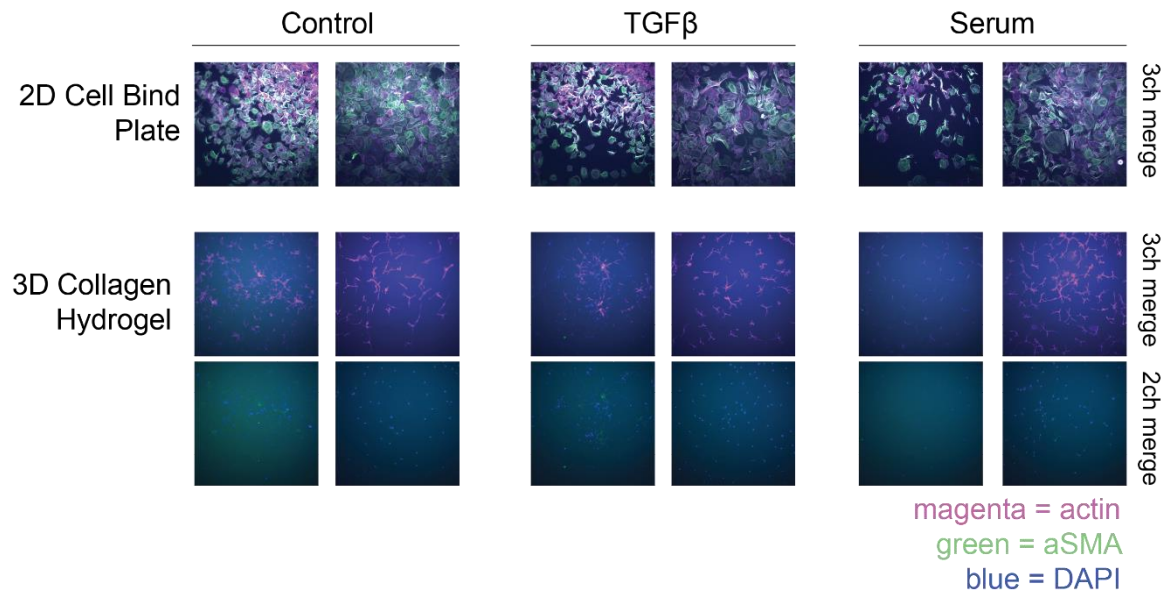


Figure 5.1: α SMA expression in adult rat cardiac fibroblasts in 2D and 3D culture. Adult rat cardiac fibroblasts were cultured for 48 hour on a cell bind 2D plate or in a 3D collagen hydrogel and stained as indicated in methods. Shown are representative experiments from two separate isolations. 2ch merge images show just the aSMA and DAPI stain for the image above.

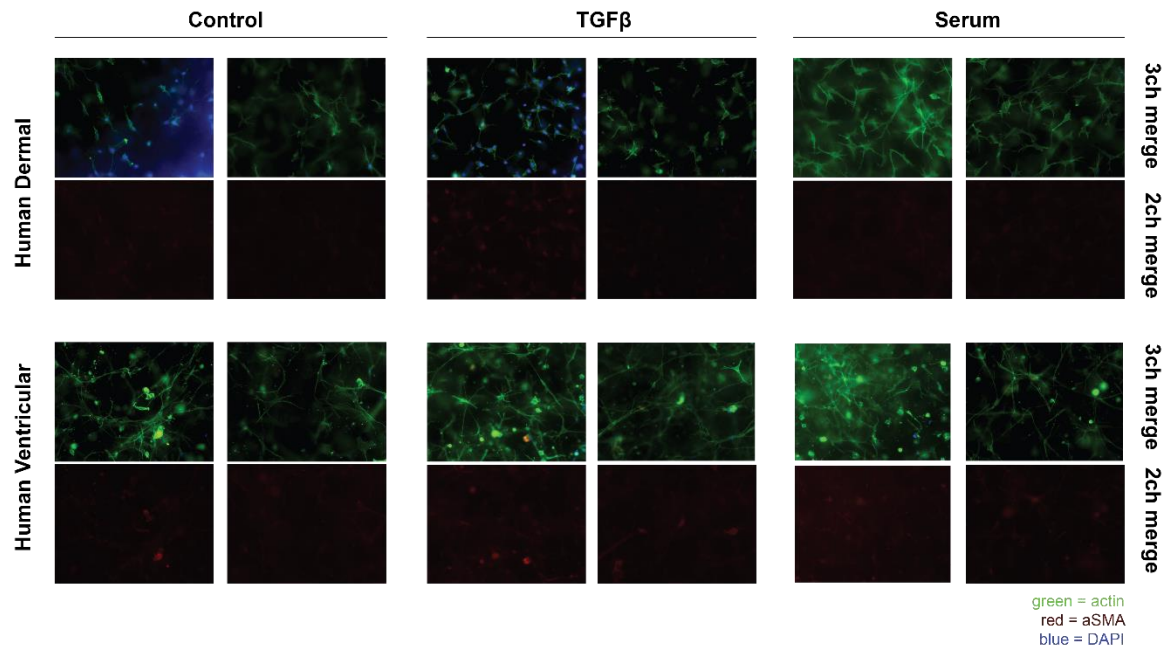


Figure 5.2: α SMA expression in human dermal and human ventricular fibroblasts. Human primary fibroblasts were cultured for 24 hours in a 3D collagen hydrogel, then allowed to contract for 6 hours in 10% FBS. Shown are representative images from two separate experiments. 2ch merge images show only aSMA stain for the image above.

5.4.2 Contractile properties of different fibroblast types

The contractile properties of human primary fibroblasts treated with TGF β and IL1 were tested (Fig. 5.3). The serum condition was meant as a positive control, but, while ventricular fibroblasts strongly increased contraction in response to 10% serum, dermal fibroblasts did not have a significant increase in contraction when treated with serum. This could be because dermal fibroblasts were treated with a different type of serum (as was recommended by the vendor), and serum is a highly variable mixture of signaling proteins. Human dermal fibroblasts were more responsive to both TGF β (increasing contraction) and IL1 (decreasing contraction) than the ventricular fibroblasts. Human ventricular fibroblasts were more contractile in the untreated control condition than human dermal fibroblasts (Table 5.1), which could explain the lack of a

response to TGF β or IL1. Although the difference shown is not statistically significant, experiments with human ventricular fibroblasts were performed at a lower density of cells because when seeded with 75,000 (as is done for experiments with dermal fibroblasts), gels were contracted down to 30% well area and no further contraction with the positive control (serum) was observed (Data not shown). Thus, under the same experimental conditions, ventricular cells are more contractile.

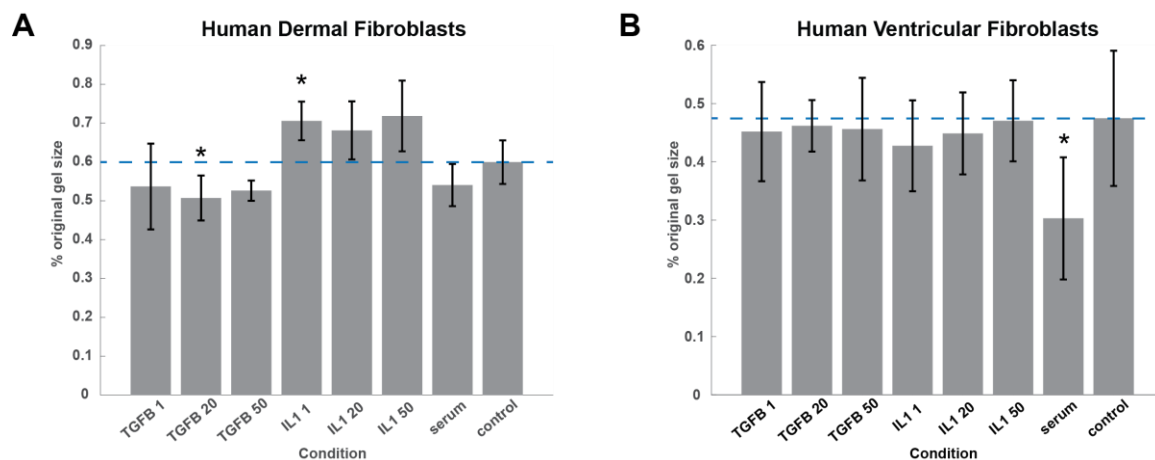


Figure 5.3: Contraction of human primary fibroblasts. Primary cells were seeded into a 3D collagen hydrogel and treated for 24 hours before being allowed to contract in full serum for 6 hours. 1 = 1ng/mL, 20 = 20ng/mL, 50ng/mL, serum = 10% FBS, control = 0% FBS. Error bars indicate standard deviation. n = 3 experiments of 3 gels

5.4.3 Collagen production from different fibroblast types

The collagen production by primary human fibroblasts was measured using a 2D picrosirius assay (Fig. 5.4). Both dermal and ventricular fibroblasts increase collagen production in response to the serum positive control and both cells have an approximately 20% increase in collagen following treatment with 20ng/mL TGF β . Previous studies have shown an $\sim 2x$ increase in collagen protein production by ventricular fibroblasts following treatment with TGF β as

measured by western (Kapoun et al. 2004) and H³-proline incorporation (Swaney et al. 2005). Ventricular fibroblasts increase collagen output in response to 20ng/mL IL1, but collagen production by dermal fibroblasts was not response to IL1. As with contraction, human ventricular fibroblasts had higher levels of collagen production in the untreated control than did human dermal fibroblasts (Table 5.1).

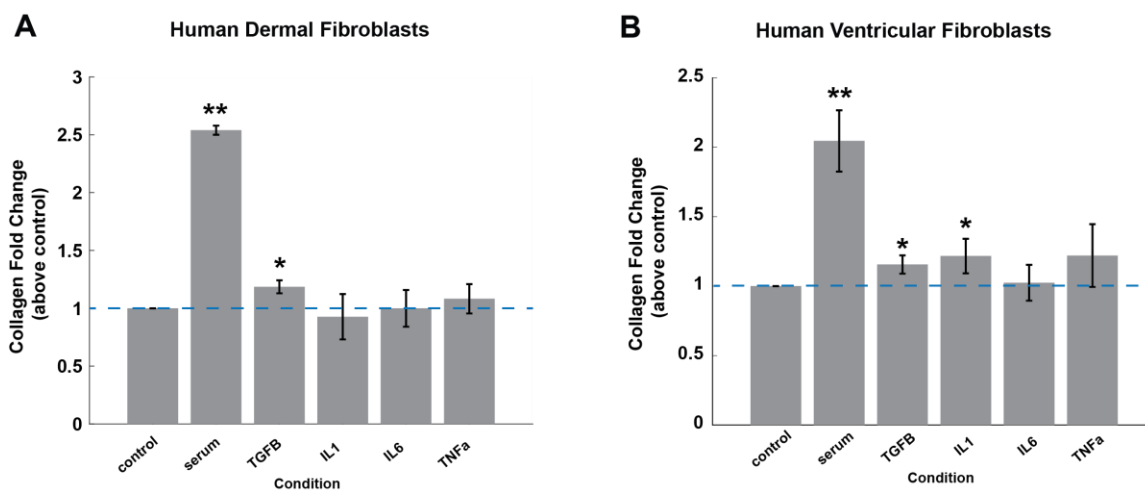


Figure 5.4: Collagen production by primary human fibroblasts. Human primary fibroblasts were treated for 72 hours on a 2D tissue culture treated plate, and collagen was measured using picrosirius stain. TGFβ, IL1, IL6, TNFα were used at a concentration of 20ng/mL. Error bars indicate standard deviation. *p<0.05, **p<0.01, n=3 experiments of 3 wells

5.5 Discussion

Fibroblasts from different organs

We show in this study that human dermal and ventricular fibroblasts have distinct phenotypes and respond differently to IL1 and TGF β as measured by both contraction and collagen production. This could partially be explained by the fact that these cells come from ATCC and PromoCell, respectively, and therefore would likely be isolated and frozen differently. However, it has been shown that fibroblasts from different organs have different properties (Rinn et al. 2006). If the results shown here are primarily due to the different source organ, then it can be concluded that ventricular fibroblasts express more α SMA and are more contractile at baseline. Furthermore, the morphology of untreated human ventricular fibroblasts has a more activated, “blown out”, appearance than either human dermal or rat cardiac fibroblasts; they have a larger cell body, higher actin content, and longer cell processes (see Fig. 5.2). Human ventricular fibroblasts also had higher baseline collagen production as is shown in Table 5.1. This activated phenotype at baseline could explain why these cells are unresponsive to further stimulation by TGF β when measured by either contraction or α SMA content.

The response to inflammatory versus growth factor stimuli is also different in human dermal and human ventricular fibroblasts. For example, IL1 increases collagen output in ventricular fibroblasts, but not in dermal fibroblasts. We previously predicted a role for IL1 in increasing collagen in ventricular fibroblasts (chapter 3), and IL1 has been shown to be pro-fibrotic in a cardiovascular setting (Hwang et al. 2001). But its role in regulating dermal fibroblasts is less clear. In dermal fibroblasts we observed that IL1 does not affect collagen output, but that IL1 decreases contraction in dermal fibroblasts. IL1 has been shown to decrease TGF β -induced upregulation of myofibroblast-like genes including α SMA (Koskela von Sydow et al. 2015), and this could explain how IL1 reduces contractility in dermal fibroblasts. The role

of IL1 in regulation of collagen is not fully consistent across studies. Although one *in vitro* study showed collagen expression decreased with IL1 stimulation in dermal fibroblasts (Mauviel et al. 1991), other studies have shown an increase in collagen expression by dermal fibroblasts when stimulated with IL1 (Kähäri, Heino, and Vuorio 1987; Duncan and Berman 1989; Artlett et al. 2017). Therefore, our lack of observed response could be due to the measurement technique. The picrosirius assay is likely less sensitive than PCR or H³ proline measurements (which could also explain why our observed collagen induction by TGFβ is slightly less than has been previously shown). IL1 is, in general, thought to be an anti-fibrotic, anti-myofibroblast stimulus in the skin (Guo and Dipietro 2010; Pereira et al. 2016; Werner and Grose 2003), but one study showed that IL1 knock out doesn't affect dermal wound healing (Graves et al. 2001). A lack of a strong response to IL1 by dermal fibroblasts could explain the general lack of consensus in the data. Further investigation into the organ-specific role of IL1 is needed to understand whether IL1 inducing treatment is a viable option for prevention of cardiac fibrosis post-MI (as indicated in chapter 4).

Fibroblasts versus Myofibroblasts

Alpha smooth muscle actin is typically used as a marker of myofibroblast differentiation both *in vitro* and *in vivo* (Willems et al. 1994; Squires et al. 2005; Huan Wang et al. 2012). We have shown in this study that fibroblasts cultured on a 2D surface express high levels of αSMA without treatment, which is consistent with previous finding (Huan Wang et al. 2012; Sadeghi et al. 2017). Fibroblasts cultured in 3D expressed lower levels of αSMA, but we found that αSMA levels do not significantly increase with TGFβ or full serum treatment in 3D. Therefore, is unclear whether αSMA levels are the best metric to determine whether a cell is a myofibroblast.

Human ventricular fibroblasts are both more contractile and have higher expression levels of α SMA. However, dermal fibroblasts in 3D do not increase α SMA levels in response to 10% serum or TGF β , but do become more contractile with those treatments. Therefore, it can be concluded that α SMA levels do not always correspond to a contractile phenotype in human primary fibroblasts. Additionally, as with rat ventricular fibroblasts (Figure 1), neither human dermal fibroblasts nor human ventricular fibroblasts significantly change α SMA expression in response to serum, TGF β , or IL1 when cultured on a 2D substrate (data not shown), but collagen production is altered in response to these stimuli. Thus, we conclude that collagen expression and α SMA expression do not always correlate. Further study, including the identification of other markers of myofibroblasts, are needed to fully understand how cytoskeletal protein expression, matrix alteration (e.g.: changes in EDAFN or periostin expression), contraction, and collagen production are related in fibroblasts versus myofibroblasts.

5.6 Conclusion

In this chapter we demonstrate that cultured primary human ventricular and human dermal fibroblasts have distinct phenotypes. Ventricular fibroblasts appear to be more active at baseline, which likely contributes to their differential response to IL1, TGF β , and serum. This study has a clear limitation in that these primary cells were purchased from different vendors and treated with different serum types. To have a more clear understanding of organ-specific differences in fibroblast phenotype, these experiments should be repeated with more consistent experimental conditions.

Chapter 6

Discussion and Conclusions

6.1 Global Aims

The goal of this dissertation was to understand how cardiac fibroblasts respond to complex or competing stimuli. In order to investigate fibroblast decision-making we aimed to use computational modeling and in vitro experimentation to develop testable hypotheses. In achieving this objective we have:

- Developed and validated a large-scale manually-curated computational model of cardiac fibroblast signaling
- Used the computational model to identify putative exogenous and endogenous regulators of the post-MI fibroblast phenotype.
- Developed a pipeline for high-throughput *in silico* drug simulation.
- Predicted the effect of FDA-approved drugs on fibroblast phenotype in signaling contexts related to cardiac diseases.
- Characterized differences in fibroblast phenotype from different species and organs.

6.1.1 Relationship between network topology and function

One benefit to having a large-scale computational model is that there are a variety of short (1-2 edge) and long (5+ edge) motifs in the signaling network. Therefore the function of a node within the model can be compared to the topology of the network around that node for many different topological characteristics. Although this manually curated network is necessarily smaller than many of the networks inferred from high-throughput datasets that have previously been used to link topology to function, this network is directed and can make predictions that are easier to match with a mechanistic function.

Previous studies have shown a relationship between local or network connectivity and essentiality of a gene (Yu et al. 2007; Jeong et al. 2001; Hahn and Kern 2005; Yu et al. 2004; Batada, Hurst, and Tyers 2006) However, this connection, while statistically significant, is often weak, and although essential genes are more likely to have high connectivity, topological metrics alone have failed to predict gene essentiality (Z. Wang and Zhang 2007; Batada, Hurst, and Tyers 2006; L. Yang et al. 2014). Machine learning approaches have incorporated cellular localization, gene expression, and biological function along with topological information to predict gene involvement in a phenotype (Acencio and Lemke 2009; P. R. Costa, Acencio, and Lemke 2010; L. Yang et al. 2014), and shown that topology alone is not as predictive as incorporating other characteristics. As shown in chapter 2, we found that the connectivity of the node does not completely determine the functional influence of the node over the entire network.

It has been hypothesized that degree correlates with essentiality due to an increased probability of connection to an essential gene or inclusion in a tightly connected module of essential genes (X. He and Zhang 2006; Zotenko et al. 2008). However, it is possible that other topological characteristics such as the location of a node in a pathway (upstream, cross-talk,

downstream), the logic of interactions upstream of a node, and the longer motifs in a pathway (e.g. autocrine loops) could have implications for function - especially when considering context-dependent function. The model developed in chapter 2 would be useful with other similar models to further investigate the role of more complex topological motifs in determining signal outcome particularly in different signaling contexts.

Beyond identifying essential nodes, this study has implications for drug efficacy. It has previously been shown that the topology of a pathway will determine whether knock down or competitive inhibition are more efficacious (Jensen, Moyer, and Janes 2016). In Chapter 4 we showed that in a toy model, having one versus two upstream activators changes the effect of the drug. Further studies will be needed to provide more comprehensive evidence of how specific topologies affect drug action.

6.1.2 Post-MI wound healing

As with wound healing in other organs, cardiac post-infarct healing involves the characteristic inflammatory, proliferative, and maturation phase. However, there is a wide variety in outcomes following a myocardial infarction, and some patients develop heart failure. Certainly, infarct size is a major predictor of pathologic remodeling (Pfeffer and Braunwald 1990), but the wound healing process itself can affect the resulting organ function (Dobaczewski et al. 2010; Hwang et al. 2001). Fibroblasts play a role throughout the time course of healing, and therefore are ideal for investigating how the entire healing process affects tissue composition (Fishbein, Maclean, and Maroko 1978).

The design of this post-MI study led us to the question, what is the ideal fibroblast phenotype for optimal infarct healing? This question has not been answered in full temporal detail. It has been shown that infarct expansion is more likely to occur within the first 24 hours (Richardson and Holmes 2015). Low collagen production early can contribute to dilation and rupture risk as the provisional scar is too weak to hold up against the high pressure in the ventricle (Hwang et al. 2001; Frantz et al. 2008). However, sustained or remote collagen production can result in fibrosis, which leads to diastolic dysfunction (Volders PG1, Willems IE, Cleutjens JP, Arends JW, Havenith MG 1993; Litwin et al. 1991; Beltrami et al. 1994). It has been hypothesized that the timing of collagen expression is an important determinant of the health of post-infarct cardiac tissue (Clarke, Richardson, and Holmes 2016; Frantz et al. 2008; N. A. Turner and Porter 2013). Based on this, we can assume that collagen production in the early time points post-MI is important for structural integrity of the heart, and a return to normal expression levels at long-term time points prevents fibrosis.

In chapter 3, we leveraged the dynamic properties of the large-scale model to predict how exogenous and endogenous signals affect the dynamics of collagen production by fibroblasts post-MI. As has been previously shown (K T Weber 1989; Dobaczewski et al. 2010; Frantz et al. 2008), TGF β is a major regulator of collagen expression dynamics and fibrosis risk, but we further predicted that the timing of TGF β signaling in post-MI healing is an important determinant of fibrosis risk. We also predicted that random variation in y_{max} (expression) values can lead to fibroblasts that persistently expression collagen long after infarction. This indicates that the timing of certain signals and differences in expression are integral to healthy post-infarct healing. More detailed simulations followed up by in vivo experimentation can elucidate which dynamic signals and expression profiles are most important for determining pathologic healing.

The next two sections outline further conclusions that can be drawn from the post-infarct simulations.

6.1.3 Pipeline for *in silico* drug screening

Due to the high cost and long time commitment involved in FDA-approval (Lipsky and Sharp 2001; Rouse et al. 2017), there is a clear benefit to identifying ways to screen drugs for efficacy and adverse side effects early in the drug discovery pipeline. It is also beneficial to identify currently approved drugs that could be re-purposed for use in different diseases. *In vitro* screening using tissue engineered constructs has helped, but *in silico* screening methods are faster and cheaper and could provide a useful filtering of drug structures or targets even before *in vitro* experimentation (Rouse et al. 2017; Ekins, Mestres, and Testa 2007). Additionally, *in silico* screening can be used to identify putative targets against a specific phenotype even when there is no drug currently known to affect that target and can provide hypotheses regarding the mechanism of a drug's actions (Guney et al. 2016). For example, in Chapter 3, we used the fibroblast computational model to predict modulators of fibroblast activity in post-MI wound healing, and we identified pro-fibrotic nodes which could potentially be inhibited to attenuate the risk of post-MI fibrosis such as NOX and PKC. Some of these potential targets for fibrosis do not have current FDA-approved therapeutics against them, and therefore could be novel putative targets against fibrosis.

In Chapter 4, we specifically modeled the effect of FDA-approved drugs on fibroblast phenotype in different disease-related signaling contexts. We identified drugs with potentially pro- or anti-fibrotic effects, some of which were context-dependent. In this study, we accurately

predicted the adverse, pro-fibrotic effect of anti-thymocyte globulin in the heart (Chu et al. 2012; Soignet et al. 2001; Yeh and Bickford 2009). This demonstrates the usefulness of this method in screening for fibrosis-related adverse side effects.

This method is also useful for repurposing drugs as promising therapeutics. Triflusal was predicted to promote beneficial fibroblast activity post-MI by increasing collagen output during the first two weeks post-MI without increasing collagen expression long term. Triflusal is already used post-MI to prevent clot formation (Bover et al. 2009; Cruz-Fernández et al. 2000; J. Costa et al. 2006), but it is worth further investigation to determine whether this drug prevents adverse remodeling. In general, fibroblast signaling is an important example for drug screening since there are no current therapeutics designed to reverse fibrosis in any organ, and other anti-fibrotic therapeutics do not directly target fibroblast signaling. Therefore, this method could be applied to predict which drugs could be used to prevent fibrosis in other contexts. Furthermore, this pipeline could be applied to any Hill ODE-based model to screen for therapeutic function or adverse effects of drugs as applied to other signaling networks.

6.1.4 Context-dependent signaling and cell decision-making

The main goal of this project was to determine how fibroblasts decide to adopt certain phenotypes. As shown in chapters 2 and 3, in different signaling contexts (input levels) some nodes will have a different affect on fibroblast phenotype. Drug efficacy is also dependent on the signaling context as is shown in chapter 4 where the change in activity in the drug target was dependent on the signaling context. Marimastat was even predicted to increase MMP activity in

some contexts but reduce it in others. This difference in effect on the drug target is translated into a difference in outcome (collagen I mRNA). Therefore, context-dependence is an important consideration when using drugs, particularly ones that would be applied to a dynamic signaling event such as wound healing.

The key to cellular decision-making is cross-talk between pathways. We showed in chapter 2 that beta-integrin signaling recruits TGF β signaling to induce α SMA expression. In chapter 3, increased inflammatory signaling post-MI, typically thought of as an anti-fibrotic stimulus, was predicted to ultimately increase the collagen area fraction, again through recruitment of the TGF β autocrine pathway (data not shown). Additionally, all nodes that were predicted to reduce collagen when upregulated, directly inhibit the TGF β pathway (see Chapter 3).

Together these indicate that TGF β activation is a key determinant in myofibroblast differentiation and collagen production, an unsurprising finding considering TGF β has been shown to be a potent pro-fibrotic stimulus (Meng, Nikolic-Paterson, and Lan 2016; Murtha et al. 2017; Wynn 2008), and loss of TGF β signaling limits collagen production and worsens healing post-MI (Ikeuchi et al. 2004; Frantz et al. 2008).

However, the prediction that inflammatory cytokines are pro-fibrotic is less understood. Previous *in vitro* experiments in cardiac fibroblasts have had contradictory results (Siwik, Chang, and Colucci 2000; Peng et al. 2002; Voloshenyuk et al. 2011). It has been previously shown that blocking IL1 leads to adverse remodeling in the heart through loss of collagen production (Hwang et al. 2001), but the CANTOS trial recently showed that blocking IL1 reduced adverse vascular remodeling in atherosclerosis (Baylis et al. 2017; Libby 2017). Therefore, the role of IL1 in regulating cardiac fibroblast phenotype remains unclear. In our hands, IL1 did increase

collagen production in human ventricular fibroblasts but not in human dermal fibroblasts (see Chapter 5). As mentioned in Chapter 3, many pathways, including inflammatory ones, in the cardiac fibroblast network are pro-fibrotic. This could mean that the model is predicting a cardiac-specific pro-fibrotic bias in signaling that includes a pro-fibrotic role for IL1 in the heart.

The organ-specificity of fibroblast signaling has not been fully investigated. It has been shown that pro-fibrotic myofibroblasts are still present in the heart long after infarction, but this does not happen during wound healing in the skin (Willems et al. 1994; Palatinus, Rhett, and Gourdie 2010). Fibrosis in different organs is initiated by different causes, which indicates a need for organ-specific response programs in fibroblasts (Zeisberg et al. 2007; Murtha et al. 2017). It has been proposed that epigenetic signatures might underlie these differences (Zeisberg et al. 2007), and, in fact, Rinn et al found that fibroblasts from different anatomic sites have distinct expression profiles which suggest epigenetic marking during development (Rinn et al. 2006). We showed in Chapter 5 that human ventricular fibroblasts and human dermal fibroblasts have different phenotypes at baseline, but it's unclear what drives that difference. The computational model developed in Chapter 2 could be used to investigate differences in signaling between dermal and ventricular or other fibroblasts by either simulating stimulation with organ-specific inputs or defining y_{max} parameters to capture organ-specific expression levels.

6.2 Future Directions

Experimental hypothesis testing

This study has generated many testable hypotheses that will require follow-up study both *in vitro* (to validate the predicted mechanism) and *in vivo* (to validate wound healing responses). The role of inflammatory signaling in up-regulating collagen post-MI will require an *in vivo* infarct study, specifically the prediction that moderately increased IL1 signaling can improve infarct healing. CANTOS, the clinical trial testing the IL1-receptor inhibitor, canakinumab, has recently concluded, and the results of that trial may inform the role of IL1, specifically, post-MI. Also, the prediction that delayed TGF β up-regulation post-infarct can exacerbate the risk for fibrosis should be tested with *in vivo* infarct experimentation.

Finally, we predicted that arsenic trioxide and anti-thymocyte globulin can worsen post-infarct remodeling, and this is in part supported by *in vivo* and clinical data (Soignet et al. 2001; Yeh and Bickford 2009; Chu et al. 2012; Nash et al. 2007). However, the promising prediction that triflusal can reduce the risk of dilation and wall rupture without increasing the risk of cardiac fibrosis will need to be tested *in vivo* and clinically.

Further Modeling

There are many ways in which the current fibroblast model can be improved. For example, pathways related to insulin and FGF signaling could be added to capture the physiology of fibroblasts in a patient with diabetes. There is an increased understanding that extracellular matrix plays a large role in signaling (Spinale et al. 2016). Therefore, the composition of the matrix is an important consideration in any study of fibrosis. Although the current fibroblast signaling network contains collagen I, collagen III, EDA-fibronectin, PAI-1, CTGF, and MMPs and TIMPS, the interactions between these proteins is not fully captures in

the network. Also, degradation products of collagen can be modulators of signaling. In order to capture these extracellular interactions more accurately, they would likely need to be modeled with a Michaelis Menten-based kinetic ODE in order to capture the stoichiometric dependence of these reactions. Overall, I hope this model serves as a first draft that can be continually improved and added to as more details on the mechanisms of fibroblast signaling are discovered.

This model can also be used in multi-scale modeling to describe how populations of fibroblasts determine ECM composition at the tissue level. Already, the first draft of such a model is being developed in collaboration with the Holmes and Pierce labs. This multi-scale model uses the signaling model to inform behavior of fibroblast turtles in an agent based model of cardiac fibrosis. In the future this model can be used to investigate the mechanism by which changes in fibroblast signaling lead to tissue fibrosis in response to a variety of stressors.

Organ-specificity

It is possible that much of the observed difference in fibroblast phenotype from different organs is due to differential signaling. We have already shown in chapters 2-4 that fibroblasts respond to signaling in a context-dependent way. If there was data to support different input levels characteristic of different organs, these could be used to define organ-specific baseline inputs in order to use the model to make predictions about how this signaling affects baseline fibroblast phenotype.

Since organ-specificity could come from differences in baseline expression (Rinn et al. 2006), the model developed in chapter 2 could be used to develop hypotheses about what drives fibroblast signaling in different organs. We showed in chapter 3 that random variation in the y_{max} parameter (analogous to expression of each node) was predicted to result in very different collagen expression dynamics post-MI, which indicates model sensitivity to y_{max} values. Therefore this parameter could be defined according to experimentally measured expression values - like those measured by Rinn et al (Rinn et al. 2006). The signaling model could then be used to predict organ-specific response to wound healing. Model predictions combined with further literature curation can determine whether expression differences alone can explain organ-specific fibroblast phenotypes. Alternatively, organs have unique profiles of extracellular signals which might be creating different phenotypes in concert with genetic differences.

6.3 Conclusions

Fibrosis is a poorly-understood process that is modulated by fibroblast activity. Fibroblasts integrate signals during injury and adopt a variety of phenotypes that affect the wound healing process. In this study we developed a computational model of cardiac fibroblast signaling in order to investigate how fibroblasts make decisions in complex signaling contexts. We demonstrate the application of this model in the study of dynamic wound healing and in screening for potential pro- or anti-fibrotic drugs. In this study we identified two major testable hypotheses: IL1 is potentially a cardiac-specific pro-collagen stimulus and triflusal is possibly a treatment that can be protective post-MI. Ultimately, this dissertation highlights a computational model of cardiac fibroblast signaling as a powerful tool in studying fibrosis. The model and the

in silico drug screening pipeline can further increase our understanding of the mechanisms by which fibroblasts respond to complex signaling and contribute to the prevention or development of fibrosis.

Appendix A

Large-Scale Fibroblast Signaling Model Description

Adapted from AC Zeigler, WJ Richardson, JW Holmes, JJ Saucerman “A computational model of cardiac fibroblast signaling predicts Context-Dependent Drivers of Myofibroblast Differentiation” *Journal of Molecular and Cellular Biology* Vol 94 pp 72-81 (2016), with permission from Elsevier

Table A.1 Network Description

Here we describe the fibroblast signaling model by outlining all network species and reactions with supporting experimental data

Table A1.a: Model species information.

Species information							
<u>module</u>	<u>ID</u>	<u>name</u>	<u>Yinit</u>	<u>Ymax</u>	<u>tau</u>	<u>type</u>	<u>gene name</u>
g-coupled	AngII	angiotensin II	0	1	1	protein	AGT
g-coupled	AT1R	angiotensin II receptor type 1	0	1	0.1	protein	AGTR1;AGTR2
g-coupled	AGT	angiotensinogen	0	1	10	protein	AGT
g-coupled	ACE	angiotensin converting enzyme	0	1	0.1	protein	ACE;ACE2
g-coupled	NOX	NAD(P)H oxidase	0	1	0.1	protein	NOX4;NOX5
g-coupled	ROS	reactive oxygen species	0	1	0.1	protein	
g-coupled	ET1	endothelin 1	0	1	1	protein	EDN1
g-coupled	ETAR	endothelin 1 receptor A	0	1	0.1	protein	EDNRA
g-coupled	DAG	diacyl-glycerol	0	1	0.1	small	
g-coupled	PKC	protein kinase C	0	1	0.1	protein	PRKCA;PRKCE;
g-coupled	TRPC	transient receptor potential canonical	0	1	0.1	protein	TRPC6;TRPC3
g-coupled	NE	norepinephrine	0	1	1	small	
g-coupled	BAR	beta adrenergic receptor 1 or 2	0	1	0.1	protein	ADRB1;ADRB2
g-coupled	Forskolin		0	1	1	small	
g-coupled	AC	adenylate cyclase	0	1	0.1	protein	ADCY6
g-coupled	cAMP	cyclic adenosine monophosphate	0	1	0.1	small	
g-coupled	PKA	protein kinase A	0	1	0.1	protein	PRKACA
g-coupled	CREB	cAMP response-element binding protein	0	1	0.1	protein	CREB1;CREB3
g-coupled	CBP	CREB - binding protein	0	1	0.1	protein	CREBBP
growth factor	TGFB	transforming growth factor beta 1	0	1	1	protein	TGFB1
growth factor	TGFB1R	TGFB receptor	0	1	0.1	protein	TGFBR1;TGFBR2

growth factor	smad3	small mothers against decapentaplegic 2 and 3	0	1	0.1	protein	SMAD2; SMAD3
growth factor	smad7		0	0.5	10	protein	SMAD7
growth factor	latentTGFB	TGFB1 with latent protein complex	0	1	10	protein	
growth factor	BAMBI	BMP and activin bound inhibitor	0	1	0.1	protein	BAMBI
growth factor	PDGF	platelet derived growth factor	0	1	1	protein	PDGFA; PDGFB; PDGFD
growth factor	PDGFR	platelet derived growth factor receptor	0	1	0.1	protein	PDGFRA; PDGFRB
stretch	NP	natriuretic peptide	0	1	1	protein	NPPA; NPPB
stretch	NPRA	natriuretic peptide receptor	0	1	0.1	protein	NPR1; NPR2; NPR3
stretch	cGMP	cyclic guanosine monophosphate	0	1	0.1	small	
stretch	PKG	protein kinase G	0	1	0.1	protein	PRKG1
stretch	mechanical	stretch	0	1	1	process	
stretch	B1int	beta 1 integrin	0	1	0.1	protein	ITGB1
stretch	Rho	a Rho-dependent GTPase	0	1	0.1	protein	RHOA
stretch	ROCK	rho associated protein kinase	0	1	0.1	protein	ROCK1
stretch	Ca	calcium	0	1	0.1	small	
stretch	calcineurin	calcineurin	0	1	0.1	protein	PPP3CA; PPP3CB
stretch	NFAT	nuclear factor of activated T-cells	0	1	0.1	protein	NFATC1
cytokine	IL6	interleukin-6	0	1	1	protein	IL6
cytokine	gp130	IL-6 receptor complexed to gp130 for signal transduction	0	1	0.1	protein	IL6ST; IL6R
cytokine	STAT	signal transducers and activators of transcription 1 and 3	0	1	0.1	protein	STAT1; STAT3
cytokine	IL1	interleukin-1 alpha and beta	0	1	1	protein	IL1B;IL1A

cytokine	IL1RI	IL1 receptor type I	0	1	0.1	protein	IL1R1
cytokine	TNFa	tissue necrosis factor alpha	0	1	1	protein	TNF
cytokine	TNFaR	TNF alpha receptor	0	1	0.1	protein	TNFRSF1A;TNFRSF1B
cytokine	NFKB	nuclear factor kappa-light-chain-enhancer of activated B cells	0	1	0.1	protein	NFKB1
cytokine	PI3K	phosphoinositide 3-kinase	0	1	0.1	protein	PIK3CA
cytokine	Akt	protein kinase B	0	1	0.1	protein	AKT1; AKT2; AKT3
MAPK	p38	a MAP kinase	0	1	0.1	protein	MAPK14
MAPK	TRAF	tnf receptor associated factor either 2/6	0	1	0.1	protein	TRAF6
MAPK	ASK1	apoptosis signal related kinase 1	0	1	0.1	protein	MAP3K5
MAPK	MKK3	mitogen activated protein kinase kinase	0	1	0.1	protein	MAP2K3
MAPK	PP1	protein phosphatase 1	0	1	0.1	protein	PPP1CA; PPP1CB; PPP1CC
MAPK	JNK	a MAP kinase	0	1	0.1	protein	MAPK8
MAPK	abl	abl tyrosine kinase	0	1	0.1	protein	ABL1; ABL2
MAPK	Rac1	a Rho-dependent GTPase	0	1	0.1	protein	RAC1
MAPK	MEKK1	a MAP3K associated with p38 and JNK	0	1	0.1	protein	MAP3K1
MAPK	MKK4	a MAP2K associated with p38 and JNK	0	1	0.1	protein	MAP2K4
MAPK	ERK	a MAP kinase	0	1	0.1	protein	MAPK1; MAPK3
MAPK	Ras	representing the family of GTPases	0	1	0.1	protein	KRAS
MAPK	Raf	family of raf protein serine/threonine kinases	0	1	0.1	protein	RAF1

MAPK	MEK1	a MAP2K mainly specific to ERK	0	1	0.1	protein	MAP2K1
adhesion	FAK	focal adhesion kinase	0	1	0.1	protein	PTK2
adhesion	epac	exchange protein activated by cAMP 1	0	1	0.1	protein	RAPGEF3
adhesion	Factin	polymerized actin	0	1	1		ACTG1
adhesion	FA	formation of focal adhesions	0	1	1	complex	
adhesion	migration	mobility	0	1	10	event	
growth	cmyc	myc transcription factor	0	1	0.1	protein	MYC
growth	CTGF	connective tissue growth factor	0	1	0.1	protein	CTGF
growth	proliferation	proliferation	0	1	10	event	
differentiation	SRF	serum response factor	0	1	0.1	protein	SRF
differentiation	EDAFN	extra domain A of fibronectin	0	1	10	protein	FN1
differentiation	aSMA	alpha-smooth muscle actin	0	1	10	protein	ACTA2
ECM	AP1	activator protein 1	0	1	0.1	protein	JUN; FOS
ECM	TIMP1	tissue inhibitor of metalloproteinase 1	0	0.5	10	protein	TIMP1
ECM	TIMP2	tissue inhibitor of metalloproteinase 2	0	0.5	10	protein	TIMP2
ECM	PAI1	plasminogen activator inhibitor 1	0	1	10	protein	SERPINE1
ECM	proMMP14	inactive MMP14	0	1	1	protein	
ECM	proMMP1	inactive MMP1	0	1	1	protein	
ECM	proMMP2	inactive MMP2	0	1	1	protein	
ECM	proMMP9	inactive MMP9	0	1	1	protein	
ECM	MMP1	metalloproteinase-1	0	1	10	protein	MMP1
ECM	MMP2	metalloproteinase-2	0	1	10	protein	MMP2
ECM	MMP9	metalloproteinase-9	0	1	10	protein	MMP9
ECM	MMP14	metalloproteinase-14	0	1	10	protein	MMP14
ECM	fibronectin	fibronectin	0	1	10	protein	FN1
ECM	periostin	periostin	0	1	10	protein	POSTN

ECM	CImRNA		0	1	1	transcript	
ECM	CIII mRNA		0	1	1	transcript	
ECM	CI	collagen I	0	1	10	protein	COL1A1
ECM	CIII	collagen III	0	1	10	protein	COL3A1

Table A.1b: Model Reaction Information

<u>Reaction Information</u>					
<u>Rule</u>	<u>Weight</u>	<u>n</u>	<u>EC50</u>	<u>PMID</u>	
=> AngII	0.25	1.4	0.6	10362677	
=> TGFB	0.25	1.4	0.6	20538689	
=> mechanical	0.25	1.4	0.6	9547793	
=> IL6	0.25	1.4	0.6	19234091	
=> IL1	0.25	1.4	0.6	19631653	
=> TNFa	0.25	1.4	0.6	10591022	
=> NE	0.25	1.4	0.6	3948363	
=> PDGF	0.25	1.4	0.6	20538689	
=> ET1	0.25	1.4	0.6	12695528	
=>NP	0.25	1.4	0.6	17991884	
=> Forskolin	0.25	1.4	0.6		
MMP9 & latentTGFB => TGFB	1	1.4	0.6	10652271, 12226090	
MMP2 & latentTGFB => TGFB	1	1.4	0.6	10652271, 12226090	
ACE & AGT => AngII	1	1.4	0.6	10790312, 13295487	
CREB + CBP => IL6	1	1.4	0.6	11597988, 16466739, 10405202	
NFKB => IL6	1	1.4	0.6	11597988, 16466739	
AP1 => IL6	1	1.4	0.6	11597988, 16466739	
AP1 => ET1	1	1.4	0.6	12695528, 1918021	
AngII => AT1R	1	1.4	0.6	8348686, 16024575	
AT1R => NOX	1	1.4	0.6	15106793, 11597988	

NOX => ROS	1	1.4	0.6	15106793, 16531806
IL6 => gp130	1	1.4	0.6	19234091, 1602143
ROS => ERK	1	1.4	0.6	11597988, 14642698, 2695528
ROS => p38	1	1.4	0.6	11597988, 24882408, 12695528
ROS => JNK	1	1.4	0.6	11597988, 12695528
IL1RI => NFKB	1	1.4	0.6	11597988, 1906501
B1int => Rac1	1	1.4	0.6	21131638, 12376560
B1int => Rho	1	1.4	0.6	21131638, 17456553
gp130 => STAT	1	1.4	0.6	19234091, 9874564
TNFaR => PI3K	1	1.4	0.6	17560598, 17612514
!AT1R & !JNK & p38 => AGT	1	1.4	0.6	18926830, 21131638, 11192370
TGFB1R & !PKG & !smad7 => smad3	1	1.4	0.6	17513491, 9335507, 9215638, 17991884, 17038494
smad3 & CBP & ERK => CTGF	1	1.4	0.6	18586263, 22749815, 11013125, 12368229, 16959941
STAT => proMMP2	1	1.4	0.6	15350851, 24573038
STAT => proMMP9	1	1.4	0.6	19234091, 18258475
smad3 & CBP => periostin	1	1.4	0.6	21367774, 24004653, 16959941
CREB & CBP => periostin	1	1.4	0.6	21367774, 24577408, 16959941

ERK => NFKB	1	1.4	0.6	17921324, 21757573
p38 => NFKB	1	1.4	0.6	17921324, 11259436
NFKB & AP1 & !smad3 => proMMP1	1	1.4	0.6	17921324, 11502752, 12525489
ETAR => ROS	1	1.4	0.6	12695528, 16391241
ERK => AP1	1	1.4	0.6	12695528, 10862759
AP1 => proMMP2	1	1.4	0.6	17921324, 12371906
AP1 & NFKB => proMMP9	1	1.4	0.6	17560598, 975585
AP1 => TIMP1	1	1.4	0.6	17921324, 9182725
AP1 => TIMP2	1	1.4	0.6	17921324, 8112602
PKC & mechanical => B1int	1	1.4	0.6	15949469, 12110574, 21131638
cAMP => PKA	1	1.4	0.6	11054474, 21977288
smad3 & CBP => fibronectin	1	1.4	0.6	16707625, 11013125
!smad3 => CBP	1	1.4	0.6	16959941, 10918613
!CREB => CBP	1	1.4	0.6	16959941, 8028671
mechanical => B1int	1	1.4	0.6	21131638, 15760908
NFAT => EDAFN	1	1.4	0.6	23178899, 23142541
TGFB1R => ACE	1	1.4	0.6	11967821, 18223028
proMMP14 => MMP14	1	1.4	0.6	
proMMP9 & !TIMP1 => MMP9	1	1.4	0.6	7674941, 19184368
proMMP1 & !TIMP1 => MMP1	1	1.4	0.6	7674941, 1311314
proMMP9 & !TIMP2 => MMP9	1	1.4	0.6	7674941, 19184368
proMMP2 & MMP14 & !TIMP1 => MMP2	1	1.4	0.6	7674941, 10827175

proMMP2 & MMP14 => MMP2	1	1.4	0.6	7674941, 10827175
TGFB & !BAMBI => TGFB1R	1	1.4	0.6	22960625, 24078695
AP1 => proliferation	1	1.4	0.6	23500546, 17483238
PKA => CREB	1	1.4	0.6	11054474, 11909979
CREB => proliferation	1	1.4	0.6	11054474, 17483238
NE => BAR	1	1.4	0.6	11054474, 7700241
ET1 => ETAR	1	1.4	0.6	12695528, 8313418
CTGF => proliferation	1	1.4	0.6	11013125, 174832
IL1 => IL1RI	1	1.4	0.6	8327496, 7769098
PKC => proliferation	1	1.4	0.6	10756114, 17483238
smad3 & CBP & !epac=> CImRNA	1	1.4	0.6	17513491, 17513491, 11279127, 18434542, 23845590
smad3 & CBP & !epac=> CIIImRNA	1	1.4	0.6	17513491, 17513491, 11279127, 18434542, 23845590
!MMP1 & CImRNA => CI	1	1.4	0.6	8999957, 11513874
!MMP1 & CIIImRNA => CIII	1	1.4	0.6	8999957
!MMP2 & CImRNA => CI	1	1.4	0.6	8999957, 11513874
!MMP2 & CIIImRNA => CIII	1	1.4	0.6	8999957
AP1 => proMMP14	1	1.4	0.6	22287584, 17348021
PDGF => PDGFR	1	1.4	0.6	11230972, 24427322
BAR => AC	1	1.4	0.6	12711600, 17934720
BAR & AT1R => AC	1	1.4	0.6	12711600, 1330500
AC => cAMP	1	1.4	0.6	12711600, 15075208

FAK =>MEKK1	1	1.4	0.6	17409352, 12458213, 21131638
AP1 => latentTGFB	1	1.4	0.6	20141610, 21367774, 22429882, 19374881
cAMP => epac	1	1.4	0.6	18434542, 9853756
Rho => ROCK	1	1.4	0.6	16043513, 17456553
MMP9 => migration	1	1.4	0.6	17560598, 21925853
MMP2 => migration	1	1.4	0.6	12970340, 21385940
TNFa => TNFaR	1	1.4	0.6	17560598, 23337087
NP => NPRA	1	1.4	0.6	16986166, 11595171
NPRA => cGMP	1	1.4	0.6	17991884, 16986166
cGMP => PKG	1	1.4	0.6	17991884, 21282499
Ras => Raf	1	1.4	0.6	9486662, 8668210
Raf & !ERK => MEK1	1	1.4	0.6	12388314, 8668210, 21943356, 24489118
MEK1 & !PP1=> ERK	1	1.4	0.6	12388314, 12167697, 11259586, 15972258, 25659900
p38 => PP1	1	1.4	0.6	11259586, 15972258, 25659900
MKK3 => p38	1	1.4	0.6	11259586, 15778394
TGFB1R => TRAF	1	1.4	0.6	22749815, 18922473
Rac1 => MEKK1	1	1.4	0.6	7600582, 9674706
MEKK1 => MKK4	1	1.4	0.6	7600582, 12401521

MKK4 & !NFKB => JNK	1	1.4	0.6	7600582, 16076903, 11713530, 11466617
PDGFR => abl	1	1.4	0.6	16076903, 10500097
abl => Rac1	1	1.4	0.6	16076903, 15039778
JNK => cmyc	1	1.4	0.6	16076903, 14523011
cmyc => proliferation	1	1.4	0.6	16076903, 15195135
TNFaR => TRAF	1	1.4	0.6	9774977, 17560598, 10523862
TRAF => ASK1	1	1.4	0.6	9774977, 10523862
ASK1 => MKK3	1	1.4	0.6	8974401, 10912795
ASK1 => MKK4	1	1.4	0.6	8974401, 9774977, 19494316
IL1RI => ASK1	1	1.4	0.6	15778394, 10912795
smad3 => PAI1	1	1.4	0.6	17991884, 11279127, 9606191
!PKA & epac => migration	1	1.4	0.6	18434542, 24725364
NFKB => proMMP14	1	1.4	0.6	11112697, 20855151
Ras => p38	1	1.4	0.6	21367774, 14593117
PI3K => Akt	1	1.4	0.6	23500546, 21498085, 15166238
TGFB1R => PI3K	1	1.4	0.6	21498085, 16288034
PDGFR => PI3K	1	1.4	0.6	21943356, 11230972
FAK => PI3K	1	1.4	0.6	15166238, 25900259
TGFB1R => NOX	1	1.4	0.6	16179589, 26096997, 25858818

Akt => NFkB	1	1.4	0.6	18064631, 10485711
NFkB => fibronectin	1	1.4	0.6	18064631, 17252537, 23141425
JNK => AP1	1	1.4	0.6	21757573, 12695528
IL1RI & TGFB => BAMBI	1	1.4	0.6	24078695, 23734837
Forskolin => AC	1	1.4	0.6	12711600, 15075208
STAT => smad7	1	1.4	0.6	10067896, 11927620, 22751114
SRF => CImRNA	1	1.4	0.6	20558820, 24732378
Rho & !Rac1 => p38	1	1.4	0.6	21131638, 25007875
MKK4 & !Rho => JNK	1	1.4	0.6	21131638, 7600582
ROCK => Factin	1	1.4	0.6	21385940, 17456553
Factin => SRF	1	1.4	0.6	24732378, 18334560
B1int & Factin => FA	1	1.4	0.6	
SRF => CIIImRNA	1	1.4	0.6	20558820, 24732378
SRF & asmad3 & CBP=> aSMA	0	1.4	0.6	16179589, 20558820, 24732378
calcineurin => NFAT	1	1.4	0.6	22403241, 23178899
AT1R => Ras	1	1.4	0.6	9486662, 21367774
ROCK => FAK	1	1.4	0.6	203008429, 15923313
smad3 & CBP => aSMA	1	1.4	0.6	16179589, 26738448
SRF=> aSMA	1	1.4	0.6	17456553, 15855636
ETAR => DAG	1	1.4	0.6	1809396, 10676846
AT1R => DAG	1	1.4	0.6	7653525, 17982962

DAG => TRPC	1	1.4	0.6	17533154, 22992321, 25521631
TRPC => Ca	1	1.4	0.6	23827314, 22992321
Ca => calcineurin	1	1.4	0.6	26191219, 23022034
DAG => PKC	1	1.4	0.6	23800645, 17071619

Table A.2 References for validation of the large-scale fibroblast signaling model

Red text indicates contradicting sources.

<u>Input</u>	<u>Output</u>	<u>'prediction'</u>	<u>Measurement</u>	<u>Reference</u>	<u>Cell Type</u>	<u>Add. Ref</u>
TGFB	ClmRNA	'Increase'	Increase	23583823	human atrial cardiac fibroblasts	
TGFB	CIII mRNA	'Increase'	Increase	23583823	human atrial cardiac fibroblasts	
TGFB	Cl	'Increase'	Increase	15625103	rat cardiac fibroblast	14726474, 10864917
TGFB	CIII	'Increase'	Increase	15625103	rat cardiac fibroblast	10864917
TGFB	aSMA	'Increase'	Increase	15625103	rat cardiac fibroblast	14726474, 11600408, 23845590, 24085841, 23583823
TGFB	PAI1	'Increase'	Increase	14726474	human primary cardiac fibroblasts	10715259
TGFB	fibronectin	'Increase'	Increase	11600408	adult male rat cardiac fibroblasts	14726474
TGFB	MMP2	'Increase'	Increase	15194465	adult rat cardiac fibroblast	
TGFB	MMP14	'Increase'	Increase	15194465	adult rat cardiac fibroblast	
TGFB	migration	'Increase'	Increase	15194465	adult rat cardiac fibroblast	17706606
TGFB	CTGF	'Increase'	Increase	23583823	human atrial cardiac fibroblasts	14726474
TGFB	IL6	'Increase'	Increase	14726474	human primary cardiac fibroblasts	23583823
TGFB	TIMP2	'Increase'	Increase	15194465	adult male rat cardiac fibroblasts	
TGFB	latentTGFB	'Increase'	Increase	10715259	disease human cardiac fibroblast	

AngII	CI	'Increase'	Increase	23141425	adult rat cardiac fibroblast	23526266, 15625103, 12480812, 18278065
AngII	CIII	'Increase'	Increase	23141425	adult rat cardiac fibroblast	23526266, 12480812, 15625103, 18278065
AngII	aSMA	'Increase'	Increase	11600408	adult rat cardiac fibroblast	15625103
AngII	PAI1	'Increase'	Increase	18278065	neonatal rat cardiac fibroblast	10715259
AngII	proliferation	'Increase'	Increase	23526266	adult rat cardiac fibroblast	7635942, 10715259, 23141425, 21819443
AngII	ET1	'Increase'	Increase	7635942	neonatal rat cardiac fibroblast	
AngII	CTGF	'Increase'	Increase	23141425	adult rat cardiac fibroblasts	
AngII	MMP2	'Increase'	Increase	23526266	rat cardiac fibroblast	
AngII	MMP9	'Increase'	Increase	23526266	rat cardiac fibroblast	
AngII	fibronectin	'Increase'	Increase	11600408	adult male rat cardiac fibroblasts	10715259, 23141425, 18278065
AngII	latentTGFB	'Increase'	Increase	18278065	neonatal rat cardiac fibroblast	10715259
stretch	CI	'Increase'	Increase	15254965	neonatal and adult rat cardiac fibroblasts	17686880, 14985070, 2054929
stretch	CIII	'Increase'	Increase	2054929	neonatal rat cardiac fibroblast	17686880, 15254965
stretch	aSMA	'Increase'	Increase	12842814	rat cardiac fibroblasts	
stretch	proliferation	'Decrease'	Decrease	15254965	neonatal rat cardiac fibroblast	
stretch	latentTGFB	'Decrease'	Increase	10939632	neonatal rat cardiac fibroblast	
TNFa	CI	'Increase'	Increase	21893029	adult rat cardiac fibroblasts	11070088, 10864917, 12480812
TNFa	CIII	'Increase'	Increase	21893029	adult rat cardiac fibroblasts	11070088, 10864917, 12480812

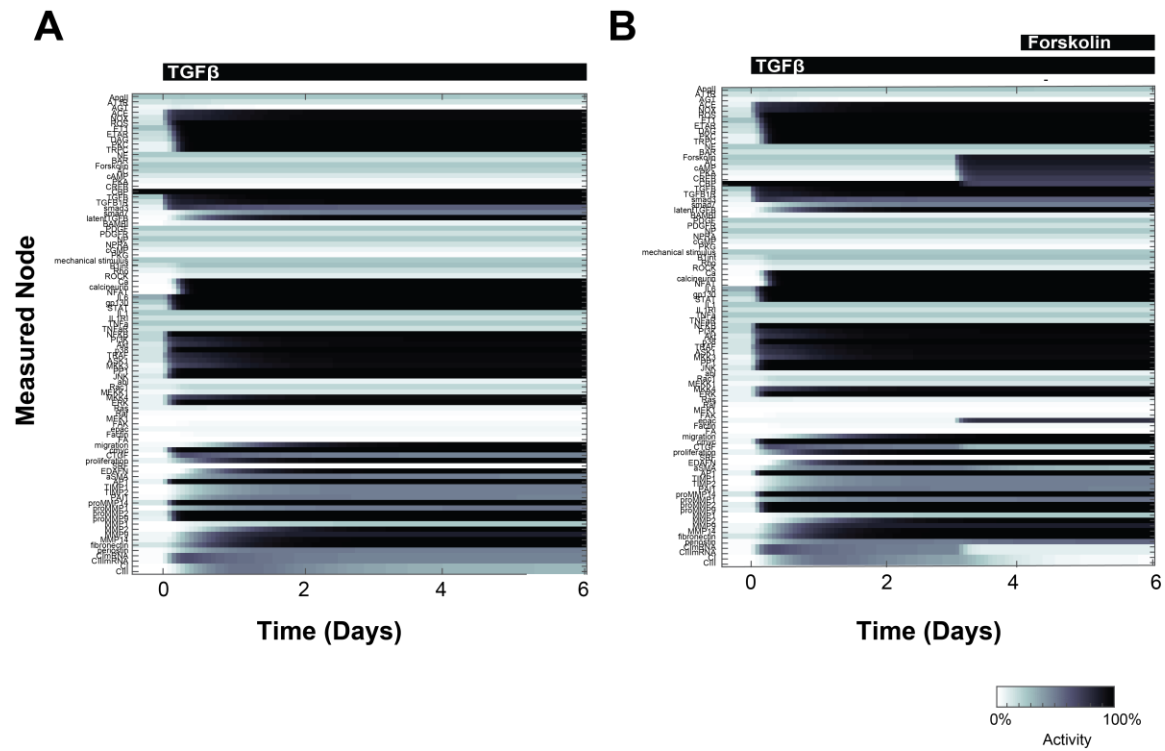
TNFa	MMP9	'Increase'	Increase	15537504	human atrial cardiac fibroblast	20619343
TNFa	MMP2	'Increase'	Increase	15194465	adult rat cardiac fibroblast	12480812, 20619343
TNFa	TIMP1	'Increase'	Increase	12480812	neonatal rat cardiac fibroblast	
TNFa	migration	'Increase'	Increase	17706606	rat cardiac fibroblast	17085539, 15537504
TNFa	latentTGFB	'Increase'	Increase	21893029	adult rat cardiac fibroblast	
IL1	ClmRNA	'Decrease'	No Change	23583823	human atrial cardiac fibroblast	20619343
IL1	Cl	'Decrease'	Decrease	10864917	rat cardiac fibroblast	
IL1	CIII	'Decrease'	Decrease	10864917	rat cardiac fibroblast	
IL1	aSMA	'Decrease'	No Change	23583823	human atrial cardiac fibroblasts	
IL1	proliferation	'Increase'	Decrease	9748252	neonatal rat cardiac fibroblast	21819443
IL1	MMP1	'Increase'	Increase	20619343	human atrial cardiac fibroblasts	
IL1	MMP9	'Increase'	Increase	20619343	human atrial cardiac fibroblast	17706606
IL1	MMP2	'Increase'	No Change	20619343	human atrial cardiac fibroblast	17706606
IL1	IL6	'Increase'	Increase	23583823	human atrial cardiac fibroblast	
IL1	CTGF	'Decrease'	No Change	23583823	human atrial cardiac fibroblasts	
IL1	migration	'Increase'	Increase	17706606	rat cardiac fibroblast	17085539
Forskolin	Cl	'Decrease'	Decrease	15625103	adult rat cardiac fibroblast	23845590
Forskolin	aSMA	'Decrease'	Decrease	15625103	adult rat cardiac fibroblast	
Forskolin	migration	'Increase'	Increase	23845590	neonatal rat CF and CMF	
Forskolin	proliferation	'Increase'	Decrease	12652658	rat cardiac fibroblast	11304509
NE	Cl	'Decrease'	Decrease	19575289	adult rat cardiac fibroblast	23845590, 20637865, 25134464, 22914642
NE	MMP2	'Increase'	Increase	22914642	adult rat cardiac fibroblast	20167215

NE	latentTGFB	'No Change'	Increase	19575289	adult rat cardiac fibroblast	
NE	CI mRNA	'Decrease'	Increase	19575289	rat cardiac fibroblast	
NE	CIII mRNA	'Decrease'	Increase	19575289	rat cardiac fibroblast	
NE	proliferation	'Increase'	Increase	12652658	rat cardiac fibroblast	11304509, 12619890
NE	IL6	'Increase'	Increase	12619890	rat cardiac fibroblast	
IL6	CI	'Decrease'	Decrease	10864917	neonatal and adult rat cardiac fibroblasts	
IL6	CIII	'Decrease'	Decrease	10864917	neonatal and adult rat cardiac fibroblasts	
IL6	proliferation	'No Change'	Increase	12619890	rat cardiac fibroblast	
ET1	CI	'Increase'	Increase	17533154	neonatal rat cardiac fibroblast	
ET1	CIII	'Increase'	Increase	17533154	neonatal rat cardiac fibroblast	
ET1	aSMA	'Increase'	Increase	17533154	neonatal rat cardiac fibroblast	
ET1	proliferation	'Increase'	Increase	7635942	neonatal rat cardiac fibroblast	
PDGF	CI	'Increase'	Increase	23585135	adult rat cardiac fibroblast	25628782
PDGF	CIII	'Increase'	Increase	25628782	neonatal rat CF	
PDGF	aSMA	'Increase'	Increase	23585135	adult rat cardiac fibroblast	25628782, 24427322
PDGF	proliferation	'Increase'	Increase	23585135	adult rat cardiac fibroblast	25628782
PDGF	MMP1	'Increase'	Increase	23585135	adult rat cardiac fibroblast	25628782
PDGF	latentTGFB	'Increase'	Increase	23585135	adult rat cardiac fibroblast	
PDGF	migration	'Increase'	Increase	23585135	rat cardiac fibroblast	19136609
NP	CI	'Decrease'	No Change	23526266	rat cardiac fibroblast	14726474
NP	CTGF	'Decrease'	No Change	14726474	human cardiac fibroblast	
NP	fibronectin	'Decrease'	No Change	14726474	human cardiac fibroblast	
NP	proliferation	'No Change'	No Change	23526266	adult rat cardiac fibroblast	

NP	aSMA	'Decrease'	No Change	14726474	human cardiac fibroblast
NP	IL6	'No Change'	No Change	14726474	human cardiac fibroblast
NP	PAI1	'Decrease'	No Change	14726474	human cardiac fibroblast
NP	CIII	'Decrease'	No Change	23526266	rat cardiac fibroblast
NP	MMP9	'No Change'	No Change	23526266	rat cardiac fibroblast
NP	MMP2	'No Change'	No Change	23526266	rat cardiac fibroblast

Figure A.1: Full simulation of TGF- β versus forskolin treatment.

Predicted dynamic activity of all nodes for 6 days of TGF- β alone (A) or for 4 days of TGF- β followed by 2 days of TGF- β + forskolin. The difference in activation of each node with and without forskolin stimulation is plotted on the network to map the specific pathways altered in these two conditions (C).



C

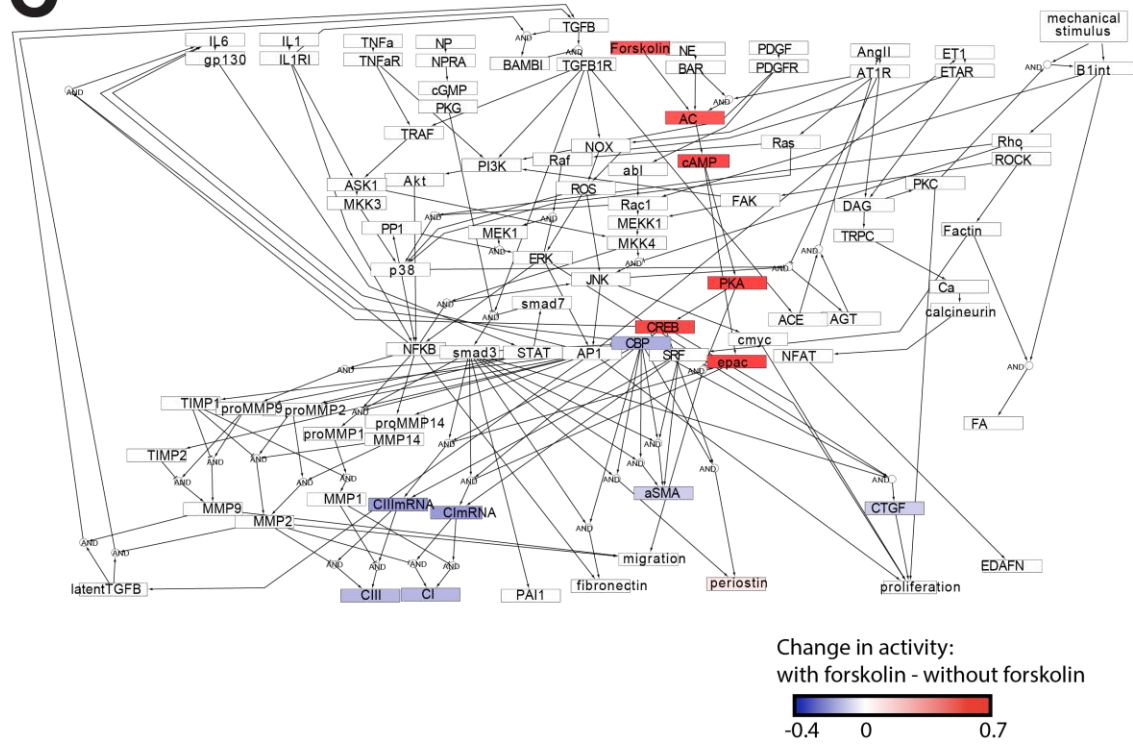


Figure A.2: Other validated relationships.

Model prediction and comparison to experimental validation data for all relationships not included in the subset shown in Figure 3. Color indicates model prediction (blue for decrease, white for no change, red for increase) and the check indicates agreement with literature where an x indicates disagreement. Inputs are shown on the vertical axis and outputs are shown on the horizontal axis. Relationships are grouped by input.

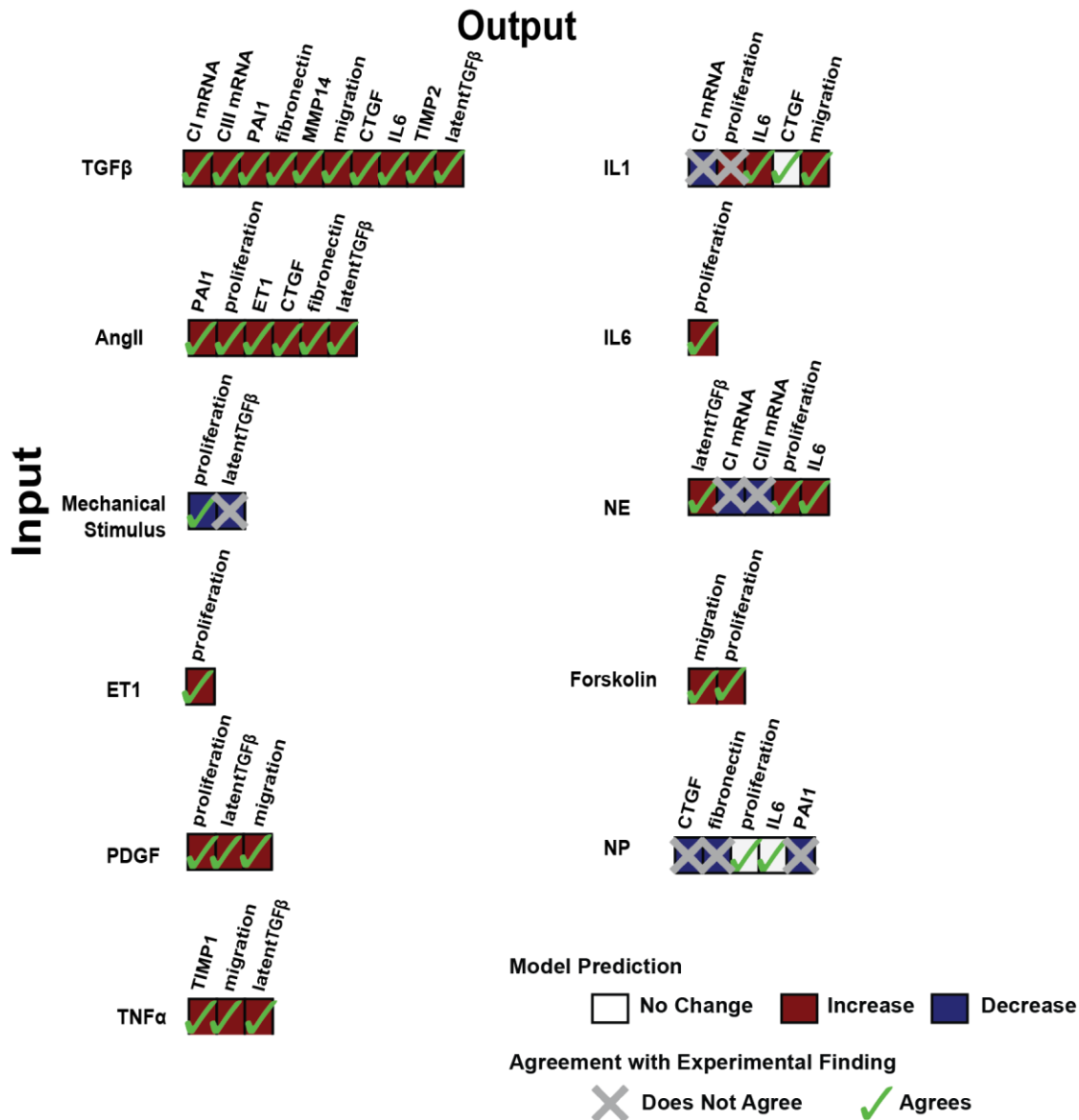
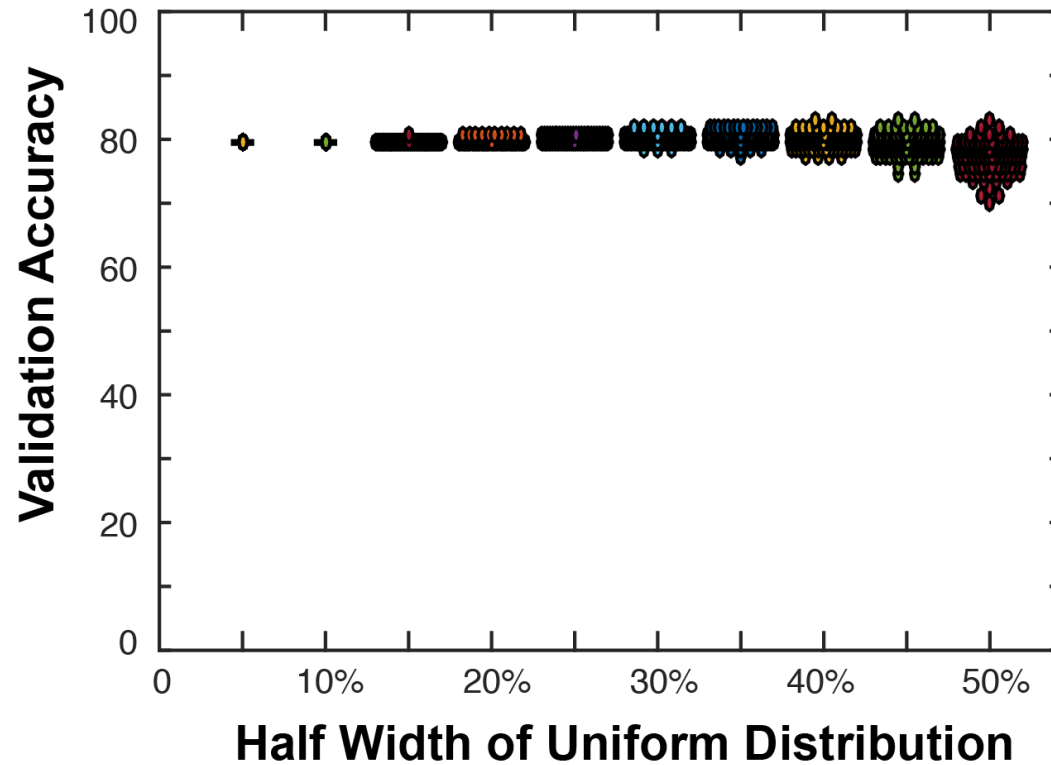


Figure A.3: Robustness of validation accuracy to changes in baseline input levels.

The baseline input levels were varied within a uniform distribution of width 5%-50% of the original value (25% activity). This uniform distribution was sampled 100 times, and the validation accuracy was calculated for each random sampling represented at a dot in the plot. The validation accuracy is robust to variation within 12-37% activity.



C

Signaling Context: Mechanical Stimulus

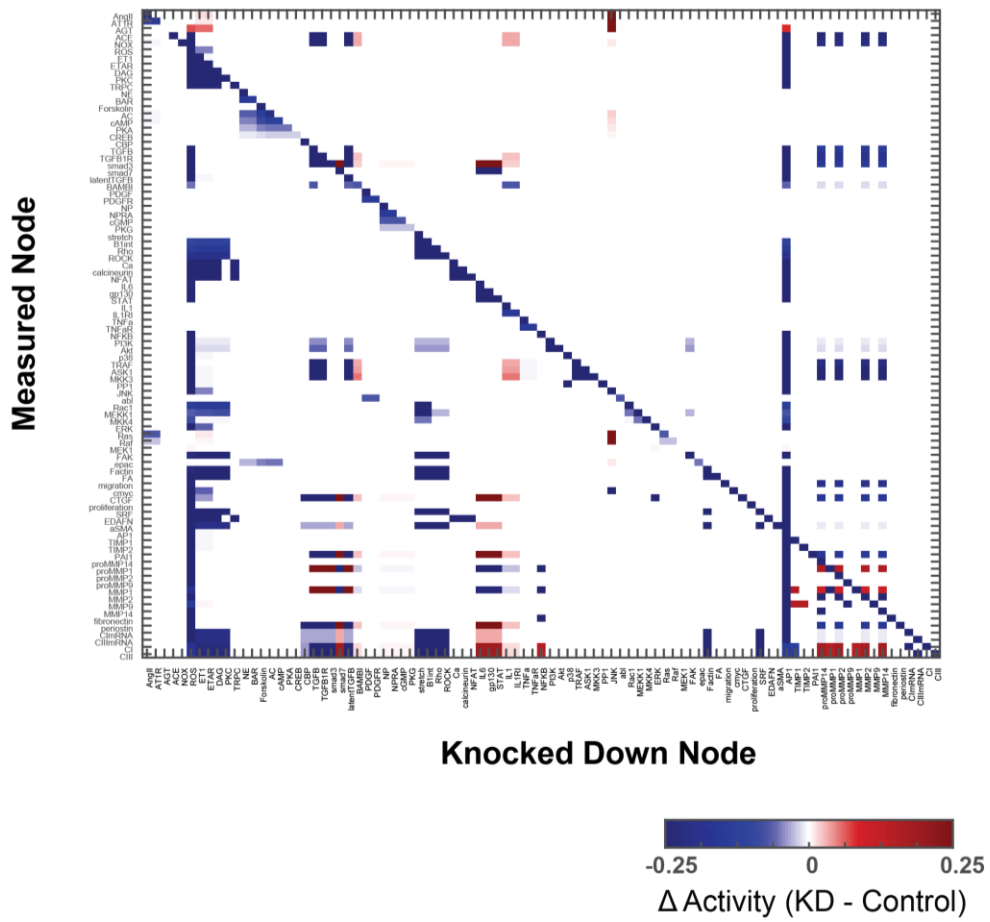
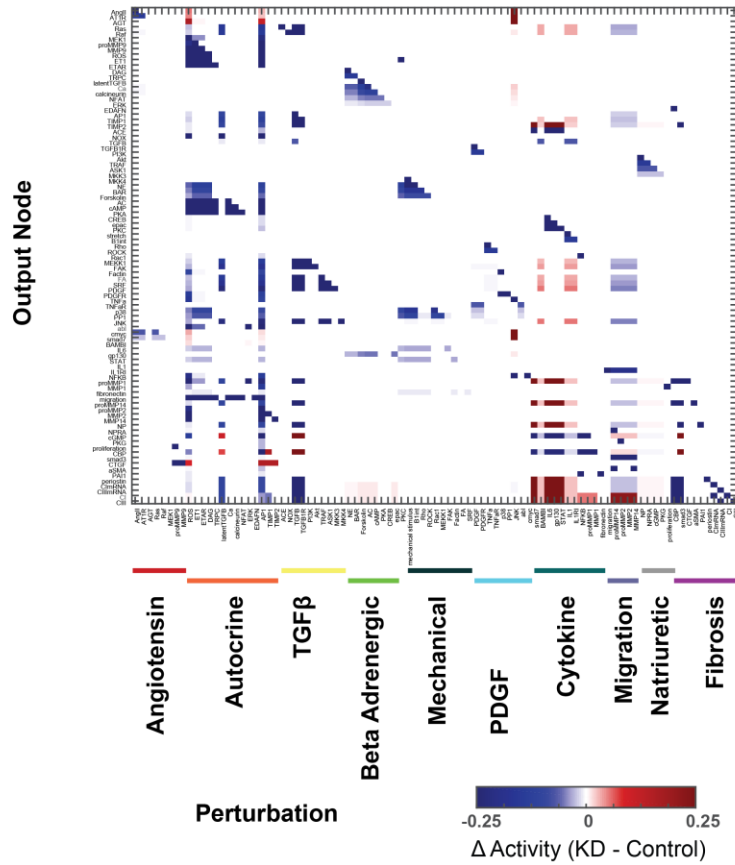


Figure A.5: Clustering analysis

(A) The full sensitivity analysis under high TGFβ signaling context ordered by cluster on both axes. (B) The full network with each node colored by module as labeled in A.

A



B

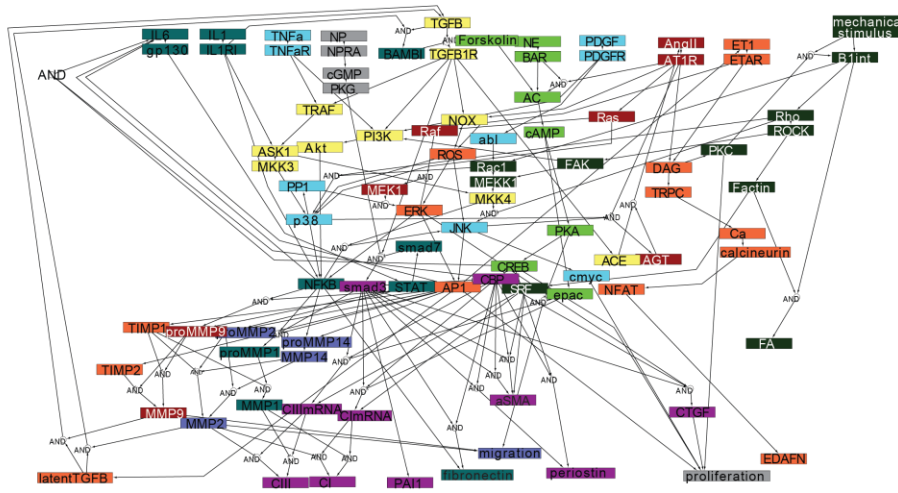


Figure A.6: Full comparison of topological features versus influence

Each topological feature is plotted against influence. R2 values are shown.

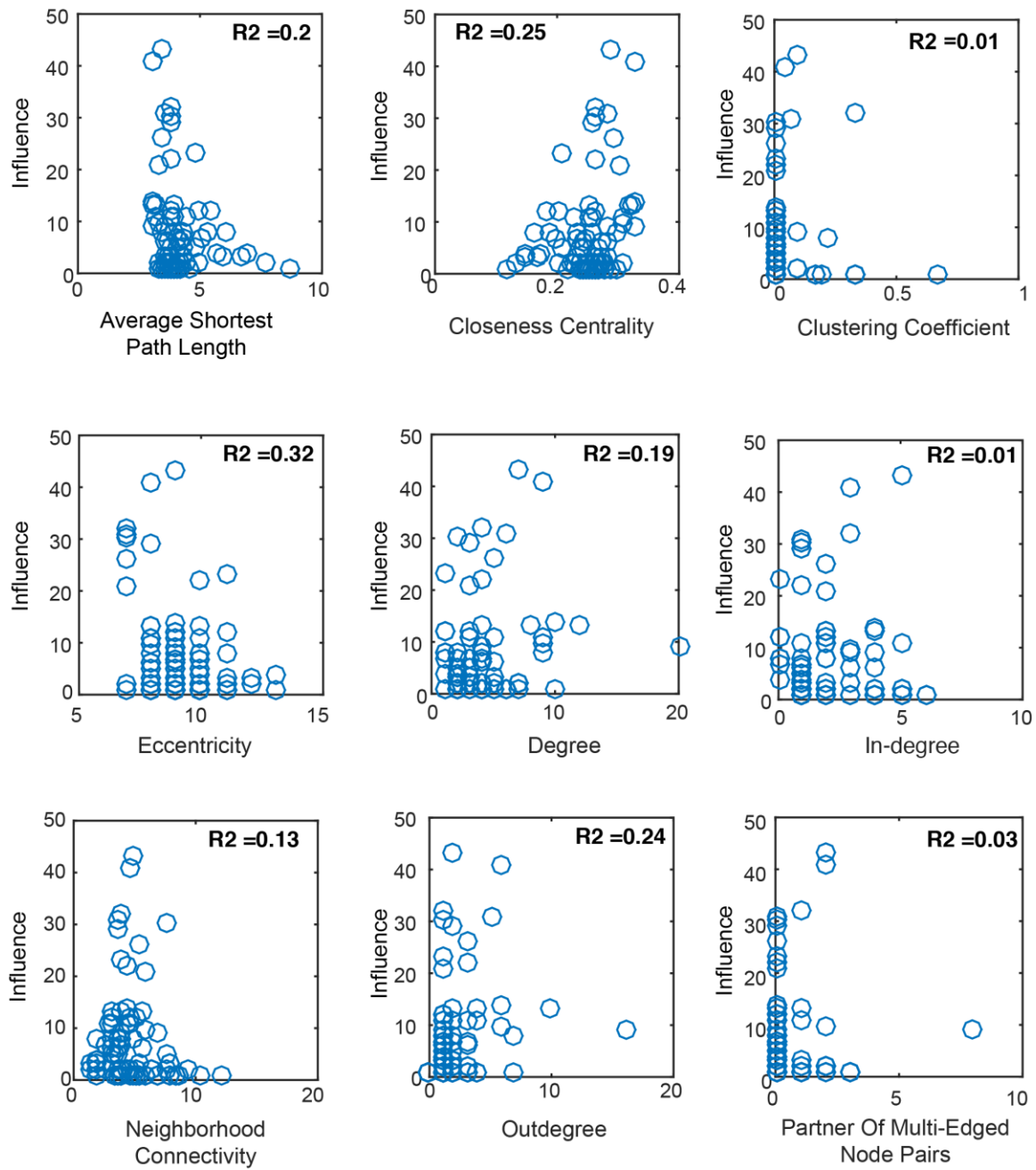


Table A.3: Definitions of network topology metrics

Each topological feature as defined by Assenov et al in the NetworkAnalyzer plugin for Cytoscape used for topological analysis of the network [27],[28].

Topology Metric	Definition
betweenness centrality	number of shortest paths from all nodes to all others that pass through node n
out-degree	number of edges that exit node n
in-degree	number of edges that enter node n
edge count	total number of edges connected to node n
eccentricity	maximal length of a shortest path between node n and any other node in the network
neighborhood connectivity	average number of neighbors for all neighbors of node n
ave shortest path length	average shortest path between node n and any other node
closeness centrality	the reciprocal of the average shortest path length from node n (interpreted as a measure of how quickly information spreads from node n)
clustering coefficient	measure of the degree to which node n 's neighbors form a complete graph
partner of multi-edged node pairs	how many nodes is node n a partner of that has multiple edges

Appendix B

Modeling the Dynamic Post-MI Environment

Table B.1: Post-Infarct Measurements of Model Inputs

Species Name	0 day	<1 day peak	1 day	3 day	7 day	2 week	4 week	6 week	7 week	Citation
AngII	20.551803	24.608421		28.113235		18.7024				11717612
AngII	0.27								0.64	8181153
TGFb	0.047392	0.414658	0.094737		0.903393					7856752
TGFb	0.041558	0.316883	0.093506		0.264935					7856752
TGFb		8.487281	7.72866	4.203505	4.566422	15.044658	25.950254			11444923
IL6	0.014285	0.763522	0.066663		0.112539					7856752
	0.009565	0.358523	0.023829		0.02078					7856752
		46.5625	10.625	1.5625	1.5625	0.62	0			12123772
IL1b	0.029577	0.490141	0.088732		0.54507					7856752
	0.030435	0.56087	0.065217		0.082609					7856752
		36.7248	19.2607	6.4476	6.69404	7.9671	11.817			12123772
TNFa	0.075342	0.43505	0.107747		0.884695					7856752
	0.064	0.549333	0.032		0.165333					7856752
		0.1625					0.23125			11399901
		659.57446								
NE	289.3617	8		455.319		468.0851				11717612
ET1	0.695535	1.530866		1.129083		1.120692				11717612
BNP	7.423295	56.664773		70.602271		81.357955				11717612
PDGF	1.015		0.4	1.092	2.708	3.138	2.323	1.308		21767547
	0.968		0.255	2.776	3.638	4.521	2.808	2.117		21767547

Color indicates whether the value at that time point is a peak. Pink indicates a low peak (<3x change), red indicates a high peak (>3x change), blue indicates a dip. All values obtained using digitize2.m (<https://www.mathworks.com/matlabcentral/fileexchange/928-digitize2-m>).

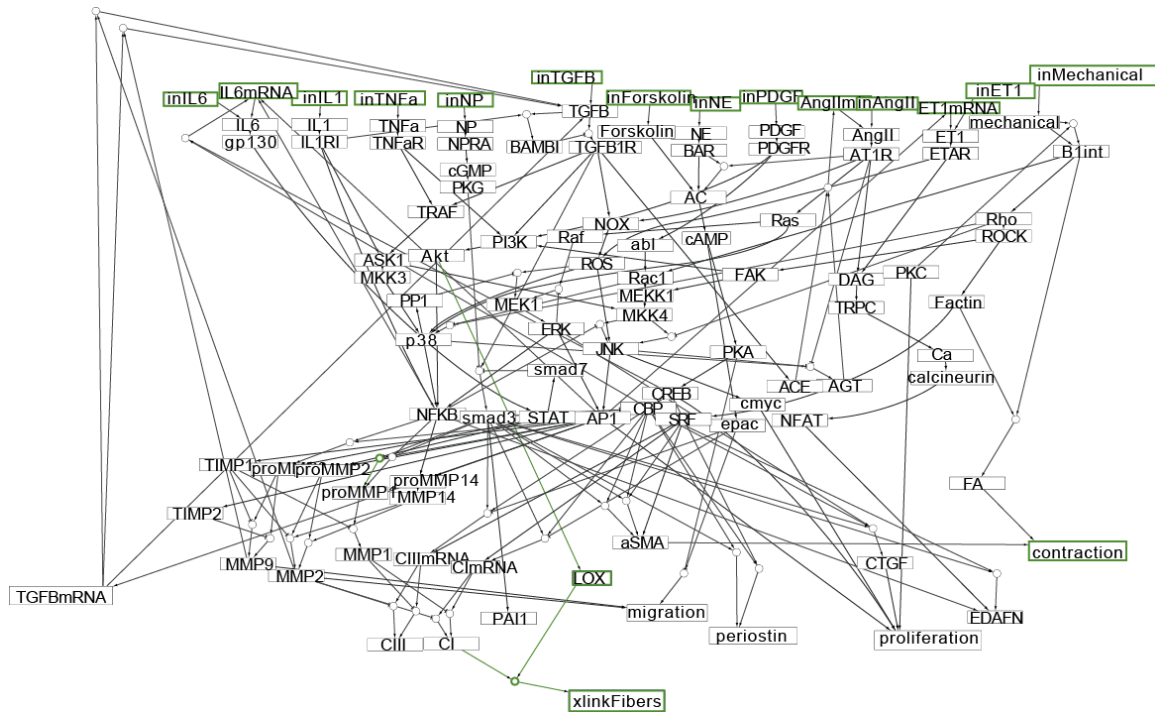


Figure B.1: Network Modifications. Network diagram of model used for post-MI studies (chapter 3) where green color highlights the interactions and nodes not included in the original model (chapter 2).

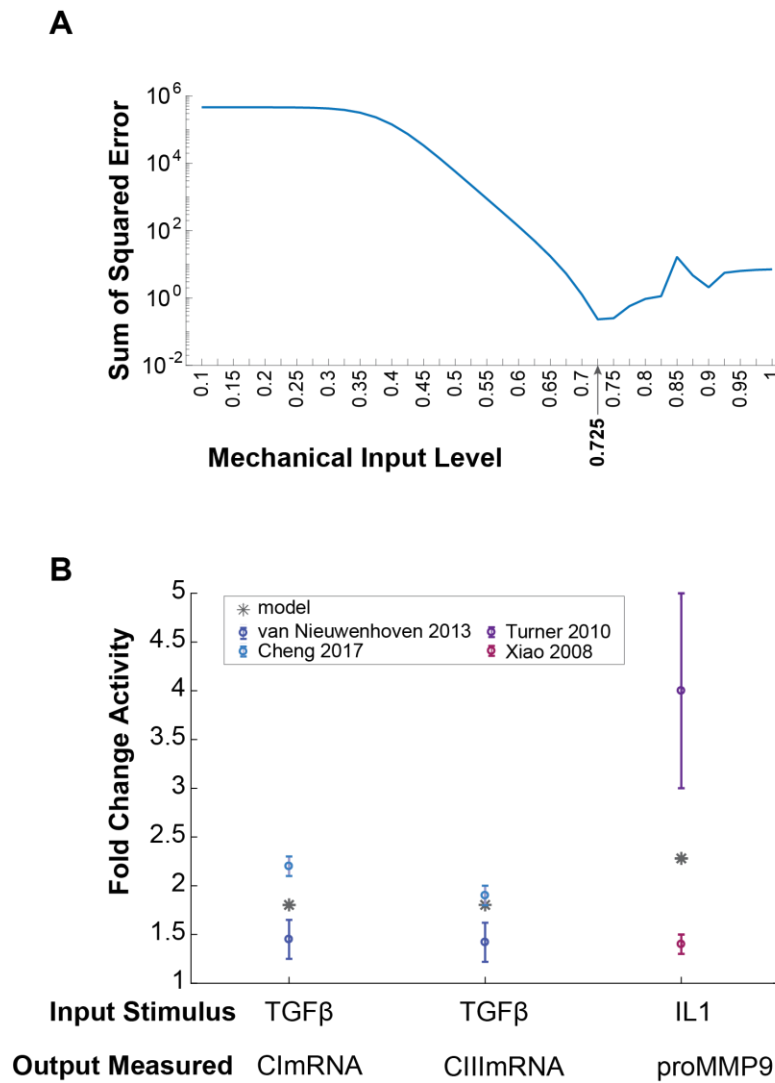


Figure B.2: Training mechanical input levels to validation data. The mechanical input level that defines the stimulus for the control model was identified by brute force optimization. A: For each mechanical input level, the sum of squared area from model prediction was calculated. B: Experimentally determined fold change in the indicated outputs following stimulation with the input is compared to the predicted fold change in specific outputs when the input indicated is added above the optimal control mechanical input.

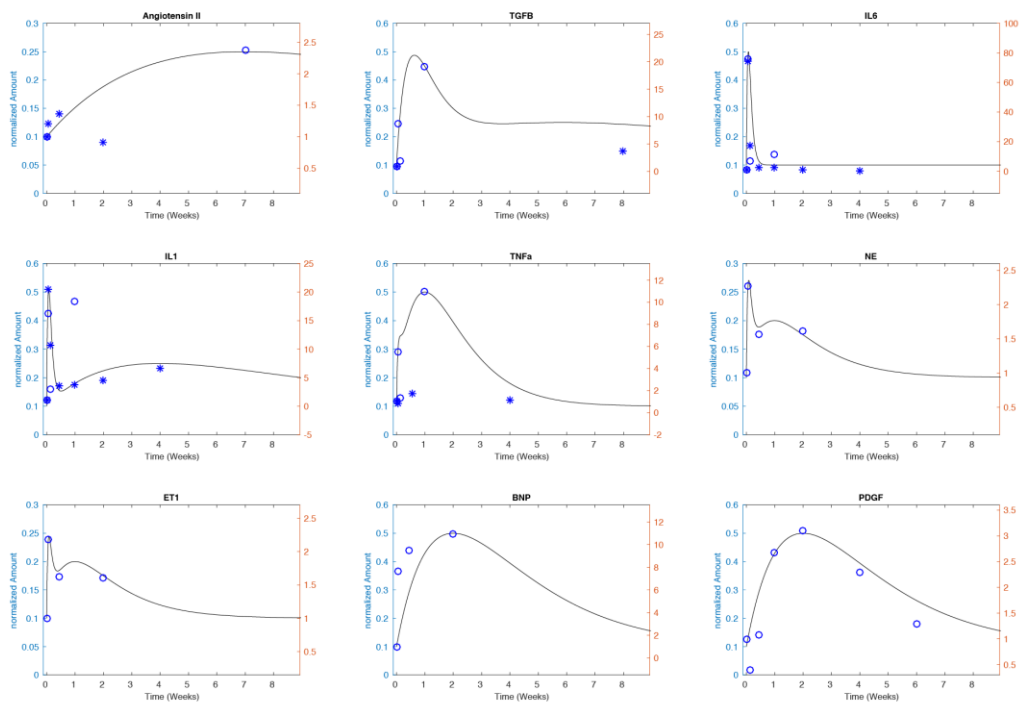


Figure B.3: Inputs for Dynamic MI simulations and their relationship to data. Shown are idealized input curves plotted against the fold change of the levels of the indicated input in rat or human infarcts. Data is summarized in Table B.1

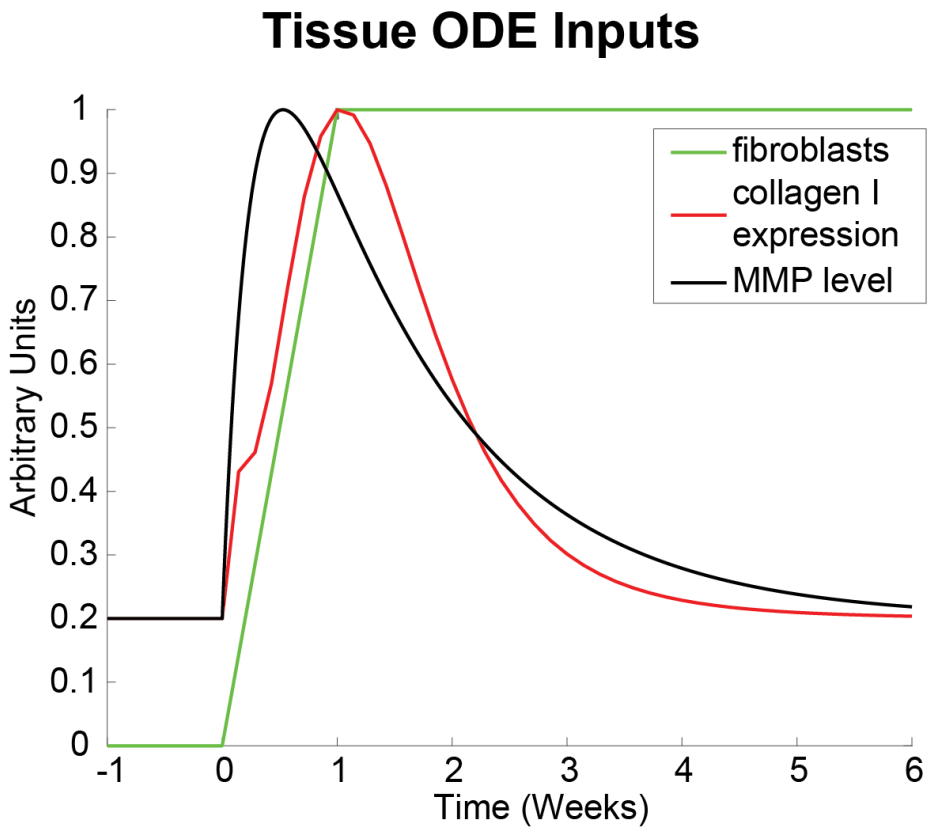


Figure B.4: Inputs to tissue-level model for control (pre-infarct) simulations. Shown are curves that input to the tissue-level model. Fibroblast number and MMP levels are defined by an idealized input curve based on post-MI data. Collagen I expression is the collagen I mRNA level predicted by the network model normalized to a max value of 1.

Appendix C

Drug Target Pairs

Table C.1: All drug-target pairs identified from DrugBank’s database of FDA-approved drugs with a known target within the fibroblast network.

Node Name	Gene Name	Drug Bank ID	Drug Name
'AT1R'	'AGTR1'	'DB00177'	'Valsartan'
'AT1R'	'AGTR1'	'DB00275'	'Olmesartan'
'AT1R'	'AGTR1'	'DB00678'	'Losartan'
'AT1R'	'AGTR1'	'DB00796'	'Candesartan'
'AT1R'	'AGTR1'	'DB00876'	'Eprosartan'
'AT1R'	'AGTR1'	'DB00966'	'Telmisartan'
'AT1R'	'AGTR1'	'DB01029'	'Irbesartan'
'AT1R'	'AGTR1'	'DB01342'	'Forasartan'
'AT1R'	'AGTR1'	'DB01347'	'Saprisartan'
'AT1R'	'AGTR1'	'DB01349'	'Tasosartan'
'AT1R'	'AGTR1'	'DB08822'	'Azilsartan medoxomil'
'AT1R'	'AGTR1'	'DB00177'	'Valsartan'
'AT1R'	'AGTR1'	'DB00275'	'Olmesartan'
'AT1R'	'AGTR1'	'DB00966'	'Telmisartan'
'AT1R'	'AGTR1'	'DB01029'	'Irbesartan'
'ACE'	'ACE'	'DB00178'	'Ramipril'
'ACE'	'ACE'	'DB00492'	'Fosinopril'
'ACE'	'ACE'	'DB00519'	'Trandolapril'
'ACE'	'ACE'	'DB00542'	'Benazepril'
'ACE'	'ACE'	'DB00584'	'Enalapril'
'ACE'	'ACE'	'DB00691'	'Moexipril'
'ACE'	'ACE'	'DB00722'	'Lisinopril'
'ACE'	'ACE'	'DB00790'	'Perindopril'
'ACE'	'ACE'	'DB00881'	'Quinapril'
'ACE'	'ACE'	'DB01180'	'Rescinnamine'
'ACE'	'ACE'	'DB01197'	'Captopril'
'ACE'	'ACE'	'DB01340'	'Cilazapril'
'ACE'	'ACE'	'DB01348'	'Spirapril'
'ACE'	'ACE'	'DB00542'	'Benazepril'
'ACE'	'ACE'	'DB00722'	'Lisinopril'
'ACE'	'ACE'	'DB00881'	'Quinapril'
'ACE'	'ACE2'	'DB00691'	'Moexipril'
'ACE'	'ACE2'	'DB00722'	'Lisinopril'
'ACE'	'ACE2'	'DB00722'	'Lisinopril'
'ETAR'	'EDNRA'	'DB00559'	'Bosentan'
'ETAR'	'EDNRA'	'DB06268'	'Sitaxentan'
'ETAR'	'EDNRA'	'DB06403'	'Ambrisentan'
'ETAR'	'EDNRA'	'DB08932'	'MACITENTAN'

'ETAR'	'EDNRA'	'DB00559'	'Bosentan'
'ETAR'	'EDNRA'	'DB06268'	'Sitaxentan'
'ETAR'	'EDNRA'	'DB06403'	'Ambrisentan'
'BAR'	'ADRB1'	'DB00187'	'Esmolol'
'BAR'	'ADRB1'	'DB00195'	'Betaxolol'
'BAR'	'ADRB1'	'DB00221'	'Isoetarine'
'BAR'	'ADRB1'	'DB00264'	'Metoprolol'
'BAR'	'ADRB1'	'DB00335'	'Atenolol'
'BAR'	'ADRB1'	'DB00368'	'Norepinephrine'
'BAR'	'ADRB1'	'DB00373'	'Timolol'
'BAR'	'ADRB1'	'DB00489'	'Sotalol'
'BAR'	'ADRB1'	'DB00521'	'Carteolol'
'BAR'	'ADRB1'	'DB00571'	'Propranolol'
'BAR'	'ADRB1'	'DB00598'	'Labetalol'
'BAR'	'ADRB1'	'DB00612'	'Bisoprolol'
'BAR'	'ADRB1'	'DB00668'	'Epinephrine'
'BAR'	'ADRB1'	'DB00841'	'Dobutamine'
'BAR'	'ADRB1'	'DB00866'	'Alprenolol'
'BAR'	'ADRB1'	'DB00960'	'Pindolol'
'BAR'	'ADRB1'	'DB01064'	'Isoprenaline'
'BAR'	'ADRB1'	'DB01102'	'Arbutamine'
'BAR'	'ADRB1'	'DB01118'	'Amiodarone'
'BAR'	'ADRB1'	'DB01136'	'Carvedilol'
'BAR'	'ADRB1'	'DB01193'	'Acebutolol'
'BAR'	'ADRB1'	'DB01203'	'Nadolol'
'BAR'	'ADRB1'	'DB01210'	'Levobunolol'
'BAR'	'ADRB1'	'DB01214'	'Metipranolol'
'BAR'	'ADRB1'	'DB01295'	'Bevantolol'
'BAR'	'ADRB1'	'DB01297'	'Practolol'
'BAR'	'ADRB1'	'DB01359'	'Penbutolol'
'BAR'	'ADRB1'	'DB01363'	'Ephedra'
'BAR'	'ADRB1'	'DB01580'	'Oxprenolol'
'BAR'	'ADRB1'	'DB04846'	'Celiprolol'
'BAR'	'ADRB1'	'DB04861'	'Nebivolol'
'BAR'	'ADRB1'	'DB06262'	'Droxidopa'
'BAR'	'ADRB1'	'DB08807'	'Bopindolol'
'BAR'	'ADRB1'	'DB08808'	'Bupranolol'
'BAR'	'ADRB1'	'DB00264'	'Metoprolol'
'BAR'	'ADRB1'	'DB00571'	'Propranolol'
'BAR'	'ADRB1'	'DB01118'	'Amiodarone'
'BAR'	'ADRB1'	'DB01136'	'Carvedilol'
'BAR'	'ADRB1'	'DB01359'	'Penbutolol'
'BAR'	'ADRB1'	'DB04846'	'Celiprolol'

'BAR'	'ADRB1'	'DB04861'	'Nebivolol'
'BAR'	'ADRB1'	'DB06262'	'Droxidopa'
'BAR'	'ADRB2'	'DB00368'	'Norepinephrine'
'BAR'	'ADRB2'	'DB00373'	'Timolol'
'BAR'	'ADRB2'	'DB00449'	'Dipivefrin'
'BAR'	'ADRB2'	'DB00489'	'Sotalol'
'BAR'	'ADRB2'	'DB00521'	'Carteolol'
'BAR'	'ADRB2'	'DB00598'	'Labetalol'
'BAR'	'ADRB2'	'DB00668'	'Epinephrine'
'BAR'	'ADRB2'	'DB00816'	'Orciprenaline'
'BAR'	'ADRB2'	'DB00866'	'Alprenolol'
'BAR'	'ADRB2'	'DB00867'	'Ritodrine'
'BAR'	'ADRB2'	'DB00871'	'Terbutaline'
'BAR'	'ADRB2'	'DB00938'	'Salmeterol'
'BAR'	'ADRB2'	'DB00983'	'Formoterol'
'BAR'	'ADRB2'	'DB01001'	'Salbutamol'
'BAR'	'ADRB2'	'DB01064'	'Isoprenaline'
'BAR'	'ADRB2'	'DB01210'	'Levobunolol'
'BAR'	'ADRB2'	'DB01214'	'Metipranolol'
'BAR'	'ADRB2'	'DB01274'	'Arformoterol'
'BAR'	'ADRB2'	'DB01288'	'Fenoterol'
'BAR'	'ADRB2'	'DB01291'	'Pirbuterol'
'BAR'	'ADRB2'	'DB01359'	'Penbutolol'
'BAR'	'ADRB2'	'DB01363'	'Ephedra'
'BAR'	'ADRB2'	'DB01366'	'Procaterol'
'BAR'	'ADRB2'	'DB01407'	'Clenbuterol'
'BAR'	'ADRB2'	'DB01408'	'Bambuterol'
'BAR'	'ADRB2'	'DB04846'	'Celiprolol'
'BAR'	'ADRB2'	'DB05039'	'Indacaterol'
'BAR'	'ADRB2'	'DB06262'	'Droxidopa'
'BAR'	'ADRB2'	'DB09080'	'Olodaterol'
'BAR'	'ADRB2'	'DB09082'	'Vilanterol'
'BAR'	'ADRB2'	'DB00983'	'Formoterol'
'BAR'	'ADRB2'	'DB01274'	'Arformoterol'
'BAR'	'ADRB2'	'DB01359'	'Penbutolol'
'BAR'	'ADRB2'	'DB04846'	'Celiprolol'
'BAR'	'ADRB2'	'DB06262'	'Droxidopa'
'PDGFR'	'PDGFRA'	'DB01268'	'Sunitinib'
'PDGFR'	'PDGFRA'	'DB06589'	'Pazopanib'
'PDGFR'	'PDGFRA'	'DB08896'	'Regorafenib'
'PDGFR'	'PDGFRA'	'DB01268'	'Sunitinib'
'PDGFR'	'PDGFRB'	'DB00102'	'Becaplermin'
'PDGFR'	'PDGFRB'	'DB00398'	'Sorafenib'

'PDGFR'	'PDGFRB'	'DB01268'	'Sunitinib'
'PDGFR'	'PDGFRB'	'DB06589'	'Pazopanib'
'PDGFR'	'PDGFRB'	'DB08896'	'Regorafenib'
'PDGFR'	'PDGFRB'	'DB00102'	'Becaplermin'
'PDGFR'	'PDGFRB'	'DB00398'	'Sorafenib'
'PDGFR'	'PDGFRB'	'DB01268'	'Sunitinib'
'NPRA'	'NPR1'	'DB00325'	'Nitroprusside'
'NPRA'	'NPR1'	'DB00727'	'Nitroglycerin'
'NPRA'	'NPR1'	'DB00883'	'Isosorbide Dinitrate'
'NPRA'	'NPR1'	'DB01612'	'Amyl Nitrite'
'NPRA'	'NPR1'	'DB01613'	'Erythrityl Tetranitrate'
'NPRA'	'NPR1'	'DB00727'	'Nitroglycerin'
'NPRA'	'NPR2'	'DB01613'	'Erythrityl Tetranitrate'
'B1int'	'ITGB1'	'DB00098'	'Anti-thymocyte Globulin (Rabbit)'
'IL6'	'IL6'	'DB09036'	'Siltuximab'
'gp130'	'IL6R'	'DB06273'	'Tocilizumab'
'IL1'	'IL1B'	'DB05260'	'Gallium nitrate'
'IL1'	'IL1B'	'DB06168'	'Canakinumab'
'IL1'	'IL1B'	'DB05260'	'Gallium nitrate'
'IL1'	'IL1B'	'DB06168'	'Canakinumab'
'IL1RI'	'IL1R1'	'DB00026'	'Anakinra'
'TNFa'	'TNF'	'DB00005'	'Etanercept'
'TNFa'	'TNF'	'DB00051'	'Adalimumab'
'TNFa'	'TNF'	'DB00065'	'Infliximab'
'TNFa'	'TNF'	'DB01041'	'Thalidomide'
'TNFa'	'TNF'	'DB06674'	'golimumab'
'TNFa'	'TNF'	'DB08904'	'Certolizumab pegol'
'TNFa'	'TNF'	'DB08910'	'Pomalidomide'
'TNFa'	'TNF'	'DB00005'	'Etanercept'
'TNFa'	'TNF'	'DB01041'	'Thalidomide'
'NFKB'	'NFKB1'	'DB01041'	'Thalidomide'
'NFKB'	'NFKB1'	'DB08814'	'Triflusal'
'NFKB'	'NFKB1'	'DB01041'	'Thalidomide'
'abl'	'ABL1'	'DB01254'	'Dasatinib'
'abl'	'ABL1'	'DB04868'	'Nilotinib'
'abl'	'ABL1'	'DB06616'	'Bosutinib'
'abl'	'ABL1'	'DB08896'	'Regorafenib'
'abl'	'ABL1'	'DB08901'	'Ponatinib'
'abl'	'ABL1'	'DB01254'	'Dasatinib'
'abl'	'ABL1'	'DB04868'	'Nilotinib'
'ERK'	'MAPK1'	'DB01169'	'Arsenic trioxide'
'ERK'	'MAPK1'	'DB01169'	'Arsenic trioxide'

'ERK'	'MAPK3'	'DB01169'	'Arsenic trioxide'
'ERK'	'MAPK3'	'DB01169'	'Arsenic trioxide'
'Raf'	'RAF1'	'DB00398'	'Sorafenib'
'Raf'	'RAF1'	'DB08896'	'Regorafenib'
'Raf'	'RAF1'	'DB08912'	'Dabrafenib'
'Raf'	'RAF1'	'DB00398'	'Sorafenib'
'MEK1'	'MAP2K1'	'DB05239'	'Cobimetinib'
'MEK1'	'MAP2K1'	'DB08911'	'Trametinib'
'EDAFN'	'FN1'	'DB08888'	'Ocriplasmin'
'AP1 '	'JUN'	'DB01169'	'Arsenic trioxide'
'AP1 '	'JUN'	'DB01169'	'Arsenic trioxide'
'PAI1'	'SERPINE1'	'DB00013'	'Urokinase'
'PAI1'	'SERPINE1'	'DB00013'	'Urokinase'
'MMP1'	'MMP1'	'DB00786'	'Marimastat'
'MMP1'	'MMP1'	'DB00786'	'Marimastat'
'MMP2'	'MMP2'	'DB00786'	'Marimastat'
'MMP2'	'MMP2'	'DB00786'	'Marimastat'
'MMP9'	'MMP9'	'DB00786'	'Marimastat'
'MMP9'	'MMP9'	'DB01296'	'Glucosamine'
'MMP9'	'MMP9'	'DB00786'	'Marimastat'
'MMP14'	'MMP14'	'DB00786'	'Marimastat'
'MMP14'	'MMP14'	'DB00786'	'Marimastat'

Bibliography

- Acencio, Marcio L, and Ney Lemke. 2009. "Towards the Prediction of Essential Genes by Integration of Network Topology, Cellular Localization and Biological Process Information." *BMC Bioinformatics* 10 (1): 290. <https://doi.org/10.1186/1471-2105-10-290>.
- Albert, Réka. 2005. "Scale-Free Networks in Cell Biology." *Journal of Cell Science* 118 (Pt 21): 4947–57. <https://doi.org/10.1242/jcs.02714>.
- . 2007. "Network Inference, Analysis, and Modeling in Systems Biology." *The Plant Cell* 19 (11): 3327–38. <https://doi.org/10.1105/tpc.107.054700>.
- Artlett, Carol M., Sihem Sassi-Gaha, Jennifer L. Hope, Carol A. Feghali-Bostwick, and Peter D. Katsikis. 2017. "Mir-155 Is Overexpressed in Systemic Sclerosis Fibroblasts and Is Required for NLRP3 Inflammasome-Mediated Collagen Synthesis during Fibrosis." *Arthritis Research & Therapy* 19 (1): 144. <https://doi.org/10.1186/s13075-017-1331-z>.
- Asbun, Juan, and Francisco J. Villarreal. 2006. "The Pathogenesis of Myocardial Fibrosis in the Setting of Diabetic Cardiomyopathy." *Journal of the American College of Cardiology*. <https://doi.org/10.1016/j.jacc.2005.09.050>.
- Ashihara, Takashi, Ryo Haraguchi, Kazuo Nakazawa, Tsunetoyo Namba, Takanori Ikeda, Yuko Nakazawa, Tomoya Ozawa, Makoto Ito, Minoru Horie, and Natalia A. Trayanova. 2012. "The Role of Fibroblasts in Complex Fractionated Electrograms during Persistent/permanent Atrial Fibrillation: Implications for Electrogram-Based Catheter

Ablation.” *Circulation Research* 110 (2): 275–84.

<https://doi.org/10.1161/CIRCRESAHA.111.255026>.

Assenov, Yassen, Fidel Ramírez, S. E Sven Eric Schelhorn, Thomas Lengauer, and Mario

Albrecht. 2008. “Computing Topological Parameters of Biological Networks.”

Bioinformatics 24 (2): 282–84. <https://doi.org/10.1093/bioinformatics/btm554>.

Bajikar, Sameer S, and Kevin A Janes. 2012. “Multiscale Models of Cell Signaling.” *Annals of*

Biomedical Engineering 40 (11): 2319–27. <https://doi.org/10.1007/s10439-012-0560-1>.

Batada, Nizar N., Laurence D. Hurst, and Mike Tyers. 2006. “Evolutionary and Physiological

Importance of Hub Proteins.” *PLoS Computational Biology* 2 (7): 0748–56.

<https://doi.org/10.1371/journal.pcbi.0020088>.

Baylis, Richard A., Delphine Gomez, Ziad Mallat, Gerard Pasterkamp, and Gary K. Owens.

2017. “The CANTOS Trial One Important Step for Clinical Cardiology but a Giant Leap for Vascular Biology.” *Arterioscler Thromb Vasc Biol* 37: e174–77.

Bazil, Jason N., Karl D. Stamm, Xing Li, Raghuram Thiagarajan, Timothy J. Nelson, Aoy

Tomita-Mitchell, and Daniel A. Beard. 2014. “The Inferred Cardiogenic Gene Regulatory Network in the Mammalian Heart.” *PLoS ONE* 9 (6).

<https://doi.org/10.1371/journal.pone.0100842>.

Beltrami, C. A., N. Finato, M. Rocco, G. A. Feruglio, C. Puricelli, E. Cigola, F. Quaini, E. H.

Sonnenblick, G. Olivetti, and P. Anversa. 1994. “Structural Basis of End-Stage Failure in Ischemic Cardiomyopathy in Humans.” *Circulation* 89 (1): 151–63.

<https://doi.org/10.1161/01.CIR.89.1.151>.

- Benton, Julie A., Benjamin D. Fairbanks, and Kristi S. Anseth. 2009. "Characterization of Valvular Interstitial Cell Function in Three Dimensional Matrix Metalloproteinase Degradable PEG Hydrogels." *Biomaterials* 30 (34): 6593–6603.
<https://doi.org/10.1016/j.biomaterials.2009.08.031>.
- Birk, D E, and R L Trelstad. 1986. "Extracellular Compartments in Tendon Morphogenesis: Collagen Fibril, Bundle, and Macroaggregate Formation." *The Journal of Cell Biology* 103 (1): 231–40.
- Blais, Edik M., Kristopher D. Rawls, Bonnie V. Dougherty, Zhuo I. Li, Glynis L. Kolling, Ping Ye, Anders Wallqvist, and Jason A. Papin. 2017. "Reconciled Rat and Human Metabolic Networks for Comparative Toxicogenomics and Biomarker Predictions." *Nature Communications* 8. <https://doi.org/10.1038/ncomms14250>.
- Bogen, D K, S A Rabinowitz, A Needleman, T A McMahon, and W H Abelmann. 1980. "An Analysis of the Mechanical Disadvantage of Myocardial Infarction in the Canine Left Ventricle." *Circulation Research* 47 (5): 728–41.
- Bondarenko, Vladimir E, Gyula P Szigeti, Glenna C L Bett, Song-Jung Kim, and Randall L Rasmusson. 2004. "Computer Model of Action Potential of Mouse Ventricular Myocytes." *American Journal of Physiology. Heart and Circulatory Physiology* 287 (3): H1378-403.
<https://doi.org/10.1152/ajpheart.00185.2003>.
- Borne, Susanne W.M. Van Den, Javier Diez, W. Matthijs Blanckesteijn, Johan Verjans, Leo Hofstra, and Jagat Narula. 2010. "Myocardial Remodeling after Infarction: The Role of Myofibroblasts." *Nature Reviews Cardiology*. <https://doi.org/10.1038/nrcardio.2009.199>.
- Bover, R, F Perez-Gomez, M P Maluenda, S Asenjo, R Perez-Saldana, A Igea, M Suarez, D

- Coletto, and C Fernandez. 2009. "Long-Term Follow-up of Atrial Fibrillation Patients in the NASPEAF Study. Prospective Evaluation of Different Antiplatelet Treatments." *Rev Esp Cardiol* 62 (9): 992–1000. <https://doi.org/13140541> [pii].
- Brown, Bryan N., Ian M. Price, Franklin R. Toapanta, Dilhari R. DeAlmeida, Clayton a. Wiley, Ted M. Ross, Tim D. Oury, and Yoram Vodovotz. 2011. "An Agent-Based Model of Inflammation and Fibrosis Following Particulate Exposure in the Lung." *Mathematical Biosciences* 231 (2). Elsevier Inc.: 186–96. <https://doi.org/10.1016/j.mbs.2011.03.005>.
- Bujak, Marcin, and Nikolaos G Frangogiannis. 2007. "The Role of TGF-Beta Signaling in Myocardial Infarction and Cardiac Remodeling." *Cardiovascular Research* 74 (2): 184–95. <https://doi.org/10.1016/j.cardiores.2006.10.002>.
- Campbell, Stuart G, and Andrew D McCulloch. 2011. "Multi-Scale Computational Models of Familial Hypertrophic Cardiomyopathy: Genotype to Phenotype." *Journal of the Royal Society, Interface / the Royal Society* 8 (64): 1550–61. <https://doi.org/10.1098/rsif.2011.0184>.
- Canty, Elizabeth G, Yinhui Lu, Roger S Meadows, Michael K Shaw, David F Holmes, and Karl E Kadler. 2004. "Coalignment of Plasma Membrane Channels and Protrusions (Fibripositors) Specifies the Parallelism of Tendon." *The Journal of Cell Biology* 165 (4): 553–63. <https://doi.org/10.1083/jcb.200312071>.
- Carpenter, Anne E, Thouis R Jones, Michael R Lamprecht, Colin Clarke, In Han Kang, Ola Friman, David a Guertin, et al. 2006. "CellProfiler: Image Analysis Software for Identifying and Quantifying Cell Phenotypes." *Genome Biology* 7 (10): R100. <https://doi.org/10.1186/gb-2006-7-10-r100>.

- Checa, Sara, Manuel K Rausch, Ansgar Petersen, Ellen Kuhl, and Georg N Duda. 2014. “The Emergence of Extracellular Matrix Mechanics and Cell Traction Forces as Important Regulators of Cellular Self-Organization.” *Biomechanics and Modeling in Mechanobiology*, April. <https://doi.org/10.1007/s10237-014-0581-9>.
- Chilton, L, S Ohya, D Freed, E George, V Drobic, Y Shibukawa, K A Maccannell, et al. 2005. “K⁺ Currents Regulate the Resting Membrane Potential, Proliferation, and Contractile Responses in Ventricular Fibroblasts and Myofibroblasts.” *American Journal of Physiology. Heart and Circulatory Physiology* 288 (6): H2931–39. <https://doi.org/10.1152/ajpheart.01220.2004>.
- Chistiakov, Dimitry A., Alexander N. Orekhov, and Yuri V. Bobryshev. 2016. “The Role of Cardiac Fibroblasts in Post-Myocardial Heart Tissue Repair.” *Experimental and Molecular Pathology*. <https://doi.org/10.1016/j.yexmp.2016.09.002>.
- Chu, Wenfeng, Cui Li, Xuefeng Qu, Dan Zhao, Xuelian Wang, Xiangru Yu, Fulai Cai, et al. 2012. “Arsenic-Induced Interstitial Myocardial Fibrosis Reveals a New Insight into Drug-Induced Long QT Syndrome.” *Cardiovascular Research* 96 (1): 90–98. <https://doi.org/10.1093/cvr/cvs230>.
- Clancy, Colleen E., and Yoram Rudy. 2002. “Na⁺ Channel Mutation That Causes Both Brugada and Long-QT Syndrome Phenotypes: A Simulation Study of Mechanism.” *Circulation* 105 (10): 1208–13. <https://doi.org/10.1161/hc1002.105183>.
- Clarke, Samantha A., William J. Richardson, and Jeffrey W. Holmes. 2016. “Modifying the Mechanics of Healing Infarcts: Is Better the Enemy of Good?” *Journal of Molecular and Cellular Cardiology*. <https://doi.org/10.1016/j.yjmcc.2015.11.028>.

- Cleutjens, J P, M J Verluyten, J F Smiths, and M J Daemen. 1995. "Collagen Remodeling after Myocardial Infarction in the Rat Heart." *The American Journal of Pathology* 147 (2): 325–38.
<http://www.pubmedcentral.nih.gov/articlerender.fcgi?artid=1869816&tool=pmcentrez&rendertype=abstract>.
- Colatsky, Thomas, Bernard Fermini, Gary Gintant, Jennifer B. Pierson, Philip Sager, Yuko Sekino, David G. Strauss, and Norman Stockbridge. 2016. "The Comprehensive in Vitro Proarrhythmia Assay (CiPA) Initiative — Update on Progress." *Journal of Pharmacological and Toxicological Methods* 81: 15–20.
<https://doi.org/10.1016/j.vascn.2016.06.002>.
- Costa, João, José M. Ferro, Jordi Matías-Guiu, José Alvarez-Sabin, and Ferran Torres. 2006. "Triflusal for Preventing Serious Vascular Events in People at High Risk." *Stroke* 37 (8): 2193–95. <https://doi.org/10.1161/01.STR.0000231642.59626.74>.
- Costa, Pedro R, Marcio L Acencio, and Ney Lemke. 2010. "A Machine Learning Approach for Genome-Wide Prediction of Morbid and Druggable Human Genes Based on Systems-Level Data." *BMC Genomics* 11 (Suppl 5): S9. <https://doi.org/10.1186/1471-2164-11-S5-S9>.
- Creemers, E. E.J.M., J. P.M. Cleutjens, J. F.M. Smits, and M. J.a.P. Daemen. 2001. "Matrix Metalloproteinase Inhibition After Myocardial Infarction: A New Approach to Prevent Heart Failure?" *Circulation Research* 89 (3): 201–10.
<https://doi.org/10.1161/hh1501.094396>.
- Cruz-Fernández, J. M., L. López-Bescós, D. García-Dorado, V. López García-Aranda, A. Cabadés, L. Martín-Jadraque, J. A. Velasco, et al. 2000. "Randomized Comparative Trial of

- Triflusal and Aspirin Following Acute Myocardial Infarction.” *European Heart Journal* 21 (6): 457–65. <https://doi.org/10.1053/euhj.1999.1874>.
- Cucoranu, Ioan, Roza Clempus, Anna Dikalova, Patrick J. Phelan, Srividya Ariyan, Sergey Dikalov, and Dan Sorescu. 2005. “NAD(P)H Oxidase 4 Mediates Transforming Growth Factor- β 1-Induced Differentiation of Cardiac Fibroblasts into Myofibroblasts.” *Circulation Research* 97 (9): 900–907. <https://doi.org/10.1161/01.RES.0000187457.24338.3D>.
- Czubryt MP, Safi HA, Nagalingam RS. 2016. “Gaining Myocytes or Losing Fibroblasts: Challenges in Cardiac Fibroblast Reprogramming for Infarct Repair.” *Journal of Molecular and Cellular Cardiology*.
- Dallon, J C, J A Sherratt, and P K Maini. “Modeling the Effects of Transforming Growth Factor-Beta on Extracellular Matrix Alignment in Dermal Wound Repair.” *Wound Repair and Regeneration : Official Publication of the Wound Healing Society [and] the European Tissue Repair Society* 9 (4): 278–86.
- . 1999. “Mathematical Modelling of Extracellular Matrix Dynamics Using Discrete Cells: Fiber Orientation and Tissue Regeneration.” *Journal of Theoretical Biology* 199 (4): 449–71. <https://doi.org/10.1006/jtbi.1999.0971>.
- Dallon, J, J Sherratt, P Maini, and M Ferguson. 2000. “Biological Implications of a Discrete Mathematical Model for Collagen Deposition and Alignment in Dermal Wound Repair.” *IMA Journal of Mathematics Applied in Medicine and Biology* 17 (4): 379–93.
- Dawn, Buddhadeb, Yu-Ting Xuan, Yiru Guo, Arash Rezazadeh, Adam B Stein, Greg Hunt, Wen-Jian Wu, Wei Tan, and Roberto Bolli. 2004. “IL-6 Plays an Obligatory Role in Late Preconditioning via JAK-STAT Signaling and Upregulation of iNOS and COX-2.”

Cardiovascular Research 64 (1): 61–71. <https://doi.org/10.1016/j.cardiores.2004.05.011>.

Desai, Poonam, Jun Yang, Bing Tian, Hong Sun, Mridul Kalita, Hyunsu Ju, Adriana Paulucci-Holthauzen, Yingxin Zhao, Allan R Brasier, and Rovshan G Sadygov. 2015. “Mixed-Effects Model of Epithelial-Mesenchymal Transition Reveals Rewiring of Signaling Networks.” *Cellular Signalling* 27 (7): 1413–25.
<https://doi.org/10.1016/j.cellsig.2015.03.024>.

Deten, A, A Hölzl, M Leicht, W Barth, and H G Zimmer. 2001. “Changes in Extracellular Matrix and in Transforming Growth Factor Beta Isoforms after Coronary Artery Ligation in Rats.” *Journal of Molecular and Cellular Cardiology* 33 (6): 1191–1207.
<https://doi.org/10.1006/jmcc.2001.1383>.

Deten, Alexander, Hans Christian Volz, Wilfried Briest, and Heinz-Gerd Zimmer. 2002. “Cardiac Cytokine Expression Is Upregulated in the Acute Phase after Myocardial Infarction. Experimental Studies in Rats.” *Cardiovascular Research* 55 (2): 329–40.
<https://doi.org/S0008636302004133> [pii].

Díaz-Araya, G, R Vivar, C Humeres, P Boza, S Bolivar, and C Muñoz. 2015. “Cardiac Fibroblasts as Sentinel Cells in Cardiac Tissue: Receptors, Signaling Pathways and Cellular Functions.” *Pharmacological Research : The Official Journal of the Italian Pharmacological Society*, July. <https://doi.org/10.1016/j.phrs.2015.07.001>.

Dobaczewski, Marcin, Marcin Bujak, Na Li, Carlos Gonzalez-Quesada, Leonardo H. Mendoza, Xiaiao Fan Wang, and Nikolaos G. Frangogiannis. 2010. “Smad3 Signaling Critically Regulates Fibroblast Phenotype and Function in Healing Myocardial Infarction.” *Circulation Research* 107 (3): 418–28. <https://doi.org/10.1161/CIRCRESAHA.109.216101>.

- Downing, Nicholas S., Nilay D. Shah, Jenerius A. Aminawung, Alison M. Pease, Jean-David Zeitoun, Harlan M. Krumholz, and Joseph S. Ross. 2017. "Postmarket Safety Events Among Novel Therapeutics Approved by the US Food and Drug Administration Between 2001 and 2010." *JAMA* 317 (18): 1854. <https://doi.org/10.1001/jama.2017.5150>.
- Driesen, Ronald B., Chandan K. Nagaraju, Joëlle Abi-Char, Tamara Coenen, Paul J. Lijnen, Robert H. Fagard, Karin R. Sipido, and Victor V. Petrov. 2014. "Reversible and Irreversible Differentiation of Cardiac Fibroblasts." *Cardiovascular Research* 101 (3): 411–22. <https://doi.org/10.1093/cvr/cvt338>.
- Driessen, Niels J B, Carlijn V C Bouten, and Frank P T Baaijens. 2005. "Improved Prediction of the Collagen Fiber Architecture in the Aortic Heart Valve." *Journal of Biomechanical Engineering* 127 (2): 329–36.
- Driessen, Niels J B, Martijn A J Cox, Carlijn V C Bouten, and Frank P T Baaijens. 2008. "Remodelling of the Angular Collagen Fiber Distribution in Cardiovascular Tissues." *Biomechanics and Modeling in Mechanobiology* 7 (2): 93–103. <https://doi.org/10.1007/s10237-007-0078-x>.
- Driessen, Niels J, Ralf A Boerboom, Jacques M Huyghe, Carlijn V Bouten, and Frank P Baaijens. 2003. "Computational Analyses of Mechanically Induced Collagen Fiber Remodeling in the Aortic Heart Valve." *Journal of Biomechanical Engineering* 125 (4): 549–57.
- Duncan, Matthew R., and Brian Berman. 1989. "Differential Regulation of Collagen, Glycosaminoglycan, Fibronectin, and Collagenase Activity Production in Cultured Human Adult Dermal Fibroblasts by Interleukin 1-Alpha and Beta and Tumor Necrosis Factor-

Alpha and Beta.” *The Journal of Investigative Dermatology* 92 (5): 699–706.

Dutta-Moscato, Joyeeta, Alexey Solovyev, Qi Mi, Taichiro Nishikawa, Alejandro Soto-Gutierrez, Ira J. Fox, and Yoram Vodovotz. 2014. “A Multiscale Agent-Based in Silico Model of Liver Fibrosis Progression.” *Frontiers in Bioengineering and Biotechnology* 2 (May): 1–10. <https://doi.org/10.3389/fbioe.2014.00018>.

Ekins, S., J. Mestres, and B. Testa. 2007. “In Silico Pharmacology for Drug Discovery: Applications to Targets and beyond.” *British Journal of Pharmacology*.
<https://doi.org/10.1038/sj.bjp.0707306>.

Fedosov, Dmitry A, Hiroshi Noguchi, and Gerhard Gompper. 2014. “Multiscale Modeling of Blood Flow: From Single Cells to Blood Rheology.” *Biomechanics and Modeling in Mechanobiology* 13 (2): 239–58. <https://doi.org/10.1007/s10237-013-0497-9>.

Fishbein, M. C., D. Maclean, and P. R. Maroko. 1978. “The Histopathologic Evolution of Myocardial Infarction.” *Chest* 73 (6): 843–49. <https://doi.org/10.1378/chest.73.6.843>.

Folger, Ori, Livnat Jerby, Christian Frezza, Eyal Gottlieb, Eytan Ruppin, and Tomer Shlomi. 2011. “Predicting Selective Drug Targets in Cancer through Metabolic Networks.” *Molecular Systems Biology* 7. <https://doi.org/10.1038/msb.2011.35>.

Fomovsky, Gregory M, and Jeffrey W Holmes. 2010. “Evolution of Scar Structure, Mechanics, and Ventricular Function after Myocardial Infarction in the Rat.” *American Journal of Physiology. Heart and Circulatory Physiology* 298 (1): H221-8.
<https://doi.org/10.1152/ajpheart.00495.2009>.

Fomovsky, Gregory M, Jesse R Macadangdang, Gorav Ailawadi, and Jeffrey W Holmes. 2011.

“Model-Based Design of Mechanical Therapies for Myocardial Infarction.” *Journal of Cardiovascular Translational Research* 4 (1): 82–91. <https://doi.org/10.1007/s12265-010-9241-3>.

Fomovsky, Gregory M, Andrew D Rouillard, and Jeffrey W Holmes. 2012. “Regional Mechanics Determine Collagen Fiber Structure in Healing Myocardial Infarcts.” *Journal of Molecular and Cellular Cardiology* 52 (5). Elsevier Ltd: 1083–90. <https://doi.org/10.1016/j.yjmcc.2012.02.012>.

Frantz, Stefan, Kai Hu, Anna Adamek, Jürgen Wolf, Abed Sallam, Sebastian K G Maier, Scott Lanning, Hong Ling, Georg Ertl, and Johann Bauersachs. 2008. “Transforming Growth Factor Beta Inhibition Increases Mortality and Left Ventricular Dilatation after Myocardial Infarction.” *Basic Research in Cardiology* 103 (5): 485–92. <https://doi.org/10.1007/s00395-008-0739-7>.

Furtado, Milena B., Mauro W. Costa, Edward A. Pranoto, Ekaterina Salimova, Alexander R. Pinto, Nicholas T. Lam, Anthony Park, et al. 2014. “Cardiogenic Genes Expressed in Cardiac Fibroblasts Contribute to Heart Development and Repair.” *Circulation Research* 114 (9): 1422–34. <https://doi.org/10.1161/CIRCRESAHA.114.302530>.

Galvão, Viviane, J. G V Miranda, and Ricardo Ribeiro-dos-Santos. 2008. “Development of a Two-Dimensional Agent-Based Model for Chronic Chagasic Cardiomyopathy after Stem Cell Transplantation.” *Bioinformatics* 24 (18): 2051–56. <https://doi.org/10.1093/bioinformatics/btn362>.

Galvão, Viviane, and José Garcia Vivas Miranda. 2010. “A Three-Dimensional Multi-Agent-Based Model for the Evolution of Chagas’ Disease.” *Bio Systems* 100 (3): 225–30.

<https://doi.org/10.1016/j.biosystems.2010.03.007>.

Gaudesius, Giedrius, Michele Miragoli, Stuart P. Thomas, and Stephan Rohr. 2003. "Coupling of Cardiac Electrical Activity over Extended Distances by Fibroblasts of Cardiac Origin."

Circulation Research 93 (5): 421–28.

<https://doi.org/10.1161/01.RES.0000089258.40661.0C>.

Gottdiener, J S, a M Arnold, G P Aurigemma, J F Polak, R P Tracy, D W Kitzman, J M Gardin,

J E Rutledge, and R C Boineau. 2000. "Predictors of Congestive Heart Failure in the

Elderly: The Cardiovascular Health Study." *Journal of the American College of Cardiology*

35 (6): 1628–37. [https://doi.org/10.1016/S0735-1097\(00\)00582-9](https://doi.org/10.1016/S0735-1097(00)00582-9).

Graves, D T, N Nooh, T Gillen, M Davey, S Patel, D Cottrell, and S Amar. 2001. "IL-1 Plays a

Critical Role in Oral, but Not Dermal, Wound Healing." *Journal of Immunology (Baltimore,*

Md. : 1950) 167 (9): 5316–20. <https://doi.org/10.4049/jimmunol.167.9.5316>.

Greenwald, Eric C., John M. Redden, Kimberly L. Dodge-Kafka, and Jeffrey J. Saucerman.

2014. "Scaffold State Switching Amplifies, Accelerates, and Insulates Protein Kinase c

Signaling." *Journal of Biological Chemistry* 289 (4): 2353–60.

<https://doi.org/10.1074/jbc.M113.497941>.

Greisas, Ariel, and Sharon Zlochiver. 2012. "Modulation of Spiral-Wave Dynamics and

Spontaneous Activity in a Fibroblast/myocyte Heterocellular Tissue - A Computational

Study." *IEEE Transactions on Biomedical Engineering* 59 (5): 1398–1407.

<https://doi.org/10.1109/TBME.2012.2188291>.

Grinnell, Frederick. 1994. "Fibroblasts, Myofibroblasts, and Wound Contraction." *Journal of*

Cell Biology. <https://doi.org/10.1083/jcb.124.4.401>.

Guney, Emre, Jörg Menche, Marc Vidal, and Albert-László Barabási. 2016. “Network-Based in Silico Drug Efficacy Screening.” *Nature Communications* 7.

<https://doi.org/10.1038/ncomms10331>.

Guo, S, and L A Dipietro. 2010. “Factors Affecting Wound Healing.” *J Dent Res* 89 (3): 219–29.

<https://doi.org/10.1177/0022034509359125>.

Hahn, Matthew W., and Andrew D. Kern. 2005. “Comparative Genomics of Centrality and Essentiality in Three Eukaryotic Protein-Interaction Networks.” *Molecular Biology and Evolution* 22 (4): 803–6. <https://doi.org/10.1093/molbev/msi072>.

Hao, W., B. H. Rovin, and a. Friedman. 2014. “Mathematical Model of Renal Interstitial Fibrosis.” *Proceedings of the National Academy of Sciences* 111 (39): 14193–98.

<https://doi.org/10.1073/pnas.1413970111>.

Harris, A K, D Stopak, and P Wild. 1981. “Fibroblast Traction as a Mechanism for Collagen Morphogenesis.” *Nature* 290 (5803): 249–51.

Hartwell, L H, J J Hopfield, S Leibler, and A W Murray. 1999. “From Molecular to Modular Cell Biology.” *Nature* 402 (6761 Suppl): C47–52. <https://doi.org/10.1038/35011540>.

Haug, C, A Metzele, J Steffgen, M Kochs, V Hombach, and A Grunert. 1994. “Increased Brain Natriuretic Peptide and Atrial Natriuretic Peptide Plasma Concentrations in Dialysis-Dependent Chronic Renal Failure and in Patients with Elevated Left Ventricular Filling Pressure.” *Clin Investig*. <http://www.ncbi.nlm.nih.gov/pubmed/7950153>.

Hautaniemi, Sampsa, Sourabh Kharait, Akihiro Iwabuchi, Alan Wells, and Douglas A.

Lauffenburger. 2005. “Modeling of Signal-Response Cascades Using Decision Tree

Analysis.” *Bioinformatics* 21 (9): 2027–35. <https://doi.org/10.1093/bioinformatics/bti278>.

Hayenga, H, B Thorne, P Yen, J Papin, Shayn M Peirce, and Jay D Humphrey. 2013.

“Multiscale Computational Modeling in Vascular Biology: From Molecular Mechanisms to Tissue-Level Structure and Function.” In *Multiscale Computer Modeling in Biomechanics and Biomedical Engineering*, edited by A. Gefen, 209–40. Berlin, Heidelberg: Springer Berlin Heidelberg.

He, J, L G Ogden, L A Bazzano, S Vupputuri, C Loria, and P K Whelton. 2001. “Risk Factors for Congestive Heart Failure in US Men and Women: NHANES I Epidemiologic Follow-up Study.” *Archives of Internal Medicine* 161 (7): 996–1002.
<https://doi.org/10.1001/archinte.161.7.996>.

He, Xionglei, and Jianzhi Zhang. 2006. “Why Do Hubs Tend to Be Essential in Protein Networks?” *PLoS Genetics* 2 (6): 0826–34. <https://doi.org/10.1371/journal.pgen.0020088>.

Herskowitz, a, S Choi, a a Ansari, and S Wesselingh. 1995. “Cytokine mRNA Expression in Postischemic/reperfused Myocardium.” *The American Journal of Pathology* 146 (2): 419–28.

Holland, David O, Nicholas C Krainak, and Jeffrey J Saucerman. 2011. “Graphical Approach to Model Reduction for Nonlinear Biochemical Networks.” *PloS One* 6 (8): e23795.
<https://doi.org/10.1371/journal.pone.0023795>.

Holmes, J W, J A Nuñez, and J W Covell. 1997. “Functional Implications of Myocardial Scar Structure.” *The American Journal of Physiology* 272 (5 Pt 2): H2123-30.

Hu, Guanghui, and Pankaj Agarwal. 2009. “Human Disease-Drug Network Based on Genomic

Expression Profiles.” *PLoS ONE* 4 (8). <https://doi.org/10.1371/journal.pone.0006536>.

Huang, Xiangwei, Naiheng Yang, Vincent F. Fiore, Thomas H. Barker, Yi Sun, Stephan W.

Morris, Qiang Ding, Victor J. Thannickal, and Yong Zhou. 2012. “Matrix Stiffness-Induced Myofibroblast Differentiation Is Mediated by Intrinsic Mechanotransduction.” *American Journal of Respiratory Cell and Molecular Biology* 47 (3): 340–48.

<https://doi.org/10.1165/rcmb.2012-0050OC>.

Hunter, Peter J., Wilfred W. Li, Andrew D. McCulloch, and Denis Noble. 2006. “Multiscale

Modeling: Physiome Project Standards, Tools, and Databases.” *Computer* 39 (11): 48–54.

<https://doi.org/10.1109/MC.2006.392>.

Hwang, M W, A Matsumori, Y Furukawa, K Ono, M Okada, A Iwasaki, M Hara, T Miyamoto,

M Touma, and S Sasayama. 2001. “Neutralization of Interleukin-1beta in the Acute Phase of Myocardial Infarction Promotes the Progression of Left Ventricular Remodeling.”

Journal of the American College of Cardiology 38 (5): 1546–53. [https://doi.org/S0735-1097\(01\)01591-1](https://doi.org/S0735-1097(01)01591-1) [pii].

Ikeuchi, Masaki, Hiroyuki Tsutsui, Tetsuya Shiomi, Hidenori Matsusaka, Shouji Matsushima,

Jing Wen, Toru Kubota, and Akira Takeshita. 2004. “Inhibition of TGF-?? Signaling

Exacerbates Early Cardiac Dysfunction but Prevents Late Remodeling after Infarction.”

Cardiovascular Research 64 (3): 526–35. <https://doi.org/10.1016/j.cardiores.2004.07.017>.

Jacquemet, Vincent, and Craig S Henriquez. 2008. “Loading Effect of Fibroblast-Myocyte

Coupling on Resting Potential, Impulse Propagation, and Repolarization: Insights from a

Microstructure Model.” *American Journal of Physiology. Heart and Circulatory Physiology*

294 (5): H2040–52. <https://doi.org/10.1152/ajpheart.01298.2007>.

Jacquemet, Vincent, and Craig S. Henriquez. 2007. "Modelling Cardiac Fibroblasts: Interactions with Myocytes and Their Impact on Impulse Propagation." *Europace : European Pacing, Arrhythmias, and Cardiac Electrophysiology : Journal of the Working Groups on Cardiac Pacing, Arrhythmias, and Cardiac Cellular Electrophysiology of the European Society of Cardiology* 9 Suppl 6. <https://doi.org/10.1093/europace/eum207>.

Jensen, Karin J., Farshid S. Garmaroudi, Jingchun Zhang, Jun Lin, Seti Boroomand, Mary Zhang, Zongshu Luo, et al. 2013. "An ERK-p38 Subnetwork Coordinates Host Cell Apoptosis and Necrosis during Coxsackievirus B3 Infection." *Cell Host and Microbe* 13 (1): 67–76. <https://doi.org/10.1016/j.chom.2012.11.009>.

Jensen, Karin J., Christian B. Moyer, and Kevin A. Janes. 2016. "Network Architecture Predisposes an Enzyme to Either Pharmacologic or Genetic Targeting." *Cell Systems* 2 (2): 112–21. <https://doi.org/10.1016/j.cels.2016.01.012>.

Jeong, H., S. P. Mason, A. L. Barabási, and Z. N. Oltvai. 2001. "Lethality and Centrality in Protein Networks." *Nature* 411 (6833): 41–42. <https://doi.org/10.1038/35075138>.

Jin, Yu-Fang, Hai-Chao Han, Jamie Berger, Qiuxia Dai, and Merry L Lindsey. 2011. "Combining Experimental and Mathematical Modeling to Reveal Mechanisms of Macrophage-Dependent Left Ventricular Remodeling." *BMC Systems Biology* 5 (1). BioMed Central Ltd: 60. <https://doi.org/10.1186/1752-0509-5-60>.

John, Jeffrey, Angela Throm Quinlan, Chiara Silvestri, and Kristen Billiar. 2010. "Boundary Stiffness Regulates Fibroblast Behavior in Collagen Gels." In *Annals of Biomedical Engineering*, 38:658–73. <https://doi.org/10.1007/s10439-009-9856-1>.

Kähäri, Veli Matti, Jyrki Heino, and Eero Vuorio. 1987. "Interleukin-1 Increases Collagen

Production and mRNA Levels in Cultured Skin Fibroblasts.” *BBA - Molecular Cell Research* 929 (2): 142–47. [https://doi.org/10.1016/0167-4889\(87\)90169-8](https://doi.org/10.1016/0167-4889(87)90169-8).

Kamentsky, Lee, Thouis R. Jones, Adam Fraser, Mark Anthony Bray, David J. Logan, Katherine L. Madden, Vebjorn Ljosa, Curtis Rueden, Kevin W. Eliceiri, and Anne E. Carpenter. 2011. “Improved Structure, Function and Compatibility for Cellprofiler: Modular High-Throughput Image Analysis Software.” *Bioinformatics* 27 (8): 1179–80. <https://doi.org/10.1093/bioinformatics/btr095>.

Kapoun, Ann M., Faquan Liang, Gilbert O’Young, Deborah L. Damm, Diana Quon, R. Tyler White, Kimberly Munson, Andrew Lam, George F. Schreiner, and Andrew A. Protter. 2004. “B-Type Natriuretic Peptide Exerts Broad Functional Opposition to Transforming Growth Factor- β in Primary Human Cardiac Fibroblasts: Fibrosis, Myofibroblast Conversion, Proliferation, and Inflammation.” *Circulation Research* 94 (4): 453–61. <https://doi.org/10.1161/01.RES.0000117070.86556.9F>.

Kharait, Sourabh, Sampsa Hautaniemi, Shan Wu, Akihiro Iwabu, Douglas A Lauffenburger, and Alan Wells. 2007. “Decision Tree Modeling Predicts Effects of Inhibiting Contractility Signaling on Cell Motility.” *BMC Systems Biology* 1: 9. <https://doi.org/10.1186/1752-0509-1-9>.

Kinugawa, S, H Tsutsui, S Hayashidani, T Ide, N Suematsu, S Satoh, H Utsumi, and A Takeshita. 2000. “Treatment with Dimethylthiourea Prevents Left Ventricular Remodeling and Failure after Experimental Myocardial Infarction in Mice: Role of Oxidative Stress.” *Circulation Research* 87 (5): 392–98. <https://doi.org/10.1161/01.RES.87.5.392>.

Kliment, Corrine R., Judson M. Englert, Lauren P. Crum, and Tim D. Oury. 2011. “A Novel

Method for Accurate Collagen and Biochemical Assessment of Pulmonary Tissue Utilizing One Animal.” *International Journal of Clinical and Experimental Pathology* 4 (4): 349–55.

Klingberg, Franco, Melissa L Chow, Anne Koehler, Stellar Boo, Lara Buscemi, Thomas M Quinn, Mercedes Costell, Benjamin A Alman, Elisabeth Genot, and Boris Hinz. 2014. “Prestress in the Extracellular Matrix Sensitizes Latent TGF- β 1 for Activation.” *The Journal of Cell Biology* 207 (2): 283–97. <https://doi.org/10.1083/jcb.201402006>.

Kohl, P, A G Kamkin, I S Kiseleva, and D Noble. 1994. “Mechanosensitive Fibroblasts in the Sino-Atrial Node Region of Rat Heart: Interaction with Cardiomyocytes and Possible Role.” *Experimental Physiology* 79 (6): 943–56.

Kohl, Peter, and Robert G. Gourdie. 2014. “Fibroblast-Myocyte Electrotonic Coupling: Does It Occur in Native Cardiac Tissue?” *Journal of Molecular and Cellular Cardiology* 70: 37–46. <https://doi.org/10.1016/j.yjmcc.2013.12.024>.

Koskela von Sydow, A, C Janbaz, C Kardeby, D Repsilber, and M Ivarsson. 2015. “IL-1alpha Counteract TGF-Beta Regulated Genes and Pathways in Human Fibroblasts.” *Journal of Cellular Biochemistry*. <https://doi.org/10.1002/jcb.25455>.

Kraeutler, Matthew J, Anthony R Soltis, and Jeffrey J Saucerman. 2010. “Modeling Cardiac β -Adrenergic Signaling with Normalized-Hill Differential Equations: Comparison with a Biochemical Model.” *BMC Systems Biology* 4 (1): 157. <https://doi.org/10.1186/1752-0509-4-157>.

Krul, Sébastien P J, Wouter R Berger, Nicoline W Smit, Shirley C M van Amersfoort, Antoine H G Driessen, Wim Jan van Boven, Jan W T Fiolet, et al. 2015. “Atrial Fibrosis and Conduction Slowing in the Left Atrial Appendage of Patients Undergoing Thoracoscopic

- Surgical Pulmonary Vein Isolation for Atrial Fibrillation.” *Circulation. Arrhythmia and Electrophysiology* 8 (2): 288–95. <https://doi.org/10.1161/CIRCEP.114.001752>.
- Kupfer, Peter, René Huber, Michael Weber, Sebastian Vlais, Thomas Häupl, Dirk Koczan, Reinhard Guthke, and Raimund W Kinne. 2014. “Novel Application of Multi-Stimuli Network Inference to Synovial Fibroblasts of Rheumatoid Arthritis Patients.” *BMC Medical Genomics* 7 (1): 40. <https://doi.org/10.1186/1755-8794-7-40>.
- Lai, Ka-Bik, John E Sanderson, and Cheuk-Man Yu. 2009. “Suppression of Collagen Production in Norepinephrine Stimulated Cardiac Fibroblasts Culture: Differential Effect of Alpha and Beta-Adrenoreceptor Antagonism.” *Cardiovascular Drugs and Therapy / Sponsored by the International Society of Cardiovascular Pharmacotherapy* 23 (4): 271–80. <https://doi.org/10.1007/s10557-009-6183-6>.
- Lavecchia, Antonio, and Carmen Cerchia. 2016. “In Silico Methods to Address Polypharmacology: Current Status, Applications and Future Perspectives.” *Drug Discovery Today*. <https://doi.org/10.1016/j.drudis.2015.12.007>.
- Li, Song, Sarah M. Assmann, and Réka Albert. 2006. “Predicting Essential Components of Signal Transduction Networks: A Dynamic Model of Guard Cell Abscisic Acid Signaling.” *PLoS Biology* 4 (10): 1732–48. <https://doi.org/10.1371/journal.pbio.0040312>.
- Libby, Peter. 2017. “Interleukin-1 Beta as a Target for Atherosclerosis Therapy: Biological Basis of CANTOS and Beyond.” *Journal of the American College of Cardiology*. <https://doi.org/10.1016/j.jacc.2017.09.028>.
- Lindsey, Merry L, and Rogelio Zamilpa. 2012. “Temporal and Spatial Expression of Matrix Metalloproteinases and Tissue Inhibitors of Metalloproteinases Following Myocardial

- Infarction.” *Cardiovascular Therapeutics* 30 (1): 31–41. <https://doi.org/10.1111/j.1755-5922.2010.00207.x>.
- Lipsky, Martin S, and Lisa K Sharp. 2001. “From Idea to Market: The Drug Approval Process.” *The Journal of the American Board of Family Practice / American Board of Family Practice* 14 (5): 362–67. <http://www.ncbi.nlm.nih.gov/pubmed/11572541>.
- Litwin, S E, C M Litwin, T E Raya, a L Warner, and S Goldman. 1991. “Contractility and Stiffness of Noninfarcted Myocardium after Coronary Ligation in Rats. Effects of Chronic Angiotensin Converting Enzyme Inhibition.” *Circulation* 83: 1028–37. <https://doi.org/10.1161/01.CIR.83.3.1028>.
- Lu, David, Nakon Aroonsakool, Utako Yokoyama, Hemal H Patel, and Paul a Insel. 2013. “Increase in Cellular Cyclic AMP Concentrations Reverses the Profibrogenic Phenotype of Cardiac Myofibroblasts: A Novel Therapeutic Approach for Cardiac Fibrosis.” *Molecular Pharmacology* 84 (6): 787–93. <https://doi.org/10.1124/mol.113.087742>.
- Luckett, L R, and R M Gallucci. 2007. “Interleukin-6 (IL-6) Modulates Migration and Matrix Metalloproteinase Function in Dermal Fibroblasts from IL-6KO Mice.” *Br J Dermatol* 156 (6): 1163–71. <https://doi.org/10.1111/j.1365-2133.2007.07867.x>.
- Luo, Fayong, Yan Zhuang, Mark D Sides, Cecilia G Sanchez, Bin Shan, Eric S White, and Joseph A Lasky. 2014. “Arsenic Trioxide Inhibits Transforming Growth Factor- β 1-Induced Fibroblast to Myofibroblast Differentiation in Vitro and Bleomycin Induced Lung Fibrosis in Vivo.” *Respiratory Research* 15 (1): 51. <https://doi.org/10.1186/1465-9921-15-51>.
- Ma, Yonggang, Ganesh V. Halade, Jianhua Zhang, Trevi A. Ramirez, Daniel Levin, Andrew Voorhees, Yu Fang Jin, Hai Chao Han, Anne M. Manicone, and Merry L. Lindsey. 2013.

“Matrix Metalloproteinase-28 Deletion Exacerbates Cardiac Dysfunction and Rupture after Myocardial Infarction in Mice by Inhibiting M2 Macrophage Activation.” *Circulation Research* 112 (4): 675–88. <https://doi.org/10.1161/CIRCRESAHA.111.300502>.

MacCannell, K Andrew, Hojjat Bazzazi, Lisa Chilton, Yoshiyuki Shibukawa, Robert B Clark, and Wayne R Giles. 2007. “A Mathematical Model of Electrotonic Interactions between Ventricular Myocytes and Fibroblasts.” *Biophysical Journal* 92 (11): 4121–32. <https://doi.org/10.1529/biophysj.106.101410>.

Mahadevan, R, and B O Palsson. 2005. “Properties of Metabolic Networks: Structure versus Function.” *Biophysical Journal* 88 (1): L07–09. <https://doi.org/10.1529/biophysj.104.055723>.

March-Vila, Eric, Luca Pinzi, Noé Sturm, Annachiara Tinivella, Ola Engkvist, Hongming Chen, and Giulio Rastelli. 2017. “On the Integration of in Silico Drug Design Methods for Drug Repurposing.” *Frontiers in Pharmacology* 8 (MAY). <https://doi.org/10.3389/fphar.2017.00298>.

Masci, Pier Giorgio, Constantinos Doulaptsis, Erika Bertella, Alberico Del Torto, Rolf Symons, Gianluca Pontone, Andrea Barison, et al. 2014. “Incremental Prognostic Value of Myocardial Fibrosis in Patients with Non-Ischemic Cardiomyopathy without Congestive Heart Failure.” *Circulation: Heart Failure* 7 (3): 448–56. <https://doi.org/10.1161/CIRCHEARTFAILURE.113.000996>.

Matsubara, H. 1998. “Pathophysiological Role of Angiotensin II Type 2 Receptor in Cardiovascular and Renal Diseases.” *Circulation Research* 83 (12): 1182–91. <https://doi.org/10.1161/01.RES.83.12.1182>.

Mauviel, A, J Heino, V M Kähäri, D J Hartmann, G Loyau, J P Pujol, and E Vuorio. 1991.

“Comparative Effects of Interleukin-1 and Tumor Necrosis Factor-Alpha on Collagen Production and Corresponding Procollagen mRNA Levels in Human Dermal Fibroblasts.”

The Journal of Investigative Dermatology 96 (2): 243–49.

<https://doi.org/papers3://publication/uuid/A4C0FB75-F258-4BA4-815A-5CD59D80B425>.

McDougall, Steven, John Dallon, Jonathan Sherratt, and Philip Maini. 2006. “Fibroblast

Migration and Collagen Deposition during Dermal Wound Healing: Mathematical

Modelling and Clinical Implications.” *Philosophical Transactions. Series A, Mathematical,*

Physical, and Engineering Sciences 364 (1843): 1385–1405.

<https://doi.org/10.1098/rsta.2006.1773>.

McDowell, Kathleen S., Hermenegild J. Arevalo, Mary M. Maleckar, and Natalia A. Trayanova.

2011. “Susceptibility to Arrhythmia in the Infarcted Heart Depends on Myofibroblast

Density.” *Biophysical Journal* 101 (6): 1307–15. <https://doi.org/10.1016/j.bpj.2011.08.009>.

Meng, Xiao Ming, David J. Nikolic-Paterson, and Hui Yao Lan. 2016. “TGF- β : The Master

Regulator of Fibrosis.” *Nature Reviews Nephrology*.

<https://doi.org/10.1038/nrneph.2016.48>.

Miragoli, Michele, Giedrius Gaudesius, and Stephan Rohr. 2006. “Electrotonic Modulation of

Cardiac Impulse Conduction by Myofibroblasts.” *Circulation Research* 98 (6): 801–10.

<https://doi.org/10.1161/01.RES.0000214537.44195.a3>.

Moreo, Antonella, Giuseppe Ambrosio, Benedetta De Chiara, Min Pu, Tam Tran, Francesco

Mauri, and Subha V Raman. 2009. “Influence of Myocardial Fibrosis on Left Ventricular

Diastolic Function: Noninvasive Assessment by Cardiac Magnetic Resonance and Echo.”

Circulation. Cardiovascular Imaging 2 (6): 437–43.

<https://doi.org/10.1161/CIRCIMAGING.108.838367>.

Moyer, Christian B, Patrick T Norton, John D Ferguson, and Jeffrey W Holmes. 2015. “Changes in Global and Regional Mechanics Due to Atrial Fibrillation: Insights from a Coupled Finite-Element and Circulation Model.” *Annals of Biomedical Engineering* 43 (7): 1600–1613. <https://doi.org/10.1007/s10439-015-1256-0>.

Murtha, Lucy A., Michael J. Schuliga, Nishani S. Mabotuwana, Sean A. Hardy, David W. Waters, Janette K. Burgess, Darryl A. Knight, and Andrew J. Boyle. 2017. “The Processes and Mechanisms of Cardiac and Pulmonary Fibrosis.” *Frontiers in Physiology*. <https://doi.org/10.3389/fphys.2017.00777>.

Nahrendorf M, Sam F, Hulsmans M. 2016. “Monocyte and Macrophage Contributions to Cardiac Remodeling.” *Journal of Molecular and Cellular Cardiology*.

Nash, Richard A., Peter A. McSweeney, Leslie J. Crofford, Muneer Abidi, Chien Shing Chen, J. David Godwin, Theodore A. Gooley, et al. 2007. “High-Dose Immunosuppressive Therapy and Autologous Hematopoietic Cell Transplantation for Severe Systemic Sclerosis: Long-Term Follow-up of the US Multicenter Pilot Study.” *Blood* 110 (4): 1388–96. <https://doi.org/10.1182/blood-2007-02-072389>.

Neagu, Adrian, Vladimir Mironov, Ioan Kosztin, Bogdan Barz, Monica Neagu, Ricardo A Moreno-Rodriguez, Roger R Markwald, and Gabor Forgacs. 2010. “Computational Modeling of Epithelial-Mesenchymal Transformations.” *Bio Systems* 100 (1): 23–30. <https://doi.org/10.1016/j.biosystems.2009.12.004>.

Nieuwenhoven, Frans A van, Karen E Hemmings, Karen E Porter, and Neil A Turner.

- “Combined Effects of Interleukin-1 α and Transforming Growth Factor- β 1 on Modulation of Human Cardiac Fibroblast Function.” *Matrix Biology : Journal of the International Society for Matrix Biology* 32 (7–8): 399–406. <https://doi.org/10.1016/j.matbio.2013.03.008>.
- Nim, Hieu T, Sarah E Boyd, and Nadia A Rosenthal. 2015. “Systems Approaches in Integrative Cardiac Biology: Illustrations from Cardiac Heterocellular Signalling Studies.” *Progress in Biophysics and Molecular Biology* 117 (1): 69–77. <https://doi.org/10.1016/j.pbiomolbio.2014.11.006>.
- Nishtala, Krishnatej, Truong Q Phong, Leif Steil, Martina Sauter, Manuela G Salazar, Reinhard Kandolf, Heyo K Kroemer, et al. 2011. “Virus-Induced Dilated Cardiomyopathy Is Characterized by Increased Levels of Fibrotic Extracellular Matrix Proteins and Reduced Amounts of Energy-Producing Enzymes.” *Proteomics* 11 (22): 4310–20. <https://doi.org/10.1002/pmic.201100229>.
- Oren, Ronit V., and Colleen E. Clancy. 2010. “Determinants of Heterogeneity, Excitation and Conduction in the Sinoatrial Node: A Model Study.” *PLoS Computational Biology* 6 (12). <https://doi.org/10.1371/journal.pcbi.1001041>.
- Palatinus, Joseph A., J. Matthew Rhett, and Robert G. Gourdie. 2010. “Translational Lessons from Scarless Healing of Cutaneous Wounds and Regenerative Repair of the Myocardium.” *Journal of Molecular and Cellular Cardiology*. <https://doi.org/10.1016/j.yjmcc.2009.06.013>.
- Peng, JianFeng, Devorah Gurantz, Van Tran, Randy T. Cowling, and Barry H. Greenberg. 2002. “Tumor Necrosis Factor- α -Induced AT1 Receptor Upregulation Enhances Angiotensin II-Mediated Cardiac Fibroblast Responses That Favor Fibrosis.” *Circulation Research* 91

(12): 1119–26. <https://doi.org/10.1161/01.RES.0000047090.08299.D5>.

Pereira, Livia De P., Mario R.L. Mota, Luiz A.C. Brizeno, Francisca C. Nogueira, Elda G.M.

Ferreira, Maria G. Pereira, and Ana M.S. Assreuy. 2016. “Modulator Effect of a Polysaccharide-Rich Extract from *Caesalpinia Ferrea* Stem Barks in Rat Cutaneous Wound Healing: Role of TNF- α , IL-1 β , NO, TGF- β .” *Journal of Ethnopharmacology* 187: 213–23. <https://doi.org/10.1016/j.jep.2016.04.043>.

Pfeffer, M. A., and E. Braunwald. 1990. “Ventricular Remodeling after Myocardial Infarction.

Experimental Observations and Clinical Implications.” *Circulation* 81 (4): 1161–72. <https://doi.org/10.1161/01.CIR.81.4.1161>.

Planavila, Anna, Ricardo Rodriguez-Calvo, Alberto Fernandez de Arriba, Rosa M Sanchez, Juan

C Laguna, Manuel Merlos, and Manuel Vazquez-Carrera. 2006. “Inhibition of Cardiac Hypertrophy by Triflusal (4-Trifluoromethyl Derivative of Salicylate) and Its Active Metabolite.” *Molecular Pharmacology* 69 (4): 1174–81.

<https://doi.org/10.1124/mol.105.016345>.

Pržulj, Nataša. 2011. “Protein-Protein Interactions: Making Sense of Networks via Graph-

Theoretic Modeling.” *BioEssays*. <https://doi.org/10.1002/bies.201000044>.

Quinn, Robert A., Louis Felix Nothias, Oliver Vining, Michael Meehan, Eduardo Esquenazi, and

Pieter C. Dorrestein. 2017. “Molecular Networking As a Drug Discovery, Drug Metabolism, and Precision Medicine Strategy.” *Trends in Pharmacological Sciences*.

<https://doi.org/10.1016/j.tips.2016.10.011>.

Rabkin, E, M Aikawa, J R Stone, Y Fukumoto, P Libby, and F J Schoen. 2001. “Activated

Interstitial Myofibroblasts Express Catabolic Enzymes and Mediate Matrix Remodeling in

Myxomatous Heart Valves.” *Circulation* 104 (21): 2525–32.

<https://doi.org/10.1161/hc4601.099489>.

Ramirez, R J, S Nattel, and M Courtemanche. 2000. “Mathematical Analysis of Canine Atrial Action Potentials: Rate, Regional Factors, and Electrical Remodeling.” *American Journal of Physiology. Heart and Circulatory Physiology* 279 (4): H1767–85.

Rangamani, Padmini, Marc Antoine Fardin, Yuguang Xiong, Azi Lipshtat, Olivier Rossier, Michael P. Sheetz, and Ravi Iyengar. 2011. “Signaling Network Triggers and Membrane Physical Properties Control the Actin Cytoskeleton-Driven Isotropic Phase of Cell Spreading.” *Biophysical Journal* 100 (4): 845–57.

<https://doi.org/10.1016/j.bpj.2010.12.3732>.

Reinhardt, James W, and Keith J Gooch. 2014. “Agent-Based Modeling Traction Force Mediated Compaction of Cell-Populated Collagen Gels Using Physically Realistic Fibril Mechanics.” *Journal of Biomechanical Engineering* 136 (2): 21024.

<https://doi.org/10.1115/1.4026179>.

Richardson, William J., and Jeffrey W. Holmes. 2015. “Why Is Infarct Expansion Such an Elusive Therapeutic Target?” *Journal of Cardiovascular Translational Research*.

<https://doi.org/10.1007/s12265-015-9652-2>.

Richardson WJ, Clarke SA, Holmes JW. 2016. “Modifying the Mechanics of Healing Infarcts: Better the Enemy of Good?” *Journal of Molecular and Cellular Cardiology*.

Rinn, John L., Chanda Bondre, Hayes B. Gladstone, Patrick O. Brown, and Howard Y. Chang. 2006. “Anatomic Demarcation by Positional Variation in Fibroblast Gene Expression

Programs.” *PLoS Genetics* 2 (7): 1084–96. <https://doi.org/10.1371/journal.pgen.0020119>.

- Rohr, Stephan. 2009. "Myofibroblasts in Diseased Hearts: New Players in Cardiac Arrhythmias?" *Heart Rhythm : The Official Journal of the Heart Rhythm Society* 6 (6): 848–56. <https://doi.org/10.1016/j.hrthm.2009.02.038>.
- Rosenfeldt, H. 2000. "Fibroblast Quiescence and the Disruption of ERK Signaling in Mechanically Unloaded Collagen Matrices." *Journal of Biological Chemistry* 275 (5): 3088–92. <https://doi.org/10.1074/jbc.275.5.3088>.
- Rouillard, Andrew D, and Jeffrey W Holmes. 2012. "Mechanical Regulation of Fibroblast Migration and Collagen Remodelling in Healing Myocardial Infarcts." *The Journal of Physiology* 590 (Pt 18): 4585–4602. <https://doi.org/10.1113/jphysiol.2012.229484>.
- . 2014. "Coupled Agent-Based and Finite-Element Models for Predicting Scar Structure Following Myocardial Infarction." *Progress in Biophysics and Molecular Biology*, July. <https://doi.org/10.1016/j.pbiomolbio.2014.06.010>.
- Rouse, Rodney, Naomi Kruhlak, James Weaver, Keith Burkhart, Vikram Patel, and David G. Strauss. 2017. "Translating New Science Into the Drug Review Process: The US FDA's Division of Applied Regulatory Science." *Therapeutic Innovation & Regulatory Science*.
- Ryall, Karen A., Vassilios J. Bezzerides, Anthony Rosenzweig, and Jeffrey J. Saucerman. 2014. "Phenotypic Screen Quantifying Differential Regulation of Cardiac Myocyte Hypertrophy Identifies CITED4 Regulation of Myocyte Elongation." *Journal of Molecular and Cellular Cardiology* 72: 74–84. <https://doi.org/10.1016/j.yjmcc.2014.02.013>.
- Ryall, Karen A, David O Holland, Kyle A Delaney, Matthew J Kraeutler, Audrey J Parker, and Jeffrey J Saucerman. 2012. "Network Reconstruction and Systems Analysis of Cardiac Myocyte Hypertrophy Signaling." *The Journal of Biological Chemistry* 287 (50): 42259–

68. <https://doi.org/10.1074/jbc.M112.382937>.

Sachse, Frank B., A. P. Moreno, G. Seemann, and J. A. Abildskov. 2009. "A Model of Electrical Conduction in Cardiac Tissue Including Fibroblasts." *Annals of Biomedical Engineering* 37 (5): 874–89. <https://doi.org/10.1007/s10439-009-9667-4>.

Sachse, Frank B., Alonso P. Moreno, and J. A. Abildskov. 2008. "Electrophysiological Modeling of Fibroblasts and Their Interaction with Myocytes." *Annals of Biomedical Engineering* 36 (1): 41–56. <https://doi.org/10.1007/s10439-007-9405-8>.

Sadeghi, Amir Hossein, Su Ryon Shin, Janine C. Deddens, Giuseppe Fratta, Serena Mandla, Iman K. Yazdi, Gyan Prakash, et al. 2017. "Engineered 3D Cardiac Fibrotic Tissue to Study Fibrotic Remodeling." *Advanced Healthcare Materials* 6 (11). <https://doi.org/10.1002/adhm.201601434>.

Sarrazy, Vincent, Anne Koehler, Melissa L. Chow, Elena Zimina, Chen X. Li, Hideyuki Kato, Christopher A. Caldarone, and Boris Hinz. 2014. "Integrins $\alpha\beta 5$ and $\alpha\beta 3$ Promote Latent TGF- $\beta 1$ Activation by Human Cardiac Fibroblast Contraction." *Cardiovascular Research* 102 (3): 407–17. <https://doi.org/10.1093/cvr/cvu053>.

Schneider, Caroline a, Wayne S Rasband, and Kevin W Eliceiri. 2012. "NIH Image to ImageJ: 25 Years of Image Analysis." *Nature Methods* 9 (7): 671–75. <https://doi.org/10.1038/nmeth.2089>.

Schoeberl, Birgit, Claudia Eichler-Jonsson, Ernst Dieter Gilles, and Gertraud Müller. 2002. "Computational Modeling of the Dynamics of the MAP Kinase Cascade Activated by Surface and Internalized EGF Receptors." *Nature Biotechnology* 20 (4): 370–75. <https://doi.org/10.1038/nbt0402-370>.

- Schroer, Alison K., Larisa M. Ryzhova, and W. David Merryman. 2014. "Network Modeling Approach to Predict Myofibroblast Differentiation." *Cellular and Molecular Bioengineering* 7 (3): 446–59. <https://doi.org/10.1007/s12195-014-0344-9>.
- Shannon, Paul, Andrew Markiel, Owen Ozier, Nitin S. Baliga, Jonathan T. Wang, Daniel Ramage, Nada Amin, Beno Schwikowski, and Trey Ideker. 2003. "Cytoscape: A Software Environment for Integrated Models of Biomolecular Interaction Networks." *Genome Research* 13 (11): 2498–2504. <https://doi.org/10.1101/gr.1239303>.
- Shibukawa, Yoshiyuki, E Lisa Chilton, K Andrew Maccannell, Robert B Clark, and Wayne R Giles. 2005. "K⁺ Currents Activated by Depolarization in Cardiac Fibroblasts." *Biophysical Journal* 88 (6): 3924–35. <https://doi.org/10.1529/biophysj.104.054429>.
- Shinde, Arti V, and Nikolaos G Frangogiannis. 2014. "Fibroblasts in Myocardial Infarction: A Role in Inflammation and Repair." *Journal of Molecular and Cellular Cardiology* 70 (May). Elsevier Ltd: 74–82. <https://doi.org/10.1016/j.yjmcc.2013.11.015>.
- Siwik, D a, D L Chang, and W S Colucci. 2000. "Interleukin-1beta and Tumor Necrosis Factor-Alpha Decrease Collagen Synthesis and Increase Matrix Metalloproteinase Activity in Cardiac Fibroblasts in Vitro." *Circulation Research* 86 (12): 1259–65.
- Soares, M B, K N Silva-Mota, R S Lima, M C Bellintani, L Pontes-de-Carvalho, and R Ribeiro-dos-Santos. 2001. "Modulation of Chagasic Cardiomyopathy by Interleukin-4: Dissociation between Inflammation and Tissue Parasitism." *The American Journal of Pathology* 159 (2): 703–9. [https://doi.org/10.1016/S0002-9440\(10\)61741-5](https://doi.org/10.1016/S0002-9440(10)61741-5).
- Soares, Milena B P, Ricardo S Lima, Leonardo L Rocha, Christina M Takyia, Lain Pontes-de-Carvalho, Antonio C Campos de Carvalho, and Ricardo Ribeiro-dos-Santos. 2004.

“Transplanted Bone Marrow Cells Repair Heart Tissue and Reduce Myocarditis in Chronic Chagasic Mice.” *The American Journal of Pathology* 164 (2): 441–47.

Sohraby, Farzin, Milad Bagheri, Masoud Aliyar, and Hassan Aryapour. 2017. “In Silico Drug Repurposing of FDA-Approved Drugs to Predict New Inhibitors for Drug Resistant T315I Mutant and Wild-Type BCR-ABL1: A Virtual Screening and Molecular Dynamics Study.” *Journal of Molecular Graphics and Modelling* 74: 234–40.
<https://doi.org/10.1016/j.jmgm.2017.04.005>.

Soignet, S L, S R Frankel, D Douer, M S Tallman, H Kantarjian, E Calleja, R M Stone, et al. 2001. “United States Multicenter Study of Arsenic Trioxide in Relapsed Acute Promyelocytic Leukemia.” *J. Clin. Oncol.* 19 (18): 3852–60.
<http://www.ncbi.nlm.nih.gov/pubmed/11559723>.

Souders, Colby A., S. L K Bowers, and Troy A. Baudino. 2009. “Cardiac Fibroblast: The Renaissance Cell.” *Circulation Research*.
<https://doi.org/10.1161/CIRCRESAHA.109.209809>.

Spach, M S, and J P Boineau. 1997. “Microfibrosis Produces Electrical Load Variations due to Loss of Side-to-Side Cell Connections: A Major Mechanism of Structural Heart Disease Arrhythmias.” *Pacing and Clinical Electrophysiology : PACE* 20 (2 Pt 2): 397–413.

Spinale, Francis G., Nikolaos G. Frangogiannis, Boris Hinz, Jeffrey W. Holmes, Zamaneh Kassiri, and Merry L. Lindsey. 2016. “Crossing into the Next Frontier of Cardiac Extracellular Matrix Research.” *Circulation Research*.
<https://doi.org/10.1161/CIRCRESAHA.116.309916>.

Squires, Christina E., G. Patricia Escobar, John F. Payne, Robert A. Leonardi, Danielle K.

- Goshorn, Nina J. Sheats, I. Matthew Mains, Joseph T. Mingoia, English C. Flack, and Merry L. Lindsey. 2005. "Altered Fibroblast Function Following Myocardial Infarction." *Journal of Molecular and Cellular Cardiology* 39 (4): 699–707.
<https://doi.org/10.1016/j.yjmcc.2005.07.008>.
- Sun, Yao, and Karl T. Weber. 2000. "Infarct Scar: A Dynamic Tissue." *Cardiovascular Research*. [https://doi.org/10.1016/S0008-6363\(00\)00032-8](https://doi.org/10.1016/S0008-6363(00)00032-8).
- Swaney, James S, David M Roth, Erik R Olson, Jennifer E Naugle, J Gary Meszaros, and Paul A Insel. 2005. "Inhibition of Cardiac Myofibroblast Formation and Collagen Synthesis by Activation and Overexpression of Adenylyl Cyclase." *Proceedings of the National Academy of Sciences of the United States of America* 102 (2): 437–42.
<https://doi.org/10.1073/pnas.0408704102>.
- Thomopoulos, Stavros, Gregory M Fomovsky, and Jeffrey W Holmes. 2005. "The Development of Structural and Mechanical Anisotropy in Fibroblast Populated Collagen Gels." *Journal of Biomechanical Engineering* 127 (5): 742–50. <https://doi.org/10.1115/1.1992525>.
- Trayanova, Natalia A., and Patrick M. Boyle. 2014. "Advances in Modeling Ventricular Arrhythmias: From Mechanisms to the Clinic." *Wiley Interdisciplinary Reviews: Systems Biology and Medicine* 6 (2): 209–24. <https://doi.org/10.1002/wsbm.1256>.
- Trelstad, R L, and K Hayashi. 1979. "Tendon Collagen Fibrillogenesis: Intracellular Subassemblies and Cell Surface Changes Associated with Fibril Growth." *Developmental Biology* 71 (2): 228–42.
- Turner, Neil A, and Karen E Porter. 2013. "Function and Fate of Myofibroblasts after Myocardial Infarction." *Fibrogenesis & Tissue Repair* 6 (1): 5.

<https://doi.org/10.1186/1755-1536-6-5>.

Turner, Neil a, Philip Warburton, David J O'Regan, Stephen G Ball, and Karen E Porter. 2010.

“Modulatory Effect of Interleukin-1 α on Expression of Structural Matrix Proteins, MMPs and TIMPs in Human Cardiac Myofibroblasts: Role of p38 MAP Kinase.” *Matrix Biol.* 29 (7): 613–20. <https://doi.org/10.1016/j.matbio.2010.06.007>.

Tusscher, K H W J ten, D Noble, P J Noble, and A V Panfilov. 2004. “A Model for Human Ventricular Tissue.” *American Journal of Physiology. Heart and Circulatory Physiology* 286 (4): H1573–89. <https://doi.org/10.1152/ajpheart.00794.2003>.

Vanhaelen, Quentin, Polina Mamoshina, Alexander M. Aliper, Artem Artemov, Ksenia Lezhnina, Ivan Ozerov, Ivan Labat, and Alex Zhavoronkov. 2017. “Design of Efficient Computational Workflows for in Silico Drug Repurposing.” *Drug Discovery Today*. <https://doi.org/10.1016/j.drudis.2016.09.019>.

Vanhoutte, Davy, Mark Schellings, Yigal Pinto, and Stephane Heymans. 2006. “Relevance of Matrix Metalloproteinases and Their Inhibitors after Myocardial Infarction: A Temporal and Spatial Window.” *Cardiovascular Research* 69 (3): 604–13. <https://doi.org/10.1016/j.cardiores.2005.10.002>.

Vempati, Prakash, Emmanouil D. Karagiannis, and Aleksander S. Popel. 2007. “A Biochemical Model of Matrix Metalloproteinase 9 Activation and Inhibition.” *Journal of Biological Chemistry* 282 (52): 37585–96. <https://doi.org/10.1074/jbc.M611500200>.

Vermolen, F, and A Gefen. 2013. “Wound Healing: Multi-Scale Modeling.” In *Multiscale Computer Modeling in Biomechanics and Biomedical Engineering*², edited by A Gefen, 321–45. Berlin, Heidelberg: Springer Berlin Heidelberg.

- Virag, Jitka Ismail, and Charles E. Murry. 2003. "Myofibroblast and Endothelial Cell Proliferation during Murine Myocardial Infarct Repair." *American Journal of Pathology* 163 (6): 2433–40. [https://doi.org/10.1016/S0002-9440\(10\)63598-5](https://doi.org/10.1016/S0002-9440(10)63598-5).
- Visser, S A G, D P de Alwis, T Kerbusch, J A Stone, and S R B Allerheiligen. 2014. "Implementation of Quantitative and Systems Pharmacology in Large Pharma." *CPT: Pharmacometrics & Systems Pharmacology* 3 (January): e142. <https://doi.org/10.1038/psp.2014.40>.
- Viswanathan, P C, R M Shaw, and Y Rudy. 1999. "Effects of IKr and IKs Heterogeneity on Action Potential Duration and Its Rate Dependence: A Simulation Study." *Circulation* 99 (18): 2466–74. <https://doi.org/10.1161/01.CIR.99.18.2466>.
- Voit, Eberhard O. 2014. "Mesoscopic Modeling as a Starting Point for Computational Analyses of Cystic Fibrosis as a Systemic Disease." *Biochimica et Biophysica Acta - Proteins and Proteomics* 1844 (1 PART B). Elsevier B.V.: 258–70. <https://doi.org/10.1016/j.bbapap.2013.03.023>.
- Volders PG1, Willems IE, Cleutjens JP, Arends JW, Havenith MG, Daemen MJ. 1993. "Interstitial Collagen Is Increased in the Non-Infarcted Human Myocardium After Myocardial Infarction." *Journal of Molecular and Cellular Cardiology*. <https://doi.org/10.1006/jmcc.1993.1144>.
- Voloshenyuk, Tetyana G., Andrew D. Hart, Elena Khoutorova, and Jason D. Gardner. 2011. "TNF-?? Increases Cardiac Fibroblast Lysyl Oxidase Expression through TGF-?? And PI3Kinase Signaling Pathways." *Biochemical and Biophysical Research Communications* 413 (2): 370–75. <https://doi.org/10.1016/j.bbrc.2011.08.109>.

Wall, Samuel T, Joseph C Walker, Kevin E Healy, Mark B Ratcliffe, and Julius M Guccione.

2006. “Theoretical Impact of the Injection of Material into the Myocardium: A Finite Element Model Simulation.” *Circulation* 114 (24): 2627–35.

<https://doi.org/10.1161/CIRCULATIONAHA.106.657270>.

Walpole, Joseph, Jason a Papin, and Shayn M Peirce. 2013. “Multiscale Computational Models

of Complex Biological Systems.” *Annual Review of Biomedical Engineering* 15 (July):

137–54. <https://doi.org/10.1146/annurev-bioeng-071811-150104>.

Wang, Hailong, Abhilash Nair, Christopher S Chen, Rebecca G Wells, and Vivek B Shenoy.

2014. “Long Range Force Transmission in Fibrous Matrices Enabled by Tension-Driven Alignment of Fibers.” *Submitted* 107 (11). Biophysical Society: 2592–2603.

<https://doi.org/10.1016/j.bpj.2014.09.044>.

Wang, Huan, Sarah M. Haeger, April M. Kloxin, Leslie A. Leinwand, and Kristi S. Anseth.

2012. “Redirecting Valvular Myofibroblasts into Dormant Fibroblasts through Light-Mediated Reduction in Substrate Modulus.” *PLoS ONE* 7 (7).

<https://doi.org/10.1371/journal.pone.0039969>.

Wang, Zhi, and Jianzhi Zhang. 2007. “In Search of the Biological Significance of Modular

Structures in Protein Networks.” *PLoS Computational Biology* 3 (6): 1011–21.

<https://doi.org/10.1371/journal.pcbi.0030107>.

Weber, Karl T, Yao Sun, Syamal K Bhattacharya, Robert A Ahokas, and Ivan C Gerling. 2013.

“Myofibroblast-Mediated Mechanisms of Pathological Remodelling of the Heart.” *Nature Reviews. Cardiology* 10 (1). Nature Publishing Group, a division of Macmillan Publishers

Limited. All Rights Reserved.: 15–26. <https://doi.org/10.1038/nrcardio.2012.158>.

- Weber, K T. 1989. "Cardiac Interstitium in Health and Disease: The Fibrillar Collagen Network." *Journal of the American College of Cardiology* 13 (7): 1637–52.
[https://doi.org/10.1016/0735-1097\(89\)90360-4](https://doi.org/10.1016/0735-1097(89)90360-4).
- Wei, Shun-guang, Yang Yu, Robert M. Weis, and Robert B. Felder. 2016. "Inhibition of Brain Mitogen-Activated Protein Kinase Signaling Reduces Central Endoplasmic Reticulum Stress and Inflammation and Sympathetic Nerve Activity in Heart Failure RatsNo Title."
- Weinberg, Eli J, Danial Shahmirzadi, and Mohammad Reza Kaazempur Mofrad. 2010. "On the Multiscale Modeling of Heart Valve Biomechanics in Health and Disease." *Biomechanics and Modeling in Mechanobiology* 9 (4): 373–87. <https://doi.org/10.1007/s10237-009-0181-2>.
- Wenk, Jonathan F, Kay Sun, Zhihong Zhang, Mehrdad Soleimani, Liang Ge, David Saloner, Arthur W Wallace, Mark B Ratcliffe, and Julius M Guccione. 2011. "Regional Left Ventricular Myocardial Contractility and Stress in a Finite Element Model of Posterobasal Myocardial Infarction." *Journal of Biomechanical Engineering* 133 (4): 44501.
<https://doi.org/10.1115/1.4003438>.
- Werner, Sabine, and Richard Grose. 2003. "Regulation of Wound Healing by Growth Factors and Cytokines." *Physiological Reviews* 83 (3): 835–70.
<https://doi.org/10.1152/physrev.00031.2002>.
- White, Michel, Jean L. Rouleau, Christian Hall, Malcolm Arnold, Francois Harel, Pierre Sirois, Sally Greaves, et al. 2001. "Changes in Vasoconstrictive Hormones, Natriuretic Peptides, and Left Ventricular Remodeling Soon after Anterior Myocardial Infarction." *American Heart Journal* 142 (6): 1056–64. <https://doi.org/10.1067/mhj.2001.119612>.

- Willems, I E, M G Havenith, J G De Mey, and M J Daemen. 1994. “The Alpha-Smooth Muscle Actin-Positive Cells in Healing Human Myocardial Scars.” *The American Journal of Pathology* 145 (4): 868–75.
- Wishart, D. S. 2006. “DrugBank: A Comprehensive Resource for in Silico Drug Discovery and Exploration.” *Nucleic Acids Research* 34 (90001): D668–72.
<https://doi.org/10.1093/nar/gkj067>.
- Wishart, David S., Yannick D. Feunang, An C. Guo, Elvis J. Lo, Ana Marcu, Jason R. Grant, Tanvir Sajed, et al. 2017. “DrugBank 5.0: A Major Update to the DrugBank Database for 2018.” *Nucleic Acids Research*. <https://doi.org/10.1093/nar/gkx1037>.
- Wong, Timothy C., Kayla Piehler, Christopher G. Meier, Stephen M. Testa, Amanda M. Klock, Ali A. Aneizi, Jonathan Shakesprere, et al. 2012. “Association between Extracellular Matrix Expansion Quantified by Cardiovascular Magnetic Resonance and Short-Term Mortality.” *Circulation* 126 (10): 1206–16. <https://doi.org/10.1161/CIRCULATIONAHA.111.089409>.
- Wynn, T a. 2008. “Cellular and Molecular Mechanisms of Fibrosis.” *The Journal of Pathology* 214 (2): 199–210. <https://doi.org/10.1002/path.2277>.
- Xie, Yuanfang, Alan Garfinkel, Patrizia Camelliti, Peter Kohl, James N Weiss, and Zhilin Qu. 2009. “Effects of Fibroblast-Myocyte Coupling on Cardiac Conduction and Vulnerability to Reentry: A Computational Study.” *Heart Rhythm : The Official Journal of the Heart Rhythm Society* 6 (11): 1641–49. <https://doi.org/10.1016/j.hrthm.2009.08.003>.
- Xie, Yuanfang, Alan Garfinkel, James N Weiss, and Zhilin Qu. 2009. “Cardiac Alternans Induced by Fibroblast-Myocyte Coupling: Mechanistic Insights from Computational Models.” *American Journal of Physiology. Heart and Circulatory Physiology* 297 (2):

H775–84. <https://doi.org/10.1152/ajpheart.00341.2009>.

Yang, Jason H., Renata K. Polanowska-Grabowska, Jeffrey S. Smith, Charles W. Shields, and Jeffrey J. Saucerman. 2014. “PKA Catalytic Subunit Compartmentation Regulates Contractile and Hypertrophic Responses to β -Adrenergic Signaling.” *Journal of Molecular and Cellular Cardiology* 66: 83–93. <https://doi.org/10.1016/j.yjmcc.2013.11.001>.

Yang, Jason H., and Jeffrey J. Saucerman. 2011. “Computational Models Reduce Complexity and Accelerate Insight into Cardiac Signaling Networks.” *Circulation Research*. <https://doi.org/10.1161/CIRCRESAHA.110.223602>.

Yang, Lei, Jizhe Wang, Huiping Wang, Yingli Lv, Yongchun Zuo, Xiang Li, and Wei Jiang. 2014. “Analysis and Identification of Essential Genes in Humans Using Topological Properties and Biological Information.” *Gene* 551 (2): 138–51. <https://doi.org/10.1016/j.gene.2014.08.046>.

Yeh, Edward T H, and Courtney L Bickford. 2009. “Cardiovascular Complications of Cancer Therapy: Incidence, Pathogenesis, Diagnosis, and Management.” *Journal of the American College of Cardiology* 53 (24): 2231–47. <https://doi.org/10.1016/j.jacc.2009.02.050>.

Yu, Haiyuan, Dov Greenbaum, Hao Xin Lu, Xiaowei Zhu, and Mark Gerstein. 2004. “Genomic Analysis of Essentiality within Protein Networks.” *Trends in Genetics*. <https://doi.org/10.1016/j.tig.2004.04.008>.

Yu, Haiyuan, Philip M. Kim, Emmett Sprecher, Valery Trifonov, and Mark Gerstein. 2007. “The Importance of Bottlenecks in Protein Networks: Correlation with Gene Essentiality and Expression Dynamics.” *PLoS Computational Biology* 3 (4): 713–20. <https://doi.org/10.1371/journal.pcbi.0030059>.

- Zeigler, A. C., W. J. Richardson, J. W. Holmes, and J. J. Saucerman. 2016. “A Computational Model of Cardiac Fibroblast Signaling Predicts Context-Dependent Drivers of Myofibroblast Differentiation.” *Journal of Molecular and Cellular Cardiology* 94: 72–81. <https://doi.org/10.1016/j.yjmcc.2016.03.008>.
- Zeigler, Angela C, William J Richardson, Jeffrey W Holmes, and Jeffrey J Saucerman. 2015. “Computational Modeling of Cardiac Fibroblasts and Fibrosis.” *Journal of Molecular and Cellular Cardiology*, November. <https://doi.org/10.1016/j.yjmcc.2015.11.020>.
- Zeisberg, Elisabeth M, Oleg Tarnavski, Michael Zeisberg, Adam L Dorfman, Julie R McMullen, Erika Gustafsson, Anil Chandraker, et al. 2007. “Endothelial-to-Mesenchymal Transition Contributes to Cardiac Fibrosis.” *Nature Medicine* 13 (8): 952–61. <https://doi.org/10.1038/nm1613>.
- Zhou, Lili, and Youhua Liu. 2016. “Wnt/ β -Catenin Signaling and Renin-Angiotensin System in Chronic Kidney Disease.” *Current Opinion in Nephrology and Hypertension* 25 (2): 100–106. <https://doi.org/10.1097/MNH.0000000000000205>.
- Zhou, Shu-xian, Yan Zhou, Yu-ling Zhang, Juan Lei, and Jing-feng Wang. 2009. “Antioxidant Probucol Attenuates Myocardial Oxidative Stress and Collagen Expressions in Post-Myocardial Infarction Rats.” *Journal of Cardiovascular Pharmacology* 54 (2): 154–62. <https://doi.org/10.1097/FJC.0b013e3181af6d7f>.
- Zimmerman, S D, D P Thomas, S G Velleman, X Li, T R Hansen, and R J McCormick. 2001. “Time Course of Collagen and Decorin Changes in Rat Cardiac and Skeletal Muscle Post-MI.” *American Journal of Physiology. Heart and Circulatory Physiology* 281 (4): H1816–22. <http://www.ncbi.nlm.nih.gov/pubmed/11557576>.

Zlochiver, Sharon, Viviana Muñoz, Karen L Vikstrom, Steven M Taffet, Omer Berenfeld, and José Jalife. 2008. “Electrotonic Myofibroblast-to-Myocyte Coupling Increases Propensity to Reentrant Arrhythmias in Two-Dimensional Cardiac Monolayers.” *Biophysical Journal* 95 (9): 4469–80. <https://doi.org/10.1529/biophysj.108.136473>.

Zotenko, Elena, Julian Mestre, Dianne P. O’Leary, and Teresa M. Przytycka. 2008. “Why Do Hubs in the Yeast Protein Interaction Network Tend to Be Essential: Reexamining the Connection between the Network Topology and Essentiality.” *PLoS Computational Biology* 4 (8). <https://doi.org/10.1371/journal.pcbi.1000140>.